The University of Nottingham

UNITED KINGDOM · CHINA · MALAYSIA

Delivery of imiquimod to intestinal lymph nodes following oral administration

Haojie Chen

School of Pharmacy

University of Nottingham

United Kingdom

Thesis submitted to the university of Nottingham for the degree of Doctor in Philosophy

Table of Contents

Acknowledgement

‘By wisdom a house is built, and through understanding it is established. Through knowledge its rooms are filled with rare and beautiful treasures.’ (Proverbs 24:3-4)

First, I would like to express my gratitude to my supervisor, Dr. Pavel Gershkovich, for his guidance, expertise, and patience throughout my PhD. His philosophy, "*Do not fight with the windmill*," offered valuable perspective during difficult times in experiments, data analysis, and writing. Whenever I felt overwhelmed and sought his advice, Pavel provided both academic and emotional support, for which I am profoundly grateful.

I also extend my deep thanks to my secondary supervisors, Dr. Michael Stocks and Dr. Dong-Hyun Kim. Dr. Stocks provided vital guidance in chemistry, while Dr. Kim offered crucial support with LC-MS/MS bioanalysis. Their expertise and supervision were essential to the completion of my research, and I am deeply grateful for their contributions.

I am especially thankful to my mother, Mrs. Yunbi Luo, and her husband, Mr. Guoxi Luo, for their ongoing support and sacrifices, including the financial assistance that allowed me to pursue my studies in the UK. I would also like to thank my father, Mr. Qiang Chen, and his wife, Mrs. Qinzhen Zhu, for their encouragement and making me feel welcome as part of their family. I am grateful to Ms. Grace Li, Dr. Long Jiang, and Dr. Erhui Sun for their support when balancing work and life became challenging. I would also like to thank my sister, Mrs. Shu Zhu, and my cousin, Mrs. Qing Chen, for their advice and constant willingness to listen.

I would like to thank all the staff at the Biodiscovery Institute, Boots Science Building, and Bio Support Unit for their help and training. Special thanks go to Dr. Eleonora Comeo for her help with chemical synthesis reactions.

I am so blessed to work with the people in Gershkovich's lab. I would like to thank Dr. Abigail Wong and Mr Liuhang Ji, who are trustworthy colleagues and great friends. I gratefully acknowledge Dr. Yenju Chu and Dr. Chaolong Qin for training me in the HPLC-UV method development and animal surgery and helping me become a senior PhD student. Thanks to Dr. Wanshan Feng for her fantastic technical support in animal work and supervision in data analysis. Special thanks to Mr. Yufei Zhu and Mr. Junting Wang for their help during the final stages of my animal studies. Lastly, I would like to thank everyone in the Gershkovich group: Dr. Alice Brookes, Dr. Adelaide Jewell, Graziamarina Sinatra, Branislav Vukovic, Fady Mina, Yunfei Zhong, Ali Ali, Yimou Zhang, Luke Kumet, Lin Zhu, Sham Nawshirawan, and Yasar Hamed.

Haojie Chen

Gershkovich group: a fake trip to Kyoto

Abstract

The lymphatic system is highly involved in the progression of colorectal cancer (CRC), providing the pathway for metastasis and the environment for the immune response to cancer. Mesenteric lymph nodes (MLNs) and iliac lymph nodes (ILNs) drain the lymph from the colorectal region and are enriched in antigen-presenting cells, such as dendritic cells (DCs), as well as different types of lymphocytes. In these lymph nodes, activated DCs can stimulate naïve T cells to differentiate to $CD8^+$ cytotoxic T cells and $CD4^+$ T helper cells by cross-presenting tumour-associated antigens to them, resulting in the anti-tumour immune response. However, in CRC patients, activated DCs are downregulated by tumour cells in the tumour-draining LNs, frequently leading to poor therapeutic outcomes for patients receiving anti-tumour immunotherapy.

Imiquimod (IMQ) is a powerful immune system activator, which can promote DCs activation *via* binding to toll-like receptor 7 on the DCs. However, the non-specific and extensive distribution of IMQ in the body may result in poor therapeutic outcomes in cancer patients and could lead to adverse effects. MLNs and ILNs are enriched in immature DCs and other lymphocytes and, therefore, are preferred tissues for immunomodulators. The delivery of IMQ into these lymph nodes in a targeted manner can promote the activation of DCs and improve the cross-presentation of tumour-associated antigens to naïve T cells. As a result, the tumour-mediated suppression of the immune system could be overcome, potentially leading to an improved therapeutic outcome in patients with CRC.

In this PhD project, the chemically unmodified IMQ was initially assessed for its potential for lymphatic transport following oral administration. Due to its low lipophilicity

and poor solubility in triglycerides, IMQ was not expected to be absorbed into the intestinal lymphatics. Therefore, the aim of this PhD project was to design highly lipophilic prodrugs of IMQ that can be transported into MLNs and ILNs, and efficiently release IMQ within these lymph nodes. This drug delivery approach takes advantage of the digestion of fat in the intestine. During the natural process of ingestion of dietary lipids, large lipoproteins, chylomicrons (CMs), are formed in the enterocytes. Due to the large size of CMs, they are absorbed into the lymph lacteals rather than blood capillaries. Thus, a drug molecule that has a high affinity to CMs has potential to be transported into the intestinal lymphatics *via* the CMs pathway.

First, we developed bioanalytical methods for the determination of the concentration of IMQ in the biological samples. The bioanalytical method using liquid chromatography equipped with ultraviolet detector (HPLC-UV) had a lower limit of quantification (LLOQ) at 15 ng/mL, which allows the determination of IMQ in *in vitro* and *ex vivo* biological samples. In addition, the bioanalytical method using liquid chromatography with tandem mass spectrometry (LC-MS/MS) was developed and validated. The calibration curve showed good linearity from 1.25 to 4,000 ng/mL, which could be used for the determination of the concentration of IMQ in *in vivo* samples. Moreover, the LC-MS/MS bioanalytical method only required a small volume of plasma sample at 100 µL, which is important for work with small laboratory animals such as rats.

Using the bioanalytical methods developed in this project, the pharmacokinetic (PK) and biodistribution (BD) profiles of IMQ in rats following oral administration were assessed. The oral bioavailability (F_{oral}) of IMQ was limited (< 10%) with or without the

presence of lipids. The plasma concentration-time profile of IMQ was prolonged and erratic following oral administration of unmodified IMQ at the dose of 8 mg/kg. In this project, we first reported the biodistribution of IMQ in the MLNs, ILNs, and other lymph nodes, which are the essential targeting areas for immune system activation. Interestingly, although IMQ is not a highly lipophilic molecule, it was widely distributed into tissues, including lymph nodes. The average concentrations of IMQ in MLNs and ILNs were 85.7 ± 103.2 ng/g and 99.8 ± 132.2 ng/g, respectively, at 1.5 h following oral administration of the drug, which was higher than its concentration in plasma (21.7 ± 20.4 ng/mL).

Next, amide prodrugs of IMQ were designed and synthesised by conjugating IMQ with saturated and unsaturated medium- to long carbon chains fatty acids. The amidation of IMQ was achieved with *N, N, N′, N′*-tetramethylchloroformamidinium hexafluorophosphate and *N*-methylimidazole in *N*-methyl-2-pyrrolidone. This reaction provided a relatively high yield for the production of the prodrugs (70 – 90 %).

The synthesised amide prodrugs were assessed for their lymphatic transport potential, determined by their *in silico* and *in vitro* affinities to CMs, as well as solubility in triglycerides. The assessments for the intestinal lymphatic transport of prodrugs showed that the developed lipophilic alkyl amide prodrugs have a substantial affinity to CMs.

A promising prodrug candidate in this work is expected to resist the enzymatic hydrolysis in the intestine, but rapidly release the active moiety in the lymphatics. The biotransformation of prodrugs in relevant enzymatic environments representing

intestinal lumen (simulated intestinal fluids with added esterase activity) and lymph (using plasma as lymph surrogate) was assessed. Additionally, in our work, brush border enzyme vesicles that were collected from rats' small intestine were used to estimate the hydrolysis of prodrugs in the gastrointestinal tract. *In vitro* and *ex vivo* results suggested that all synthesised prodrugs were stable in the intestine (except prodrug 1, which was synthesised by conjugating IMQ with decanoic acid) and could efficiently release IMQ in the lymph fluid. Moreover, it was found that the unsaturation of fatty acid could facilitate IMQ release from the prodrugs in rat plasma.

Subsequently, the most promising prodrug candidates (prodrug 5 and prodrug 8) were administered to rats to assess their pharmacokinetics and lymph nodes delivery. When prodrug 5 (synthesized by conjugating IMQ with myristoleic acid) and prodrug 8 (synthesized by conjugating IMQ with linoleic acid) were orally administered, the F_{oral} of IMQ was not increased, but the plasma concentration-time profile of IMQ was not prolonged and erratic in comparison to oral administration of IMQ itself. This result suggests that the lipophilic prodrug approach did not significantly increase the systemic exposure to IMQ but potentially changed the absorption pathway of the drug. Therefore, the BD studies of IMQ following oral administration of prodrugs 5 and 8 were conducted to evaluate the intestinal lymphatic delivery. *In vivo* studies showed that the average concentrations of prodrugs 5 and 8 in the mesenteric lymph were 50- and 11-fold higher than their concentration in the plasma, respectively, suggesting that a substantial amount of prodrugs were transported into intestinal lymphatics. Moreover, the lymph-to-plasma ratio of the concentration of IMQ (released from the prodrug) was 1.9-fold and 1.7-fold following oral administration of prodrug 5 and prodrug 8, respectively, indicating that the prodrugs efficiently released IMQ in the mesenteric

lymph. Importantly, the average concentration of IMQ in MLNs and ILNs was 11-fold and 9-fold higher, respectively, than it was in plasma at 1.5 h following oral administration of prodrug 5. Similarly, the average concentration of IMQ in MLNs and ILNs also improved following the oral administration of prodrug 8. Additionally, the BD studies showed that the non-specific distribution of IMQ into various organs and tissues was reduced following the oral administration of prodrugs in comparison to the oral administration of unmodified IMQ.

This PhD project suggests that the highly lipophilic prodrug approach is a simple but powerful method that can efficiently deliver IMQ to intestinal lymphatics following oral administration. In addition, this study demonstrates the feasibility of using amide-based prodrugs for general amine-containing compounds for intestinal lymphatic targeting.

Abbreviation

AUC – Area under the curve

AUC_{inf} – Area under the curve from time zero to infinity

AUC_{last} – Area under the curve to the last sampling time point

BD – Biodistribution

BBMVS – Brush border membrane vesicles

C_0 – concentration extrapolated to time zero

CL – Clearance

CMs – Chylomicrons

CRC – Colorectal cancer

CTLA-4 – Cytotoxic T lymphocytes-associated antigen 4

DCs – Dendritic cells

DPBS – Dulbecco's phosphate buffered saline

DMSO – Dimethylsulfoxide

FaSSIF – Fasted state simulated intestinal fluid

FDA – Food and Drug Administration

HPLC-UV – High performance liquid chromatography with ultraviolet detector

F_{oral} – Oral bioavailability

IL – Interleukin

ILNs – Iliac lymph nodes

IMQ – Imiquimod

IFN – Interferon

IS – Internal standard

IV – Intravenous administration

LC-MS/MS – Liquid chromatography with tandem mass spectrometry

LLOQ – Lower limitation of quantification

LNs – Lymph nodes

MHC – Major histocompatibility complex

MLNs – Mesenteric lymph nodes

NMI – *N*-methylimidazole

NMP – *N*-methyl-*2*-pyrrolidone

NMR – Nuclear magnetic resonance

PD-1/PD-L1 – programmed cell death protein 1/ programmed cell death ligand-1

PEG 200 – Polyethylene glycol 200

PG – Propylene glycol

PK – Pharmacokinetic

PO – Oral administration

PRRs – Pathogen recognition receptors

SD – Standard deviation

$t_{1/2}$ – Half-live

TAAs – Tumour-associated antigens

TCFH – *N, N, N′, N′*-tetramethylchloroformamidinium hexafluorophosphate

TG – Triglycerides

TGF – Transforming growth factor

TLC – Thin-layer chromatography

TLRs – Toll-like receptors

T_{max} – Maximum concentration

TME – Tumour microenvironment

V_{ss} – Volume of distribution at steady state

List of Figures

List of Tables

Chapter 1 Introduction

1.1 Colorectal cancer

1.1.1 Epidemiology of colorectal cancer

A statistical report for global cancer incidence and mortality from the GLOBOCAN database estimated that in 2018, there were18.1 million (95% UI: 17.5–18.7 million) new cancer cases and 9.6 million (95% UI: 9.3–9.8 million) people have died from cancer [1,2]. In the United Kingdom, projected data for cancer incidence in the age group from fifteen to ninety are 270,260.90 in males and 243,689.80 in females in the year 2035 [3].

Colorectal cancer (CRC) is a malignant tumour that localised in the colon and rectum [4]. Globally, CRC is the third most common cancer in humans (WHO, Cancer, accessed on Jan 2024). It was estimated that in 2020, about 2 million new cases of CRC were reported, with approximately 9.5 % death rate [5,6]. In developed countries where the diagnostic methods and treatments for CRC are well established, the estimated mortality of CRC is high: 9 % in males and 8 % in females [7]. In addition, a significant increase in CRC incidences in the young age group (0 – 49 years old) was observed in the last two decades, suggesting an increased risk of CRC in the younger age group [8,9].

It was predicted that in the future the number of deaths associated with CRC would rise by 60 % in 2035 due to the increase in population and lifespans and this number was estimated to continuously increase until 2040 [6,10].

1.1.2 Classification of CRC

The CRC can be defined as a carcinogenic neoplasia in the colon or rectum region [11]. The classification of CRC is a complex and comprehensive subject that is constantly developing. In this section, we only demonstrate some well-known classification methods of CRC.

The region of cancer can be used to classify CRC. The most common subsites of CRC in humans are proximal (39 %), rectal (30 %) and distal (24 %) colorectum [12]. Moreover, beyond the regions of neoplasia, CRC can be further divided into several subtypes, such as tubular and villous CRC, depending on the pathological features of the solid tumour [13]. Other classifications of CRC based on the pathohistology of CRC have been reviewed by Quirke *et al*. [11].

In addition to pathophysiological classification, subtypes of CRC can also be defined by their related gene mutations and molecular biomarkers. Previously, a comprehensive analysis of CRC-related genomic mutations among 276 patients showed that there were 24 genetic mutations that were highly associated with colorectal carcinoma. Therefore, based on the prevalence of these mutated genes, CRC can be divided into hypermutated CRC (occupied 16 % of the total cases) and non-hypermutated CRC [14,15].

Another CRC experts panel, across areas of pathology, immunology, oncology and clinics, had summarised current classifications of CRC and integrated them into four subtypes based on the molecular features of CRC (**Table 1-1**) [16]. Consensus molecular subtype 1 is defined as microsatellite instability immune and found in 14% of CRC. The microsatellite is a short, repeated DNA sequence that can be found in the genomes [17]. Microsatellite instability is a result of a defective DNA mismatch

repair mechanism. Consensus molecular subtype 1-CRC is hypermutated and highly associated with an unstable and strong immune activation due to a substantial production of neoantigens (tumour-associated antigens, TAAs) [18]. Consensus molecular subtype 2 is mainly characterised by the carcinogenic differentiation of epithelia and is found in 37 % of CRC [16]. It can be identified by the activation of WNT and MYC signal pathways [19]. Consensus molecular subtype 3 CRC displays a KRAS mutation and is found in 13 % of CRC [16,20]. The mutation of KRAS can result in an upregulation of energy metabolism and nutrient utilization due to its impacts on metabolic dysregulation [21]. Consensus molecular subtype 4 is found in 23 % of CRC [16]. Consensus molecular subtype 4-CRC is characterized by the overexpression of transforming growth factor beta (TGF-ß), which results in tumour angiogenesis and malignant differentiation of mesenchymal and stromal cells. Other details about the prevalence, pre-diagnostic value and clinical application can be found in these reviews: [16,22–24]

Table 1-1 Summary of Consensus molecular subtype classification of CRC and significant biological characteristics of Consensus molecular subtype subtypes. Adapted from [16].

Subtypes	Consensus molecular subtype 1	Consensus molecular subtype 2	Consensus molecular subtype 3	Consensus molecular subtype 4
Prevalence	14 %	37 %	13 %	23 %
Biomarker	Microsatellite instability, hypermutated	*SCNA* high	Mixed Microsatellite instability status, *SCNA* low, *CIMP* low	*SCNA* high
Mutation	*BRAF* mutations		*KRAS* mutations	
Significant biodifference	Immune infiltration and activation	WNT and MYC activation	Metabolic deregulation	TGF-β activation, angiogenesis

1.1.3 CRC metastasis

Metastasis describes the dissemination of malignant cells from the primary tumour and migration to distal regions. Then, the colonization will be completed after the distal tissue adopts these cells and allows them to develop into a detectable tumour [25]. It was shown that 15% - 28% of CRC patients have developed metastasis in the early stages (I to II) of CRC [26]. Riihimäki *et al.* conducted a population-based analysis of 49,096 cases of CRC. They found that rectal adenocarcinoma frequently metastasises into thoracic organs, whereas cancer cells from mucin and signet rings frequently metastasise into the peritoneum. Importantly, the authors indicated that the destination of metastasis is associated with the route of cancer cell migration. For example, adenocarcinoma from the distal rectal can migrate into the lungs *via* blood circulation. By contrast, the mucinous adenocarcinoma can migrate into the lungs through the gastrointestinal lymphatics passing by the cisterna chyli [27]. Compared to the vascular wall of blood vessels, lymphatic vessel layers consist of loosely connected endothelium [28]. As a result, the lymphatics vasculature offers an easy and convenient route for cancers to enter and migrate to other organs. A review article on lymphangiogenesis in cancer models reported that tumour-produced vascular endothelial growth factors, such as vascular endothelial growth factor C and vascular endothelial growth factor D, were highly expressed in rodent models of cancer [29]. Although the importance of these growth factors in malignant lymphangiogenesis is unclear, the presence of the vascular endothelial growth factors in the tumour environment reinforces the evidence that cancer cells can potentially migrate to other tissue *via* the lymphatic system.

In clinical studies, it has been reported that the metastasis of CRC frequently happens through the gastrointestinal lymphatic system, often resulting in a poor survival rate and a high recurrence in patients who received surgical resection [30–32]. It was shown that primary tumour in the colorectal tissue can invade pericolic and perirectal lymph nodes (small lymph nodes located around the colon and rectum, respectively) and eventually reach large lymph nodes (such as iliac and mesenteric lymph nodes) via lymphatic vessels (**Figure 1-1**) [32]. This suggests that mesenteric lymph nodes (MLNs) and iliac lymph nodes (ILNs) are important targets for the prevention and treatment of CRC progression and metastasis [32–34].

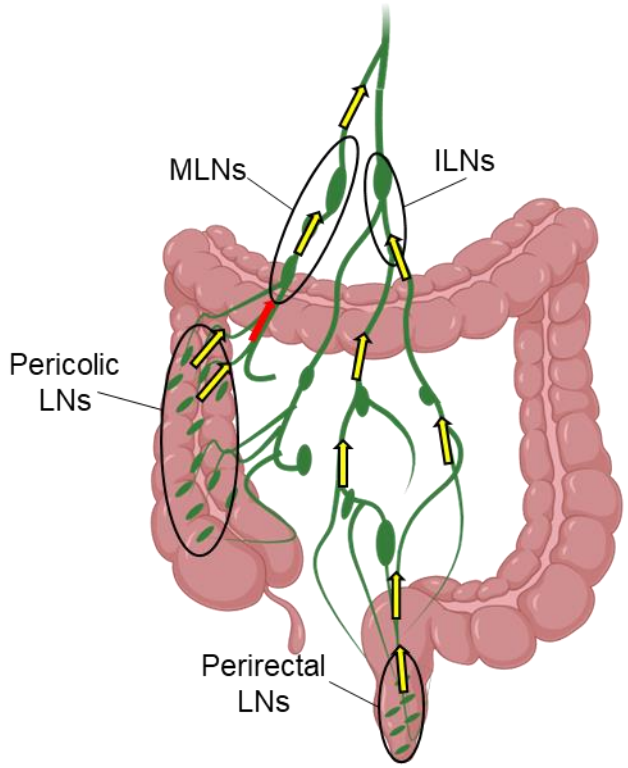

Figure 1-1 Colorectal cancer metastasis. Yellow arrows show the direction of cancer cell migration *via* the lymphatic system [32–34]. Mesenteric lymph nodes, MLNs; iliac lymph nodes, ILNs; lymph nodes, LNs. (Created with BioRender.com)

1.1.4 CRC treatments and their limitation

According to the National Institute for Health and Care Excellence (NICE) guidelines for CRC (2020), surgical resection is the gold standard treatment for patients diagnosed with CRC when it is possible. For patients with unresectable colorectal tumours or with recurrence after surgical resection, chemotherapies and anti-tumour immunotherapies can be used to alleviate the cancer progression [35].

1.1.4.1 Chemotherapy of CRC

For patients who cannot receive surgical resection of CRC or need adjuvant chemotherapy after surgery, 5-fluorouracil, capecitabine, oxaliplatin, and irinotecan are recommended as the first-line chemotherapy [35–37].

5-fluorouracil and 5-fluorouracil-based chemotherapy are highly recommended in patients with hypermutated CRC or MSI-CRC [4]. The 5-fluorouracil is an analogue to pyrimidine (uracil) with a fluorine at the C-5 position. The 5-fluorouracil can be transported into the cytoplasm *via* the same mechanism as uracil and then converted into its active metabolites fluorodeoxyuridine mono/triphosphate and fluorouridine triphosphate. These uracil-like active moieties can be involved in the transcription process in the tumour cells, resulting in the disruption of ribonucleic acid (RNA) synthesis [38]. However, 5-fluorouracil cannot be orally administered due to its rapid metabolism in the liver, resulting in off-target carcinogenic toxicity. Therefore, a prodrug of 5-fluorouracil, capecitabine, was developed. Following the oral administration of the prodrug, capecitabine can be converted to *5'-deoxy-5-fluorouridine* by the hepatic carboxylesterase. Then, *5'-deoxy-5-fluorouridine* will be

further converted by cytidine deaminase to *5'-deoxy-5-fluorocytidine,* which is the active form of the drug [39].

Oxaliplatin is recommended in combination with 5-fluorouracil based treatment [35,37]. It has been shown that including oxaliplatin in the treatment plan can effectively improve therapeutic outcomes in patients affected by CRC [40]. Oxaliplatin is the third generation of platin-based chemotherapy. It has a similar pharmacological mechanism as cisplatin, but oxaliplatin is effective in cisplatin-resistant cancer [41]. It can be uptaken into cells *via* the copper membrane transporter 1. In the cytoplasm, the strong electrophilic hydrolysed product of oxaliplatin can interact with nucleic acids, resulting in deoxyribonucleic acid (DNA) damage in the malignant cells [42].

The combination of irinotecan with 5-fluorouracil based chemotherapy was also recommended for patients with unresectable CRC [37]. Irinotecan is a topoisomerase 1 inhibitor approved by the American Food and Drug Administration (FDA) for the treatment of metastatic CRC [36]. Topoisomerase 1 is highly expressed in the supercoiled chromatin regions. Topoisomerase can release the supercoiled DNA (*a.k.a* tight DNA strands) and break the unrotated DNA strands for the replication process. Therefore, the inhibition of topoisomerase 1 with irinotecan directly interrupts the DNA synthesis, resulting in cell apoptosis [43]. Irinotecan is a prodrug of the active moiety SN-38 and can be orally administered to humans. The area under the curve (AUC) of irinotecan following oral administration has linearly correlation with the dose. By contrast, its active metabolite SN-38 does not have such linear correlation. Irinotecan can be metabolised to SN-38 *via* a carboxylesterase-mediated pathway. It can also be metabolised by CYP3A4 to *7-ethyl-10-[4-N-(5-aminopentanoic acid)-1-piperidino]- carbonyloxycamptothecin* and

7-ethyl-10-[4-(1-piperidino)-1-amino]-carbonyloxycamptothecin, which can be hydrolysed to SN-38 later with carboxylesterase [44,45].

1.1.4.2 Immunotherapy of CRC

The interaction between the immune system and cancer is introduced in **Section 1.2**. In this section, we mainly focus on the current options of immunotherapy for the treatment of CRC.

Although the role of immunotherapy in CRC treatment is not crystal clear, many clinical trials have shown promising therapeutic benefits of immunotherapy in patients [46,47].

The programmed cell death protein 1/ programmed cell death ligand-1 (PD-1/PD-L1) inhibitor, also called checkpoint inhibitors, is currently the most well-known immunotherapy used in cancer treatment. PD-1 is an immune checkpoint receptor that is expressed on the surface of macrophages, natural killer cells, antigen-presenting cells (APCs) and lymphocytes, such as T cells [48]. PD-L1 is one of the ligands for PD-1 and is usually expressed on the surface of macrophages, activated T cells and B cells, dendritic cells and epithelia in inflammatory conditions [49]. PD-1/PD-L1 is an important pathway that regulates cell apoptosis in healthy conditions. However, tumour cells can overexpress PD-L1, which suppresses T cell-mediated cytotoxicity and the activation of activated T cells, diminishing the anti-tumour immune response [48,50,51]. Nivolumab is a human monoclonal antibody and is the first PD-1 inhibitor approved by the FDA in patients with metastatic/unresectable melanoma [52]. In 2017, nivolumab was approved for use in patients with lymph-node-positive metastatic melanoma by the FDA. Nivolumab has been tested in clinical trials in the combination of oxaliplatin, 5-fluorouracil and irinotecan in patients with metastatic CRC. The improved overall response rate in the treatment groups resulted in the approval of

nivolumab for this group of patients [53]. Pembrolizumab is another FDA-approved PD-1 inhibitor [52]. In a phase III clinical trial, it significantly extended progression-free survival compared to chemotherapy, resulting in approval as a first-line treatment for microsatellite instability-high/mismatch repair-deficient (MIS/dMMR) metastatic CRC [54].

Another well-known and important immune checkpoint is the cytotoxic T lymphocytes-associated antigen 4 (CTLA-4). CTLA-4 is an intracellular protein in resting T cells. After T cells are activated via their extracellular molecules, T cell receptor (TCR) and CD28 bind to the major histocompatibility complex (MHC) and B7, respectively, on the dendritic cells (DCs). CLTA-4 translocates to the extracellular surface of activated T cells [55]. CLTA-4 has a high affinity to B7 on the DCs, which competes with CD28. This competitive binding can diminish the stimulatory signalling pathway that is regulated by the binding between CD28 and B7, indirectly resulting in the inactivation of T cells [55–57]. In healthy conditions, the regulatory T cells constitutively express CLTA-4 on their surface to balance the activation/inactivation state of effector T cells [58]. Cancer cells can attract the regulator T cells into the tumour environment, which is highly infiltrated with activated T cells. The recruitment of the regulatory T cells in the tumour site results in the suppression of anti-cancer immune response via the inhibitory signalling between regulatory T cells, DCs and activated T cells [59]. In 2011, ipilimumab became the first approved monoclonal antibody as a CLTA-4 inhibitor for the indication of metastatic/unresectable melanoma [52]. A Phase II clinical trial showed that including a low dose of ipilimumab in treatment with nivolumab for MIS/dMMR in metastatic CRC was well-tolerated and resulted in an overall response rate of 69 % [60]. Other potential options, such as cytokine therapy, have been reviewed in [61–63].

1.1.4.3 Limitations of CRC treatment

In most cases, patients who received chemotherapy tolerate and respond well to their treatment, resulting in a significant increase in the survival rate [38,40,64,65]. However, the treatment plan involving chemotherapy could be complexed in some scenarios.

Firstly, it could be difficult to balance the therapeutic benefits and inevitable cytotoxic effects of chemotherapy. For example, the wound healing process could be prolonged with the addition of chemotherapy in patients who receive surgical resection and are in the postoperative period [66]. Additionally, the administration of chemotherapy is of highly concern for patients who are pregnant due to its severe cytotoxic effects on both mother and child [67]. The potential interactions between chemotherapy and other medications should be carefully evaluated, particularly in elderly patients who are often on polypharmacy regimens, as their metabolic rates and drug clearance can differ significantly from those of younger adults [68]. Moreover, it was reported that the genotoxic effects of chemotherapy (such as FU-based treatments and oxaliplatin) could accelerate the progression of CRC [69].

Secondly, drug-resistant tumours could develop during chemotherapies *via* mechanisms involving detoxification, intracellular transporters, DNA repair, cell death and epigenetic mutations [70]. For example, the mutation of *p35* can lead to an increase in drug efflux and enhanced intracellular drug metabolism, which attenuates the efficacy of 5-fluorouracil based drugs [71]. The perturbation of DNA caused by chemotherapy can introduce DNA self-repair, which neutralises the therapeutic effects of irinotecan [72]. The transcription factor NF-*k*B has been shown to be frequently deregulated in colorectal tumours, and it is associated with increased proliferation and resistance to apoptosis induced by chemotherapeutic agents [73]. In fact, the

mechanisms of tumour resistance to chemotherapy are complex and normally involves multiple signalling pathways, which have been well-reviewed in [74–76].

It has been shown that tumour cells that are killed by chemotherapies can release damaged associated molecule patterns, which can be captured by APCs, such as DCs. Then, the APCs present damaged associated molecule patterns to other lymphocytes, such as T cells, activating the anti-tumour immune response [77]. Therefore, combining immunotherapy with other chemotherapy can potentially overcome the resistance of CRC to chemotherapy.

However, the combination of immunotherapy in the treatment of CRC is not always effective due to the immunogenicity of different CRC. For example, Consensus molecular subtype 1 and 4 CRC are ‘hot’ tumours where immune cells are highly infiltrated into the solid tumours, suggesting that the PD-1/PD-L1 or CTLA-4 treatment may be effective. Opposite to Consensus molecular subtype 1 and 4, Consensus molecular subtype 2 and 3 are less- to non-immunogenic tumours (a.k.a ‘cold’ tumours), resulting in limited response to immunotherapy [78]. Additionally, the tumour-mediated suppressive signals in the tumour microenvironment (TME), such as IL-14 and IL-10, that are associated with the activation of T cells are also responsible for the ineffectiveness of immunotherapy [77,79].

1.2 The role of the immune system in cancer

1.2.1 The interaction between cancer and the immune system

The interactions between the immune system and malignancy were first described by Burnet and Thomas in 1967. They suggested a hypothesis, termed as *immunological surveillance*, that the immune system does not only monitor and defend external microorganisms but also protects mammals from potential neoplasia [80].

Dunn *et al.* reviewed the key evidence that supports *immune surveillance* theory [81]. Firstly, it was shown that interferon (IFN)-α, an important cytokine for innate and adaptive immune immunity, protects the host from external malignancy. Secondly, it was observed that innate immunity can protect organisms from carcinogens-induced tumours. Moreover, *in vitro* results were consistent with clinical observations that in ovarian cancer patients with large amounts of infiltrated CD8+ T lymphocytes (CTLs) and natural killer cells (NKs) in the solid tumour, a better prognosis was found in comparison to patients who were deficient in infiltrated lymphocytes [82].

Interestingly, the role of the immune system in tumour progression is not always favourable. In some cases, it was reported to be controversial. It was shown that tumours formed in immunodeficient groups have higher immunogenicity than tumours that appear in immunocompetent groups [81,83]. Consequently, highly immunogenic tumours are more frequently detected and eliminated by the immune system. However, less immunogenic counterparts may be able to escape the scanning by the immune system [83].

Taken together, it was found that immunity not only eradicates potentially harmful cancer cells but also shapes the tumour growth pattern during cancer's progression.

Therefore, since the first decade of the 21st century, scientists have started to use the broader term "*immunoediting*" instead of "*immunological surveillance*" to describe the interaction between tumours and the immune system [25].

1.2.2 The immune system identifies cancer *via* tumour-associated antigens

Both innate and adaptive immunity monitor and regulate the progression of cancerous tumours. At the early stage of CRC, tumour-associated antigens (TAAs) can be detected by innate or adaptive immunity, which results in the elimination of cancer cells [84]. TAAs are proteins that are specifically overexpressed in the cancer cells compared to normal cells [85,86]. For example, mucin 1 is one of the first identified TAAs. It is a large glycoprotein that is secreted by epithelial cells and significantly glycosylated [87]. It was found that mucin 1 was highly expressed in the malignant epithelia in patients affected by CRC [88]. As a result, the overexpressed mucin 1 is presented to T cells by tumour cells themselves and by antigen-presenting cells (APCs) *via* cross-presenting, initiating the anti-tumour immune response. In addition, the peptide-major histocompatibility complex class I (MHC I) and MHC II produced on the surface of tumour cells can also be recognized by T helper cells, which induce anti-tumour immune responses as well [89].

Immunotherapy that targets the TAAs has been previously designed [90]. For example, tecemotide, a mimetic lipopeptide of TAAs, has been used as a tumour vaccine to provoke the immune response against Mucin 1 [91]. Moreover, it was shown that tumours with high expression of TAAs demonstrated an elevated immunogenicity, resulting in an effective response to immunotherapy [92].

1.2.3 The immune system identifies tumours *via* dendritic cells

1.2.3.1 Classification of dendritic cells

Dendritic cells (DCs) are a type of antigen-presenting cell widely distributed in the human body. Compared to tumour cells and other APCs, the DCs have the most powerful antigen-presenting capacity for presenting TAAs to other lymphocytes [93].

DCs are members of mononuclear phagocytes, which also include monocytes and macrophages [94]. It is difficult to define DCs based on single or multiple biomarkers since the extracellular protein expression could vary among different subtypes of DCs [95]. In general, DCs are described as cells with stellate morphology that present immune signals *via* MHC on their surface to other lymphocytes efficiently [94].

To the best of our knowledge, there is no clear agreement for the classification of DCs subtypes. Sato *et al.* suggested that DCs subtypes can be divided into Langerhans cells (or dermal DCs) and interstitial DCs based on their anatomical localisation [96]. Langerhans DCs can be found in the skin and mucous membranes, such as pulmonary mucous [97,98]. Interstitial DCs are resident DCs in most organs, such as liver and spleen [99].

Merad *et al.* classify DCs into plasmacytoid DCs and classic DCs (refers to all other subtypes except plasmacytoid DCs) [100]. Plasmacytoid DCs mainly accumulate in the blood and lymphoid tissue (such as the spleen and thymus) and can migrate to lymph nodes (LNs) after activation. They only express a few pattern-recognition receptors, such as toll-like receptors 7 and 9. Classic DCs occupy about 1-5 % of tissue cells, depending on the organs.

The role of each subtype of DCs in immune responses has not been fully understood. Generally, DCs in the mature stage can i) present antigens to lymphocytes; 2) induce an adaptive immune response by cross-presenting or producing proinflammatory cytokines, and 3) drive innate immune response *via* producing related chemokines, such as MCP-1, IL-8, and MDC [101,102].

1.2.3.2 Maturation of DCs

It was reported that the low infiltration of mature DCs in advanced colorectal cancer was frequently observed, indicating that the infiltration of mature DCs is associated with poor prognosis in CRC [93]. This suggests that the involvement of mature DCs is important for the immune system against CRC.

The capacity of DCs to present tumour antigens to other lymphocytes depends on their maturation stage. The pathogen recognition receptors (PRRs) on the surface of immature DCs can be activated by damaged associated molecule patterns or pathogen-associated molecular patterns, resulting in DC maturation [103].

Previously, Gulubova *et al.* found that the mature DCs, characterized as presenting the CD83 marker, were more frequently observed in lymph nodes (LNs) nearest to the tumour-invasive regions than in the tumour stroma [93]. This observation suggested that DCs could migrate to the draining LNs after activation, increasing DCs infiltration in LNs.

In general, nonlymphoid-resident DCs increase their motility during maturation through reorganisation of their structures and expression of high levels of chemokine receptor CCR7. Chemokines CCL19 and CCL21 are ligands of CCR7 and can be produced by macrophages, mature DCs and natural killer cells in the T-cell zone of LNs [104].

Additionally, CCL21 is also produced by endothelial cells in the lymphatic vessels [105]. Then, with the help of CCL19 and CCL21, mature DCs start to migrate to the nearest lymphoid vessels *via* the hapatotaxis effects. The hapatotaxis describes the cell movement directed by molecular concentration gradients inducing cell movement from the low-concentration regions to high-concentration regions. In this case, DCs move from a low concentration of CCL21/19 areas to a high concentration of CCL21/19 areas where the LNs are located. After entering the lymphoid tissue, it takes 24 to 72 hours for activated DCs to migrate towards the paracortex of LNs, where the T cell enriched area is, and interact with naïve lymphocytes [103].

Similar to nonlymphoid DCs, DCs located in lymphoid tissue, such as lymphatic sinus endothelium, also respond to the concentration gradient of CCL19 and CCL20, resulting in migration to T cell-rich regions. However, compared to their counterparts, those lymphoid-resident DCs induce T-cell responses much faster [106].

1.2.4 Dendritic cells-mediated anti-tumour immune response

The anti-cancer T cell response can be initiated by DCs through two mechanisms: 1) DCs detect TAAs and stimulate the cytotoxic T cell differentiation *via* cross-presenting, and 2) DCs polarise the T helper cell differentiation to orientate the anti-cancer immune response [107]. The helper T cells and the cytotoxic T cells are the two main subtypes of T lymphocytes, which are identified as presenting CD4 and CD8 markers on their surfaces, respectively [108].

Immature DCs are widely spread in the host's body and are able to capture TAAs. Then, the TAAs can be processed into immunogenic peptides on the MHC I complex. The immunogenic molecules on the MHC I can be presented to naïve CD8+ T cells (cytotoxic T cells), known as cross-presentation [93]. The activated cytotoxic T

lymphocytes can induce the target-cell death program, which initiates the formation of pores in the cell membrane of the targeted tumour cells. The killing program is achieved by CD8+ T cells secreting granzymes, cathepsin C, granulysin and perforin which are transported into tumour cells by endocytosis [109].

In addition, DCs can present the immunogenic peptides on the MHC II to T helper cells, resulting in Th 1 cells polarising to $CD4^+$ T cells. The $CD4^+$ T cells deliver proliferation and differentiation signals to cytotoxic $CD8^+$T cells and stimulate them through reciprocal activation of antigen-presenting cells (such as DCs), enhancing their migration (also known as infiltration) to lymph nodes and tumour sites [110]. The CD4+ helper T cells can be further divided into two subtypes: Th1 and Th2 T cells. The cytokines that are predominantly produced by those two types of cells are known as Th1-type cytokines and Th2-type cytokines [108]. In the tumour environment, the activation of cytotoxic T lymphocytes can be enhanced by Th 1 T cells *via* a) direct interaction with cytotoxic T cells through co-stimulatory molecules, such as CD27, CD134 and MHC II; b) indirect regulation through IL-12 which are released by Th 1 cells; and c) stimulation of APCs (such as DCs) which contributes to improving TAAs present to T cells [89].

In addition to presenting TAAs *via* MHC, cytokines and chemokines that are largely secreted by mature DCs can also stimulate the response of naïve lymphocytes. The interferon (IFN)-α produced by pDCs can induce the activation and proliferation of CD4+ T [111].

DCs activate naïve B cells by causing CD4+ T helper cell activation, which, in turn, stimulates lymphocyte B cell growth and antibody production [108]. Moreover, natural

killer cells (NKs) can be stimulated by interleukin-12 (IL-12) secreted by activated DCs [112].

1.2.5 Suppression of immune system by CRC

It was shown that a high inhibition of DCs in tumour environments could lead to a lower survival rate (over the period of 3 years) in patients affected by CRC in comparison to a low inhibition of DCs [113]. This suggests that the balance of the activation and inhibition of DCs impacts the immune system activity against cancer.

During cancer progression, tumour cells can build up a suitable TME where they can escape the detection and elimination by the immune system and suppress the immune response. The TME consists of cells surrounding the tumour, intercellular signalling molecules and abnormal physical environments (such as changes in oxygen level and pH value) [114].

It was shown that the maturation of DCs in TME can be suppressed by transforming growth factor (TGF)-ß, IL-10, IL-6 and prostaglandin E2, which are secreted by tumour cells [115]. TGF-ß is a potent inhibitory cytokine that regulates cell differentiation and proliferation, which allows its function as a tumour suppressor [116]. However, it is also derived from tumour cells, being responsible for the downregulation of DC maturation [117]. IL-10 is a human cytokines synthesis inhibitory factor, which is an anti-inflammatory cytokine. It is regulated by tumour cells in the TME, which has shown inhibitory effects on the maturation and the T cell stimulatory ability of DCs [118,119]. In cancer patients, the increased serum level of IL-10 was found to be associated with the deficiency and maturation of DCs. IL-6 is a cytokine which has been known to be associated with cell proliferation, differentiation and immune cell migration during the progression of cancer. *In vitro* studies showed that the inhibition of the STAT3 pathway

by IL-6 can result in limited the maturation of DCs [117,118]. PGE2 is a mediator for inflammation and vasoconstriction. An elevated level of PGE2 in the CRC has been shown to be related to the growth of tumour size, as well as the decreased differentiation of precursor to DCs [117].

In addition to the tumour-mediated inhibitory effects on the maturation of DCs, the infiltration of DCs in TME is also suppressed by tumour cells. For example, the high mobility groupbox-1 is a tumour-produced cytokine which can induce the apoptosis of DCs. It was reported that the concentration of mobility groupbox-1 in regional lymph nodes, which drain lymph from the colorectal regions was high in patients with positive-lymph nodal metastatic CRC, resulting in depletion of mature DCs in the tumour-draining LNs [120].

The TME can also inhibit the anti-tumour response by inducing T-cell programmed death. PD-L1 and PD-L2 are the binding ligands for programmed death 1 co-stimulatory receptors on the surface of cytotoxic T cells [56]. The PD-L1 and PD-L2 can be overexpressed on the surface of tumour cells, which can suppress the anti-tumour immune response by triggering the T-cell programmed death [109]. Moreover, the IFN-γ that is highly produced by tumour cells can also upregulate the production of PD-L1 and PD-L2 from macrophages and dendritic cells [121].

Taken together, immunity's anti-tumour effects can be depleted by cancer cells through decreasing the maturation and infiltration of DCs. Therefore, immunomodulators that can enhance the maturation of DCs can potentially overcome the tumour-mediated suppression in the TME, improving the immunotherapy outcomes in patients affected by CRC.

1.3 Toll-like receptor agonists: a promising target for cancer treatment

1.3.1 Toll-like receptors

Innate immunity and adaptive immunity are regulated by APCs, such as DCs, *via* the pattern recognition receptors [122]. Toll-like receptors (TLRs) are one type of the PRRs. There are 13 subtypes of TLRs reported, but only TLRs 1-10 are expressed in humans [123]. TLR 1, 2, 4, 5 and 6 are expressed on the cell membrane, while TLR 3, 7, 8, 9 and 10 are found in the endosomal membrane [124].

The roles of different subtypes of TLRs in various disease are complex and the mechanisms of all functions has not been clearly understood. It was shown that TLR 3, 7, 8 and 9 can recognise the nucleic acid from organisms, such as viruses and bacteria [124]. TLR 7, 8 or 9 are associated with anti-cancer and anti-tumour therapy since the activation of those receptors could induce a high production of INF- α, promoting anti-cancer and anti-viral action [125].

All toll-like receptors are activated through myeloid differentiation primary-response protein 88–dependent pathway, except TLR 3 [126]. There are two important compartments in TLRs: toll-interleukin-1 receptors and toll-interleukin-1 receptors domain leucine-rich repeats [123]. After binding to ligands (such as TAAs), the TLRs recruit the primary-response protein 88 for the activation of the nuclear factor kappa signalling pathway. The activation of the nuclear factor kappa signalling pathway can further promote the translocation of interferon regulatory factor 7, which increases the production of type I interferon, as well as facilitate the maturation of DCs [124,126].

1.3.2 Toll-like receptor 7

Toll-like receptor 7 (TLR 7) can be found in antigen-presenting cells, lymphocytes and cancer cells. The DCs express a high level of TLR 7, which enables DCs to recognise viral nucleic acids and endogenous mutant tumour antigens [106]. TLR 7 has two ligand binding sites. The first binding pocket is similar to the TLR 8, which can recognize both viral nucleotides and TAAs. The second binding pocket allows the binding of the ssRNA, which facilitates the activation of the first binding site [127].

The activation of TLR 7 on tumour-resident DCs stimulates the maturation of DCs and increases the production of proinflammatory cytokines (such as IFN-α, IL-12 and TNF-α) [124]. Consequently, the cross-presenting of DCs to naïve T cells is improved, resulting in the increase in T cell infiltration in the tumour sites. Therefore, the activation of TLR 7 can potentially convert the 'cold' tumour into a 'hot' tumour and facilitate the immune system to overcome the tumour-mediated immune suppression [78,128]. Moreover, it has been shown that the activation of the NF-κB transcription factor pathway stimulated by the activation of TLR 7 could amplify the cross-presenting between DCs and T cells, suggesting that the proinflammatory-cytokines environment in the TME is important for the effectiveness of the PD-1/PD-L1 treatment [129].

However, the function of TLR 7 could be controversial in cancer therapy. It was reported that a high systemic level of type I IFN (such as IFN-α) could upregulate the expression of PD-1 and indoleamine-pyrrole 2,3-dioxygenase (IDO), which are immunosuppressive factors, on the DCs themselves and cytotoxic T cells, diminishing the anti-tumour immune response [122]. Moreover, it was shown that the unspecific overactivity of TLR 7 on DCs and lymphocytes could build up a tumour resistance to immunotherapy, facilitating tumour growth, survival and metastasis in cancer patients

[130]. Therefore, systemic activation of TLR 7 in immune cells may not be beneficial for cancer treatment, suggesting that a specific activation of TLR 7 in the targeted regions is required.

1.3.3 Imiquimod: a powerful TLR 7 agonist

Imiquimod (IMQ) was the first small-molecule TLR agonist on the market [125]. It was approved for basal cell carcinoma and genital warts by the Food and Drug Administration (FDA) in 2012 [131]. Imiquimod has been well-studied and an increasing number of research works for imiquimod focus on its antitumour effects [125,126,128,132].

IMQ use as an anti-cancer agent was first investigated as it is a potent proinflammatory cytokines inducer [126]. It was reported that IFN-α treatment has been used for solid tumours as the IFN-α can regulate tumour apoptosis and reduce tumour cell proliferation. Additionally, high-dose of IFN-α injection demonstrated a potent antiangiogenic capacity, which results in slower tumour growth [61].

It has been reported that imiquimod is a potent IFN-α inducer in animal models and humans [133–135]. It was shown that the effect on the production of IFN-α with the oral administration of IMQ was dose-dependent [134,135]. A preclinical study showed that the increase in production of IFN-α in rats was observed when the dose was higher than 3 mg/kg [134]. Moreover, it was found that the production of proinflammatory cytokines was significantly higher in rats treated with IMQ in comparison to rats challenged with lipopolysaccharides (LPS). Interestingly, a hyporesponsive state of IFN-α to IMQ was found in the daily administration group (30 mg/kg, consecutively for five days). This result suggests that the interferon resistance mechanism may exist with the long-term administration of imiquimod [134].

It has been reported that the blockage of TNF-α resulted in a depletion of anti-tumour effects, which suggests the production of TNF-α is associated with anti-tumour immune response [61]. TMX-101 is a liquid formulation of IMQ, which has been investigated for the treatment of non-muscle invasive bladder cancer *via* intravesical administration in animal studies on rats and pigs [136,137]. The results showed that IMQ leads to higher production of TNF-α in comparison to other treatment agents.

A phase I clinical trial suggested that IMQ is a powerful interferon inducer in humans as well [133]. It was shown that the serum level of IFN-α increased to 100-2300 U/mL with a 300-500 mg imiquimod dose (p.o.) over 24 hours. The increase in the serum level of IFN-α was higher in comparison to direct injection of IFN-α or administration of another IFN-α inducer (in this study, polyICLC) at equivalent doses.

It was also shown that there was no severe haematological toxicity of IMQ found at the does range of 100-500 mg (p.o.), but several minor adverse side effects (such as fever and headache) were observed, which are probably related to the increase of levels of IFN-α in the systemic circulation [133]. Another phase I clinical trial, which recruited patients affected with asymptomatic human immunodeficiency virus, reported dose-limiting toxicity of IMQ in patients receiving >200 mg of the drug weekly [138]. Additionally, it was reported that the low-dose IMQ treatment (25mg per day) was found to have no adverse effects in humans [139]. However, no increase in IFN-α level was detected in this group. This limited production of IFN-α following oral administration of the drug may be a result of low oral bioavailability (F_{oral}) of imiquimod (< 47 %) in humans and limited exposure to targeted cell types, such as DCs [140].

Since 2002, the pharmacological effects of IMQ as a TLR 7 agonist in the immunotherapy of cancer have also been investigated. The current clinical

applications of IMQ is mainly based on its topical formulation. Improved therapeutic outcomes after using IMQ cream have been found in patients affected by cutaneous cancer or cutaneous metastasis (such as T-cell lymphoma), pre-neoplastic and malignant on the skin (such as squamous cell carcinoma and melanoma), and accessible epithelial cancer (such as vaginal and cervical cancers) [131]. By 2018, IMQ had been tested in combination with neoadjuvant, 5-fluorouracil based chemotherapy, and checkpoint inhibitors in the treatment of cancer, as well as tested as a preventive agent for tumour recurrence in the postoperative period [141]. Other investigations of IMQ as an adjuvant for virus or tumour vaccine have been reviewed in [142,143]. It should be noted that the use of IMQ *via* other administration routes, such as intravenous (IV) bolus or subcutaneous administration is limited due to its poor solubility, as well as its low F_{oral} (< 47%) [136,137,140].

1.3.4 Application of IMQ in CRC

To the best of our knowledge, clinical trials investigating the therapeutic effects of IMQ in patients with colorectal cancer (CRC) are limited. This may be due to the fact that the currently available formulation of IMQ is a topical cream, which is not suitable for targeting tumours in deep tissues.

However, the clinical use of IMQ has been reported in the treatment of anal epithelial neoplasia and anal squamous intraepithelial lesions, where topical administration is feasible. Dindo *et al.* reported that, until 2010, 80.4% of dermatologists and 28.2% of surgeons in the EU and Austria had prescribed IMQ as a non-invasive treatment for patients with human papillomavirus (HPV) or human immunodeficiency virus (HIV) who were diagnosed with anal intraepithelial neoplasia[144]. It has been shown that 77% of patients achieved complete clearance of anal intraepithelial neoplasia following

a 16-week treatment with 5% IMQ cream or IMQ suppositories. Although IMQ is not approved by the FDA for intra-anal administration in the United States, it has been used as an off-label prescription in HIV patients who were diagnosed with high-grade squamous intraepithelial lesions[145]. Studies have shown that 35% of patients with anal squamous intraepithelial lesions achieved complete healing following treatment with IMQ suppositories.

In a previous *in vitro* study, Caco-2 cells were incubated with IMQ for 3 days. A significant change in the expression of BCL-2 (a pro-apoptotic biomarker) was found following the IMQ treatment. Additionally, a significantly increased number of autophagic vesicles was observed in the treatment group in comparison to the control group [146]. Results suggested that IMQ have a direct anti-tumour activity on human-derived colon adenocarcinoma cell lines through the modulation of autophagy.

Additionally, the anti-tumour effects of IMQ have been evaluated in CRC mouse models. In a previous *in vivo* study, a CRC model was established by injecting mouse colorectal cancer cells into the flank of BALB/c mice. Once the tumour reached a size of $\geqslant$50 mm^3, IMQ was administered intraperitoneally at 2.5 mg/kg weekly for one month. The results demonstrated that IMQ significantly suppressed tumour growth, leading to an improvement in survival rate over a 60-day observation period [147]. Furthermore, synergistic effects of IMQ in combination with other therapies have been observed in CRC models. Rostamizadeh et al. reported that IMQ combined with HIF-1α inhibitors significantly enhanced pro-inflammatory cytokines (such as IFN-γ and IL-12) in the tumour microenvironment, resulting in a notable reduction in tumour growth in CRC-bearing mice [148]. In another study, Yang *et al.* developed an injectable hydrogel for intra-tumoral administration of doxorubicin, tumour-associated antigens,

and IMQ, enabling a sustained and localized release of chemotherapy and vaccine components at the tumour site. In this study, IMQ was used as an adjuvant to enhance the immune response in the CRC mouse model. The results showed that the addition of IMQ in hydrogel increased immune cell infiltration within tumours and promoted CD8+ T cell activation in the injected regions. This led to tumour suppression and prevention of metastasis to distant organs, such as the lungs [149].

1.4 Intestinal lymph nodes are important targets for toll-like receptor agonist

The lymphatic system in humans consists of a complex vessel network. Lymph contains many proteins, fluids and molecules derived from interstitial spaces due to the high permeability of lymphatic vessels related to their open-junction structures. Therefore, the formation and drainage of lymph can regulate tissue fluid homeostasis [150]. In addition to regulating fluid balance, the lymphatic system also serves as an important environment for immune response [150] and offers a transport pathway for immune cells and metastatic cancer cells [151]. During the progression of cancer, vascular endothelial growth factor C (a lymphangiogenic factor) is produced, activating the growth of lymphatic vessels [29]. As a result, lymphatic vessels with loose epithelial structures facilitate tumour metastasis [33,152]. In the metastasis of CRC, the tumour invasion pathway partially follows the mesenteric lymph nodes (MLNs) and retroperitoneal lymph nodes (such as iliac lymph nodes, ILNs), draining the lymph from the colorectal regions (**Figure 1-1**) [30,32,34,153]. It was reported that in the TME and lymph nodes (LNs), the maturation of DCs is suppressed, and the infiltration of mature DCs is reduced, resulting in the diminished ability of the immune system to recognise cancer cells [93,120].

Additionally, the LNs within the lymphatic system, containing a large population of macrophages, lymphocytes and dendritic cells, are the primary immunity response place [154]. It was shown that naïve T cells that are located in the paracortex zone of LNs are not attracted towards activated DCs through chemotactic gradient but rather interact with them by chance. Normally, mature/activated DCs can efficiently cross-present tumour antigens to T cells at the ratio of one DC to ten T cells [155]. However, in the tumour-draining lymph nodes, immature/inactivated DCs can be inhibited from activation by two pathways. They can respond to immune suppression cytokines released from cancer cells, such as TGF-ß, or by uptaking debris derived from apoptotic cancer cells, resulting in incomplete T-cell activation [156,157].

Therefore, targeted delivery of immune activators, such as IMQ, to the lymph nodes draining the colorectal region (MLNs and ILNs) could facilitate the activation of DCs and overcome the inhibitory immune responses that are regulated by cancer cells, potentially improving the treatment outcomes of people affected by CRC.

1.5 Targeted delivery of IMQ to the intestinal lymphatics following oral administration

In general, therapeutic molecules can be delivered to specific regions of the lymphatic system *via* different administration routes [158,159]. Peripheral lymphatics targeting can be achieved via subcutaneous or intradermal administrations that allow therapeutic agents to be transported into the lymphatic system involving peripheral local-drainage lymph nodes [158]. In addition, it was reported that monoclonal antibody checkpoint inhibitors can be directly delivered to tumour-draining LNs through intra-tumour injection [160]. However, compared to parental administrations, lymphatic targeting following oral administration benefits from exposure to the largest lymph

node system in the body (mesenteric and retroperitoneal lymphatic systems) and can maintain a systemic plasma concentration at multi-dosage regimens. The concept of delivering small molecules into the intestinal lymphatics in a targeted manner following an oral administration takes the benefit of the intestinal absorption of lipids, which is explained in the following sections.

1.5.1 Absorption of lipids *via* the intestinal lymphatics

The diagram of the lipids digestion and absorption is shown in **Figure 1-2**. The digestion of food-derived lipids (which mainly come in the form of triglycerides, TG) starts in the stomach. The initial crude emulsion is formed with partial hydrolysis of TG (10 – 30 %) by gastric acid lipase, producing free fatty acids and diglycerides *via* a preferentially cleaving on the sn-1 or sn-3 position of TG [161,162]. After stomach emptying, the digested products stimulate the secretion of bile salts and pancreatic lipase, which facilitates the hydrolysis of up to 70 % of TG [163]. The emulsion will further convert to a small-droplet emulsion with phospholipids and cholesterol surrounding its surface [164]. The diglycerides are effectively digested into sn-2 monoglycerides and fatty acids due to the emulsification with bile salts [162]. In the small intestine, hydrolysed products of lipids, together with bile salts and phospholipids, form amphiphilic micelles, which can cross the unstirred water layer to the border of enterocytes [165]. Then, these lipidic substances cross the apical membrane of the enterocytes by the mechanism of passive diffusion or by active transport via lipid-binding proteins [165,166]. In the enterocytes, fatty acids with short or medium carbon chains ($C<12$) can directly enter the systematic circulation *via* the portal vein [164]. In contrast, long-chain fatty acids ($C\geq12$) are transported to the endoplasmic reticulum of enterocytes and are esterified into fatty acyl-CoA by acyl-CoA synthetase [164,167].

Then, the fatty acyl-CoA are resynthesized into diglycerides with monoglycerides and subsequently TGs by monoacylglycerol acyltransferases and diacylglycerol acyltransferases, respectively [167]. The resynthesized TGs form pre-chylomicrons (pre-CMs) with integrating lipoprotein B48 in the endoplasmic reticulum and are transported to the Golgi apparatus by pre-chylomicron transport vesicles [168,169]. Mature chylomicrons (CMs) that are stored in the Golgi apparatus are secreted and eventually enter the lymphatic vessels [169].

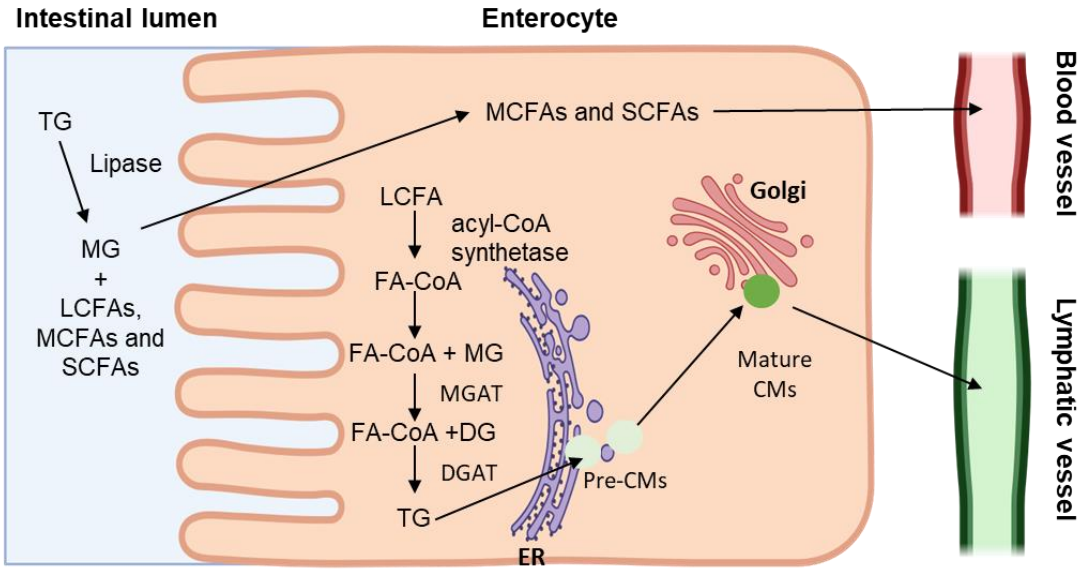

Figure 1-2 The digestion and transport of lipids. Triglycerides (TGs) are first digested into monoglycerides (MGs) and fatty acids in the intestinal lumen. In the enterocytes, the short- to medium-chain fatty acids (SCFAs and MCFAs) are directly absorbed into blood vessels. The long-chain fatty acids (LCFAs) are resynthesized into TG with MG and diglycerides (DGs) by monoacylglycerol acyltransferases (MGAT) and diacylglycerol acyltransferases (DGAT). The resynthesized TG form pro-chylomicrons (pre-CMs) on the endoplasmic reticulum (ER) and then are transported to the Golgi apparatus. The mature CMs are eventually secreted and absorbed into lymphatic vessels. (Created with BioRender.com

1.5.2 Lymphatic targeting *via* lipophilic prodrug approach

Following oral administration, molecules are usually transported into blood capillaries, as opposed to lymphatic lacteals, and then absorbed into the systemic circulation after potential first-pass metabolism in the liver. This is because the flow rate of the blood in the intestinal capillaries is approximately 500-fold and 750-fold faster than the flow

rate of the intestinal lymph in rodents and humans, respectively [170–172]. The CMs that are assembled in the enterocytes have a particle size covering the range from 75 to 1,500 nm [173,174]. Due to the tight zipper-like junctions of the vascular structure of intestinal capillaries, macro-size CMs cannot enter the blood vessels. The intestinal lymphatic vessels have a relatively loose button-like vascular structure, which allows the passage of CMs [175]. Therefore, drug molecules with a high affinity for CMs can be transported into the intestinal lymphatics using CMs as a carrier. Additionally, drugs that are absorbed into the intestinal lymphatic capillaries will flow with the lymph through the mesenteric duct, cisterna chyli and thoracic duct, and they will eventually enter the blood circulation via the left subclavian vein [176–178].

Cannabinoid (CBD) is a lipophilic molecule that demonstrated high affinity for CMs in *in vitro* and *ex vivo* assessments [179]. Following oral administration to rats, it was found that the concentration of CBD in the mesenteric lymph is 250-fold higher than its concentration in the plasma [180], indicating the feasibility of lymphatic targeting *via* the CMs pathway.

However, a high affinity to CMs is not always found in drug molecules, especially for hydrophilic compounds. It has been suggested that only molecules that meet certain physicochemical properties and have high solubility in triglycerides (> 50 mg/mL) are likely to associate with CMs in the enterocytes [181–184], being transported into the intestinal lymphatic following an oral administration.

Previously, chemical modification was applied to hydrophilic molecules to improve their affinity for CMs. Porter's group has developed a series of prodrug structures that mimic the chemical structure of TG or digested product of TG [185–189]. In these studies, the active parent molecules are attached to the sn-2 position of the TG

structure, which avoids the enzymatic hydrolysis by lipase in the intestinal lumen and enables the TG-mimetic prodrugs to assemble into pre-CMs along with natural TGs. Additionally, Porter's group suggested that the TG-mimetic chemical modifications are more effectively involved in the association with CMs in comparison to other lipidic structures, such as simple alkyl groups.

Our group has previously targeted bexarotene, retinoic acid, and lopinavir, which have limited affinities to CMs, into intestinal lymphatics using activated alkyl prodrug structures [190,191]. The *in vivo* studies showed that the concentrations of bexarotene and retinoic acid were 17-fold and 2.4-fold in MLNs, respectively, in comparison to orally administered unmodified drugs [190]. Additionally, the concentration of lopinavir in the MLNs was significantly improved and reached the protein binding-adjusted concentration required of 90% viral inhibition [191]. Interestingly, the TG-mimetic structure of bexarotene did not efficiently release the active molecules in the intestinal LNs, although a substantial amount of TG-mimetic prodrugs was transported into the intestinal lymphatics [190].

Previous studies by us and others suggested that simple alkyl prodrug structures were not able to efficiently release the parent drug in the mesenteric lymph and LNs, although the highly lipophilic prodrugs themselves were transported into the intestinal lymphatics via the CMs pathway [170,185,190,191]. However, previously Yenju et al. showed that a simple alkyl structure of dolutegravir significantly increased the concentration of dolutegravir in the mesenteric lymph and MLNs by 9.4- and 4.8-fold following an oral administration in comparison to the administration of unmodified parent drug [192].

1.6 Aim of this PhD project

DCs is an important APCs that cross-present the TAAs to other lymphocytes, such as naïve T cells, stimulating anti-tumour immune response. The maturation process of the DCs is the key to their antigen-presenting capacity. However, the activation/maturation of the DCs is downregulated by the tumour-mediated immunosuppressive signals in the patients affected by CRC, especially in the MLNs and iliac LNs. These LN drain lymph from the colorectal regions and are enriched in DCs. IMQ is the currently only approved TLR 7 agonist, which can facilitate the maturation of DCs. However, in the pre-clinical studies and clinical trials, limited therapeutic outcomes and dose-limiting toxicity were observed following the administration of IMQ, suggesting an unspecific distribution of IMQ. Therefore, in this project, we aimed to deliver IMQ in a targeted manner to intestinal LNs using a lipophilic prodrug approach to facilitate the maturation of DCs in these regions, potentially enhancing the anti-tumour immune response and eventually improving the therapeutic outcomes in patients affected by CRC.

The specific objectives of this work are described as follows:

Chapter 3

1. Developing a bioanalytical method for the determination of IMQ and its prodrugs in biological samples
2. Partial validation of developed bioanalytical methods

Chapter 4

1. *In silico* and *in vitro* assessment of the lymphatic transport potential of unmodified IMQ.

2. Developing safe formulations of IMQ for intravenous (IV) bolus and oral administration.
3. *In vivo* pharmacokinetic (PK) studies of IMQ following IV bolus and oral administration.
4. *In vivo* biodistribution (BD) studies of IMQ following an oral administration of IMQ using lipid-based formulation.

Chapter 5

1. Design of highly lipophilic prodrugs of IMQ based on the in silico predicted affinity of prodrugs to chylomicrons (CMs).
2. Chemical synthesis of designed prodrugs using a high yield amidation reaction and characterization of the synthesized molecules.
3. Assessing the potential of intestinal lymphatic transport of prodrugs using artificial CMs.
4. Developing and validating an ex vivo model for assessing the biotransformation of prodrugs to the parent drug using brush border enzyme vesicles (BBMVs).
5. Evaluation of the biotransformation of prodrugs to the parent drug in the intestinal lumen, enterocytes and lymphatics using *in vitro* and *ex vivo* assays.
6. *In vivo* PK studies of IMQ and prodrugs 5 and 8 following IV bolus and oral administration of prodrugs.
7. *In vivo* BD studies of IMQ and prodrugs 5 and 8 following IV bolus and oral administration of prodrugs.

Chapter 2 Materials and Methodology

2.1 Materials

Imiquimod (CAS: 99011-02-6) was purchased from Key Organics Ltd. (Cornwall, UK). Lauroyl chloride, fatty acids (decanoic acid, myristic acid, palmitic acid, stearic acid, myristoleic acid, palmitoleic acid, oleic acid and linoleic acid), propranolol, *d*-chloroform, Intralipid®, Dulbecco's phosphate buffered saline (DPBS), serum triglycerides kits, porcine hepatic esterase, ethylenediaminetetraacetic acid (EDTA), sodium, sesame oil, sodium chloride (NaCl), sodium hydroxide (NaOH) pellet, sodium fluoride (NaF), Bradford reagents and bovine albumin standard (1 mg/mL) were all purchased from Merck Life Science (Gillingham, UK). Calcium chloride ($CaCl_2$) was purchased from Alfa Aesar (Lancashire, UK). The alkaline phosphatase assay kit and leucine aminopeptidase activity assay kit were purchased from Abcam (Cambridge, UK). Rat plasma (pooled male Sprague Dawley rat plasma) was purchased from BIOIVT (Burgess Hill, UK). Propylene glycol (European Pharmacopoeia grade), Polyethylene glycol 200 (PEG200), Polyethylene glycol 400 (PEG400), Dimethylsulfoxide (DMSO), L-alpha-phosphatidylcholine from egg yolk, ammonium formate (LC-MS grade), methyl tertiary-*butyl* ether, and Costar Spin-X centrifuge tube filters were purchased from Fisher Scientific (Leicestershire, UK). Other agents and solvents were purchased from commercially available sources and were HPLC or LC-MS grade.

2.2 *In silico* prediction of association of drugs with chylomicrons

The lymphatic transport of IMQ and its prodrugs via the chylomicrons (CM) pathway following oral administration were initially evaluated using a previously reported *in silico* model [182].

This model was developed based on the experimental CM association of 6 tested drug molecules (probucol, vitamin E, benzopyrene, vitamin D, halofantrine and DDT) and their physiochemical properties. The correlation between the experimental CM association and the physicochemical properties of tested compounds was assessed using a partial least squares model.

The physicochemical properties, including LogP, $LogD_{7.4}$, polar surface area (PSA), number of H-bond donors (H-donors) and H-bond acceptors (H-acceptors), number of free rotated bonds (FRB), density and molar volume of tested molecules were calculated using ACD-I/LAB (Advanced Chemistry Development Inc., Toronto, ON, Canada).

The *in silico* predicted CM association of a drug molecule is calculated using the following equation,

$$In\ silico\ predicted\ CM\ Association\ (\%) = 100\ \times \frac{10^{Y}}{(1+10^{Y})}$$

The Y is a numeric sum of calculated physicochemical properties. Each physicochemical property is multiplexed by its corresponding unscaled regression coefficient constant. The equation for the calculation of Y is shown as below,

$$Y = (Log\ D7.4\ \times\ 0.299879) + ((LogP\ -\ LogD7.4) \times -0.238127)$$
$$+ (PSA \times -0.00855215) + (H - acceptors \times\ -0.184359)$$
$$+ (FRB \times 0.0805226) + (Density \times\ 1.45337)$$
$$+ (Molar\ volume \times 0.00545912) + (H - donors \times 0.0823094) + K$$

K is a calculated constant (generated by the partial least squares model) equal to -5.24138.

The *in silico* predicted affinities of IMQ and its prodrugs were summarized in **Table 4-1** (**Chapter 4**) and **Table 5-1** (**Chapter 5**).

2.3 Chemical synthesis of IMQ prodrugs

The potential affinities of designed lipophilic prodrugs to CMs were first calculated as described in **Section 2.2**. Then, the designed prodrugs were synthesised as described in this section. The amidation of IMQ was achieved using three different reactions. The reaction which provided the highest yield was applied to compile the synthesis of all prodrugs.

2.3.1 Synthesis of IMQ prodrugs using acyl halides

A lipophilic prodrug of IMQ was synthesised with lauroyl chloride. This reaction followed a previously reported protocol with minor modifications [192]. Briefly, 0.4 mmol of lauroyl chloride and 0.1 mmol of IMQ were mixed in anhydrous dimethylformamide (DMF) under nitrogen at 0 ℃ for 24 hours (**Figure 2-1**).

The reaction was monitored by thin-layer chromatography (TLC) and LC-UV-MS. Products were purified by flash chromatography using a 4 g silica gel-packed column

with MeOH and dichloromethane (DCM) (50:50, v/v) as the mobile phase.

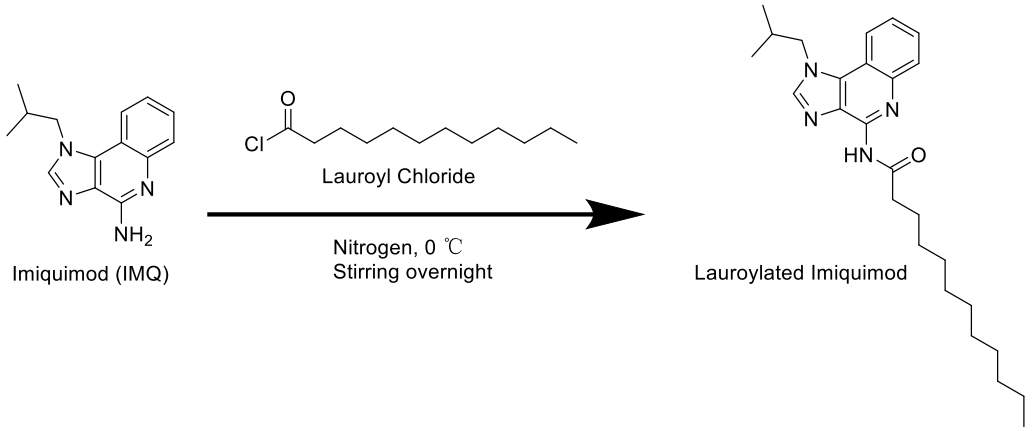

Figure 2-1 The chemical synthesis of lauroylated imiquimod.

The yield of the reaction was calculated using the following equation,

$$Yield\ (\%) = \frac{Actual\ yield\ of\ product\ (mg)}{Theoretic\ yield\ of\ prodrug\ (mg)} \times 100$$

2.3.2 Synthesis with coupling reaction

2.3.2.1 Amidation of IMQ using NHS-DCC

Based on a previously reported methodology, IMQ decanoic acid prodrug was synthesised using the amide coupling reagent combination of *N*-hydroxysuccinimide (NHS) and *N, N'*-dicyclohexylcarbodiimide (DCC) [193]. Briefly, the carboxylic acid was activated by mixing 0.1 mmol of decanoic acid, 0.2 mmol of DCC and 0.2 mmol of NHS in anhydrous DMF under N_2 at room temperature for 24 hours. After the transient NHS ester was formed, 0.1 mmol of IMQ was added. The reaction was monitored by TLC and LC-UV-MS. The schematic presentation of the chemical synthesis of the decanoic IMQ prodrug structure is shown in **Figure 2-2**. The yield of the reaction was calculated using the equation described in **Section 2.3.1**.

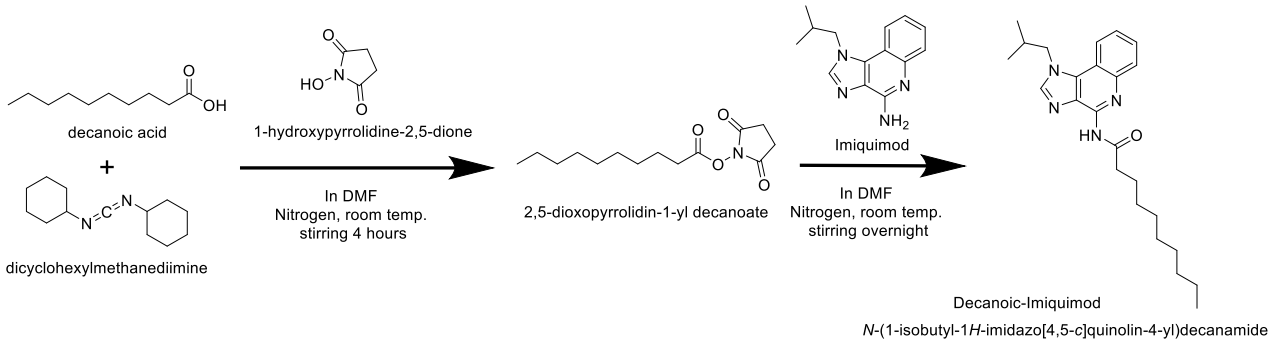

Figure 2-2 Chemical synthesis of decanoic imiquimod using NHS-DCC coupling.

2.3.2.2 Amidation of IMQ using TCFH-NMI

The amidation of imiquimod was achieved with *N, N, N′, N′*-tetramethylchloroformamidinium hexafluorophosphate (TCFH) and *N*-methylimidazole (NMI) as previously reported [194]. The corresponding fatty acids (0.3 mmol) were activated with TCFH (0.35 mmol) and NMI (1.05 mmol) in 2 mL anhydrous *N*-methyl-2-pyrrolidone (NMP) and stirred under nitrogen at 45 ℃ for 30 mins. Then, imiquimod (0.39 mmol) was added and the mixture was stirred for 24 hours. The reaction process was monitored by thin-layer chromatography (TLC) and LC-UV-MS. The crude reaction product was purified by flash chromatography using a 12 g silica gel-packed column and hexane-ethyl acetate (50:50, v/v) as the mobile phase. The schematic presentation of chemical synthesis and all IMQ prodrug structures are shown in **Figure 2-3**. The yield of the reaction was calculated using the equation described in **Section 2.3.1**.

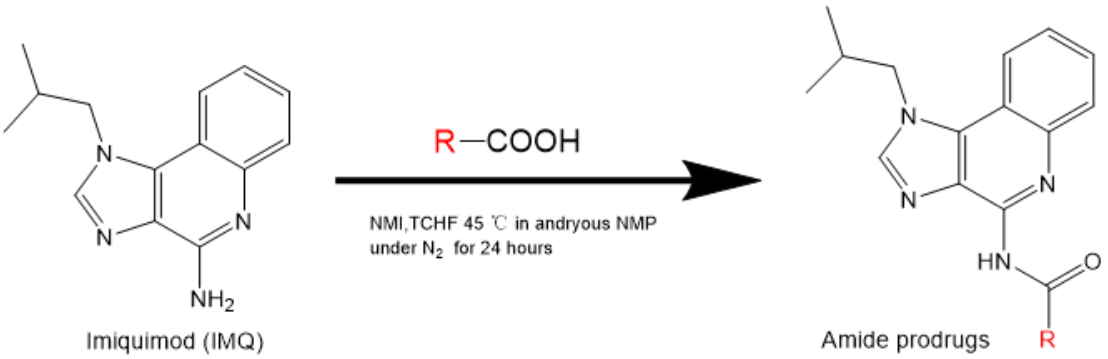

Saturated fatty acid	Unsaturated fatty acid
1:R=$CH_3(CH_2)_8$	5:R=$CH_3(CH_2)_3CH{=}CH(CH_2)_7$
2:R=$CH_3(CH_2)_{12}$	6:R=$CH_3(CH_2)_5CH{=}CH(CH_2)_7$
3:R=$CH_3(CH_2)_{14}$	7:R=$CH_3(CH_2)_7CH{=}CH(CH_2)_7$
4:R=$CH_3(CH_2)_{16}$	8:R=$CH_3(CH_2)_4CH{=}CHCH_2CH{=}CH(CH_2)_7$

Figure 2-3 Chemical synthesis of IMQ lipophilic prodrugs using TCFH-NMI.

2.3.3 Characterisation of synthesised prodrugs

Purified prodrugs were dissolved in chloroform-*d* for NMR examination. ^{1}H NMR and ^{13}C NMR spectra of the synthesised prodrugs were obtained using a Bruker 400 Ultrashield Spectrometer at 400 and 100 MHz, respectively. NMR spectra were analysed using MestReNova (Version 14.2.2, Mestrelab). Chemical shifts (δ) are reported as parts per million (ppm) relative to chloroform-d (^{1}H, δ = 7.24 ppm; ^{13}C, δ = 77.16 ppm). High-resolution mass spectrometry was also conducted to characterise the prodrugs using a Bruker MicroTOF.

II with electrospray (ESI). Characterisations of all synthesised prodrugs are shown in **Appendix**.

2.4 *In vitro* assessment of lymphatic transport potential of imiquimod and prodrugs following oral administration

The affinities of IMQ and prodrugs to CM were assessed with artificial CMs. The preparation of artificial CMs is described in **section 2.4.1**. Tested compounds were incubated with artificial CMs, as described in **section 2.4.2**.

The percentages of compounds associated with CM were determined using the following equation:

$$Chylomicrions\ association\ (\%) = \frac{(Amount\ of\ compound\ in\ CMs\ \div 0.9)}{Amount\ of\ compound\ in\ method\ recovery} \times 100$$

2.4.1 Preparation of artificial emulsion from Intralipid®

A CM-like emulsion was prepared by diluting 20% intralipid® ((Merck Life Science, Gillingham, UK)) with Dulbecco's phosphate buffered saline (DPBS) to yield an emulsion with the triglyceride concentration at 100 mg/dL. The triglyceride concentration in the emulsions was measured using a serum triglyceride determination kit as per the manufacturer's instructions (Cat.RT100, Sigma Aldrich, Dorset, UK). Briefly, the triglycerides in the intralipid® were hydrolysed by the lipase (provided within the kit) to glycerols and free fatty acids. The released glycerols were further reacted with adenosine-*5'*-triphosphate (provided within the kit), forming glycerol-1-phosphate, adenosine-*5'*- diphosphate and hydrogen peroxide. The hydrogen peroxide that was formed during the reaction was then reacted with substrates (provided within the kits), producing a quinoneimine dye that has an absorbance at 540 nm. The amount of triglycerides in the intralipid® was determined using a

calibration curve that was generated with the triglyceride standard solution (provided within the kits).

2.4.2 Association with CMs assay procedure

The assessment of CM affinity for IMQ and its prodrugs followed previously reported methodology with minor modifications [182,190,191,195,196]. The stock solutions of tested compounds were prepared in DMSO at 1 mM. The density solutions were made by adding the appropriate amount of KBr into DPBS to reach the density at 1.006, 1.019 and 1.063 mg/mL.

Experimental CMs association and mass recovery samples were established by adding 2 µL of stock solutions into 998 µL of CM-like emulsion to reach the final concentration of prodrug at 2 µM. A control sample was made by spiking 2 µL of stock solutions into 998 µL of DPBS. All samples were incubated in a 37 ℃ water bath for 1 hour with magnetic stirring at 170 rpm. After the incubation, mass recovery groups were stored at 15 ℃ until processed for HPLC-UV analysis. On the other hand, 900 µL of incubation mixture from CM association groups and control groups and quality control were transferred into polyallomer ultracentrifuge tubes and mixed with the appropriate amount of KBr to reach the density of 1.1 g/mL. The density gradient was built up by gently layering density solutions in the following order: 4 mL of 1.063 mg/mL, 4 mL of 1.019 mg/mL and 2 mL of 1.006 mg/mL. Following the completion of the density gradient, tubes were transferred into an ultracentrifuge (SORVALL® equipped with TH-641 rotor, Thermo Fisher Scientific, UK) for ultracentrifugation at 268,350 *g* at 15°C for 35 mins. The white artificial CMs floating on the top in the testing group were collected. In the quality control groups, 1 mL of the top layer was collected. All samples

collected from CM association, mass recovery and control groups were processed for HPLC analysis described in **section 2.8.3.** All experiments were performed in triplicates.

2.5 In vitro and *ex vivo* assessment of biotransformation of prodrugs to IMQ

The rate of biotransformation of prodrugs to IMQ was described as the stability (half-life, $t_{1/2}$) of the prodrug in biorelevant media. In general, concentration-time profiles of prodrugs were obtained by incubating prodrugs with biorelevant media (FaSSIF+esterase and BBMVs media) and rat plasma. The preparations of FaSSIF supplemented with esterase and the BBMVs media are described in **section 2.5.2** and **section 2.5.3**, respectively.

The logarithmic scale was used to calculate the slope. The half-life of a prodrug in incubational biorelevant media was calculated as:

$$Half - life = \frac{-0.693}{k}$$

Results generated in this section are shown in **Chapter 5**.

2.5.1 Collection of brush border membrane vesicles from rat small intestine

The extraction of brush border membrane vesicles (BBMVs) from rats' small intestines was performed as previously described with some adjustments[197]. Fresh jejunum and ileum were harvested from SD male rats (weight 270 – 350 g) and were flushed with ice-cold saline to remove the intestinal contents. Harvested small intestines were stored at -80℃ until used.

On the day of the experiments, 20 g of the rat's small intestine samples were cut into small pieces (about 1 g) after being thawed to room temperature. Processed tissues were immersed in 12 mM Tris/Chloride buffer (pH = 7.1), which contained 300 mM mannitol in a 250 mL baker. After vortexing for 5 mins, connective tissues were discarded using a 1 mm Buchner funnel. The suspension was diluted with ice-cold water at a 1:6 ratio and then homogenised (POLYTRON® PT 10-35 GT, Kinematica AG, Luzern, Switzerland) at $20{,}000\ rpm$ for 3 mins in an ice bath. Calcium chloride powder was added into the ice-cold suspension and well-mixed to reach a final concentration of 10 mM. The suspension was kept on the ice bath for 15 mins to allow cell components to interact fully with calcium ions. The suspension was then spun down at $3{,}000 \times g$ at 4 ℃ and the precipitates were discarded. At this stage, the BBMVs were distributed in the supernatant. The supernatant was continuously centrifuged at $27{,}000g$ at 4 ℃ for 30 mins to collect crude BBMVs pellets. Collected pellets were purified by resuspending into 40 mL of 10 mM Tris/chloride buffer (pH = 7.1) plus 50 mM of mannitol and centrifuged at $27{,}000g$ at 4 ℃ for 30 mins. The purified white BBMVs pellets were collected and resuspended in a small volume (less than 1 mL) of 50 mM sodium maleate buffer (pH = 6.8) and stored at -20 ℃ until used [198]. Extraction procedures were repeated several times until sufficient quantities of BBMV pellets were obtained to perform the experiments described in **sections 2.5.4**.

Alkaline phosphatase (ALP) and leucine aminopeptidase (LAP) were selected as representative control enzymes in BBMVs, and their activities were measured with commercial kits (Abcam, Cambridge, UK) to monitor the enzymatic activity of BBMVs.

Briefly, these two commercial kits measured the activity of ALP or LAP using a colourimetric assay. Purified BBMVs pellets were diluted 10,000 times with assay buffers (provided within the kits). Diluted pellets were then incubated with *p*NPP

(substrate for ALP, provided with the kits) or AMC (substrate for LAP, provided with the kits) in a 96-well plate for 45 – 60 min at 37 ℃. The fluorescence of examined samples was monitored at 368/460 nm (for LAP assay) or 405 nm (for ALP assay). The amount of fluorescent products was determined using standard solutions (provided within the kits). The final activity of the enzymes was calculated as:

$$Enzyme\ activity\ (\mu mol/min/mL\ or\ U/mL) = (\frac{B}{T \times V}) \times D$$

Where B is the amount of fluorescent products in the sample well calculated from the standard curve (μmol); T is the reaction time (min); V is the volume of sample added into the reaction well (mL); D is the sample dilution factor. All measurements were performed in triplicates.

The purification of BBMVs was confirmed by the enzymatic activities of alkaline phosphatase and leucine aminopeptidase, which increased by at least 30-fold compared to the homogenised suspension.

2.5.2 Development and validation of brush border membrane vesicles *ex vivo* model

In the initial experiment where the total protein concentration of BBMVs in this model was investigated, bovine albumins were used as surrogate proteins for BBMVs. The concentrations of bovine albumin solutions were determined using Bradford reagents (ThermoFisher SCIENTIFIC, UK) with bovine albumin as standard. Albumin solutions at concentrations of 0, 0.1, 0.5 and 1 mg/mL (in 25 mM HEPES/Tris buffer, pH = 7), were pre-heated to 37 ℃. The incubation was started by spiking prodrug 1 (IMQ conjugated with decanoic acid) into albumin solutions at a concentration of 10 μM and

shaking at 200 rpm on a thermo-controlled incubator (ThermoFisher SCIENTIFIC, MaxQ4000, MA, USA) for two hours. One hundred and twenty microliters of the incubated mixture were collected at pre-determined time points and immediately added into 360 µL of -20 ℃ acetonitrile to terminate the reaction. After the addition of 10 µL of 50,000 ng/mL of propranolol as internal standard (IS), the concentration of prodrug 1 in the mixture was assessed using HPLC-UV bioanalytical method as described in **Section 2.8.3** Preparation of HPLC-UV samples

In the experiments in which the enzymatic kinetic parameters were determined for 1 mg/mL BBMVs proteins, procedures were performed using a similar protocol as previously reported [199]. Prodrug 1 was spiked into 25 mM HEPES/Tris buffer (pH = 7), which contained 1 mg/mL (total protein level) of BBMVs, to reach the final concentrations of 0.5, 1, 2, 4, 6 and 8 µM. At pre-determined time points, 120 µL of the incubated mixture was sampled as described earlier. After the addition of the same amount of IS, the mixture was processed for HPLC analysis. The peak area ratio between the peak area of prodrug 1 and the peak area of IS was used for the determination of the concentrations of prodrug 1 in the samples.

The concentrations of prodrug 1 in samples collected at different time points and sampling times were plotted on an X-Y graph to determine the slope. Subsequently, these slopes, obtained from incubating various substrate (prodrug 1) concentrations with BBMVs and their corresponding substrate concentrations, were assessed using GraphPad Prism (version 10, GraphPad Software, Inc., San Diego, CA, USA). The maximum rate of reaction (V_{max}) is visually predicted using the GraphPad Prism Kinetics model. The correlation between V_{max} and Michaelis constant (K_m) is shown below,

$$Y = \frac{Vmax \times X}{(Km + X)}$$

Where Y is the enzyme velocity (μM/min) at a known concentration of substrate; X is the concentration of substrate (μM); V_{max} is the maximum enzyme velocity (μM) predicted using GraphPad Prism; K_m is Michaelis-Menten constant (μM/min). Therefore, when Y = 1/2 V_{max}, the K_m is equal to the X.

All experiments were performed in triplicates. Samples generated in this section were processed as described in **section 2.8.2** and analysed using HPLC-UV. Results are shown in **section 5.3.5.**

2.5.3 Incubation media to simulate fasted state intestinal fluid

The fasted state simulated intestinal fluid (FaSSIF) was prepared using a previously reported protocol [200]. The ingredients in the FaSSIF can be found in Table 2-1. After the dissolution of all ingredients in water, the FaSSIF solution was stored in a refrigerator at 4°C, with a maximum storage duration of one month. On the day of the experiments, porcine hepatic esterase was added to the FaSSIF media to reach a concentration of esterase at 20 IU/mL.

Table 2- 1 The recipe of fasted state simulated intestinal fluid (FaSSIF) [200].

Materials	Concentration
Sodium taurocholate	3 mM
Lecithin	0.75 mM
NaOH (pellets)	0.174 g
$NaH_2PO_4.H_2O$	1.977 g
NaCl	3.093 g
Water (HPLC grade)	500 mL
Media has a pH of 6.50 and an osmolality of about 270 mOsmol/kg.	

2.5.4 Biotransformation of prodrugs in biorelevant media

The rate of biotransformation of prodrugs to IMQ was assessed as the stability of prodrugs in varying biorelevant media which mimic the gastrointestinal environment in rats. **Figure 2-4** demonstrates the general workflow of *in vitro* and *ex vivo* assessment of prodrug stabilities. Experiments performed in this section followed the previously reported protocols with minor modifications [190–192].

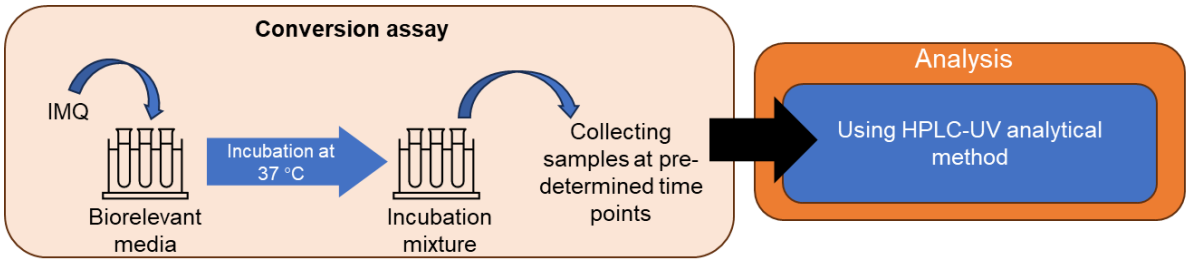

Figure 2-4 Schematic diagram of biotransformation assay for prodrugs.

Incubation media used in assessments, including BBMVs, FaSSIF (supplemented with 20 IU/mL of esterase) and rat plasma, were freshly prepared before experiments. FaSSIF supplemented with esterase was prepared as described in **section 2.5.3**. The BBMVs pellets were extracted as described in **section 2.5.1** and suspended into 25 mM HEPES/Tris buffer (pH = 7) to reach the total protein concentration at 1 mg/mL. It is important to note that all prodrugs were tested with the same bench of BBMVs pellets. This approach aimed to minimise the potential impact of varied enzymatic activities of BBMVs among different batches.

Stock solutions of prodrugs were prepared by dissolving appropriate amounts of prodrugs in DMSO at concentrations of 1,000, 500 and 200 µM. Incubations were initiated by spiking 10 µL of prodrugs stock solution into 990 µL of media, which were

pre-heated to 37°C. Then, the mixture was incubated at 37°C, stirring at 200 rpm on a temperature-controlled orbital shaker. One hundred and twenty microliters of the mixture were collected into a fresh testing tube, and 360 µL of acetonitrile (-20 ℃) were immediately added to terminate the enzymatic hydrolysis of prodrugs. Initial concentrations of prodrugs added into biorelevant media and sampling times are shown in **Table 2-2**.

Table 2-2 The initial concentration of prodrugs added into the incubation media and sampling times.

Biorelevant matrix	Initial concentration of prodrug (µM)	Sampling times (min)
Rat plasma[a]	5	0, 5, 10, 15, 30, 60 and 120
BBMVs[b]	2	0, 60, 120, 180, 240, 300 and 360
FaSSIF + esterase[c]	10	0, 2, 4, 6, 10, 15 and 20[d] or 0, 5, 10, 15, 30, 60 and 120[e]

[a] Pooled male Sprague-Dawley rat plasma;
[b] 1 mg/mL BBMVs pellets suspended into 25 mM HEPES/Tris buffer (pH = 7);
[c] FaSSIF supplemented with 20 IU/mL of porcine hepatic esterase
[d] Sampling time for prodrug 1 in FaSSIF + esterase media
[e] Sampling time for prodrug 2-8 in FaSSIF + esterase media

Collected samples were processed for HPLC analysis as described in **section 2.8.3** and analysed by the HPLC-UV method. Calibration curves were also generated using the same batch of stock solutions in relevant matrix. All experiments were performed in triplicates.

2.6 Triglyceride solubility measurements

As previously reported, the solubilities of tested compounds in long-chain triglycerides were assessed using olive oil [192,195]. Six mg of the tested compound was added to 100 µL of olive oil at 37℃ and stirred for 72 hours. After incubation, the remaining drug

particles were removed using Costar Spin-X Centrifuge tubes with a 0.22 μm filter via centrifugation at 2,400 *g* for 10 min at 37 ◦C. The filtrates were 10-fold diluted with acetone, followed by 100-fold dilution with ethanol. Several diluted samples undergo another 10-fold dilution with MeOH, depending on the concentration of tested compounds in triglycerides. Concentrations of compounds were determined by means of HPLC-UV. All experiments were performed in triplicates.

2.7 Animal experiments

2.7.1 Preparation of formulations

2.7.1.1 Development of formulations for imiquimod oral and intravenous administrations

The oral administration (PO) dose of IMQ used in this work was 8 mg/kg, which was translated by allometric scaling from a previously reported clinical trial [140]. In this work, we aimed to generate a safe formulation of IMQ at 8 mg/mL and minimise the volume of liquid administered to animals via oral gavage.

Eight milligrams of IMQ powders were added into selected 1 mL of formulation vehicles, including water, normal saline, ethanol/water (20:80, v/v), propylene glycol (PG), polyethylene glycol 200 (PEG 200) and HCl at different concentrations (0.1 N, 0.05 N and 0.025 N). The mixture was stirred in a water bath at 37 ℃ for 24 hours, with regular monitoring to assess the dissolution of the IMQ powder. The complete dissolution of drug powder in the tested formulation vehicles was first visually assessed by the absence of drug particles in the solution. Subsequently, 500 μL of the transparent solution was transferred into a Spin-X Costar centrifuge tube (Fisher Scientific, Loughborough, UK) and centrifuged at 2,400 g at 37°C for 20 minutes. The filtrate was collected and subjected to a two-step dilution: first, a 100-fold dilution with

acetone, followed by another 100-fold dilution with MeOH. The final concentration of IMQ in the diluted solution was determined using the HPLC-UV method, as described in **section 2.8.3**. The solubility of IMQ in the tested vehicles was calculated based on the measured IMQ concentration multiplied by the dilution factor. Results generated in this section are presented in **section 4.3.2**. Formulation vehicles that provided IMQ solubility at 8 mg/mL and could be safely administered to animals *via* oral gavage were selected and used for pharmacokinetic and biodistribution study of IMQ.

2.7.1.2 Formulation of IMQ and prodrug 5 and 8

The doses of IMQ via intravenous (IV) bolus administration and oral administration (PO) were 0.8 mg/kg and 8 mg/kg, respectively. The dose safety was confirmed by previous literature [140,201].

The oral lipid-free formulation of IMQ was prepared by dissolving IMQ powder in 0.05 N HCl (pH = 2.8 to 3.2) at 8 mg/mL. The IV formulation of IMQ was obtained by a 10-fold dilution from the oral lipid-free formulation with 80:20 propylene glycol/water (v/v) at 0.8 mg/mL. The pH of the IMQ IV formulation was adjusted to 6.5 -7 with 4 N NaOH.

Prodrugs 5 and 8 were administered to the animals at a molar equivalent dose of IMQ. The oral formulations of prodrugs 5 and 8 were prepared by dissolving prodrugs in olive oil at 14.9 mg/mL and 16.9 mg/mL for the doses at 14.9 mg/kg and 16.9 mg/kg, respectively. The IV bolus formulations of prodrugs 5 and 8 were prepared by dissolving prodrugs in vehicles (80:10:10 propylene glycol/water/ethanol, v/v) at 1.49 mg/mL and 1.69 mg/mL for the doses at 1.49 mg/kg and 1.69 mg/kg, respectively.

2.7.2 Animals

The protocols for pharmacokinetic and biodistribution study for IMQ and its prodrugs were reviewed and approved by the University of Nottingham Ethical Committee under the Animals [Scientific Procedures] Act 1986. Male Sprague Dawley rats weighing 275–300 g were purchased from Charles River Laboratories (UK) and housed in the Bio Support Unit at the University of Nottingham in an environmentally controlled room (12 h light/dark cycle) with free access to food and water for at least seven days. The weight of rats before the pharmacokinetics (PK) or biodistribution (BD) study was 300-350 g.

2.7.3 Pharmacokinetic study

The right jugular vein cannulation surgery was performed on each rat under general anaesthesia (3 % isoflurane in oxygen) following previously reported protocol [190–192,195,196,202,203]. After the surgery, animals were allowed to recover for two nights with free access to food and water. Animals were fasted for 10 hours prior to the drug administration with free access to water. Food was given to animals 5-6 hours after the drug administration.

2.7.3.1 Pharmacokinetic study of IMQ

In the IMQ pharmacokinetic (PK) study, rats were divided into IV bolus, oral lipid-free and oral lipid-based groups.

For the IV groups, the IMQ IV formulation was administered via the jugular vein cannula as the IV bolus for over 30 seconds. Following IV administration, 0.25 mL of heparinised saline (100 IU/mL) was administered through the cannula to remove any residual IV formulation in the cannula. At pre-determined time points 5, 15, 30, 60, 90,

120, 180, 240, 300 and 360 mins, 0.25 mL of whole blood was sampled from the cannula.

For the oral lipid-free groups, the IMQ lipid-free formulation was administered to rats by oral gavage and followed by an administration of 1 mL of water. In the preliminary lipid-free PK study, whole blood (0.25 mL) was sampled at pre-determined time points 0.25, 0.5, 1, 2, 4, 8, 12, 16, 24, and 36 h. In the full-scale study, whole blood was sampled at 0.5, 1, 2, 4, 8, 12, 16, 20, 24 and 28 hours.

For the oral lipid-based groups, the IMQ lipid-free formulation was administered to rats by oral gavage, followed by the same volume of olive oil as the lipid-free formulation. After the formulation administration, 1 mL of water was administered via oral gavage to facilitate the emulsification of the administered oil. Following the administration, blood samples were collected at pre-determined time points: 0.5, 1, 2, 4, 8, 12, 16, 20, 24 and 28 h.

2.7.3.2 Pharmacokinetic study of prodrug 5 and 8

In the PK study of prodrug 5 and 8, rats were divided into IV and oral lipid-based groups. For the IV groups of prodrugs, IV formulations were administered to animals following the same procedures described in **section 2.7.3.1**. For the oral lipid-based groups, prodrugs prepared in olive oil were administered to animals by an oral gavage, followed by 1 mL of water. Blood was sampled at 0.5, 1, 2, 4, 8, 12, 16, 20, 24 and 28 hours.

2.7.3.3 Pharmacokinetic parameters analysis

Pharmacokinetic parameters were calculated from the plasma concentration profiles by a non-compartmental analysis approach and compartmental models using Phoenix® WinNonlin® 6.3 software (Pharsight, Mountain View, CA, USA). The method of calculation *Linear up Log down* was applied to compute the area under the curve (AUC). This method used the linear trapezoidal rule to compute the AUCs when the concentration of the drug was increasing, while it used the logarithmic trapezoidal rule to compute the AUCs when the concentration of the drug was decreasing.

Additionally, pharmacokinetic parameters were calculated from the plasma concentration-time profiles using a compartmental model. The plasma concentration-time profile of IMQ following IV bolus administration exhibited a biphasic decline (**Section 4.3.3, Figure 4-2**), indicating that a two-compartment model could provide the best fit for describing the pharmacokinetics of IMQ. To account for heteroscedasticity and minimise the influence of high concentrations, the plasma concentration of IMQ was weighted using $\mathrm{w} = \frac{1}{(\mathrm{Yhat} * \mathrm{Yhat})}$ in the two-compartment model. As a result, the selected model yielded an Akaike Information Criterion (AIC) of -15.4 ± 8.6 and a sequential Bayesian criterion (SBC) of -15.1 ± 8.6. Similarly, the pharmacokinetic parameters of the prodrugs following IV bolus administration were estimated using the two-compartment model with the same weighting method. For prodrug 5, the AIC and SBC were -8.4 ± 3.7 and -7.2 ± 3.7, respectively, while for prodrug 8, these values were -12.5 ± 4.9 and -11.9 ± 5.3, respectively.

The oral bioavailability (F_{oral}) of the drug was determined by comparing the area under the plasma concentration-time curve from time zero to the last measurable time point

($AUC_{0\text{-last}}$) following both IV bolus and oral administration. It was calculated using the following equation:

$$F_{oral}(\%) = \frac{AUC_{Oral} \times Dose_{IV}}{AUC_{IV} \times Dose_{Oral}} \times 100$$

Results generated in this section were demonstrated in **Section 4.3.3** and **Section 5.3.7.**

2.7.4 Biodistribution study of IMQ, prodrug5 and prodrug 8

IMQ formulation and prodrug formulations were prepared as described in **section 2.7.1.2**. In the biodistribution (BD) study of IMQ, IMQ was administered by oral gavage to rats using the lipid-free formulation followed by oral gavage of olive oil and water as described in **section 2.7.3.1**. In the BD study of prodrugs, prodrugs were administered to animals by an oral gavage followed by 1 mL of water.

At predetermined time points, blood samples were collected from the vena cava while animals were under terminal anaesthesia. It should be noted that BD studies of IMQ conducted at 1.5 h and 6 h were also used for a head-to-head comparison of BD studies of prodrugs (**Chapter 5, Section 5.3.8**). In the BD studies of prodrugs, NaF was added to the sample collection tubes to prevent the degradation of prodrugs (**Section 2.7.5**). NaF was also added to the sample collection tubes for the BD studies of IMQ. However, the addition of NaF also prevented the coagulation process. Therefore, the serum was not able to be separated in the BD studies of IMQ at 1.5 and 6 h.

After animals were sacrificed by cervical dislocation, the mesenteric lymph fluid was immediately withdrawn from the superior mesenteric lymph duct with a syringe connected to a 23G needle. It should be noted that the collection of mesenteric lymph

fluid was only possible in the BD studies at 1.5 h, 2 h and 6 h. Lipids (olive oil) that were orally administered to rats stimulated the increase in the production of intestinal lymph, resulting in a dilated mesenteric lymphatic duct and a white colour of lymph. However, the lymphatic duct became transparent at 28 h. Therefore, it was not possible to collect the mesenteric lymph at late time points.

Other tissues, including mesenteric lymph nodes (MLNs), iliac lymph nodes, cervical lymph nodes, brain, spleen, kidney, liver, skeleton muscle (right thigh) and intestinal contents, were harvested from the cadavers.

2.7.5 *In vivo* sample storage and processing

Whole blood and mesenteric lymph fluid obtained from PK and BD studies of IMQ were collected into 1.5 mL Eppendorf tubes with 1% 1.5M EDTA (v/v) as an anticoagulant. For serum collection, whole blood was collected into a separate 1.5 mL Eppendorf tube without any anticoagulant to allow blood coagulation. In the PK and BD studies of prodrugs, whole blood and lymph fluid were collected into 1.5 mL Eppendorf tubes containing 1% 1.5M EDTA and sodium fluoride (NaF, final concentration at 10 mg/mL). The addition of NaF aimed to prevent the release of IMQ following sample collection. Subsequently, plasma and serum were separated by centrifuging non-coagulated and coagulated whole blood at 1,160g for 10 min at 10 ℃, respectively.

After animals were culled, fresh tissues were immediately collected and frozen in dry ice. All harvested tissues were weighed. Large tissues, including kidney, brain, liver, muscle and spleen, were homogenised with 10 mg/mL NaF solution at a ratio of 1:3 (w/v) using a Polytron® PT 10–35 GT homogeniser (Kinematica, Malters, Switzerland). Intestinal contents, including liquid and solids, that were collected from small intestines,

large intestines and rectums were homogenised with NaF solution at a ratio of 1:10 or 1:20, depending on the concentration of tested compounds in contents.

Lymph nodes were placed in 1.5 mL Eppendorf tubes with 3-5 Stainless Steel Beads (Next ADVANCE, Web Scientific, USA) and NaF solution was added to obtain at least 100 µL volume of samples. Lymph nodes were homogenised using a Bullet Blender 24 Gold (Next Advance, USA).

All processed samples were kept at -80 ℃, and the analysis of samples was finished in up to one week. Concentrations of IMQ, prodrug 1 and prodrug 8 in the processed samples were determined using LC-MS/MS as described in **section 2.8.4.** Results that were generated as described in this section were demonstrated in **Section 4.3.3** and **Section 5.3.8**.

2.8 Bioanalytical procedures

2.8.1 Schematic description of procedures

Two instruments were used to determine the concentration of analytes in samples. Samples collected from *in vitro* and *ex vivo* experiments **(Sections 2.4**, **Section 2.5 and Section 2.6**) were analysed using HPLC-UV. Samples collected from *in vivo* studies (**Section 2.7**) were analysed using LC-MS/MS to achieve higher sensitivity. The general scheme of determining the concentration of analytes is shown in **Figure 2-5**.

The bioanalytical methods described in **Section 2.8** were validated following the protocols described in **Section 2.9.7** and **Section 2.9.8**. The results of method validation are shown in **Section 3.4.3** and **Section 3.4.5**.

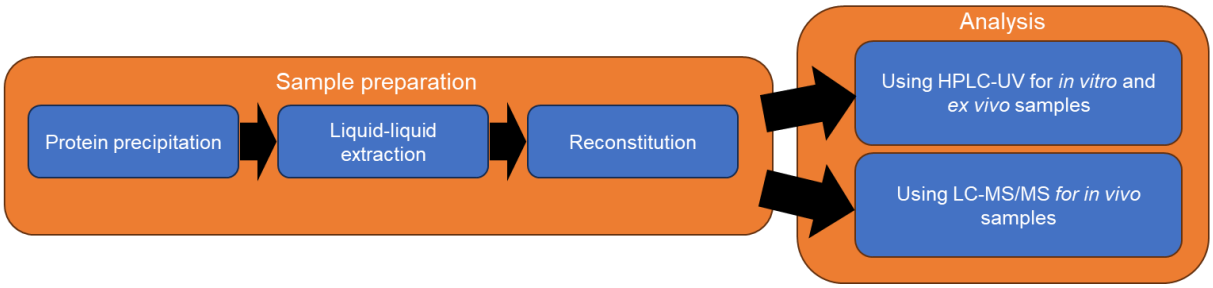

Figure 2-5 Schematic diagram of the workflow for determining the concentration of analytes using HPLC-UV or LC-MS/MS systems.

2.8.2 Instruments and chromatography conditions

2.8.2.1 HPLC-UV

The HPLC system consisted of a Waters Alliance 2695 separations module equipped with a Waters 996 photodiode array detector. The injection volume was 60 µL. Chromatographies were monitored at 319 nm for all analytes. A C18 150 x 2 mm, 5 µm particle size reverse phase column (Gemini-LC-column, Phenomenex, US) connected to a 3 µm particle size guard column (Phenomenex, Macclesfield, UK) was used as the solid phase for separation. The temperature of the column oven and autosampler was 40 ℃ and 4 ℃. The HPLC chromatography conditions and retention time for IMQ and prodrugs are shown in **Table 2-3**. Chromatograms were processed with Empower™ 2.

Table 2-3 HPLC conditions for IMQ and prodrugs

Compound	Mobile phase		Flow rate (mg/mL)	Internal standard (IS)	UV wavelength (nm)	Retention time (min)
	Buffer[a]	MeOH				
IMQ	Gradient 1[b]		0.3	Propranolol	319	8.9
Prodrug 1	Gradient 2[c]		0.3	Propranolol	319	20.6
Prodrug 2	Gradient 3[d]		0.3	Propranolol	319	36.3
Prodrug 3	Gradient 4[e]		0.3	Propranolol	319	26.5
Prodrug 4	Gradient 1[b]		0.3	Propranolol	319	31.3
Prodrug 5	Gradient 3[d]		0.3	Propranolol	319	29.4
Prodrug 6	Gradient 2		0.3	Propranolol	319	30.0
Prodrug 7	Gradient 1[b]		0.3	Propranolol	319	27.3
Prodrug 8	Gradient 2[c]		0.3	Propranolol	319	33.6

[a]10 mM Ammonium formate (pH=3)
[b]Gradient 1: 30% MeOH from 0-9 min, gradually increased to 90% from 9-14 min, maintain at 90 % from 14-30 mins, gradually decrease to 30% from 30-35 min, maintain at 30% from 35-40 min.
[c]Gradient 2: 30% MeOH from 0-9 min, gradually increased to 84% from 9-14 min, maintain at 84 % from 14-35 mins, gradually decrease to 30% from 35-40 min, maintain at 30% from 40-45 min.
[d]Gradient 3: 30% MeOH from 0-9 min, gradually increased to 80% from 9-14 min, maintain at 80 % from 14-40 mins, gradually decrease to 30% from 40-45 min, maintain at 30% from 45-50 min.
[e]Gradient 4: 30% MeOH from 0-9 min, gradually increased to 90% from 9-14 min, maintain at 90 % from 14-35 mins, gradually decrease to 30% from 35-40 min, maintain at 30% from 40-45 min
[e]Propranolol concentration is 5000 ng/mL in each sample. The retention time of propranolol is 12.9 min.

2.8.2.2 LC-MS/MS

The LC-MS/MS system consisting of an AB Sciex API Qtrap4000 tandem mass spectrometry system coupled with a SHIMADZU LC-10AD binary pump and a SHIMADZU SIL-HTc autosampler was used for analysis. The conditions of the mobile phase and solid phase were the same for the HPLC-UV (**Section 2.8.2.1**). The injection volume for the LC-MS/MS method was 10 µL.

The ionisation of analytes was conducted in positive mode with multiple reaction monitoring. The remaining MS conditions were set as follows: ion spray voltage 5,000 V; temperature 350 °C; curtain gas 30 psi; ion source gas 1 and gas 2 40 psi; entrance potential 10 V. The declustering potential (DP), collision energy (CE), collision cell exit potential (CXP) and monitored ion pairs in Q1 and Q3 are shown in **Table 2-4**.

Table 2-4 The mass spectrometry condition and monitored ion pairs of IMQ, IS, prodrug 5 and prodrug 8.

Compound	Q1 mass[a]	Q3 mass[a]	DP[b]	CE[c]	CXP[d]
Imiquimod	241.300	185.300	40.000	37.000	14.000
		141.200		62.000	14.000
		114.200		80.000	13.000
Prodrug 5	449.400	241.300	90.000	46.000	15.000
		185.100	70.000	70.000	15.000
Prodrug 8	503.500	241.300	80.000	56.000	20.000
		185.100	130.000	43.000	28.900
Propranolol (IS)	260.200	116.300	40.000	27.000	12.000

[a]mass over charges (m/z);[b]Declustering potential (DP); [c]Collision energy (CE); [d]Collision cell exit potential (CXP)

2.8.3 Preparation of HPLC-UV samples

Twelve microliters of 50,000 ng/mL propranolol as an internal standard (IS) were added to 120 µL of samples. Then, protein precipitation was achieved by addition of 360 µL of cold acetonitrile (-20 ◦C) following a previously reported protocol[204]. Liquid-liquid extraction was performed by vortexing samples with 3 mL of methyl tert-*butyl* ether for 10 mins. After centrifugation at 1160 *g* at 10 °C for 10 mins, the upper organic layer was transferred into clean testing tubes and evaporated to dryness at 40 °C under nitrogen flow. Samples were reconstituted with 100 µL of 65:35 water/methanol (v/v) and transferred into sample vials.

Fresh calibration curves were established for each experiment using the same matrix as the study samples and the same stock solution of tested compounds. The stock solutions of IMQ and IS were prepared in methanol at 100 µg/mL. The stock solutions of IMQ prodrugs were prepared in methanol at 1 mM. The working standard solutions of IMQ were serially diluted with MeOH at concentrations of 50,000, 10,000, 5,000, 1,000, 500, 300, 200 and 150 ng/mL. The working standard solutions of prodrugs were serial diluted with MeOH at 100, 50, 25, 20, 10, 5, and 3 µM. Calibration curve samples were prepared by spiking 12 µL of working standard solution into 108 µL of blank rat plasma. All calibration curve samples were processed for HPLC-UV analysis as described above. The nominal concentrations of the calibration curve for IMQ were at 5,000, 1,000, 500, 100, 50, 30, 20 and 15 ng/mL. The nominal concentrations of the calibration curve for IMQ prodrugs were at 10, 5, 2.5, 2, 1, 0.5 and 0.3 µM.

2.8.4 Preparation of LC-MS/MS samples

In vivo samples, after being processed as described in **section 2.8.4**, were prepared for analysis using the LC-MS/MS system.

Ten microliters of 5,000 ng/mL propranolol as an internal standard (IS) were added to 100 µL of samples, followed by an addition of 360 µL of cold acetonitrile (-20 ◦C) for protein precipitation. Liquid-liquid extraction was performed by vortexing samples with 3 mL of METB for 10 mins. After centrifugation at 1160 *g* at 10 °C for 10 mins, the upper organic layer was transferred into clean testing tubes and evaporated to dryness at 40 °C under nitrogen flow. Samples were reconstituted with 60 µL of 65:35 water/methanol (v/v) and transferred into sample vials.

Fresh calibration curves were created for each animal study using the same matrix as the samples. The working standard solutions of IMQ, prodrug 5 and prodrug 8 were serially diluted from formulations used in animal studies with methanol at concentrations of 2000, 1000, 500, 200, 160, 120, 80, 50, 25 and 12.5 ng/mL. Calibration curve samples were made by spiking 10 µL of working standard solution into 90 µL of commercially available male SD rat plasma. All calibration curve samples underwent the same procedures to become LC-MS/MS samples as described above. The nominal concentrations of calibration curve samples were 200, 100, 50, 20, 16, 12, 8, 5, 2.5, and 1.25 ng/mL.

2.9 Validation of bioanalytical methods

2.9.1 UV-spectrum of IMQ

The stock solution of IMQ was prepared in MeOH at a concentration of 100 µg/mL and diluted with MeOH to reach a final concentration of 1 µg/mL. The UV spectrum of IMQ

was measured using a Waters 996 photodiode array detector following an injection of 60 µL of 1 µg/mL IMQ solution into the system. A mixture of water and MeOH 50:50 (v/v) was used to elute IMQ following the injection. Additional information about the Waters HPLC-UV systems and the separation column is described in **Section 2.8.2.1**.

2.9.2 Log D of IMQ

The chemical structure of IMQ was uploaded into the ACD/I-Lab online platform. The Log D of IMQ at different pH (from pH = 0 to pH = 14) was calculated using this software.

2.9.3 Selection of buffers

Two mobile phase buffers:10 mM ammonium formate (pH = 3) and 10 mM ammonium acetate (pH = 10) were prepared. An isocratic elution method (buffer: MeOH 70:30, *v/v*) was used to generate the chromatograms of IMQ following an injection of 60 µL of 100 ng/mL IMQ (prepared in 65:35 water/MeOH, *v/v*).

2.9.4 Selection of biological matrix sample volume

Blank rat plasma at volumes of 100, 120 and 150 µL was processed for HPLC-UV analysis as described in **Section 2.8.3.** The **elution method 1** described in **Section 2.8.2.1, Table 2-3** was used to generate the chromatograms of blank rat plasma following an injection of 60 µL of samples.

2.9.5 Selection of IMQ and related ions

An IMQ solution was prepared with MeOH at a concentration of 100 ng/mL. Two hundred microliters of IMQ solution were continuously injected into the LC-MS/MS systems at a flow rate of 20 µL/min using a perfusion pump equipped with a 200 µL

Hamilton syringe. The product ions of IMQ were generated and monitored using the multiple reaction monitoring mode on the AB Sciex API QTRAP 4000. Additional information about the LC-MS/MS systems and instrument settings is described in **Section 2.8.2.2**.

2.9.6 Identifying the carryover of IMQ

To develop a bioanalytical method for the determination of IMQ in rat plasma using the LC-MS/MS system, a short elution method was first used to separate IMQ from endogenous plasma interferences (**Table 3-1**). This elution method was an empirical LC gradient method, which was previously developed by others on the QTRAP 4000 LC-MS/MS system [205]. The carryover effect of this method was assessed by injecting 5 µL of 100 ng/mL IMQ (prepared in 65:35 water/MeOH). Then, 5 µL of blank reconstitution solvent (65:35 water/MeOH) was repeatedly injected into the LC-MS/MS to monitor the carryover of IMQ.

Table 3-1 An empirical LC gradient method for the elution of IMQ using the LC-MS/MS system. The buffer used in this method was 10 mM of ammonium formate, pH = 3.

Time (mins)	Buffer pH 3 (%)	MeOH
0	90	10
4	10	90
6	10	90
6.1	90	10
10	90	10

Since an obvious carryover of IMQ was noticed with this elution method, in the next step, four needle wash solvents: 50:50 MeOH/water (v/v), 50:50 MeOH/water + 0.1 % formic acid (v/v), 25:25:25:25 MeOH/water/acetonitrile/isopropanol alcohol and 50:50

formic acid/water were used to minimise the potential contamination of IMQ in the autosampler system.

Additionally, the gradient method 1, which was previously developed for the HPLC-UV system (**Section 2.8.2.1, Table 2-3**), was also applied to the LC-MS/MS system to avoid the carryover of IMQ.

2.9.7 Validation of bioanalytical methods for the determination of the concentrations of IMQ in biological samples

The HPLC-UV method and the LC-MS/MS method used for the generation of results in **Chapters 4 and 5** were partially validated following the US Food and Drug Administration (FDA) guidelines for bioanalysis [206].

Calibration standards and instrument settings are described in **Section 2.8.2**. The validation of selectivity, sensitivity, linearity and carryover was performed for the HPLC-UV method. The validation of selectivity, sensitivity, carryover, linearity, recovery, stability, and dilution effect was assessed for the LC-MS/MS method.

2.9.7.1 Selectivity

The selectivity of bioanalytical methods was demonstrated by the absence of interference (in the biological matrix samples, such as plasma) at the same retention time of analytes and IS. The absence of interference was confirmed in six validation samples.

2.9.7.2 Carryover

The carryover was assessed for both HPLC-UV and LC-MS/MS bioanalytical methods. Rat plasma samples spiked with IMQ at the concentrations of 1 µg/mL or 100 ng/mL

were injected into the HPLC-UV system or the LC-MS/MS system, respectively. Following the injection of IMQ, blank reconstitution solvent (65:35 water/MeOH) or blank rat plasma samples were injected into the system to confirm the absence of carryover. If a carryover of IMQ is found, the peak area of the carryover should be less than 20% of the LLOQ [206].

2.9.7.3 Sensitivity

The sensitivity of the bioanalytical method for the determination of IMQ concentrations in rat plasma was demonstrated by assessing the LLOQ of IMQ. Six rat plasma samples spiked with IMQ at the LLOQ were prepared alongside a calibration curve. RE and RSD between calculated concentrations and nominal concentrations were conducted to assess compliance with acceptance criteria, ensuring RE and RSD were both ≤ ± 20% in intra-day and inter-day analysis. Additionally, for the bioanalytical method using the LC-MS/MS system, the signal-to-noise ratio between the IMQ at the LLOQ and blank biological matrix should be more than five times [206].

2.9.7.4 Linearity and accuracy

Calibration curves of IMQ with the range 15 – 5,000 ng/mL (HPLC-UV assay) or the 1.25 – 200 ng/mL (LC-MS/MS assay) were generated by spiking IMQ into rat plasma as described in **section 2.8.3** and **section 2.8.4**.

The peak area ratios between analytes and IS against nominal concentration were plotted on an X-Y graph. A least-squares linear regression ($y = ax + b$) was established using 1/x weighting factors. The linearity of the generated linear regression should be more than 0.99 (r^2 > 0.99). The acceptance criteria for accuracy and precision were described as the RE of calculated concentrations ≤ ±15% compared to nominal concentrations (except LLOQ ≤ ± 20%).

2.9.7.5 Dilution effect

Blank rat plasma samples spiked with IMQ at the concentration of 4,000 ng/mL or 200 ng/mL were 20-fold diluted with rat plasma to reach the final concentration of 200 ng/mL or 10 ng/mL. The diluted samples were processed for bioanalysis using the LC-MS/MS system. The concentration of IMQ in these diluted samples was determined using a calibration curve with a range of 1.25 – 200 ng/mL. The calculated concentrations were defined as measured concentrations multiplied by the dilution factor. The RE and RSD between nominal concentrations and calculated concentrations should be less than ≤ ±15%

3.3.7.6 Recovery

The recovery of IMQ was determined by comparing the peak areas of processed samples with the peak areas of standard solutions (prepared in reconstitution solvent 65:36 water/MeOH, v/v) at the equivalent concentration. The recovery of IS was determined in the same manner as IMQ.

2.9.7.7 Stability

The stability of samples was assessed to evaluate the degradation of IMQ in different conditions in which the samples were stored and analysed. In practice, rat plasma samples collected from an *in vivo study* were stored in the -80 °C freezer until analysis (up to one week). On the day of the analysis, processed samples were reconstituted in 65:35 water/MeOH and stored in the autosampler (4 °C) until being injected into the LC-MS/MS (within 24 hours).

Therefore, short-term stability was assessed by spiking IMQ to rat plasma and then stored at -80 °C for 1 week. Autosampler stability was assessed by storing

reconstituted samples (65:35 water/MeOH) at 4 °C for 24 hours. The stability of analytes was demonstrated as the RE and RSD ≤ ±15% (except LLOQ ≤ ± 20%).

2.9.8 Validation of bioanalytical methods for the determination of the concentrations of prodrugs in biological samples

2.9.8.1 Validation of selectivity, sensitivity and linearity

In *in vitro* assessments of prodrugs, biological samples containing prodrugs 1-8 were processed for analysis using HPLC-UV. For *in vivo* studies that assessed the lymphatic transport of prodrugs 5 and 8 (**Chapter 5**), biological samples containing prodrugs 5 and 8 were processed for analysis using LC-MS/MS. Calibration curve samples for prodrugs were prepared as described in **sections 2.8.3** and **2.8.4,** respectively. The selectivity, sensitivity and linearity of bioanalytical methods for prodrugs were assessed as described in **sections 2.9.7.1**, **3.3.7.3** and **2.9 .7.4**.

2.9.8.2 Stability of prodrugs 5 and 8

The stability of samples containing prodrugs 5 and 8 was assessed to evaluate their degradation in the on-bench conditions and autosampler.

The on-bench stability of prodrugs 5 and 8 was assessed by spiking them into rat plasma and immediately transferring the mixture into Eppendorf tubes containing 1% 1.5M EDTA and sodium fluoride (10 mg/mL) on ice. The remaining percentage of prodrugs in the plasma was monitored over a period of 6 h.

The Autosampler stability of prodrugs 5 and 8 was assessed by storing processed samples (reconstituted in 65:35 water/MeOH) at 4 °C for 24 hours. The stability of samples was demonstrated as the RE and RSD ≤ ±15% (except LLOQ ≤ ± 20%).

2.10 General statistical analysis

All results shown i**n this work a**re presented as mean ± standard deviation (SD). Statistical analysis was conducted using GraphPad Prism version 10 (GraphPad Software, Inc., San Diego, CA, USA). An outlier test based on nonlinear regression (ROUT) with assumption Q = 1% was used to remove outliers where appropriate.

A two-tailed unpaired student t-test was used to assess the statistically significant difference between the means of two independent groups. To determine if there is a significant difference between 3 or more independent groups, the one-way analysis of variance (ANOVA) was used to compare the means of groups. Additionally, post hoc comparisons (Dunnett's comparison or Tukey's multiple comparisons) were conducted following a significant one-way ANOVA to determine which specific groups differ from each other. A significant difference was stated when a *p*-value was below 0.05.

Chapter 3 Development and validation of bioanalytical methods for the determination of imiquimod and its prodrugs in biological samples

3.1 Introduction

In CRC patients, the activation of DCs is significantly suppressed by tumours in the mesenteric lymph nodes (MLNs) and iliac lymph nodes (ILNs), which are the drainage LNs for the colorectal regions [30,32,34,153]. Imiquimod (IMQ) is a small molecule of toll-like receptor 7 agonists. Preclinic studies suggested that IMQ is a potent immune activator and can facilitate the maturation process of immature DCs [111,119]. However, a poor therapeutic outcome and dose-limited toxicity of IMQ were previously observed in clinical trials [141,207]. The unsatisfactory therapeutic results and adverse side effects of IMQ may reflect the fact that IMQ was not efficiently target delivered to the affected area, such as LNs.

Therefore, in this study, we aimed to use a lipophilic prodrug approach combined with a lipid-based formulation to deliver IMQ to these LNs following oral administration. To examine the pharmacokinetic parameters and biodistribution of IMQ in the target regions, a sensitive and robust bioanalytical method for determining the concentration of IMQ in a biological sample is essential.

Interestingly, in the previous studies involving target delivery of IMQ, the success of drug delivery to the target area was not directly demonstrated. In one study, the distribution of nanoparticles was reported as a proxy to represent the local concentration of IMQ [208]. In addition, the difference in pharmacodynamic results between experimental groups (a.k.a. animals that received IMQ encapsulated in nanoparticles) and control groups (a.k.a. animals that received free IMQ molecules) was used to prove the successful target delivery of IMQ [209–211].

To our best understanding, validated analytical methods for the determination of the concentration of IMQ in *in vivo* samples were limited. Previous analytical methods for IMQ were developed for 1) identifying IMQ in topical formulations [212,213]; 2) monitoring the potential impurities and byproducts of IMQ that were produced during the chemical synthesis [214]; and 3) monitoring the stability of IMQ in various inorganic solvents or under different physical conditions [215]. These methods only allow the quantification of IMQ in a simple matrix. Sabri *et al.* previously reported an analytical method for determining IMQ in a biological sample (porcine skin). However, this method required processing samples with solid-phase extraction, which is very costly, and only achieved a poor lower limit of quantification (LLOQ) > 1 μg/mL. It has been reported that the oral bioavailability of IMQ in rats is close to zero, suggesting the actual concentration of IMQ that will be found in our work could be very low [140].

Therefore, this chapter aimed to develop a simple, sensitive, and cost-effective bioanalytical method for determining IMQ in rat plasma. Additionally, bioanalytical methods for the determination of the concentrations of lipophilic prodrugs of IMQ (synthesized as described in **Chapter 5**) in biological samples were also generated. The methods developed in this chapter were used to generate data in **Chapter 4 and Chapter 5**.

3.2 Experimental design

Figure 3-1 demonstrates the process of the development of bioanalytical methods for the determination of the concentrations of IMQ and its prodrugs in plasma. The development was initially started with high-performance liquid chromatography equipped with an ultraviolet detector (HPLC-UV). Then, the bioanalytical method was further optimized with LC equipped with tandem mass spectrometry (MS/MS) to

achieve a higher sensitivity. Bioanalytical methods using different detectors were validated according to the FDA guidelines [206].

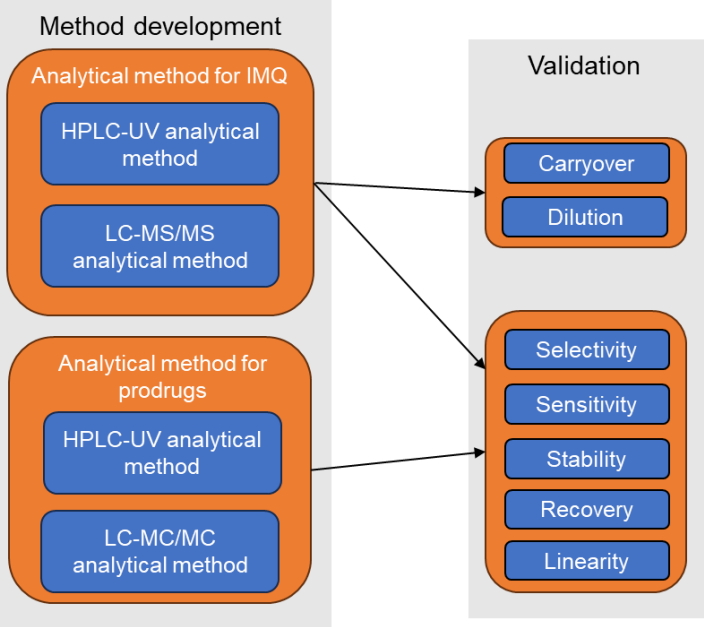

Figure 3-1 Schematic diagram of developing development of the bioanalytical methodology for the determination of the concentrations of IMQ and its prodrugs in rat plasma samples using HPLC-UV or LC-MS/MS systems.

3.4 Results

3.4.1 Development of a bioanalytical method for the determination of the concentrations of IMQ using an HPLC-UV system

It was shown that IMQ has three peaks of UV absorbance at wavelengths of 226, 244 and 319 nm (**Figure 3-2 A**). During the method development process, the unique UV spectrum of IMQ was used to identify the peak of IMQ. The Log D of IMQ at different pH levels was calculated using ACD/I-Lab. **Figure 3-2 B** shows that the lipophilicity of IMQ reaches the maximum (Log D = 3.0) when the pH $\geq$ 8. By contrast, the lipophilicity of IMQ reaches -1 when the pH $\leq$ 3.

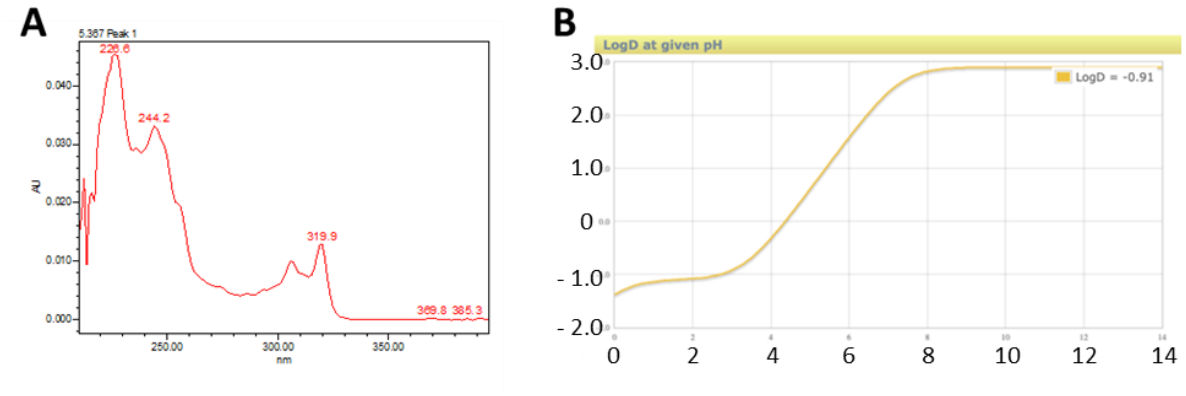

Figure 3-2 Panel (A) UV-spectrum of IMQ; Panel (B) Calculated Log P of IMQ at different pH (calculated by ACD/I-lab).

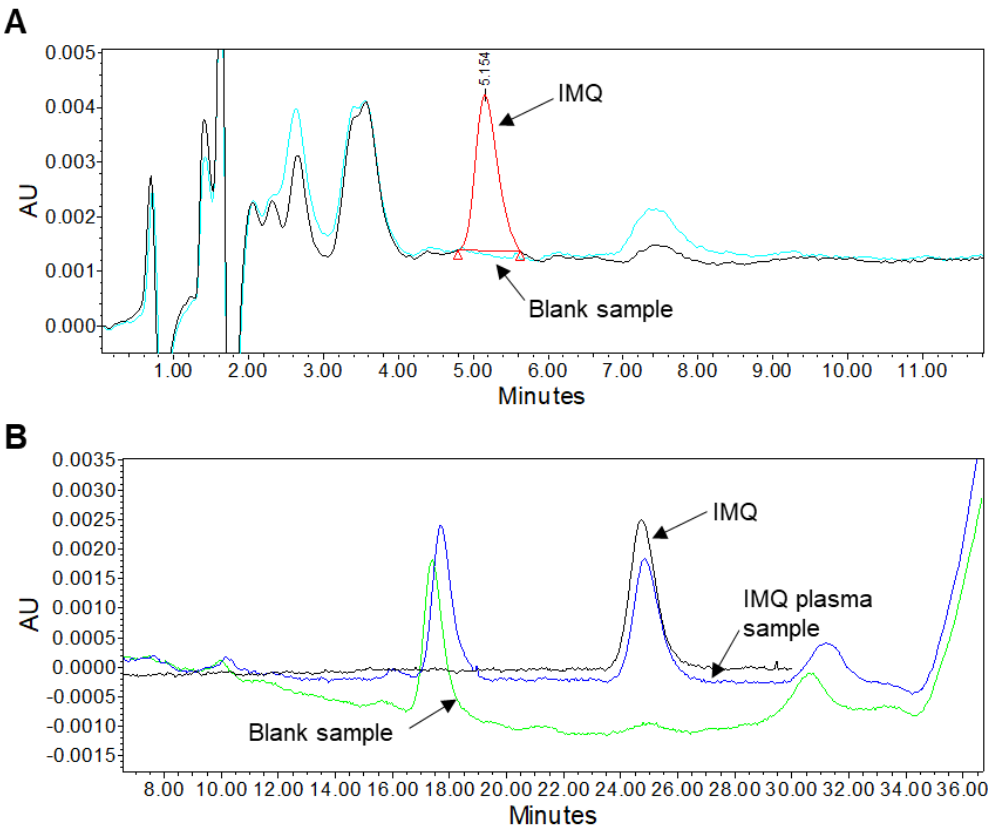

Figure 3-3 Chromatograms of 100 ng/mL IMQ stock solution (prepared in 65:35 water/MeOH, v/v) and solvent blank (65:35 water/MeOH). Panel (A) represents the chromatogram that was generated using an acidic buffer (10 mM ammonium formate, pH = 3). Panel (B) represent the chromatogram that was generated using an alkaline buffer (10 mM ammonium acetate, pH = 10). The chromatogram was monitored at the UV wavelength = 319 nm.

The chromatograms showed that peaks of IMQ were sharp and symmetric when either the acidic buffers (10 mM ammonium formate, pH = 3) or alkaline buffer (10 mM ammonium acetate, pH = 10) was used (**Figure 3-3**). The retention time of IMQ using the acidic buffer (5.1 min) was shorter than it was using the alkaline buffer (25.6 min). **Figure 3-4** shows that no interference was found in blank rat plasma samples that were prepared with 100 µL (blue) or 120 µL (red) of rat plasma. However, an obvious interference peak was noticed when 150 µL (green) of rat plasma was used.

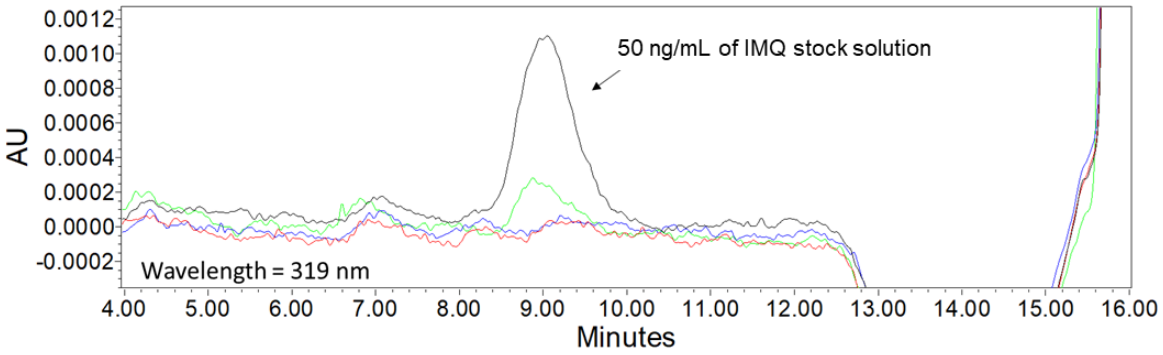

Figure 3-4 The chromatogram of 50 ng/mL IMQ solution (65:35 water/MeOH, v/v) and rat plasma blank samples that were prepared with different volumes of plasma. The blue, red and green lines represent chromatograms of blank rat plasma prepared with 100, 120 and 150 µL plasma, respectively. The black line represents the chromatogram of 50 ng/mL IMQ solution. The chromatograms were monitored at the wavelength of 319 nm.

3.4.2 Development of a bioanalytical method for the determination of IMQ using an LC-MS/MS system

Three main product ions of IMQ were found using the MRM scan mode. A product ion m/z 241.3/185.3 demonstrated the strongest signals and, therefore, was selected to monitor the presence of IMQ (**Figure 3-5**). Other product ions of IMQ, m/z 241.3/141.2 and m/z 241.3/114.2, were also selected as characteristic ions to confirm the presence of IMQ.

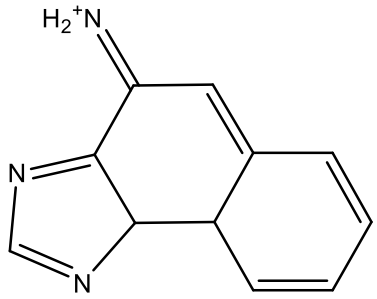

Figure 3-5 The predicted structure of IMQ product ion m/z 241.3/185.3.

An empirical gradient method (**Table 3-1**) was first used to elute IMQ on the LC-MS/MS system. Following an injection of 5 µL of 100 ng/mL IMQ (prepared in 65:35 water: MeOH, v/v), the signal of product ion m/z 241.3/185.3 was also detected in a subsequent injection of 5 µL of reconstitution solvent (65:35 water: MeOH, v/v), indicating the presence of carryover (

Table 3-2). Additionally, it was noted that the peak area of carryover was gradually decreased during the continuously repeated injections of the blank reconstitution solvent (**Table 3-3**).

Table 3-2 Carryover of IMQ after the injection of 5 µL of 100 ng/mL IMQ stock solution. (n=3)

Product ion (m/z)	The peak area of 5 µL of 100 ng/mL IMQ	The peak area of 5 µL of MeOH	Carryover (%)
241.3/185.3	3945000 ± 1477853	915500 ± 374059	27.0 ± 19.3

Table 3-3 The peak area of IMQ product ion m/z 241.3/185.3 in 100 ng/mL of IMQ stock solution and in repeated injections of the solvent blank (65:35 water: MeOH, v/v).

Injection sequence	Peak area of IMQ product ion (m/z 241.3/185.3)
5 µL of 100 ng/mL IMQ	3948000
5 µL of MeOH (1st injection)	47450
5 µL of MeOH (2nd injection)	1664
5 µL of MeOH (3rd injection)	744
5 µL of MeOH (4th injection)	812
5 µL of MeOH (5th injection)	361
5 µL of MeOH (6th injection)	479
5 µL of MeOH (7th injection)	436
5 µL of MeOH (8th injection)	547
5 µL of MeOH (9th injection)	206
5 µL of MeOH (10thinjection)	137

Initially, we considered that the carryover of IMQ was a result of contamination in the autosampler (such as injector needle and connection tubing). It meant the current needle-wash solvent, 100 % MeOH, could not efficiently remove IMQ residues in the autosampler. Therefore, we applied other needle-wash solvents to clean the autosampler between each injection. It was shown that these needle-wash solvents demonstrated certain positive impacts for minimising IMQ carryover compared to 100 % MeOH, but still could not fully avoid the carryover of IMQ (

Table 3-4). Based on the current results, the mixture of 50:50 MeOH/water was selected as the needle-wash solvent.

Table 3-4 The percentage of IMQ carryover using different needle wash solvents.

Needle wash solvent	50:50 MeOH and water	50:50 MeOH and water + 0.1% formic acid	25:25:25:25 MeOH/ACN/IPA/Water	50:50 Formic acid/Water
Carryover (%)	13.4	19.7	23.1	24

ACN, acetonitrile; IPA, isopropanol alcohol

Then, we suspected that the carryover of IMQ was derived from the separation column (C18 150 x 2 mm, 5 µm particle size, Gemini-LC-column, Phenomenex, US). This meant that substantial amounts of IMQ were retained in the column and could not be fully eluted. To evaluate this hypothesis, 5 µL of 100 ng/mL IMQ and 5 µL of reconstitution solvent were consecutively injected into the mass spectrometry bypassing the separation column. It was shown that no carryover was detected in the absence of a column, suggesting the presence of IMQ residue in the column.

Finally, we aimed to adjust the elution method to minimize the carryover of IMQ. It should be noted that no carryover of IMQ was previously detected using the gradient method 1 (**Section 2.8.2, Table 2-3**) on the HPLC-UV system. Therefore, we applied the same elution method to the LC-MS/MS system. As we expected, no carryover was found. The result suggested that elution method 1 can be used for both the HPLC-UV system and the LC-MS/MS system.

3.4.3 Method validation for bioanalytical method of IMQ

3.4.3.1 Selectivity

The selectivity of bioanalytical methods using HPLC-UV or LC-MS/MS was demonstrated as the absence of interference at the retention time of analytes and IS. The chromatograms presented in **Figure 3-6** and **Figure 3- 7** illustrate the effective selectivity of IMQ using HPLC-UV or LC-MS/MS bioanalytical methods, respectively. Chromatograms suggest that IMQ was well separated from endogenous interferences within the rat plasma.

(a) Rat plasma blank

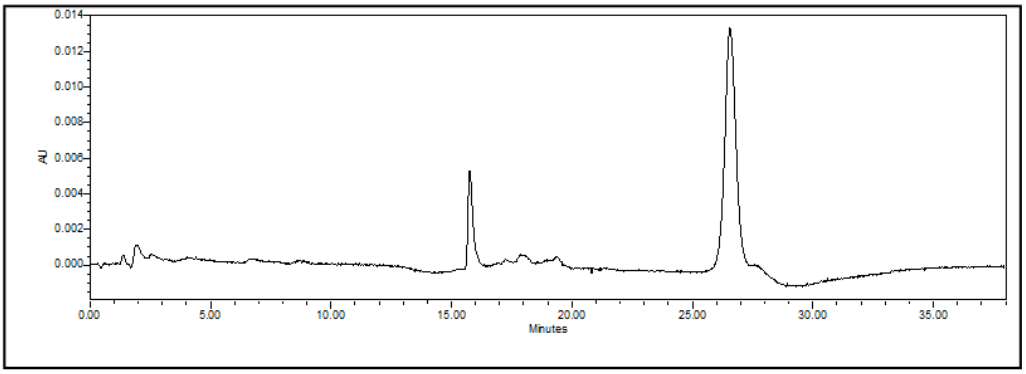

(b) Rat plasma spiked with IMQ at the concentration of 15 ng/mL.

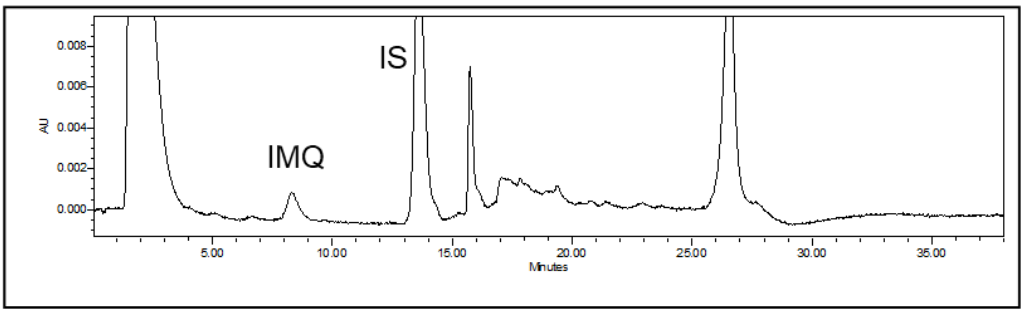

(C) Rat plasma spiked with IMQ at the concentration of 1,000 ng/mL.

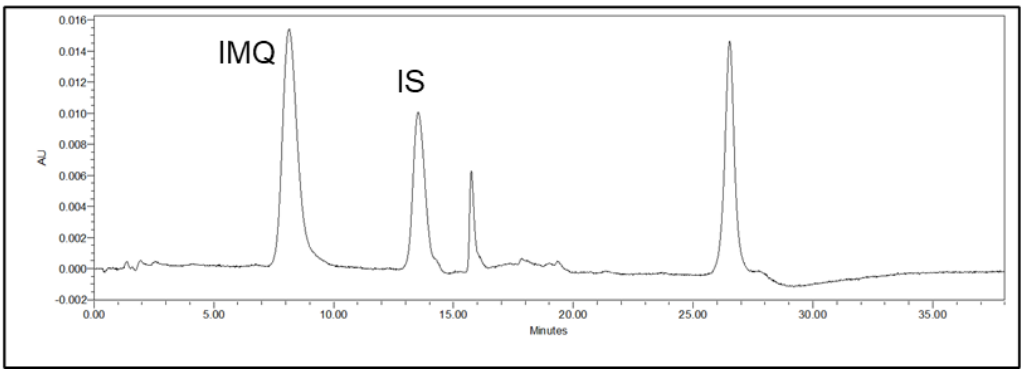

Figure 3-6 Representative HPLC-UV chromatograms of (a) rat plasma blank sample; (b) rat plasma spiked with IMQ and IS at the concentration of 15 ng/mL, and 5,000 ng/mL, respectively; (c) rat plasma spiked with IMQ and IS at the concentration of 1,000 ng/mL and 5,000 ng/mL. All chromatograms were monitored at λ = 319 nm.

(a) Blank rat plasma

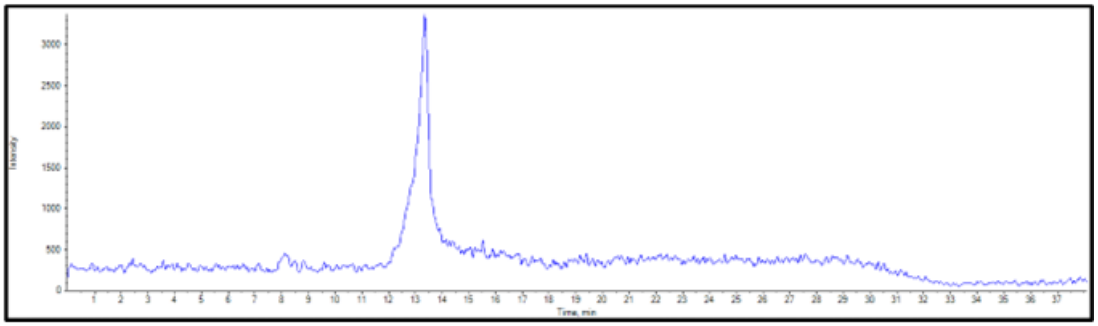

(b) 1.25 ng/mL IMQ in rat plasma

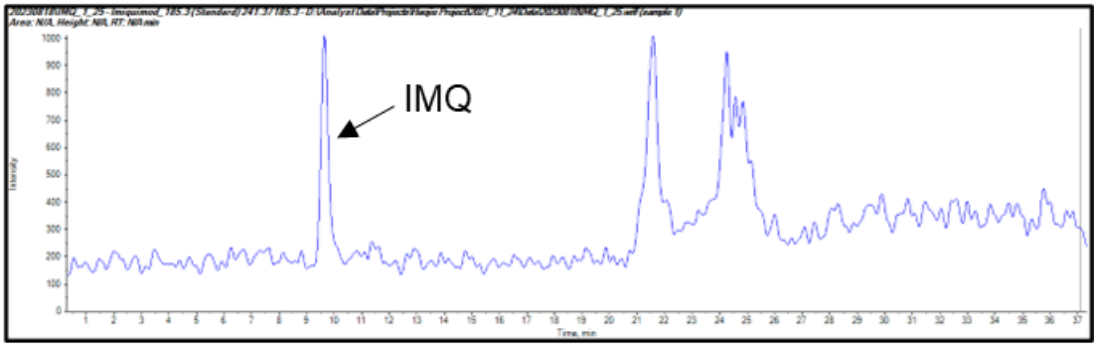

(c) 100 ng/mL of IMQ in rat plasma

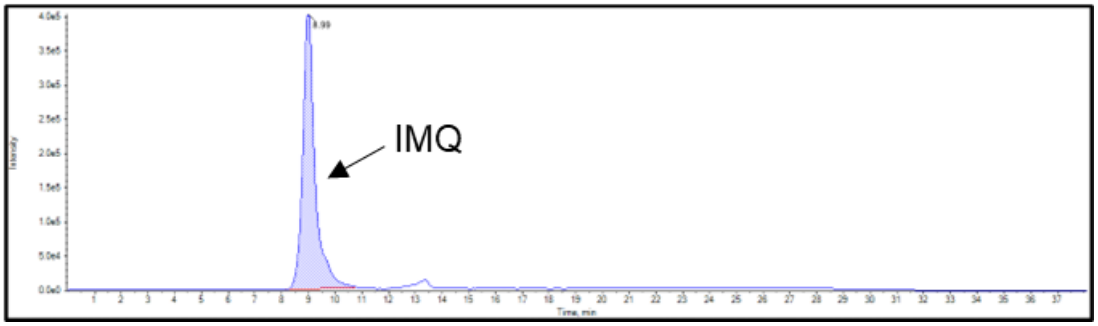

Figure 3- 7 Representative LC-MS/MS extracted ion chromatograms of (a) blank rat plasma monitoring at m/z 241.3/185.3; (b) rat plasma spiked with IMQ at the concentration of 1.25 ng/mL monitoring at m/z 241.3/185.3. (c) rat plasma spiked with IMQ at the concentration of 100 ng/mL monitoring at m/z 241.3/ 185.3.

3.4.3.2 Carryover

There was no carryover of IMQ observed when either the finalised HPLC-UV or LC-MS/MS analytical method was used.

3.4.3.3 Sensitivity

The sensitivity of bioanalytical methods was determined by the lower limit of quantification (LLOQ) of IMQ spiked into rat plasma samples. The LLOQ was assessed for its relative error (RE) and relative standard deviation (RSD) ≤ ±20% across intra-day and inter-day runs.

The LLOQ of the HPLC-UV bioanalytical method for the determination of the concentrations of IMQ in plasma was only assessed for RE and RSD across intra-day runs (n = 6) (**Table 3-5**). The result showed that the concentration of IMQ in rat plasma can be determined as low as 15 ng/mL using the HPLC-UV bioanalytical assay.

The LLOQ of the LC-MS/MS bioanalytical method for determining the concentration of IMQ in plasma was assessed for RE and RSD across both inter-day and intra-day runs (**Table 3-6**). The result indicated that 1.25 ng/mL was the LLOQ of this bioanalytical method. Additionally, the signal-to-noise ratio between IMQ at LLOQ (1.25 ng/mL) and the blank matrix sample was more than five times (intensity response

$_{(LLOQ)}$ = 38800 ± 2362 vs. intensity response $_{(blank)}$ = 6613 ± 778, n = 6), which meets the criteria in the FDA guidelines.

Table 3-5 The intra-day validation of LLOQ of IMQ using HPLC-UV.

Nominal concentration (ng/mL)	Intra-day (n =6)	
	Accuracy (RE, %)	Precision (RSD, %)
15	13.8	6.4

Table 3-6 The intra-day and inter-day validation of LLOQ of IMQ using LC-MS/MS.

Nominal concentration (ng/mL)	Intra-day (n =6)		Inter-day (n =6)	
	Accuracy (RE, %)	Precision (RSD, %)	Accuracy (RE, %)	Precision (RSD, %)
1.25	6.3	4.6	9.7	2.5

3.4.3.4 Linearity and Accuracy

The correlation coefficient (r^2) of IMQ calibration curves that were established using the HPLC-UV method was greater than 0.99 (**Table 3-7**). The calculated concentrations met the criteria of RE ≤ ±15% compared to nominal concentrations (except LLOQ ± ≤ 20%).

Peak areas of IMQ and IS that were obtained using LC-MS/MS, and nominal concentrations were uploaded into MultiQuant (version 3.0.3, USA) to generate a calibration curve. It was shown that the r^2 of the calibration curve was greater than

0.99, and the RE of calculated concentration was ≤ ±15% compared to nominal concentrations (excluding LLOQ, which met the criteria of ≤ ±20%) **(Table 3-8**).

Table 3-7 The results of validation for accuracy and linearity using the HPLC-UV method.

Nominal concentration (ng/mL)	Calculated concentration (ng/mL)	Accuracy (RE, %)	Linear regression	
15	18	19.3	Slope	0.00175
20	20	-0.7	Intercept	-0.00958
30	30	1.1	r^2	0.99916
50	45	-9.7		
100	100	0.4		
500	478	-4.3		
1,000	918	-8.1		
5,000	5104	2.1		

Table 3-8 The results of validation for accuracy and linearity using the LC-MS/MS method (data generated using MultiQuant (version 3.0.3).

Nominal concentration (ng/mL)	Calculated concentration (ng/mL)	Accuracy (RE, %)	Linear regression	
1.25	1.02	-18.4	Slope	0.00631
2.5	2.14	-14.4	Intercept	0.00468
5	5.08	1.6	r^2	0.99671
8	7.79	-2.6		
16	17.98	12.4		
20	22.94	14.7		
50	53.86	7.7		
100	105.71	5.7		
200	186.24	-6.9		

3.4.3.5 Recovery

The absolute recoveries (mean ± SD) of IMQ after sample preparation were 82.0 ± 7.2 % and 94.8 ± 8.8 % at the concentration of LLOQ and 100 ng/mL, respectively. The recovery of the IS was 90.9 ± 3.3 %. The high recovery of the analytes and IS in this assay contributed to achieving good sensitivity.

3.4.3.6 Dilution effect

The dilution effect was validated for the LC-MS/MS bioanalytical method for IMQ. **Table 3-9** shows the RE and RSD of the calculated concentrations compared to nominal concentrations were less than 10 %. Results suggest that the dilution of samples did not affect the accuracy and precision of the LC-MS/MS bioanalytical method.

Table 3-9 The results of validation of dilution effects.

Nominal concentration (ng/mL)	Calculated concentration (n = 3)	
	Accuracy (RE, %)	Precision (RSD, %)
4,000	4.5	6.8
200	7.3	2.6

3.4.3.7 Stability

The stability of IMQ in the short-term storage conditions (one week at -80 °C) and the autosampler conditions (24 h at 4 °C) were accessed and are summarized in **Table 3-10**. It was shown that IMQ was stable in these storage conditions.

Table 3-10 Stability results of IMQ in rat plasma at -80 °C for one week and IMQ in 65:35 water/MeOH at 4 °C for 24 h.

Concentration (ng/mL)	Short-term stability (-80 °C, one week) (n =6)		Autosampler stability (4 °C, 24 h) (n =6)	
	Accuracy (RE, %)	Precision (RSD, %)	Accuracy (RE, %)	Precision (RSD, %)
1.25	3.7	1.2	2.9	3.3
100	12.0	3.1	13.2	1.8

3.4.5 Validation of the bioanalytical methods for determination of prodrugs in biological samples

3.4.5.1 Selectivity, sensitivity and linearity of the bioanalytical methods for the determination of prodrugs

Figure 3-8 to **Figure 8-15** indicate the good selectivity of the HPLC-UV bioanalytical method for determining the concentration of prodrugs 1 – 8 in plasma samples. The good selectivity of LC-MS/MS bioanalytical methods, which were used to determine the concentration of prodrug 5 and prodrug 8 in plasma samples, is demonstrated in **Figure 3- 16** and **Figure 3- 17.**

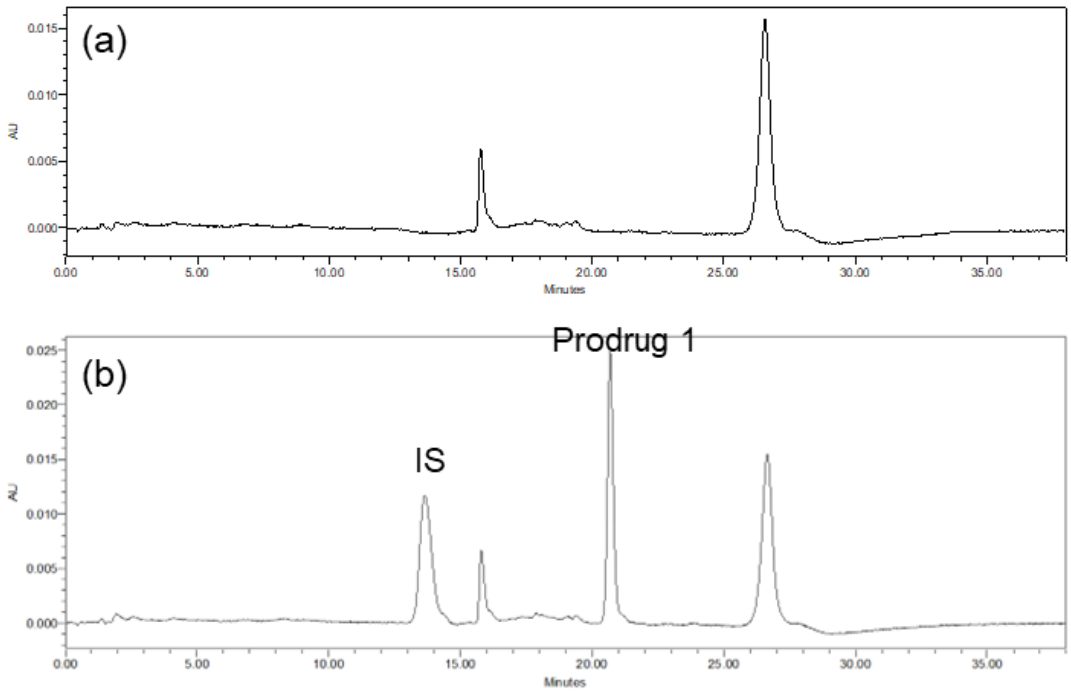

Figure 3-8 Representative chromatograms of HPLC-UV. (a) rat plasma blank sample at λ = 319 nm and (b) rat plasma spiked with prodrug 1 and IS at the concentration of 5 μM and 5,000 ng/mL, respectively, at λ = 319.

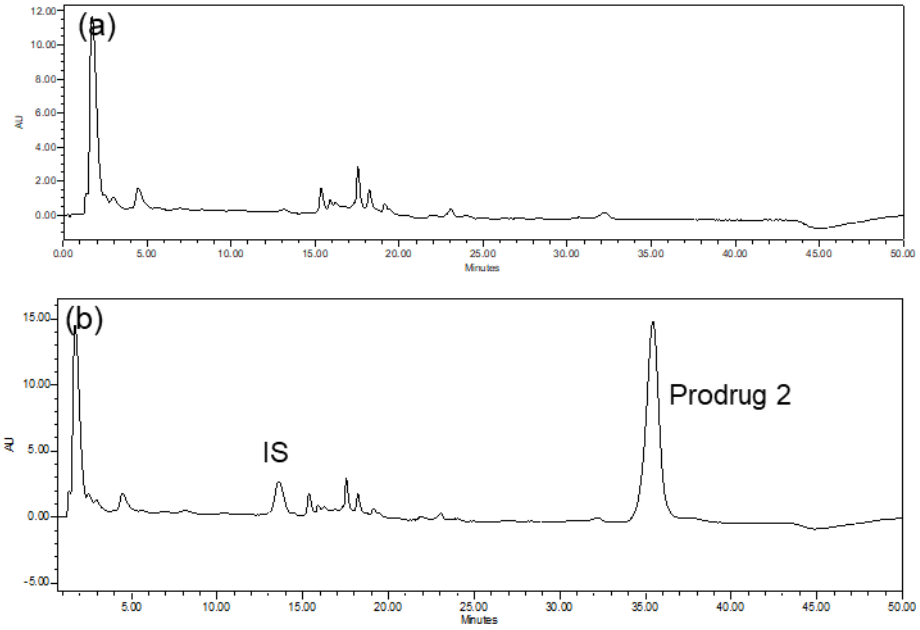

Figure 3-9 Representative chromatograms of HPLC-UV. (a) rat plasma blank sample at λ = 319 nm and (b) rat plasma spiked with prodrug 2 and IS at the concentration of 10 μM and 5,000 ng/mL, respectively, at λ = 319.

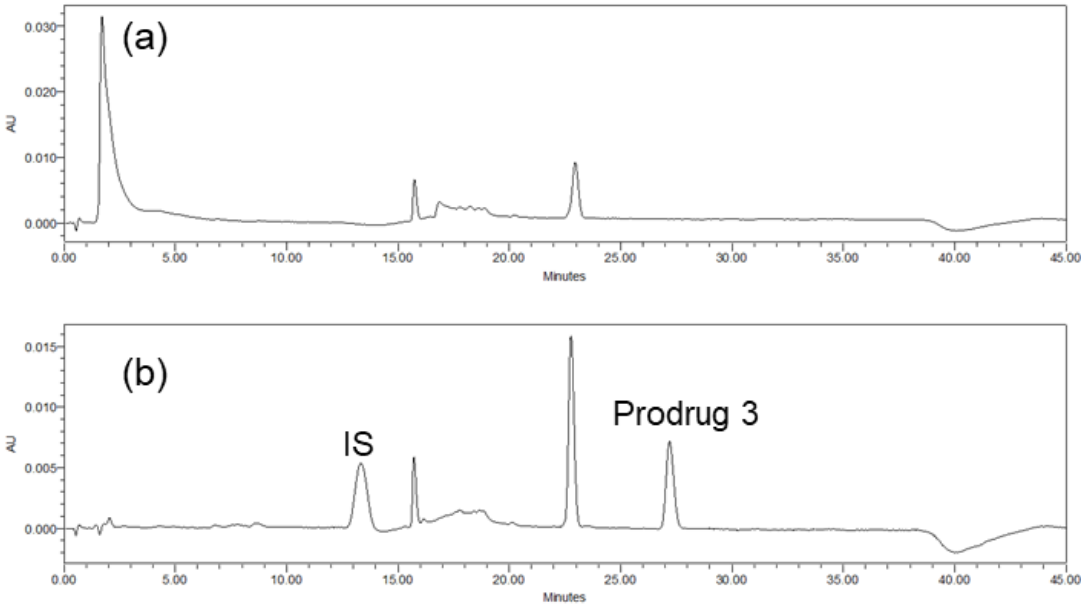

Figure 3-10 Representative chromatograms of HPLC-UV. (a) rat plasma blank sample at λ = 319 nm and (b) rat plasma spiked with prodrug 3 and IS at the concentration of 5 μM and 5,000 ng/mL, respectively, at λ = 319.

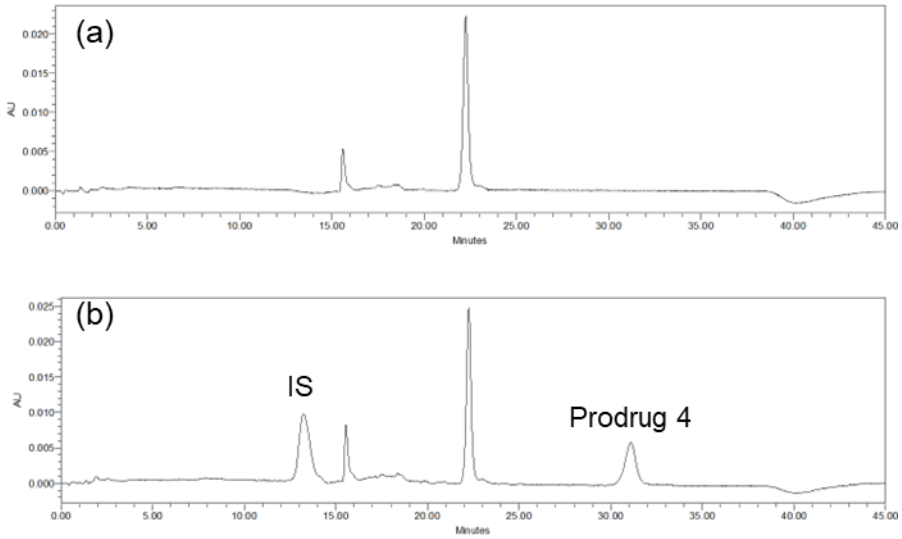

Figure 3- 11 Representative chromatograms of HPLC-UV. (a) rat plasma blank sample at λ = 319 nm and (b) rat plasma spiked with prodrug 4 and IS at the concentration of 5 μM and 5,000 ng/mL, respectively, at λ = 319

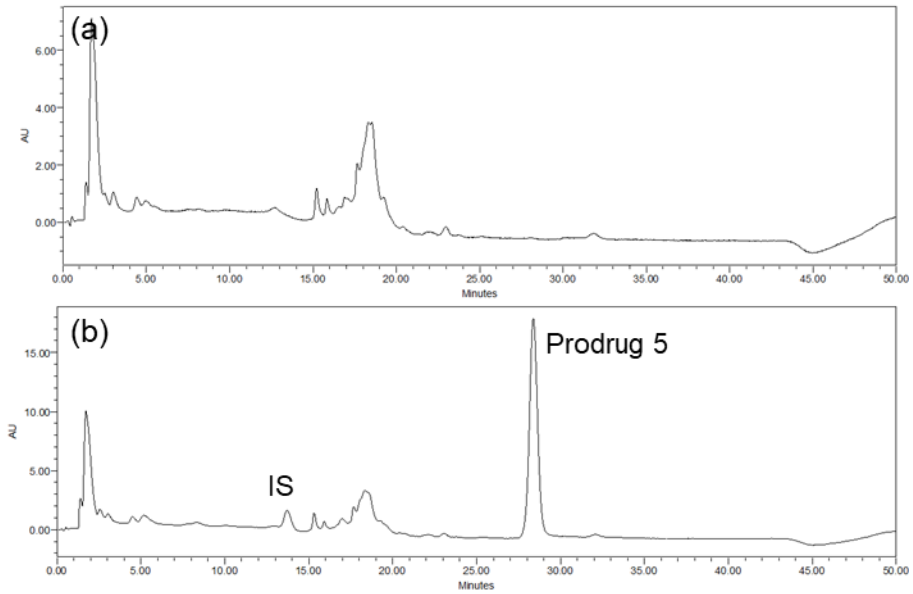

Figure 3- 12 Representative chromatograms of HPLC-UV. (a) rat plasma blank sample at λ = 319 nm and (b) rat plasma spiked with prodrug 5 and IS at the concentration of 5 μM and 5,000 ng/mL, respectively, at λ = 319.

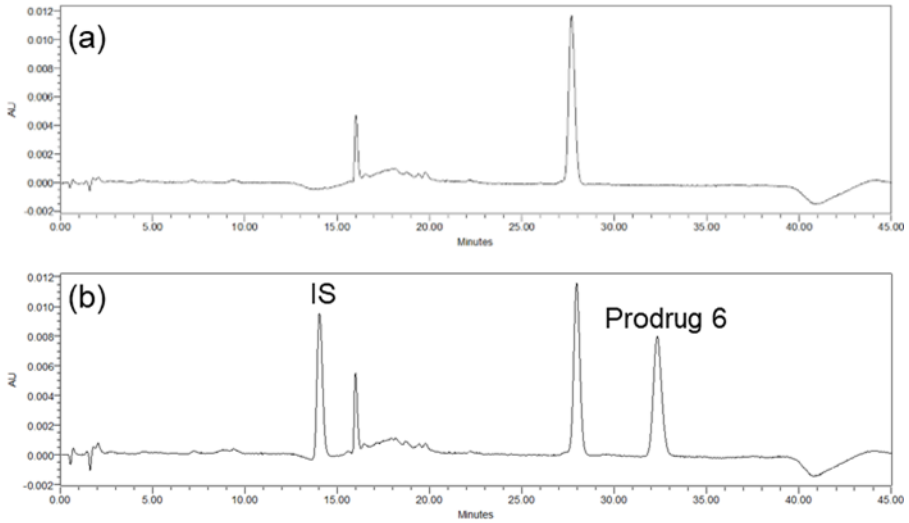

Figure 3- 13 Representative chromatograms of HPLC-UV. (a) rat plasma blank sample at λ = 319 nm and (b) rat plasma spiked with prodrug 6 and IS at the concentration of 5 μM and 5,000 ng/mL, respectively, at λ = 319.

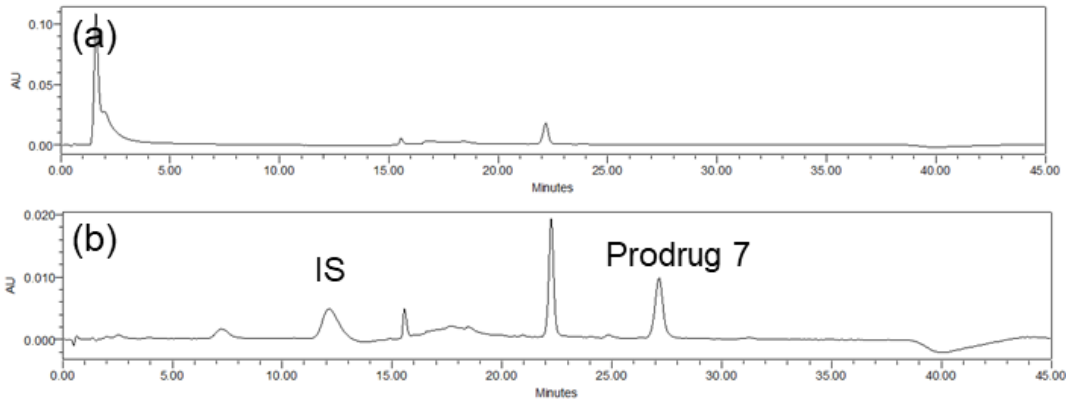

Figure 3-14 Representative chromatograms of HPLC-UV. (a) rat plasma blank sample at λ = 319 nm and (b) rat plasma spiked with prodrug 7 and IS at the concentration of 5 μM and 5,000 ng/mL, respectively, at λ = 319.

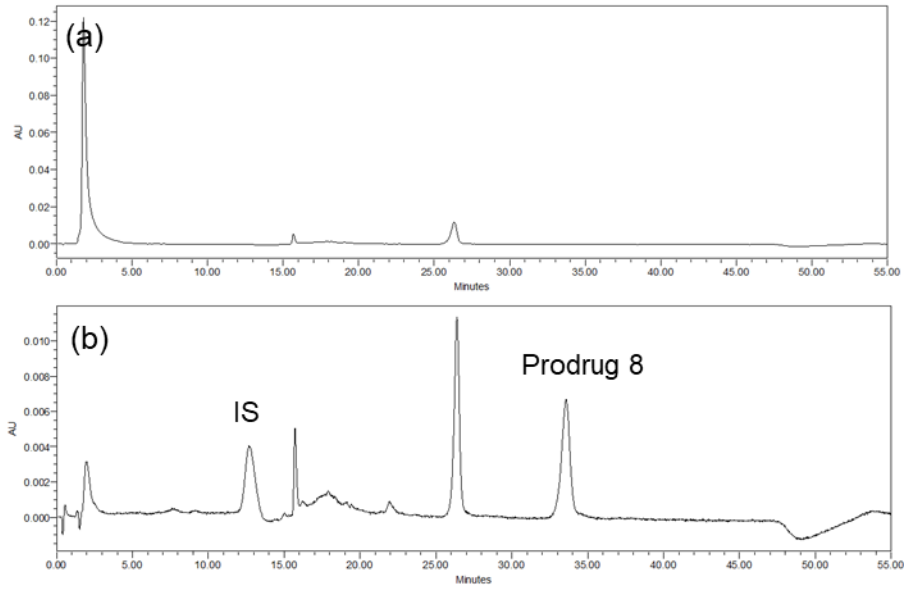

Figure 3-15 Representative chromatograms of HPLC-UV. (a) rat plasma blank sample at λ = 319 nm and (b) rat plasma spiked with prodrug 8 and IS at the concentration of 5 μM and 5,000 ng/mL, respectively, at λ = 319.

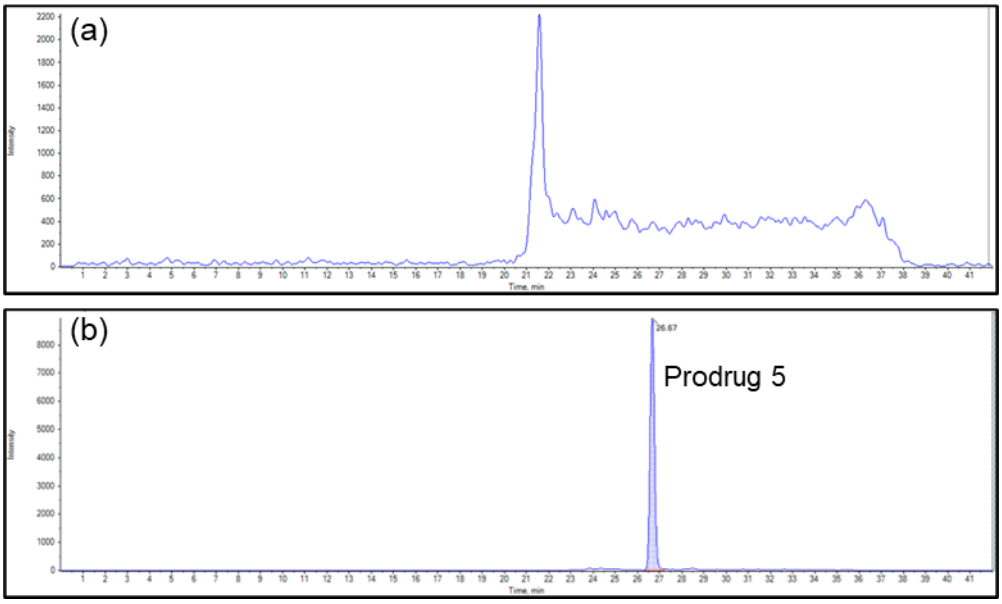

Figure 3- 16 Representative LC-MS/MS extracted ion chromatograms of (a) blank rat plasma monitoring at the product ion of m/z 449.4/241.3 and (b) rat plasma spiked with prodrug 5 at the concentration of 100 ng/mL, monitored at the product ion of m/z 449.2/241.3.

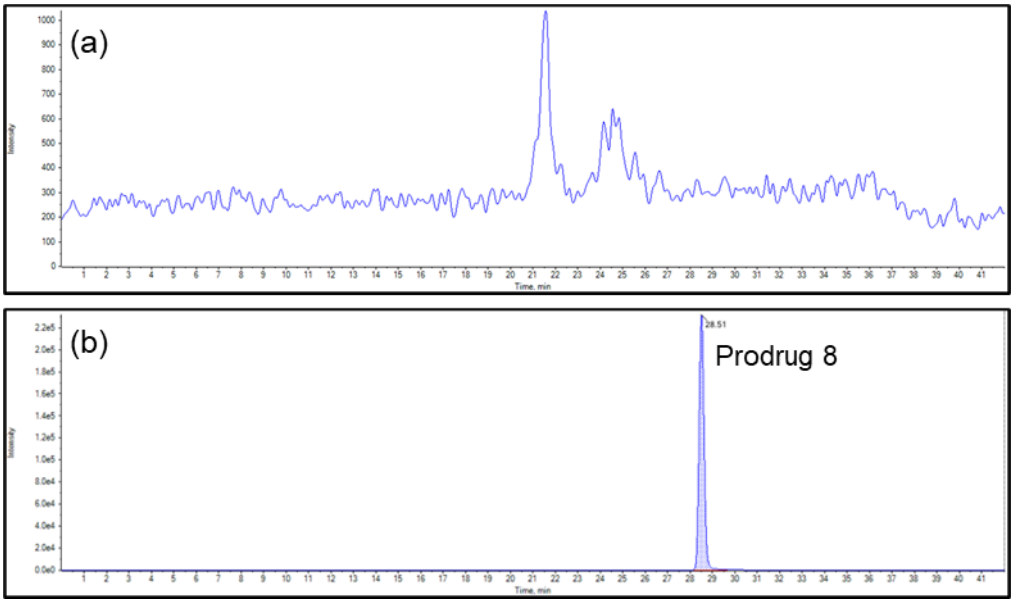

Figure 3- 17 Representative LC-MS/MS extracted ion chromatograms of (a) blank rat plasma monitoring at the product ion of m/z 503.5/241.3 and (b) rat plasma spiked with prodrug 8 at the concentration of 100 ng/mL, monitored at the product ion of m/z 503.5/241.3.

The sensitivity, linearity and accuracy of the bioanalytical methods using HPLC-UV for the determination of the concentrations of prodrugs 1-8 in rat plasma samples are summarised in **Table 3- 11** to **Table 3- 18**. The results show that 0.3 μM was the LLOQ of these assays. The LLOQ, linearity and accuracy of the bioanalytical methods using LC-MS/MS for determining the concentration of prodrugs 5 and 8 in rat plasma

samples were summarised in **Table 3- 19** and **Table 3- 20**. The results show the LLOQ of prodrugs 5 and 8 was 1.25 ng/mL using the LC-MS/MS.

Table 3- 11 The validation of LLOQ and linearity of prodrug 1 using HPLC-UV bioanalytical method.

Nominal Concentration (μM)	Cal. Conc. (μM)	ER (%)	RSD (%) (inter-day, n = 4)	Linear Regression	
10	9.9	-1.1		Slope	0.439954
5	5.1	1.3		Intercept	-0.06428
2.5	2.4	-4.3		r^2	0.998695
2	2.0	-0.3			
1	0.9	-10.7			
0.5	0.6	18.0			
0.3	0.4	22.2	8.7		

Table 3- 12 The validation of LLOQ and linearity of prodrug 2 using the HPLC-UV bioanalytical method.

Nominal Concentration (μM)	Cal. Conc. (μM)	ER (%)	RSD (%) (inter-day, n = 4)	Linear Regression	
10	10.9	10.9		Slope	0.344528
5	5.0	5.0		Intercept	0.039727
2.5	2.4	2.4		r^2	0.998047
2	2.2	2.2			
1	1.0	1.0			
0.5	0.4	0.4			
0.3	0.3	0.3	9.3		

Table 3- 13 The validation of LLOQ and linearity of prodrug 3 using HPLC-UV bioanalytical method.

Nominal Concentration (μM)	Cal. Conc. (μM)	ER (%)	RSD (%) (inter-day, n = 4)	Linear Regression	
10	9.3	-7.1		Slope	0.180251
5	7.6	8.3		Intercept	0.03868
2.5	5.7	14.2		r^2	0.991292
2	2.4	-4.1			
1	0.8	-17.0			
0.5	0.5	-7.1			
0.3	0.4	18.7	2.2		

Table 3- 14 The validation of LLOQ and linearity of prodrug 4 using the HPLC-UV bioanalytical method.

Nominal Concentration (μM)	Cal. Conc. (μM)	ER (%)	RSD (%) (inter-day, n = 4)	Linear Regression	
10	10.7	7.1		Slope	0.304874
5	5.0	1.0		Intercept	-0.02937
2.5	2.4	-6.0		r^2	0.998939
2	2.1	3.4			
1	1.0	-2.7			
0.5	0.5	2.0			
0.3	0.3	16.2	9.6		

Table 3- 15 The validation of LLOQ and linearity of prodrug 5 using HPLC-UV bioanalytical method.

Nominal Concentration (μM)	Cal. Conc. (μM)	ER (%)	RSD (%) (inter-day, n = 4)	Linear Regression	
10	9.8	-1.7		Slope	2.376726
7	7.4	6.3		Intercept	-0.27596
5	4.8	-4.1		r^2	0.998129
2.5	2.3	-7.8			
1	1.0	0.6			
0.5	0.5	9.3			
0.3	0.4	22.2	9.9		

Table 3- 16 The validation of LLOQ and linearity of prodrug 6 using HPLC-UV bioanalytical method.

Nominal Concentration (μM)	Cal. Conc. (μM)	ER (%)	RSD (%) (inter-day, n = 4)	Linear Regression	
10	9.8	-1.5		Slope	0.254421
5	5.3	5.6		Intercept	0.04471
2.5	2.4	-4.9		r2	0.999079
2	1.9	-0.8			
1	1.0	0.5			
0.5	0.4	-15.2			
0.3	0.2	-20.3	11.1		

Table 3- 17 The validation of LLOQ and linearity of prodrug 7 using HPLC-UV bioanalytical method.

Nominal Concentration (μM)	Cal. Conc. (μM)	ER (%)	RSD (%) (inter-day, n = 4)	Linear Regression	
10	10.5	5.2		Slope	0.095547
5	4.2	-16.3		Intercept	-0.00428
2	2.1	6.2		r^2	0.987066
1	1.2	17.4			
0.5	0.6	16.5			
0.3	0.2	-28.0	6.6		

Table 3- 18 The validation of LLOQ and linearity of prodrug 8 using the HPLC-UV bioanalytical method.

Nominal Concentration (μM)	Cal. Conc. (μM)	ER (%)	RSD (%) (inter-day, n = 4)	Linear Regression	
10	10.2	1.8		Slope	0.251304
5	5.1	2.3		Intercept	-0.02023
2.5	2.0	-19.5		r^2	0.988817
2	2.3	15.3			
1	1.0	0.0			
0.5	0.5	4.4			
0.3	0.3	14.5	20.2		

Table 3- 19 The validation of LLOQ and linearity of prodrug 5 using the LC-MS/MS bioanalytical method.

Nominal concentration (ng/mL)	Calculated concentration (ng/mL)	Accuracy (RE, %)	RSD (%) (inter-day, n = 6)	Linear regression	
1.25	1.41	12.8	16.1	Slope	0.00280
2.5	3.49	39.6		Intercept	0.00497
5	5.54	10.8		R^2	0.99473
8	6.88	-14.0			
16	14.46	-9.6			
20	18.05	-9.8			
50	50.57	1.1			
100	107.47	7.5			
200	206.85	3.4			

Table 3- 20 The validation of LLOQ and linearity of prodrug 8 using the LC-MS/MS bioanalytical method.

Nominal concentration (ng/mL)	Calculated concentration (ng/mL)	Accuracy (RE, %)	RSD (%) (inter-day, n = 6)	Linear regression	
1.25	1.22	-2.4	2.26	Slope	0.00693
2.5	2.34	-6.4		Intercept	0.00689
5	4.69	-6.2		R^2	0.99613
8	8.89	11.125			
16	16.32	2.0			
20	19.11	-4.45			
50	49.49	-1.02			
100	112.89	12.89			
200	187.56	-6.22			

3.4.5.2 Stability of prodrugs in storage conditions

In the pharmacokinetic and biodistribution studies of prodrugs 5 and 8 (**Chapter 5**), plasma collected from animals was stored in Eppendorf tubes that were pre-spiked with NaF (final concentration 10 mg/mL) and EDTA (1% 1.5 M) and stored on ice. The addition of NaF aimed to prevent the enzymatic hydrolysis of prodrugs in the plasma [192]. **Figure 3- 18** shows that prodrugs 5 and 8 were stable in the rat plasma with the presence of NaF and EDTA. In addition, no IMQ that could be released from prodrugs was observed.

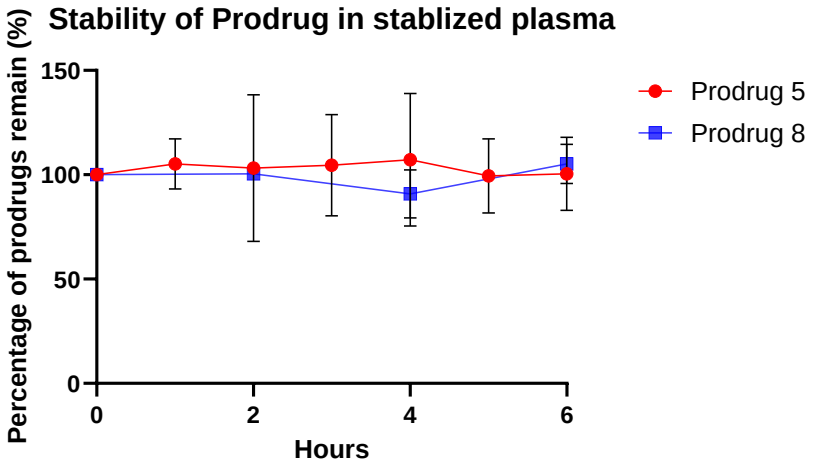

Figure 3- 18 Stability of prodrug 5 and prodrug 8 in stabilised plasma (containing NaF at 10 mg/mL) on ice.

On the day of bioanalysis, plasma samples that contained prodrugs 5 or 8 were processed for LC-MS/MS analysis. After the sample preparation, prodrugs were reconstituted in 65:35 water/MeOH and stored in the autosampler (4 °C) until being injected (within 24 h) into LC-MS/MS. Therefore, the stability of prodrugs in the reconstituted solvent in the autosampler was also assessed. **Table 3-21** shows that prodrugs 5 and 8 were stable in the autosampler.

Table 3-21 Stability results of prodrugs 5 and 8 in autosampler.

Compound	Concentration (ng/mL)	Autosampler stability (4 °C, 24 h) (n = 6)	
		Accuracy (RE, %)	Precision (RSD, %)
Prodrug 5	1.25	17.4	10.8
Prodrug 8	1.25	6.8	14.2

3.5 Discussion

To date, a number of analytical methods for the determination the concentration of imiquimod (IMQ) in non-biological samples [212–214] and biological samples [216,217] using HPLC-UV [140,216,218,219] or LC-MS/MS [220–222] have been developed. However, to the best of our understanding, no bioanalytical methods have been generated and validated for the determination of the concentrations of IMQ in the rat plasma samples. A robust, convenient and sensitive bioanalytical method is a cornerstone for pharmacokinetic (PK) and biodistribution (BD) studies. Therefore, in this chapter, we aimed to establish a bioanalytical method for IMQ, which can be used for the continuous PK and BD studies in **Chapter 4** and **Chapter 5**.

3.5.1 Bioanalytical method for the determination of IMQ using HPLC-UV

The development of the analytical method for IMQ was initiated with an HPLC-UV system. **Figure 3-2 A** shows that at a wavelength of 226 nm, IMQ has the highest UV absorbance, resulting in a higher sensitivity of detection compared to other wavelengths. This result was consistent with the previously reported HPLC-UV analytical method of IMQ [214]. However, in the previous analytical methods, only a relatively clean non-biological matrix was involved [212–214]. In biological matrices, such as plasma, there are substantial amounts of nucleotides and nucleosides, which also have large UV absorbance at wavelengths of 220 to 240 nm [216]. Therefore, in the current method, a wavelength of 319 nm was selected to monitor the chromatography of IMQ, avoiding the interference of the endogenous substances. **Figure 3-2 B** shows that the hydrophilicity of IMQ was increased with the decrease of pH, suggesting that the drug molecules will be ionised in an acidic environment. During

preliminary studies, both acidic (10 mM ammonium formate, pH = 3) and alkaline (10 mM ammonium acetate, pH = 10) buffers were tested to select the best pH range of this method. Results showed that the peak of IMQ was symmetric and without tailing when either acidic or alkaline buffer was used as the mobile phase (**Figure 3-3**). However, the retention time of IMQ using the alkaline buffer (25.6 min) was significantly longer than it was using the acidic buffer (5.1 min), suggesting the pH conditions dramatically influence the elution of IMQ. As a result, the acidic pH was selected to promote a fast elution of IMQ without tailing.

It should be noted that this bioanalytical assay was developed for *in vivo* studies. It means that the health and safety of animals (e.g. the maximum blood volume that can be safely sampled from rats) should be carefully considered when deciding the volume of matrix used in the assay. During the initial experiment, we aimed to use a higher volume of plasma to improve the LLOQ of this assay. Results showed that no endogenous interference was observed with 100 µL or 120 µL of plasma in comparison to 150 µL of plasma, where a clear interference was noticed (**Figure 3-4**). Therefore, 120 µL of plasma was selected as a sample volume for this current method. The validation of selectivity showed that IMQ was well-separated from endogenous interference in rat plasma, indicating minimum matrix effect and absence of carryover (**Figure 3-6**). Moreover, this current HPLC-UV method also demonstrated good linearity and accuracy across intra-day runs (**Table 3-7**). Most importantly, this assay was validated for the quantification of IMQ in the plasma at a concentration range of 15 – 5,000 ng/mL (**Table 3-5**), which is more sensitive than most previously reported methods [215,216,219]. Soria *et al.* previously reported an analytical method for determining the concentration of IMQ in human plasma with an LLOQ at 1 ng/mL [140].

However, in their assay, 1 mL of serum (a.k.a around 2 mL of blood) was used to achieve this sensitivity, which is not realistic to be used for studies in rodents.

3.5.2 Bioanalytical method of IMQ using LC-MS/MS

In **section 3.5.1**, an HPLC-UV bioanalytical method for the determination of IMQ in rat plasma with an LLOQ at 15 ng/mL was developed. However, it was reported that the absolute oral bioavailability of IMQ in rodents is zero [140]. This suggested that a more sensitive bioanalytical method was required to complete the pharmacokinetics (PK) of the drug in rats. Therefore, tandem mass spectrometry (MS/MS) was introduced to improve the sensitivity of the current method.

Different from the UV detector, the MS/MS can selectively monitor only the product ions of analytes. It allows for the flexibility to shorten the total run time without concerns about the overlap between the peak of IMQ and peaks of potential interferences. Therefore, in the initial experiments, an empirical LC gradient method (**Table 3-1**) was used for the elution of IMQ. However, it was found that a substantial amount of IMQ remained in the column using this empirical elution method (

Table 3-4). Other elution methods, such as an isocratic elution method using a 50:50 MeOH/ buffer (10 mM ammonium formate, pH = 3), have been tested to avoid the carryover of IMQ. Unfortunately, none of these attempts diminished the carryover of IMQ. As a result, the same elution method designed for the HPLC-UV bioanalytical assay was applied to the LC-MS/MS system, resulting in a minimum matrix effect and absence of carryover (**Figure 3- 7**).

The validation of sensitivity and linearity showed that this current LC-MS/MS method can accurately and precisely quantify IMQ in rat plasma at concentrations range of 1.25 – 200 ng/mL (**Table 3-6** and **Table 3-8**). Most importantly, the LLOQ of this assay

(1.25 ng/mL) was more sensitive in comparison to our HPLC-UV method (LLOQ = 15 ng/mL) and previously reported LC-MS/MS method (LLOQ = 10 ng/mL) [220]. Additionally, the previously reported method requires processing biological samples with a strong cation exchange solid phase extraction to avoid endogenous interferences and improve recovery. In our assay, IMQ was efficiently and rapidly extracted using methyl *tert*-butyl ether with a recovery of over 85 % [220].

Previously, Kim *et al.* developed an LC-MS/MS analytical method for the determination of IMQ at a range of 780 – 50,000 ng/mL in non-biological samples [219]. However, we noticed that the linearity of calibration curves generated using our mass spectrometry system (AB Sciex API Qtrap4000) significantly decreased when the concentration was above 200 ng/mL. Therefore, for samples with an IMQ concentration exceeding 200 ng/mL, a 20-fold dilution with plasma was applied. **Table 3-9** shows that the dilution of the sample did not affect the accuracy and precision of the bioanalysis, suggesting the range of detection was extended from 1.25 – 200 ng/mL to 1.25 – 4,000 ng/mL with dilution.

The current assay takes 40 minutes for each run. This suggests that samples need to be stored at -80 °C or autosampler for days before bioanalysis. **Table 3-10** indicate IMQ has excellent stability in storage conditions. This result is consistent with a previous report that degradation of IMQ was not observed in most storage conditions but was only found in the presence of strong oxidants [215]. As a result, the good stability of IMQ indicates the feasibility of using this current LC-MS/MS assay for bioanalysis in preclinical studies.

3.5.3 Bioanalytical method for prodrugs

Due to the fast elution of IMQ in the first 10 min, the bioanalytic method of IMQ can be easily adjusted for bioanalysis of prodrugs. Results showed that with an extension of the gradient method, peaks of prodrugs can be well-separated from endogenous interference (**Figure 3-8** to **Figure 8-15**). As a result, these bioanalytical methods can determine the concentrations of IMQ and its prodrugs within the same run.

The validation of sensitivity and linearity showed that bioanalytical methods described in **section 2.8.2.1 and section 2.8.3** could be used to determine the concentrations of the prodrugs 1-8 at the range of 0.3 – 10 µM using the HPLC-UV system (**Table 3-11** to **Table 3- 18**). The LLOQ of these assays (0.3 µM) was sensitive enough to complete the *in vitro* and *ex vivo* experiments for prodrugs in **Chapter 5**.

Additionally, the LLOQ of the analytical methods for prodrugs 5 and 8 was improved using the LC-MS/MS system to 1.25 ng/mL, allowing the application of this assay for *in vivo* studies.

To accurately describe the PK parameters of prodrugs 5 and 8 following intravenous bolus or oral administration, it was important to develop suitable storage conditions for samples that contain prodrugs. These conditions were expected to prevent the degradation of the prodrugs and the release of the parent drug in rat plasma or reconstitution solvent. Fluoride is a strong inhibitor of esterase, lipase and amide hydrolase [223–225]. In previous studies, sodium fluoride (NaF) was added to human or rat plasma to prevent the hydrolysis of unstable compounds [226]. Results showed that NaF could also prevent the hydrolysis of prodrugs 5 and 8 in rat plasma (**Figure 3- 18**). Therefore, in the PK and BD study for prodrugs, sample collection tubes were pre-spiked with NaF (10 mg/mL) to prevent the hydrolysis of prodrugs. Additionally, it

was found that prodrugs 5 and 8 were also stable in reconstitution solvent in autosampler, suggesting that the current LC-MS/MS bioanalytical method for prodrugs 5 and 8 can also be used for the preclinical research in **Chapter 5**.

3.6 Conclusion

In this chapter, two bioanalytical methods for the determination of the concentration of IMQ in rat plasma were developed. The two methods reported in this work have been partially validated with good selectivity, sensitivity, linearity and accuracy. The HPLC-UV method with an LLOQ at 20 ng/mL is technically simple to perform and can be reliably used in most in vitro or ex vivo studies involving the quantification of IMQ. In addition, a more sensitive bioanalytical method for IMQ using LC-MS/MS was also developed in this work. With the tandem mass spectrometry detector, the concentration of IMQ in the plasma as low as 1.25 ng/mL can be accurately quantified. Therefore, this method can be used in the preclinical pharmacokinetic and biodistribution studies of IMQ.

Chapter 4 Pharmacokinetics and biodistribution of imiquimod in rats

4.1 Introduction

Dendritic cells (DCs), being one of the most potent antigen-presenting cells, can activate the immune system against tumours via cross-presenting tumour-related antigens (TAAs) on the MHC II to other lymphocytes, such as naïve T cells [111,119,122]. The ability of DCs to present TAAs is dependent on the maturation of the cell. In colorectal cancer (CRC) patients, the maturation of DCs is downregulated by tumour cells in both solid tumours and lymph nodes that drain lymph from the tumour regions. As a result, the polarisation of naïve T cells to cytotoxic T cells and T helper cells is diminished, limiting the anti-cancer immune response [93,120]. The programmed cell death protein and programmed death ligands (PD-1/PD-L1) and cytotoxic T-lymphocytes antigen 4 (CTLA-4) are well-known checkpoint inhibitors. It was reported that a low therapeutic response was found in cancer patients who received only immune checkpoint inhibitors without immune adjuvants [79]. The low therapeutic effects of checkpoint inhibitors may be attributed to immune suppression by tumour cells, suggesting the addition of immune activators to cancer treatment is necessary.

Imiquimod (IMQ) is a small molecule of toll-like receptor 7 (TLR7) agonist. Its ability to stimulate immature dendritic cells (DCs) to transition into mature DCs is a critical factor in its therapeutic potential as an anti-cancer immunomodulator [131,141,207,227]. In a phase I clinical trial, IMQ was found to stimulate a detectable level of immunostimulatory cytokines following the oral administration of the drug. However, no therapeutic effects of IMQ were observed in cancer patients. Additionally, dose-dependent adverse effects, such as flu-like symptoms, of IMQ were reported [133,139].

These results could potentially suggest that IMQ was not specifically delivered into targeted areas, such as lymph nodes which are enriched in immature dendritic cells and lymphocytes [154,228].

To the best of our understanding, the reported pharmacokinetics (PK) data of IMQ are limited, especially in rodent models. Previously, several studies have investigated advanced delivery platforms for IMQ using nanoparticles and liposomes through a parenteral injection [201,208–211,229–232]. However, none of them described the PK parameters of IMQ when free drug molecules (a.k.a. without nanoparticles) were administered to animals *via* intravenous injection or oral administration. It may be related to the poor solubility of IMQ in commonly used formulation vehicles, resulting in difficulties in developing a safe injectable formulation for IMQ [233]. It should be noted that the PK profile following the IV administration of free drug molecules is generally considered the best way to describe the fundamental PK parameters of an API, providing a direct measurement of drug distribution, metabolism and elimination without the complexity introduced by formulations of the drug.

TMX-101 is an injectable formulation developed by Falke *et al.* [137]. The composition of TMX-101 has not been reported, and unfortunately, TMX-101 is not commercially available. Previously, IMQ was dissolved in 0.1 N HCl for subcutaneous injection into humans [140]. However, due to the acidic pH of 0.1 N HCl, this formulation is unsuitable for administering to rodents *via* an intravenous (IV) bolus administration. Yan *et al.* have developed a solution that contains 10 % DMSO for IMQ IV formulation. The authors did not mention any observed side effects of this formulation; however, we were concerned about the safety of this formulation since it contains such a high percentage of DMSO. Therefore, in this chapter, we first aimed to develop a safer formulation for IMQ that would allow us to generate the PK parameters of the drug in

rats. Then, the PK parameters of IMQ were calculated following IV and oral administration of the drug.

A few studies have been done for the targeted delivery of IMQ to lymph nodes (LNs) [201,208–211,229–232]. However, none of them reported the distribution of IMQ into the intestinal LNs, such as mesenteric lymph nodes (MLNs) and iliac lymph nodes (ILNs). MLNs and ILNs drain lymph from the colorectal and retroperitoneal regions and are primary reservoirs of DCs and lymphocytes (**Figure 1-1, Chapter 1**), suggesting they are important targets for IMQ [27,153,234]. It was previously shown that small molecules can be delivered into intestinal LNs following oral administration [190–192]. Therefore, in this chapter, the intestinal lymphatic absorption of IMQ and biodistribution of the drug in the intestinal LNs following oral administration were assessed. Additionally, the data generated in this chapter was used as a control/comparison group for IMQ prodrugs reported in **Chapter 5**.

4.2 Experimental design

The *in silico* and *in vitro* assessment of IMQ affinity to CMs were performed as described in **Sections 2.2, 2.4** and **Sections 2.6**. Samples generated in these sections were processed for bioanalysis using a validated HPLC-UV bioanalytical method reported in **Chapter 3**. Studies of IMQ were conducted as described in **sections 2.7.3** and **2.7.4** using the formulation developed in **Section 2.7.1.1**. *In vivo* samples were analysed using a validated LC-MS/MS bioanalytical method, as described in **Chapter 3**. The scheme of work is shown in **Figure 4-1**.

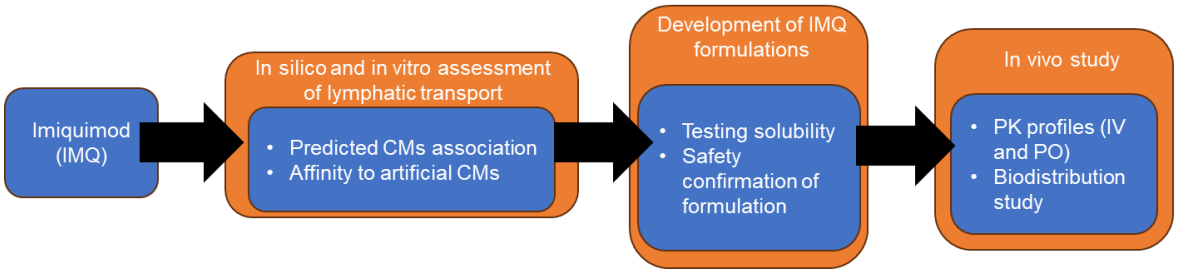

Figure 4-1 Schematic diagram of experimental design for generating pharmacokinetic profiles of IMQ.

4.3 Results

4.3.1 Physicochemical properties, predicted affinity to CMs and association with artificial CMs of IMQ

The physicochemical properties of IMQ were calculated using ACD/I-Lab and inputted into a previously reported *in silico* model to predict the affinity of IMQ to CMs (**Table 4-1**) [182]. It showed that IMQ is a moderately lipophilic compound (Log P = 3.46) and is not ionised in the plasma (Log P – Log $D_{7.4}$ = 0). The affinity of IMQ to artificial CMs was also assessed to confirm the *in silico* result following a previous protocol (**Table 4-1**) [181]. Both *in silico* and *in vitro* results showed that IMQ has a very limited affinity to CMs. Moreover, the triglyceride solubility of IMQ was 7.4 ± 1.0 μg/mL measuring with olive oil. These results strongly suggest a meagre chance of IMQ being absorbed into intestinal lymphatic systems following oral administration by the mechanism of association with CMs.

Table 4-1 The physicochemical properties and the CMs affinity of IMQ.

Tested compound	Log D 7.4[c]	Log P[c]	Log P - Log D	PSA[a,c]	H-Acceptors[c]	FRB[b,c]	Density[c]	Molar Volume[c]	H-Donors[c]	Predicted CM association (%)	Association with artificial CM (%)[d]
IMQ	3.46	3.46	0	86.11	7	19	1.28	187.7	1	1.81	< 1.78

[a] Polar surface area; [b] Free rotatable bond;
[c] Calculated by ACD/I-lab
[d] The artificial CMs association was determined by the LLOQ of the IMQ analytical method (15 ng/mL) using the HPLC-UV analytical method reported in **Chapter 3**.

4.3.2 Development of a safety formulation for imiquimod animal study

The solubilisation of 8 mg of IMQ powder in 1 mL of tested formulation vehicles was assessed and listed in

Table 4- 2. Complete dissolution was assessed by the absence of drug powder in the tested vehicles, following the determination of the IMQ concentration in the vehicles using the HPLC-UV bioanalytical method as described in **Section 2.7.1.1**.

It was found that commonly used formulation vehicles, including water, normal saline, ethanol, propylene glycol (PG), and polyethene glycol 200 (PEG 200), are inadequate for preparing an oral formulation of IMQ at a concentration of 8 mg/mL. The calculated pKa of IMQ (7.3) indicates that it is a weak base, suggesting that the solubility of IMQ may be increased in acidic formulation. Herein, 0.05 N HCl solution was selected as the most appropriate formulation vehicle for the IMQ oral formulation.

Table 4- 2 The results of the solubilisation of IMQ in tested formulation vehicles and the pH of the formulation.

Tested formulation	Sterilised water	Normal Saline	Ethanol/water (20:80, v/v)	PG[a]	PEG 200[b]	0.1 N HCl	0.05 N HCl	0.025 N HCl
Dissolved (Y/N)[c]	N	N	N	N	N	Y	Y	N
pH	5.6	5.6	N/A[d]	10.2	5.7	1.2	1.8	2.1

[a] propylene glycol glycol;
[b] polyethylene glycol 200;
[c] The dissolution test of IMQ was performed by dissolving 8 mg of IMQ powders into 1 mL of tested vehicles and stirring for up to 24 h in a 37℃ water bath. The dissolution was identified as the absence of drug powders in tested vehicles following HPLC-UV analysis of the concentration of IMQ in dissolved solution.
[d]N/A did not measure

For developing an intravenous (IV) formulation of IMQ at a concentration of 0.8 mg/mL, solubilisation experiments were repeated and mirrored those procedures performed for the development of the oral formulation. Apart from the HCl solution, the solubilities of IMQ in tested vehicles were lower than 0.8 mg/mL. Apparently, due to the low pH of the HCl solution (< 2.5), it was unsuitable for IV administration. Alternatively, we decided to prepare the IMQ IV formulation *via* a 10-fold dilution of the IMQ oral formulation (8 mg/mL in 0.05 N HCl) with water, PG, or a water-PG mixture, followed by adjusting its pH to a safe range (6 - 8). As a result, it was found that diluting the oral formulation with an 80:20 water/PG (v/v) mixture and adjusting the pH to 6 - 6.5 with a small amount of 4 N NaOH (less than 5 µL) was the current optimal approach.

4.3.3 Pharmacokinetics of IMQ in rats

The pharmacokinetic profiles of IMQ in plasma were generated following IV bolus administration and oral (PO) administration (without or with the presence of lipids) in rats (**Figure 4-2**). In **Figure 4-2** panel (A), the concentration-time profile after IV bolus administration is plotted at a semi-logarithmic scale (log concentration vs. linear time).

This approach effectively represents a wide range of drug concentrations, particularly in IV bolus administration. This is because the concentration of IMQ was initially very high but decreased to very low levels in the later phase following the IV bolus administration of the drug. The semi-logarithmic scale provides a clear visualisation of the first-order elimination kinetics of IMQ. Similarly, the concentration-time profile following oral administration is plotted at a semi-logarithmic scale in panel (B) to maintain consistency in data presentation across both panels.

Pharmacokinetic parameters derived from plasma concentration-time profiles are summarised in **Table 4- 3**.

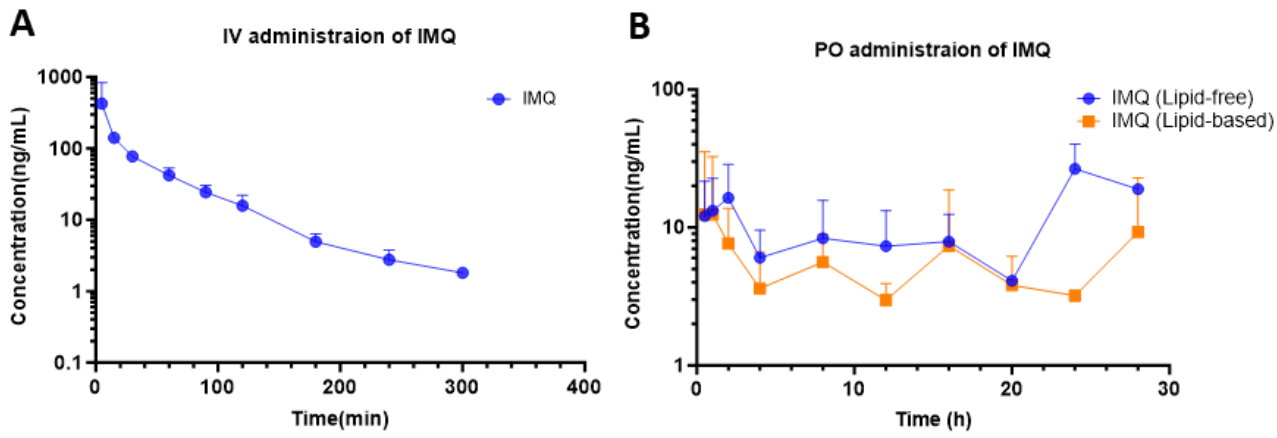

Figure 4-2 Plasma concentration-time profile in rats following administration of IMQ (mean ± SD). Panel (A) shows IV bolus of IMQ (0.8 mg/Kg, n=4); Panel (B) shows Oral administration of IMQ (8 mg/Kg) in lipid-free formulation (n=6) and with lipids (n=5).

The concentration of IMQ was lower than LLOQ (1.25 ng/mL) at 360 mins following the IV bolus administration of IMQ (**Figure 4-2 A**). Following IV administration, a relatively short half-life of IMQ (0.73 ± 0.05 mins) was found. Interestingly, although the calculated Log P of IMQ is moderate (Log P = 3.46), the volume of distribution (V_{ss}) of IMQ after IV administration was very high (3376.3 ± 1842.0 mL/Kg) (**Table 4- 3**).

Table 4- 3 Pharmacokinetic parameters of IMQ following IV administration of IMQ (0.8 mg/Kg, n=4) and oral administration of IMQ (8 mg/Kg)) with lipid (n=5) and without lipid (n=6) (mean ± SD).Parameters were calculated with a non-compartmental approach.

Compound dose	**Imiquimod**		
Route of administration	IV	PO (lipid-free)	PO (lipid-based)
$AUC_{0\text{-}inf}$ (h·ng/mL)	203.2 ± 95.4		
$AUC_{0\text{-}last}$ (h·ng/mL)	200.7 ± 96.0	168.3 ± 90.0	136.3 ± 85.3
C_0 or C_{max} (ng/mL)	274.9 ± 60.9	26.7 ± 14.6	17.1 ± 10.9
CL (mL/h/kg)	4468.5 ± 1569.8	-	-
V_{ss} (mL/kg)	3376.3 ± 1842.0	-	-
$t_{1/2}$ (h)	0.73 ± 0.05	-	-
T_{max} (h)	-	0.5 - 28	2 - 28
F_{oral} (%)	-	8.3 ±4.5^{ns}	6.7± 4.2^{ns}

$AUC_{0\text{-}inf}$ area under the curve from time zero to infinity; $AUC_{0\text{-}last}$ area under the curve from time zero to the last observed time point (0 – 300 min for IV bolus administration of IMQ; 0 – 28 h for PO administration of IMQ); C_{max}, maximum observed concentration; C_0, concentration extrapolated to time zero; CL, clearance; V_{ss}, volume of distribution at steady state; $t_{1/2}$, half-life; F_{oral}, absolute oral bioavailability.
The absolute oral bioavailability was calculated with the AUC_{last} of IMQ IV bolus.
An unpaired two-tailed t-test was used to compare the F_{oral} of IMQ between lipid-based and lipid-free groups.

In addition to data analysis with the non-compartmental PK approach, the volume of distribution of IMQ following IV administration was also calculated using two-, -compartmental PK models.

Table 4-4 shows that the distribution volume in the central compartment (V1) for IMQ was very high.

Table 4-4 Two-compartment analysis of the volume of distribution of IMQ, prodrug5 and prodrug 8.

Compound dose	IMQ
Administration route	IV (n = 4)
$AUC_{0\text{-}inf}$ (h·ng/mL)	192.8 ± 83.79
CL (mL/h/kg)	4646.0 ± 1562.4
V_1 (mL/kg)	2228.4 ± 1472.2
V_2 (mL/kg)	1448.5 ± 594.7
V_{ss} (mL/kg)	3676.9 ± 1936.4
$t_{1/2}$ (h)	0.9 ± 0.1

$AUC_{0\text{-}inf}$, the area under the curve from time zero to infinity; CL, clearance; V_1. volume of distribution in compartment 1; V_2, volume of distribution in compartment 2; V_{ss}, volume of distribution at steady state; T_{max} maximum concentration; $t_{1/2}$, elimination half-life in ß phase .

In the preliminary study of IMQ oral administration groups (n = 7, using lipid-free formulation), no IMQ was detected at 36 hours. Therefore, in the full-scale PK study, the last sampling time point was 28 hours. The plasma concentration-time profiles of

IMQ following oral administration indicated that the oral absorption of IMQ is prolonged and erratic (**Figure 4-2 B**), resulting in the difficulty of identifying T_{max} clearly (**Table 4-3**). In addition, the oral absorption varied significantly among rats, resulting in substantial differences in IMQ concentrations. In some rats, IMQ concentrations were undetectable after 20 hours, while in others, they remained notably high. Considering the 3Rs (replacement, reduction, and refinement) principle in designing animal studies, we decided not to escalate the sample size to mitigate data variability or add extra sampling points between 28 and 36 hours. As a result, the elimination phase of IMQ following oral administration was not displayed in this study. The F_{oral} of IMQ was limited (< 10 %), and there is no difference found between the F_{oral} of the IMQ lipid-free group and the F_{oral} of the IMQ lipid-based group, suggesting that the presence of lipids did not facilitate the oral absorption of IMQ.

4.3.3 Biodistribution of IMQ following oral administration of IMQ in rats

The biodistribution (BD) of IMQ at apparent T_{max} points (1.5, 2, 6 and 28 h) following oral administration of unmodified IMQ with lipids is presented in **Figure 4-3**.

It should be noted that in this figure, the concentration of IMQ in plasma, serum, lymph fluid, and whole blood is shown in ng/mL, whereas the concentration of IMQ in tissues is reported in ng/g. We were aware that the statistical analysis in this figure involves comparing values with different units. However, previous reports indicated that the density of rat plasma, serum or lymph fluid is less than 1.006 g/mL, while the density of whole blood is approximately 1.056 g/mL [235–237]. Therefore, the concentrations of IMQ in the examined biofluids expressed as ng/mL can be approximately equated to ng/g, allowing for direct comparison in the statistical analysis. Additionally, the

concentrations of IMQ in the examined biofluids are presented as ng/g in the **Appendix** (**Figure Appx.-1**).

There was no statistical difference in the concentration of IMQ in plasma, serum and whole blood at 2 h and 28 h, suggesting a low intracellular distribution of IMQ in blood cells (**Figure 4-3 B and D**)

The distribution of IMQ into the high blood-perfused tissue (spleen, liver, kidney) and into the less well-perfused tissue (skeleton muscle and brain) was determined. It should be noted that the brain was initially separated into right and left hemispheres for analysis. However, there was no difference in the concentration of IMQ between the right and left brains. Therefore, only the concentration of IMQ in the whole brain is shown in **Figure 4-3**.

The concentrations of IMQ in all analysed tissue samples were highly variable. The average concentration of IMQ in the main organs (liver, kidney, spleen, and brain) at early time points (1.5 h to 2 h) was 6- to 9-fold higher than the average concentration of IMQ in plasma, suggesting that IMQ rapidly distributes into non-targeted regions following oral administration of the drug.

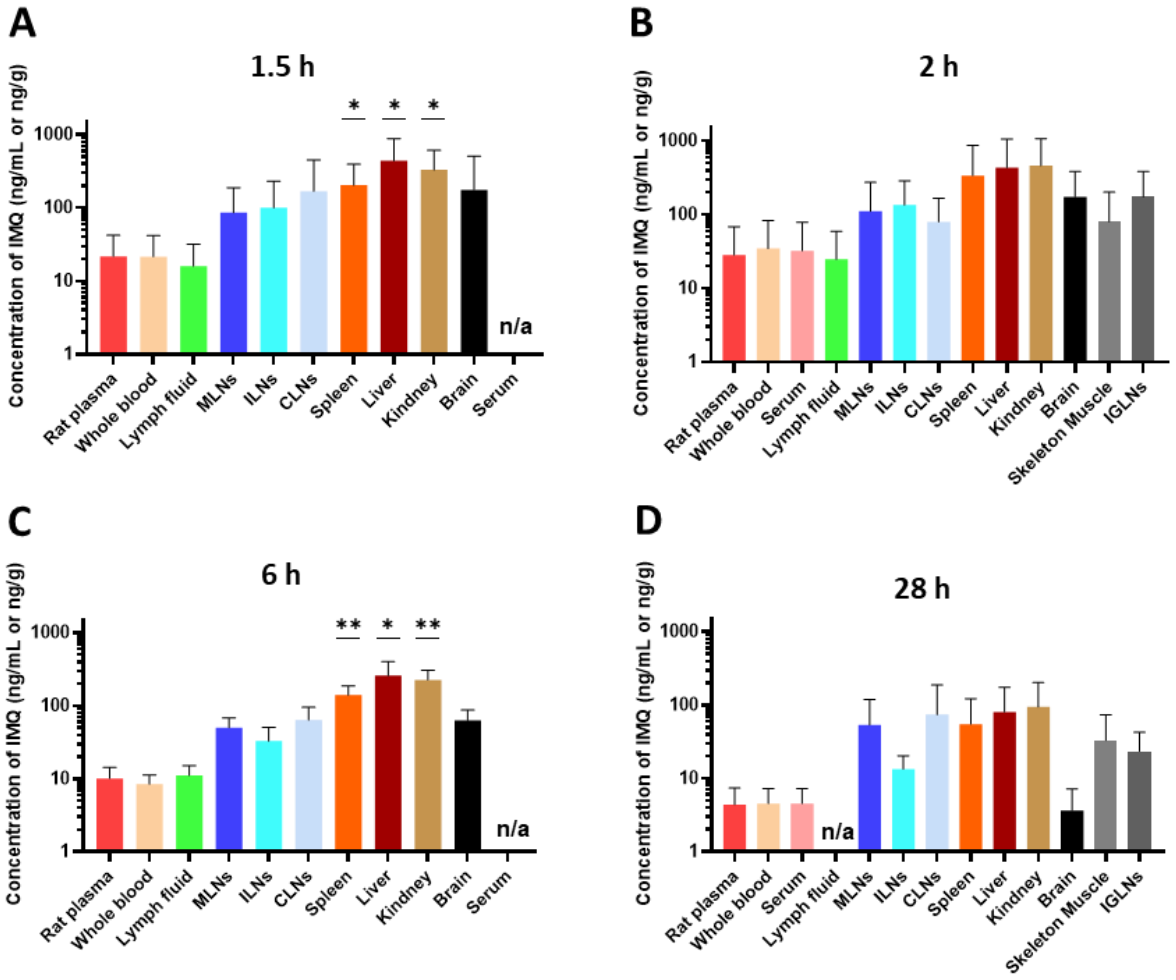

Figure 4-3 The biodistribution of IMQ following oral administration of IMQ (8 mg/kg) with lipids at local T_{max} 1.5 h, 2 h, 6 h and 28 h (mean ± SD, n = 4 to 6). MLN, mesenteric lymph node; ILNs, iliac lymph nodes; CLNs, cervical lymph nodes; IGLNs, inguinal lymph nodes. An unpaired t-test was used for the comparison of IMQ concentration in plasma and other samples. One-way ANOVA followed by Turkey's comparison was used to compare the concentration of IMQ in the plasma, serum and whole blood at 2 h and 28 h. **, $p < .05$*; ***,$p < .01$.* n/a: Samples were not collected.

Interestingly, although IMQ showed poor affinity to CM, the average concentrations of IMQ in mesenteric lymph nodes (MLNs) were 3.9-, 3.9-, 4.9- and 12-fold higher than the concentration of IMQ in plasma at 1.5 h, 2 h, 6 h and 28 h, respectively. Similarly, the average concentrations of IMQ in iliac lymph nodes (ILNs) were 4.5-, 4.7-, 3.1- and 3.0-fold higher than plasma at 1.5 h, 2 h, 6 h and 28 h, respectively. However, there is no statistical difference between the concentration of IMQ in the mesenteric lymph fluid and plasma.

The concentration of IMQ in the gastrointestinal (GI) tract was also assessed to understand the potential absorption window of IMQ in the GI tracts. After oral administration of IMQ, intestine contents (including both solids and liquid) were collected at 2 h and 28 h from small intestines (ilium and jejunum), large intestines (cecum and colon) and distal rectum (**Figure 4- 4**). It was shown that IMQ mainly remained in the small intestinal contents at 2 h. There was still a large amount of IMQ remaining within the intestinal lumen at 28 h.

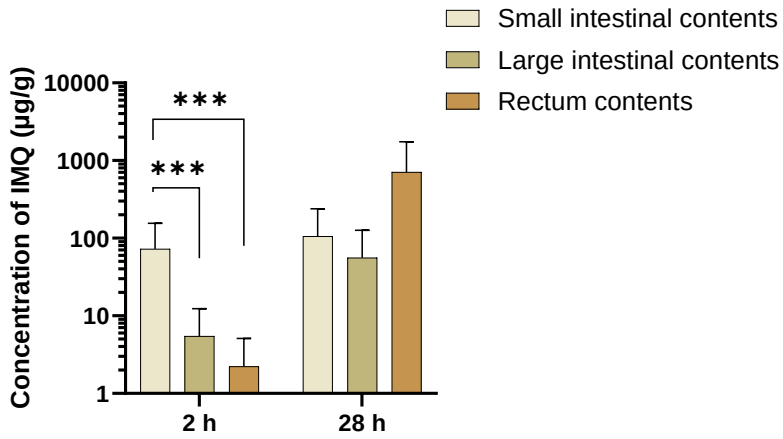

Figure 4- 4 The concentration of IMQ in small intestinal contents, large intestinal contents and rectal faeces at 2 h and 28 h following oral administration of IMQ (8 mg/kg) with lipids (n = 4). ***, p < .001.

4.4 Discussion

Imiquimod is a small-molecule of toll-like receptor 7 (TLR7) agonist. It is the first TLR agonist on the market as an immunomodulator for anti-cancer treatment. Previously, there were a large number of studies that have investigated the targeted delivery of IMQ to cancer-related regions [201,208–211,229–232]. However, none of them reported the details of the pharmacokinetic (PK) profiles of IMQ, as well as the distribution of the drug into intestinal lymph nodes, which are the primary targets for colorectal cancer. Therefore, in this work, we first described the PK parameters of IMQ

following IV and oral administration and the biodistribution of the drug into LNs and other tissues or organs.

4.4.1 Development of formulations for IMQ oral and intravenous administration

Imiquimod (IMQ) is a class IV molecule in the biopharmaceutical classification system, indicating its limited solubility in the GI tract and poor permeability across the intestinal epithelial cells when it is orally administered [238]. In general, a drug molecule with good oral bioavailability is correlated to its good solubility in the gastrointestinal (GI) tract [239,240]. This is because, in most cases, free drug molecules can be absorbed into epithelial cells and eventually enter the systemic circulation. By contrast, insoluble drugs stay as solid particles in the GI tracts, limiting their oral absorption. Previously, it was reported that IMQ has limited solubility in most commonly used solvents, such as water, ethanol and DMSO [233]. Therefore, developing an oral formulation that facilitates the solubility of IMQ is crucial for the application of IMQ in preclinical studies.

The oral dose of IMQ used in this study is 8 mg/kg, which was translated by allometric scaling from a previously reported clinical trial [140]. To minimise the volume of formulation administered to animals via oral gavage, the concentration of this formulation was designed to be at a concentration of 8 mg/mL. The solubility of IMQ in tested formulation vehicles suggested that its solubility increased when the pH of the formulation vehicles decreased (

Table 4- 2), aligning with previous findings [230,233]. Although hydrochloric acid is rarely used as a formulation vehicle for oral administration, the safety of HCl as an oral formulation vehicle was previously reported. It was shown that oral administration of 0.05 N HCl did not differ from saline in triggering gastric inflammatory response [241]. Moreover, dosing as high volume as 1 mL of low-concentration of HCl (0.05-0.35 N) orally to rats was able to protect their stomachs from necrotising agents [242]. In addition, in a clinical trial, a concentration of 0.1 N HCl was used as an injectable formulation for IMQ [140]. Based on these studies, 0.05 N HCl was selected as the optimal formulation vehicle for oral administration in the current study.

The intravenous (IV) bolus administration dose for IMQ was 0.8 mg/kg, with its safety confirmed by previous *in vivo* studies [137,201]. The IV formulation of IMQ was initially prepared by diluting the oral formulation 10-fold with only water and adjusting the pH to 6 - 6.5 using NaOH. After the pH was adjusted, IMQ precipitated, indicating the solubility of IMQ in water was lower than 0.8 mg/mL when the pH was close to neutral. Interestingly, no precipitation of IMQ was observed when the oral formulation was diluted 10-fold with the propylene glycol (PG)-water mixture (80:20, *v/v*) at the pH range of 6 - 6.5. This observation suggested that the PG-water mixture exhibits a better capacity for facilitating IMQ solubility. This enhanced capacity may be attributed to hydrotropic solubilisation by adding PG and the formation of a water-miscible cosolvent system [243–245]. PG contains both a hydrophobic group (methyl) and two hydrophilic groups (hydroxyl), allowing it to act as a hydrotrope. The addition of PG in the co-solvent system can disrupt the structured network of water molecules surrounding the poorly soluble IMQ, reducing the hydrophobic effect and improving the solubility of the drug [246]

4.4.2 An erratic and prolonged oral absorption of IMQ

IMQ, as a small molecule with a molecular mass less than 500 Da, a log P less than 5, hydrogen bond donor less than 5 and hydrogen bond acceptors less than 10 (**Table 4-1**), meets the criteria of Lipinski rule of five, suggesting its potential for oral administration. However, the concentration-time profile of IMQ following oral administration shows that the absorption of IMQ was prolonged and erratic (**Figure 4-2 B**).

We hypothesised that this prolonged absorption profile is related to the solubilisation of IMQ in the different regions of GI tracts and multiple sites of absorption of IMQ. In the PK study, IMQ was dissolved in an acidic formulation (0.05 N HCl) to facilitate its solubility for oral administration. In the first two hours after oral administration, a relatively rapid increase in plasma concentration of IMQ was found, suggesting absorption from the upper GI tract. However, with a gradual increase in pH in the lower parts of the small intestine and proximal colon, IMQ could precipitate, resulting in limited absorption from these regions [247–249]. A second peak in IMQ concentration was observed after 20 hours. At this stage, the remained IMQ in the GI tract would likely to be already in the lowest parts of the rectum. The second peak could reflect the absorption from this area, which partially avoids hepatic first-pass metabolism [250]. This hypothesis was investigated by assessing the concentration of IMQ in the intestinal contents at 2 h and 28 h, which were considered as the two apparent T_{max} points of IMQ following oral administration. It was shown that IMQ was mainly found in the small intestine at 2 hours, and a substantial amount of IMQ was trapped within the intestinal lumen up to 28 h (**Figure 4- 4**).

In general, rats are a good *in vivo* model for predicting the oral absorption of drugs in humans [55]. Additionally, the intestinal physiology of rats is similar to humans [251].

However, in the case of IMQ, an obvious difference in plasma concentration profile and PK parameters was found between rats and humans following oral administration of IMQ [140]. The oral absorption of IMQ in humans was observed between 2 to 4 hours, depending on the fasted and non-fasted states. Importantly, a clear elimination phase of IMQ from plasma was also observed in humans. Previously, it was reported that the oral bioavailability of IMQ in rats was practically zero [252]. However, in our study, it was found that the oral bioavailability of IMQ was limited (< 10 %) but not zero (**Table 4- 3**). It was shown that the oral bioavailability of IMQ was various across different species, such as 47 % in humans and 80-91 % in monkeys [140]. One of the explanations for the differences in F_{oral} is the variability of first-pass metabolism of IMQ in different species. It was reported that IMQ is primarily metabolised by cytochrome P450 (CYP450) 1A1 and 1A2 [253]. CYP1A1 and CYP1A2 in humans are 10-fold less sensitive to their substrate compared to in rats [254]. Therefore, the first-pass metabolism of IMQ in humans following oral administration may be less than in rats, resulting in higher F_{oral} of IMQ in humans than in rats.

It was previously reported that using a long-chain triglycerides lipid-based formulation for oral administration could potentially avoid the first-pass metabolism by improving intestinal lymphatic transport of drugs, resulting in increased F_{oral} [183,255]. IMQ has a limited solubility in olive oil (7.4 ± 1.0 µg/mL) and a low CMs affinity in the *in silico* and *in vitro* assessments (**Table 4-1**). Therefore, we hypothesised that the presence of lipids following the oral administration of IMQ (*a.k.a* IMQ lipid-based group) would not increase the F_{oral} of IMQ. As expected, there was no significant difference in F_{oral} of IMQ between lipid-free and lipid-based groups (**Table 4- 3**).

Although the lipophilicity of IMQ is moderate (Log P = 3.46), the V_{ss} of IMQ was found to be very high (3376.3 ± 1842.0 mL/Kg) (**Table 4- 3**). We have also calculated the V_{ss}

of IMQ following IV administration using data reported by other authors in previous work [137,201]. The results showed that this high V_{ss} found in our study was consistent with previous studies (7295.8 mL/Kg and 6784.3 mL/Kg). There was no significant difference in the concentration of IMQ between blood and plasma (**Figure 4-3 B and D**), suggesting a low distribution of IMQ into blood cells. Therefore, it could not explain the large V_{ss} of IMQ. Using a two-compartment model analysis, it was shown that IMQ has a higher volume of distribution in the central compartment (V1: 28951.4 mL/Kg) than in the peripheral compartment (V2: 14484.9 mL/Kg). The difference in the volumes of distribution of IMQ between compartments suggested that IMQ is mainly distributed in the plasma and highly blood-perfused organs (such as the liver, kidney and spleen) which are represented as the central compartment. Previously, a similar distribution of a drug molecule in the systemic compartment was also found in animals following administration of metformin [256]. Metformin is a small molecule that is used in diabetes. It is a hydrophilic molecule with a log P at –1.43. In general, for such a drug molecule, like metformin, it should have a low volume of distribution. However, Stepensky *et al.* previously reported that the V_{ss} of metformin in rats was 1310 mL/Kg [256]. The authors proposed a pharmacokinetic model to explain the disposition of metformin in rats. They suggested that, apart from plasma, the GI wall and liver could be large reservoirs that are responsible for the accumulation of metformin. Since metformin and IMQ share a similar amine structure, we suspect that the large V_{ss} of IMQ could also be a result of the disposition of IMQ in the GI wall and liver.

4.4.3 Unexpectedly high lymph nodes distribution of IMQ following oral administration

Previously, it was suggested that a high affinity of small molecules to CMs and a high solubility of drug molecules in long-chain triglycerides (> 50 mg/mL) are two important indicators for intestinal lymphatic transport following oral administration [181–184]. In previous studies, we have demonstrated that artificial CMs are a good surrogate for *ex vivo* plasma-isolated CMs, and the affinity of molecules to artificial CMs also correlated with the percentage of dose that can be transported into intestinal lymphatics [181,182]. The *in silico* prediction and the *in vitro* assessment of IMQ show the drug has a low affinity to CMs (< 1.75 %) and has limited solubility in triglycerides (7.4 ± 1.0 µg/mL), indicating that IMQ cannot be transported into the lymphatic system following oral administration even in the presence of long-chain triglycerides *via* CMs association mechanism. However, BD studies of IMQ following oral administration showed that the drug substantially accumulated in LNs, especially MLNs which are LNs draining lymph from the GI tract (**Figure 4-3**). MLNs are a large group of LNs that are allocated on the base of the mesentery. The lymph fluid that is drained from the duodenum, small intestines, ascending and transverse colon passes through superior MLNs and then enters the cisterna chyli [178]. The unexpected accumulation of IMQ in MLNs may suggest the existence of lymphatic uptake of IMQ, which is against the previous theory that the high CMs affinity and high triglyceride solubility are the key to intestinal lymphatic transport following oral administration [181]. However, it was previously reported that molecules which were transported into the intestinal lymphatic system following oral administration via the CMs pathway have a higher concentration in the superior mesenteric lymph duct compared to plasma [189–192,195,203,257]. In this study, there was no significant difference in concentrations of IMQ in plasma and

mesenteric lymph fluid (**Figure 4-3**), suggesting that the accumulation of IMQ in intestinal LNs was not the result of intestinal lymphatic transport or, at least, was not associated with CMs pathway.

In addition to MLNs, it was noted that the IMQ also accumulated in the superficial inguinal LNs and cervical LNs (**Figure 4-3**). Superficial inguinal LNs are located within the subcutaneous fat near the superficial epigastric veins and are responsible for lymph drainage from the thighs and lower abdomen [178]. Superficial and deep inguinal LNs drain into iliac lymph nodes. In this study, both superficial and deep cervical lymph nodes (CLNs) were harvested and combined together for analysis. Superficial CLNs drain lymph from the tongue and nasolabial lymphatics, whereas deep CLNs drain lymph from the brain [258]. Due to the one-way direction of lymph flow, IMQ in the intestinal LNs were directly transported into blood circulation through the cisterna chyli and thoracic duct [61]. Therefore, the accumulation of IMQ in the inguinal LNs and cervical LNs is unlikely related to the intestinal transport of IMQ, suggesting a substantial distribution of IMQ to all LNs.

Wong *et al.* reported that lamivudine (a nucleoside analogue of antiretroviral agents), which has a limited affinity to CMs, was also primarily distributed to the MLNs following oral administration [196]. The authors suggested that the lymphatic accumulation of lamivudine may be attributed to potential active transporters for nucleoside analogues, such as organic cation transporters and concentrative nucleoside transporters. However, IMQ is not a classic nucleoside analogue but is a derivative of imidazoquinoline (hetero-cyclic amine). Therefore, the active transport of IMQ to the lymphatic system is less likely to be the reason for the high accumulation of IMQ in LNs.

In addition to active transporters, IMQ-targeted cells, such as dendritic cells (DCs), macrophages and lymphocytes, may carry IMQ into the LNs. In blood, IMQ can penetrate into the DCs by passive diffusion, activating DCs by binding to the intracellular TLR7. It was reported that the activation of DCs could promote the production of type 1 interferon, leading to lymphocytes and antigen-presenting cells migration into the nearest LNs [259]. As a result, IMQ may be transported into the LNs with cell migration. However, it was observed that the cell migration into LNs normally takes several hours to initiate. The accumulation of IMQ in the LNs has been observed as early as 1.5 h following oral administration of the drug, suggesting that transportation of IMQ by DCs is unlikely to be the reason for the accumulation.

It was reported that molecules with high albumin binding can be transported into the lymphatic system by the albumin-hitchhiking mechanism [260]. The term ‘albumin-hitchhiking’ describes the phenomenon that albumin returns from the interstitial fluid to blood circulation via the lymphatic system. The concentration difference of albumin in the blood (40 mg/mL) and in interstitial fluid (< 15 mg/mL) results in a passive diffusion of albumin from high-concentration regions to low-concentration regions through a leaky vasculature, such as a lymphatic vessel. The exact affinity of IMQ to rat albumin has not been reported. However, *in vitro* assessment showed that IMQ has more than 90 % protein binding to human plasma proteins [261]. Additionally, other small molecules derived from the same chemical structure as MQ have shown a high albumin binding in the albumin [262]. Herein, we hypothesized that IMQ might also have a high affinity to rat albumin, resulting in transportation into the lymphatic vessel followed by entering MLNs due to the mechanism of albumin hitchhiking.

It was noted that the V_{ss} of IMQ is high (3.376 L/kg) (**Table 4- 3**), suggesting that the high concentration of IMQ in LNs may also be associated with high and non-specific

distribution of IMQ into various tissues and organs Therefore, we analyzed IMQ concentration in both highly blood-perfused organs (kidney, spleen and liver) and relatively low blood-perfused organs (skeleton muscle) (**Figure 4-3**). It was found that the concentration of IMQ in the highly blood-perfused organs was significantly higher than it was in plasma (**Figure 4-3 A and C**). Additionally, the high distribution of IMQ into the liver and kidney was also observed in mice that received IMQ IV injections [210].Therefore, the high non-specific distribution of IMQ could be one of the reasons for the accumulation of IMQ in the LNs. Moreover, it was noted that IMQ was also highly distributed into the brain (**Figure 4-3**). The high penetration to the central nervous system and non-specific distribution of IMQ could be the reason for the observed flu-like symptoms in patients after the administration of IMQ [131,141,207,263].

4.5 Conclusions

To the best of our knowledge, this is the first reported pharmacokinetic and biodistribution study of IMQ in rats. We found that the plasma concentration-time profile of IMQ following oral administration was prolonged and erratic, which may be attributed to a complex absorption of IMQ in the small intestines. It was observed that although IMQ has a limited affinity to CMs, it still substantially accumulated in the LNs. Additionally, IMQ was also non-specifically distributed into various organs and tissues. The unspecific systemic distribution of IMQ may be responsible for the adverse effects of IMQ and low therapeutic response in clinical trials. Therefore, in **Chapter 5**, several lipophilic prodrugs of IMQ were designed and synthesized, which were expected to minimise its non-specific distribution and improve the therapeutic effect of IMQ by targeted delivering the drug into the MLNs and ILNs.

Chapter 5 Targeted delivery of IMQ to intestinal lymph nodes using lipophilic prodrug approach

5.1 Introduction

As described in **Section 1.1.1**, CRC is the third most commonly diagnosed cancer, with a mortality rate of 10 % in both males and females [2]. In recent years, immunotherapies involving immune checkpoint blockade, such as programmed cell death protein and programmed death ligands (PD-1/PD-L1) inhibitors and adoptive cell therapy (cytotoxic T-lymphocytes antigen 4 (CTLA-4)), have demonstrated promising potential in cancer treatment [264–267]. However, these immunotherapies were less effective in CRC than in other cancer types [77,268].

In addition to the mechanism of tumour resistance to immunotherapy, described in **Section 1.1.4.3**, the tumour-mediated secretion of pro-tumorigenic cytokines, such as IL-6 and IL-17, can protect the malignant colorectal epithelium by overstimulating the production of vascular endothelial growth factor and promoting cancer cell proliferation, resulting in resistance to immunotherapy [268]. To overcome tumour resistance to the current immunotherapies, the combination of immunotherapeutics with different mechanisms of action was suggested [269]. The recruitment of dendritic cells (DCs) was proposed as an important strategy in cancer immunotherapy [106,119,122]. As described in **Section 1.2.4**, activated DCs can present tumour-associated antigens

(TAAs) to $CD8^+$ T cells and facilitate the Th1 cell differentiation of CD4+ T cells [119]. In addition to stimulation of adaptive immune response, activated DCs can also enhance the innate immune response to cancer cells by stimulating natural killer cells [269]. Therefore, the simulation of DCs is an important aspect of immunotherapy of CRC.

In the metastasis of CRC, the tumour invasion pathway partially follows the mesenteric lymph nodes (MLNs) and retroperitoneal lymph nodes (such as iliac lymph nodes, ILNs), draining the lymph from the colorectal regions [30,32,34,153]. It was reported that in the TME and lymph nodes (LNs), the maturation of DCs is suppressed, and the infiltration of mature DCs is reduced, resulting in the diminished ability of the immune system to recognise cancer cells [93,120].

Imiquimod (IMQ) is an agonist of toll-like receptor 7 (TLR 7). Early studies showed that IMQ facilitates the secretion of immunostimulatory cytokines, such as interferon-α (IFN- α), resulting in suppression of the tumour growth [134,135]. Briefly, the production of cytokines is regulated by the activation of dendritic cells (DCs) by IMQ binding to TLR7 through the MyD88 signalling pathway. After stimulation by IMQ, DCs transform into mature state, promoting both innate and adaptive immune responses to the cancerous cells [111,119]. Despite the fact that in many preclinical studies TLR agonists have demonstrated great potential as anti-tumour agents, in most clinical trials TLR agonists were not very effective for cancer treatment [141,207]. In addition, in a phase I clinical trials of IMQ, a dose-limiting toxicity of the drug (> 50 mg) was observed in patients with refractory neoplasms [139]. The systemic adverse effects, such as flu-like symptoms and nausea, and limited therapeutic success of IMQ in

clinical trials could be related to its extensive non-specific distribution into tissues, and lack of targeted delivery to relevant organs, such as draining lymph nodes, enriched in DCs [231,270,271]. Intestinal lymphatic targeting following oral administration is one of the strategies to deliver small molecules to the MLNs. This strategy is based on the physiological pathway of digestion and absorption of dietary lipids. Chylomicrons (CMs) are large lipoproteins that are assembled in the enterocytes in the presence of long-chain lipids. Due to their large size, CMs cannot penetrate blood capillaries and, therefore, are taken up selectively by lymph lacteals [164,272]. Drug molecules with high affinity to CMs can be transported efficiently into the intestinal lymphatic system [181]. Highly lipophilic compounds with Log $D_{7.4}$ > 5 and solubility in long-chain triglycerides (LCTs) > 50 mg/mL are most likely to be transported into the intestinal lymphatic system through CMs pathway [182,273].

IMQ is not a highly lipophilic compound with a calculated log $D_{7.4}$ of 3.36 (ACD/I-lab), suggesting that this molecule is unlikely to be transported into the intestinal lymphatic system following oral administration by the CM association pathway. Previously, a lipophilic prodrug approach has been used to increase lipophilicity and hence CMs affinity of drugs, achieving intestinal lymphatic targeting [186,189–192]. Successful lipophilic prodrugs should resist chemical and enzymatic hydrolysis in the gastrointestinal (GI) tract, but efficiently release active moieties in the intestinal lymphatic system. In addition, multiple works have suggested that the presence of LCTs in the lipid-based formulation facilitates the intestinal lymphatic transport of highly lipophilic compounds following oral administration [184]. The improvement in intestinal lymphatic transport using LCT lipid-based formulation has also been observed in our previous studies [179,180,182,190–192,203,255].

Therefore, the main aim of this chapter was to achieve targeted delivery of active IMQ to the intestinal lymph nodes draining from the colorectal region, with the ultimate goal of improvement in treatment outcomes of CRC.

In most previous studies, prodrug candidates for intestinal lymphatic targeting following oral administration were based on the ester bond structure [186,189–192]. However, Han *et al.* reported a lipophilic prodrug of modified mycophenolic acid (MPA) that was conjugated with an alkyl chain *via* an amide bond. The approach was found to be not efficient for targeting intestinal lymphatics following oral administration since the amide prodrug did not release the active moiety efficiently within the lymphatic system [188]. IMQ has only a primary amine as a prodrug-able functional group that can be conjugated with lipophilic groups through an amide bond. However, IMQ release from the amide prodrugs could be efficient due to the electron resonance between the amine and imidazoquinoline in IMQ.

5.2 Experimental design

The general scheme flowchart of the experimental design is shown in **Figure 5- 1**. The lipophilic prodrugs of IMQ were designed as described in **Section 2.2**. Prodrugs were synthesized and characterized as described in **Section 2.3.2.2** and **Section 2.3.3**, respectively. The *ex vivo* model of brush border membrane vesicles was developed and validated as described in **Section 2.5.1** and **Section 5.3.5**. The potential for intestinal lymphatic transport of synthesized prodrugs was assessed by their affinity to chylomicrons and solubility in long-chain triglycerides as described in **Section 2.4** and **Section 2.6**, respectively. A further selection of prodrug candidates was determined by resistance to enzymatic hydrolysis in the intestinal lumen, and release of IMQ in

the lymphatics using fasting state simulated intestinal fluid (FaSSIF) supplemented with esterases (20 UI/mL), brush border enzyme vesicles and rat plasma following the protocol described in **Section 2.5.4**. Sample collected from *in vitro* and *ex vivo* studies were processed for bioanalysis using the bioanalytical method reported in **Section 2.8.3**.

The pharmacokinetic (PK) parameters and biodistribution (BD) in rats were assessed for the most promising compounds, prodrugs 5 and 8, as described in **section 2.7.4**. Samples were collected from *in vivo* studies as described in **Section 2.7.5** and were processed for bioanalysis using the bioanalytical method reported in **Section 2.8.4.** The PK parameters were calculated as described in **Section 2.7.3.3**.

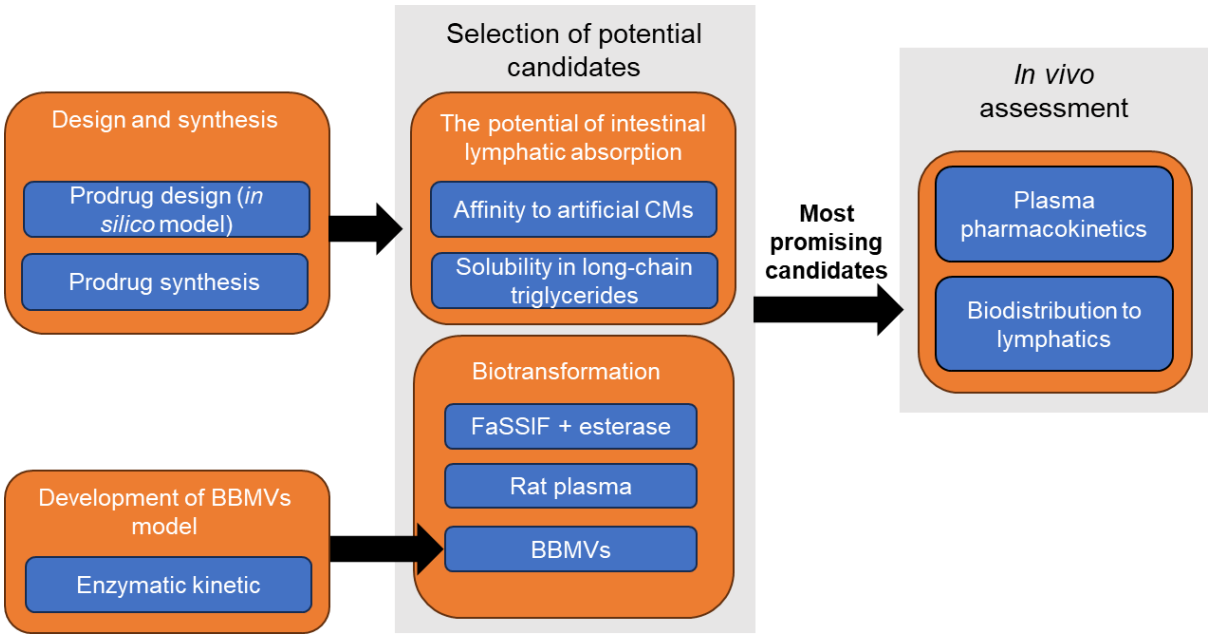

Figure 5- 1 The experimental workflow scheme of development of highly lipophilic prodrugs of IMQ for targeted delivery of IMQ to intestinal lymphatics following oral administration. FaSSIF, fast state stimulated intestinal fluid; CMs, chylomicrons; BBMVs, brush border membrane vesicles.

5.3 Results

5.3.1 Prodrug design

The high affinity of molecules to CMs is important for intestinal lymphatic absorption following oral administration of the drug molecules. Therefore, in this section, we aimed to design highly lipophilic prodrugs for IMQ that have a good affinity to CMs.

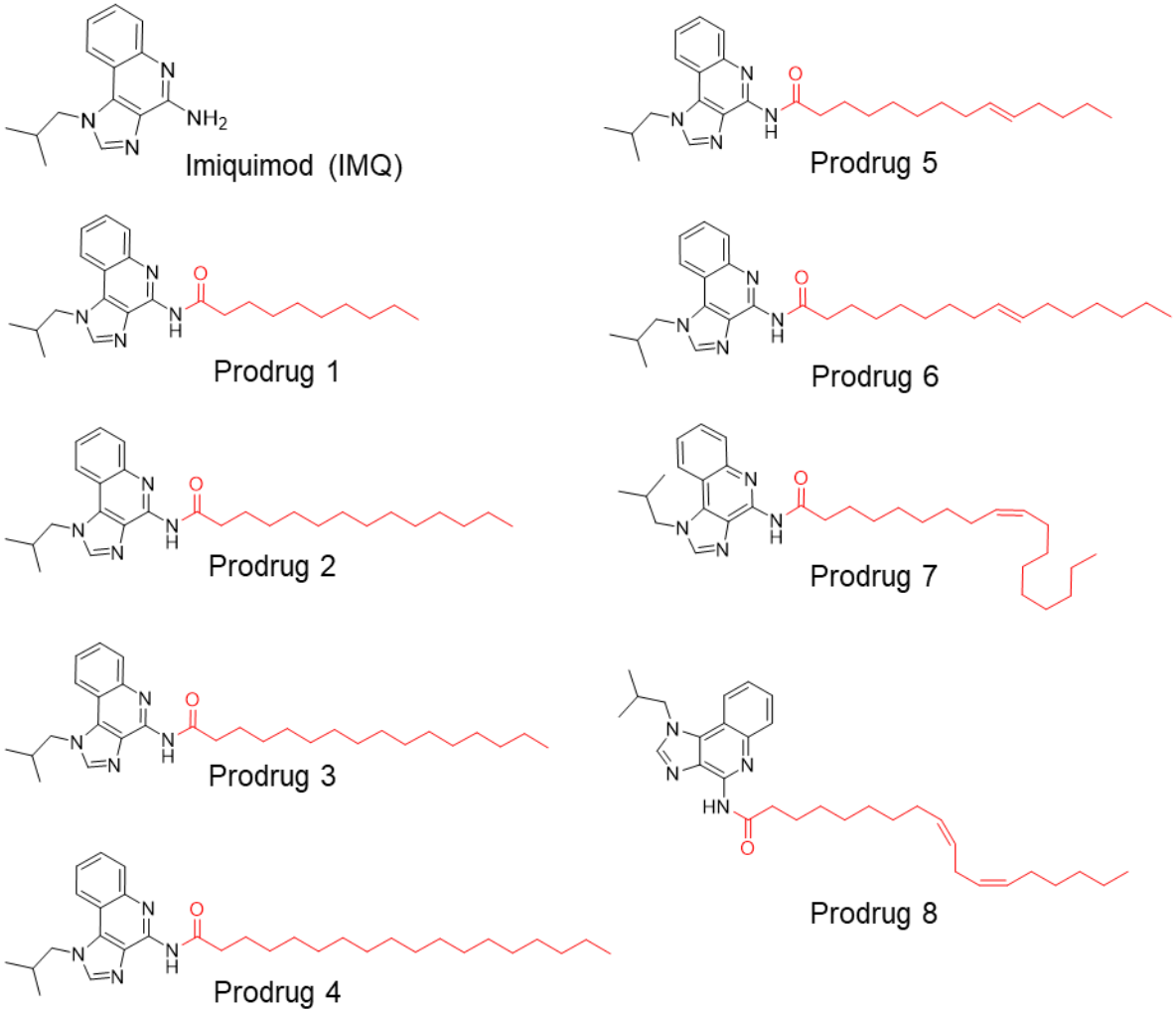

Figure 5-2 Chemical structures of IMQ and its lipophilic prodrugs 1–8.

Prodrugs 1-4 were designed by conjugating the amine group of IMQ with 10-, 14-, 16- and 18-carbon chain length saturated fatty acid. Prodrugs 5-8 were designed by conjugating the amine to unsaturated fatty acid, including myristoleic acid, palmitoleic acid, oleic acid and linoleic acid, respectively (**Figure 5-2**).

The physicochemical properties of the prodrugs were calculated by ACD/I-Lab and imported into an *in silico* model [182] to predict their affinity to CMs (as described in **Chapter 2, Section 2.2**). Results of the physicochemical properties of the prodrugs and the predicted affinity of the prodrugs to CMs are listed in **Table 5-1**. Comparing the IMQ's affinity to CMs (**Table 4-1, Chapter 4**) and the prodrugs' affinities to CMs (**Table 5-1**), it suggests that IMQ has a negligible predicted affinity to CM (< 1.75 %), while the prodrugs 1-8 have moderate (>50 %) to high (> 90 %) predicted affinity.

For prodrugs 1-4, with an extension of chain length from 10 to 14 carbons, the predicted CMs association increases from moderate to high. Additionally, unsaturated fatty acids were also used to develop prodrugs 5-8, improving the biotransformation of prodrugs to IMQ in the lymphatic system. With the introduction of unsaturation to fatty acids, the predicted CMs association of prodrugs that contain unsaturated fatty acids (prodrugs 5-8) was not obviously changed compared to prodrugs that contain the corresponding saturated fatty acids (prodrugs 1-4).

Table 5-1 Calculated physicochemical properties of designed prodrugs and their predicted affinity to CMs using an *in silico* model.

Prodrugs	1	2	3	4	5	6	7	8	9	10
Log D 7.4	6.35	8.31	9.2	10.09	7.95	8.84	9.72	9.36	5.38	10
Log P	7.12	9.24	10.31	11.37	8.73	9.79	10.85	10.33	5.98	10.91
Log P - Log D	0.77	0.93	1.11	1.28	0.78	0.95	1.13	0.97	0.63	0.91
PSA	59.81	59.81	59.81	59.81	59.81	59.81	59.81	59.81	86.11	86.11
H-Acceptors	3	3	3	3	3	3	3	3	7	7
FRB	12	16	18	20	15	17	19	18	7	18
Density	1.11	1.08	1.06	1.05	1.07	1.06	1.04	1.04	1.2	1.11
Molar Volume	352.7	416.9	449	481.1	416.9	449	481.1	481.1	389.5	534.6
H-Donors	1	1	1	1	1	1	1	1	1	1
Predicted CM association (%)	50.12	93.81	98.10	99.45	91.16	97.33	99.19	98.86	4.71	97.6

In addition to the design of lipophilic prodrugs using fatty acids, coumarin-derived prodrug structures (prodrugs 9 and 10) were also designed to improve both the affinity of CMs and the biotransformation of prodrugs to IMQ (**Figure 5-3 A).** The coumarin-based structure was expected to increase the affinity of drug molecules to CMs (**Table 5-1**) and facilitate the release of IMQ from the prodrugs (**Figure 5-3 B**).

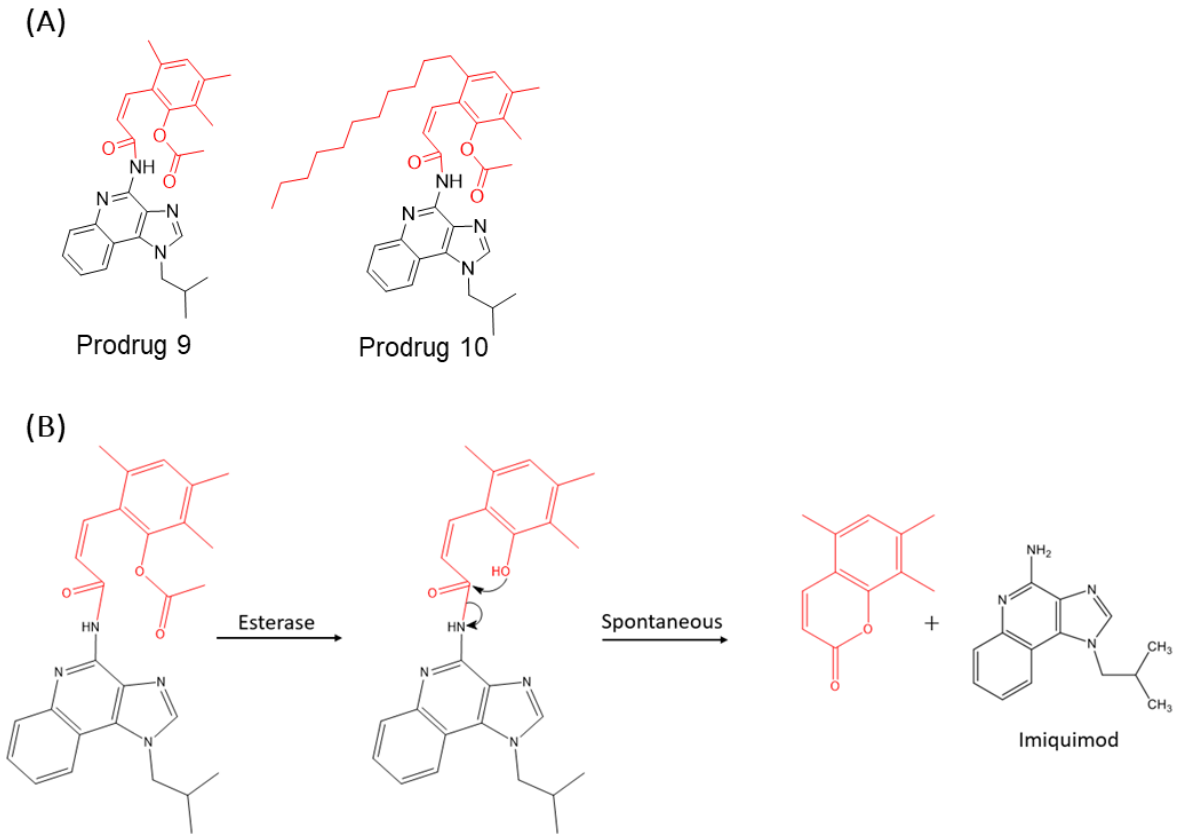

Figure 5-3 Panel (A) chemical structure of IMQ coumarin-based prodrugs 9 and 10; Panel (B) predicted mechanism of the hydrolysis of IMQ coumarin-based prodrugs 9 and 10.

5.3.2 Prodrug synthesis and structural characterisation

Due to the time frame limitation for this PhD project, only prodrugs 1-8 were synthesized. Therefore, the amidation of IMQ was performed using the three different reactions, which are described in **section 2.3**.

In the amidation reaction with acyl chloride (**Figure 2-1**), a white cloudy mixture was observed, indicating that the starting materials, particularly IMQ, were not completely dissolved in the anhydrous dimethylformamide (DMF). The formation of the product (lauroylated imiquimod) was first detected after 1 hour. The amount of the product gradually increased over the next 6 hours (monitored by HPLC-UV). However, no further increase in the amount of the product was observed for up to 24 hours, indicating that the reaction had finished. The yield of this reaction was less than 10 %.

In the next step, different coupling reactions were used to improve the yield of IMQ prodrugs (**Figure 2-2**). An amidation reaction of IMQ using a mixture of NHS and DCC was conducted following a previously reported protocol [193]. Again, a white cloudy mixture was found in the flask, indicating that starting materials were insoluble in the reaction solvent (DMF). Surprisingly, no products were found during the 24 hours of reaction.

Therefore, another coupling reaction for IMQ prodrugs using TCFH-NMI was used (**Figure 2-3**) following a previously reported protocol [194]. In this reaction, DMF was replaced by anhydrous *N*-methyl-2-pyrrolidone (NMP) to facilitate the solubility of IMQ. A dark yellow (or light yellow, depending on the fatty acids used in the reaction) and transparent mixture was observed following the initiation of the reactions, suggesting all starting materials were fully dissolved in the NMP. The yield of all prodrugs 1-8 using the TCFH-NMI coupling reaction was high (> 70 %).

The characterisation of synthesised prodrugs using HRM, NMR ^{1}H and ^{13}C are summarised in **Appendix**.

5.3.3 Affinity of prodrugs to artificial CMs

The affinity of drug molecules to artificial CMs is a reasonable predictor to estimate the potential lymphatic absorption of drugs following oral administration [181]. Compounds 1-4 are highly lipophilic prodrugs of IMQ conjugated with saturated fatty acids. As predicted, IMQ had no affinity to CM, while the affinities of prodrugs 1-4 to artificial CMs were substantial (**Figure 5-4**). The second generation of prodrugs with unsaturated fatty acids (prodrugs 5-8) was designed and synthesised. These unsaturated fatty acids are of the same chain length as saturated fatty acids used in prodrugs 1-4. No difference was found in affinity to CMs between the saturated and unsaturated prodrugs (**Figure 5-4**).

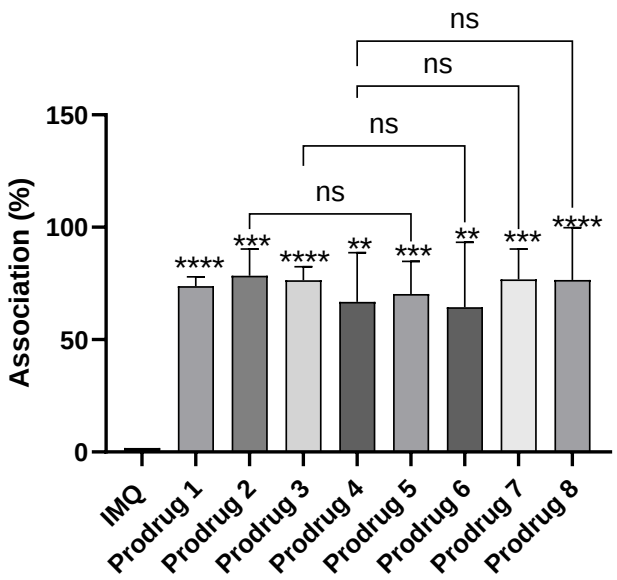

Figure 5-4 Affinities of IMQ and its prodrugs to artificial CMs. One-way ANOVA followed by Tukey's comparison was used for statistical analysis. All results are presented as mean ± SD (n = 3).^{ns}, *p > .05 *,p < .05; **,p < .01; ***,p < .001; ****,p < .0001.*

5.3.4 Long-chain triglyceride solubility of prodrugs

The long-chain triglyceride solubilities of the tested compounds were determined by dissolving 6 mg of each compound in 100 µL of olive oil at 37℃ and stirring the mixture for 72 hours, as described in **Section 2.6**. At the end of the study, if all the added compounds were completely dissolved, no additional compound would be added. The solubilities of prodrugs in olive oil are summarised in **Table 5-2**.

Prodrugs 1 and 2 were in powder form. Following a 72-hour solubility test, powder of prodrugs 1 and 2 were still noticeable in the oil phase. Prodrugs 3 and 4 were in a waxy form, while prodrugs 5-8 were in an oily form. By the end of the solubility test, prodrugs 5-8 were fully dissolved in olive oil, suggesting that triglyceride solubility exceeded 50 mg/mL for prodrugs 3-8 (**Table 5-2**).

Table 5-2 Triglycerides solubilities of prodrugs (mean ± SD, n = 3).

Compounds	Triglycerides solubility (µg/mL)
IMQ	7.4 ± 1.0
Prodrug 1	2510±210
Prodrug 2	46400 ±7300
Prodrug 3	> 50000
Prodrug 4	
Prodrug 5	
Prodrug 6	
Prodrug 7	
Prodrug 8	

5.3.5 Validation of brush border enzyme vesicles *vivo* model to access IMQ stability in the small intestine

In this work, brush border enzyme vesicles (BBMVs) were introduced to estimate the stabilities of amide prodrugs in the gastrointestinal tract (GI tract). To generate a robust *ex vivo* model, the concentration of BBMVs protein pellets and the concentration of prodrugs used in this assay need to be optimised and validated. In this section, prodrug 1 (IMQ-decanoic acid) was selected as a representative prodrug to evaluate the enzymatic kinetic parameters of prodrugs in the BBMVs. The prodrug 1 was the only available prodrug when the BBMVs model was developed and validated. In this work, we were aware that the affinity of different prodrugs to BBMVs could be various, resulting in different enzymatic kinetics.

BBMVs pellets were collected from rats' small intestine as described in **section 2.5.1**. The enzymatic activities of leucine aminopeptidase (LAP) and alkaline phosphatase (ALP) in homogenates suspension and purified BBMVs pellets are summarised in

Table 5-3. After extraction and purification, the enzymatic activities of LAP and ALP in BBMV pellets dramatically increased by 32-fold and 80-fold, respectively. The significant increase in the enzymatic activities of these two representative enzymes indicated the robust quality of purified BBMV pellets.

Table 5-3 The enzymatic activity of leucine aminopeptidase and alkaline phosphatase in homogenised suspension and purified BBMVs pellets.

Samples	Leucine aminopeptidase Activity (U/mL)[a, c]	Alkaline phosphatase Activity (U/mL)[b, c]
Homogenised suspension	3.5 ± 0.34	0.05 ± 0.001
Purified BBMVs pellets	112.7 ± 1.7****	4.0 ± 0.5****

[a] The activity of leucine aminopeptidase is measured with LAP substrates provided with the commercial kits.

[b] The activity of alkaline phosphatase is measured with p-nitrophenyl phosphate provided with the commercial kits.

[c] U/mL = μM/min/mL

**** $p<0.001$

Theoretically, when highly lipophilic prodrugs are spiked to a protein-free medium, the concentration of prodrugs can rapidly decrease due to the precipitation of lipophilic molecules but not the hydrolysis of prodrugs. Therefore, in the initial experiment, we aimed to measure the solubility of lipophilic prodrugs in solutions with various concentrations of protein.

Prodrug 1 (final concentration in media at 10 μM) was spiked into albumin solutions at different concentrations of protein. **Figure 5-5** demonstrates that the prodrugs were unable to exist as free molecules in the absence of proteins. It should be noted that no IMQ released from prodrug 1 was observed. Results suggested that the decrease in the concentration of prodrug 1 was not a result of the hydrolysis of the prodrug.

It was found that the solubility of prodrug 1 was increased with the addition of albumin. In practice term, the amount of BBMVs collected from animals was limited. Thus, the protein concentration of 1 mg/mL was selected as the optimised condition and applied

to the continuous experiments to validate the enzymatic stability of prodrugs in the BBMVs *ex vivo* assay.

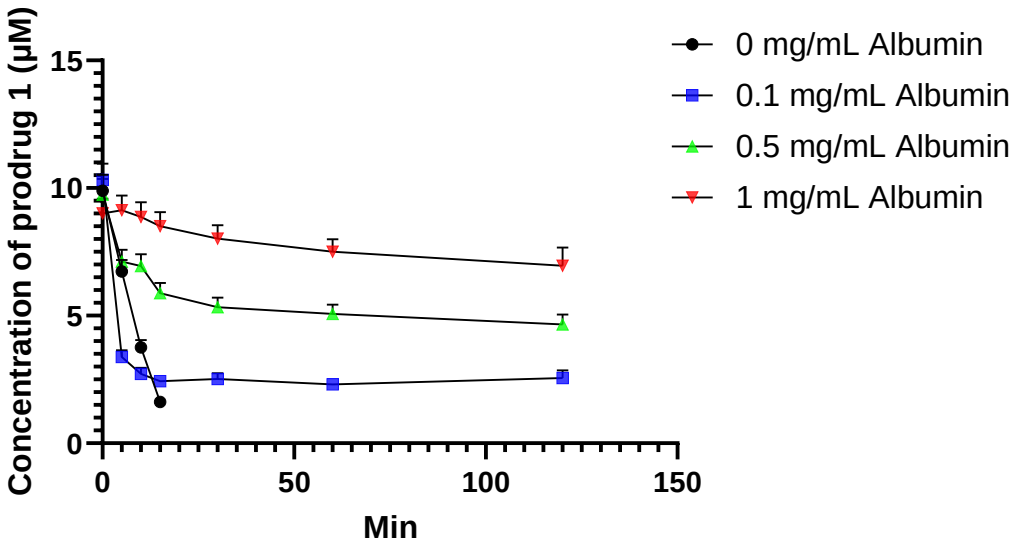

Figure 5-5 The concentration-time profile of prodrug 1 was observed following its incubation at 10 µM with a 25 mM HEPES/Tris buffer (pH = 7) that was supplemented with varying concentrations of albumin.

In the next step, we aimed to calculate the rate of reaction (V_{max}) and Michaelis constant (K_m) for prodrugs in the BBMVs suspension. Prodrug 1 (at final concentrations of 0.5, 1, 2, 4, 6 and 8 µM) was spiked into BBMVs at the protein concentration of 1 mg/mL in 25 mM HEPES/Tris buffer (pH = 7). The concentration of substrate (prodrug 1) and their corresponding velocity were input into the GraphPad Prism (**Figure 5- 6**) using the Michaelis-Menten Kinetics model to compute the V_{max} and K_m as described in **Section 2.5.2**. It was found that the V_{max} and K_m of prodrug 1 in 1 mg/mL of BBMVs proteins was 0.00688 µM per min and 4.696 µM, respectively.

To ensure an efficient enzymatic reaction between IMQ lipophilic prodrugs and 1 mg/mL of BBMVs, 2 µM (< ½ K_m) was selected as the optimised concentration of

prodrugs in the BBMVs assay. Moreover, since the V_{max} was relatively slow, the period of incubation was extended from 120 min to 360 min.

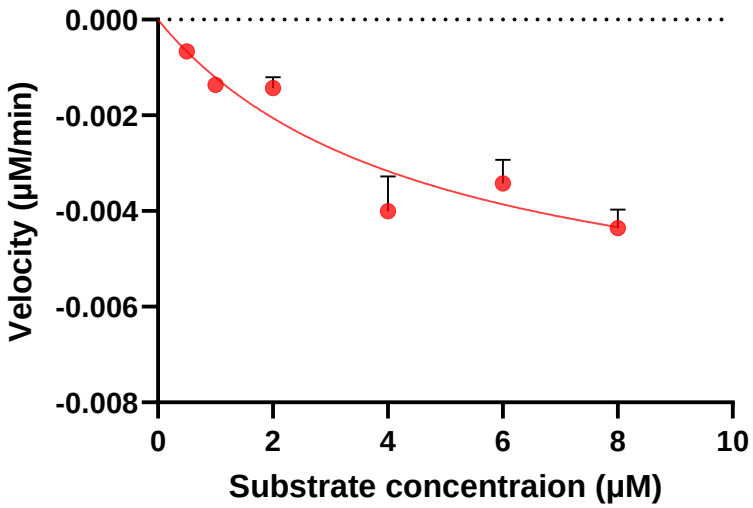

Figure 5- 6 Substrate saturation curve for prodrug 1 in 1 mg/mL protein concentration of BBMVs.

5.3.6 Biotransformation of prodrugs to IMQ in biorelevant media and rat plasma

The biotransformation of prodrugs to IMQ was assessed as described in **Section 2.5.4**. The biotransformation of prodrugs to IMQ was first estimated using two biorelevant media representing the intestinal tract: FaSSIF with added esterase activity and BBMVs, as well as rat plasma [190–192]. In this assay, rat plasma was used as a surrogate for lymph fluid as previously described, since they share similar enzymatic composition [274]. The rate of conversion was expressed as the half-lives of prodrugs and summarised in **Figure 5-7 D**. It is worth noting that the esterase used in the FaSSIF with added esterase activity assay was, in fact, a crude extract from porcine liver characterised for esterase activity, but also containing additional enzymes with not quantified activity. Despite the fact that the prodrugs designed in this study are amides (known for better stability than esters), IMQ was released from the amide

prodrugs quite efficiently with the presence of this extract in the FaSSIF. An increase in the fatty acid carbon chain from 10 to 18 (prodrugs 1-4) resulted in prolonged half-lives. Comparing the half-lives of prodrugs 2 vs 5, 3 vs 6, and 4 vs 7 or 8 in plasma, it was found that unsaturation resulted in the reduction of the half-lives (**Figure 5- 8**). In addition, BBMVs media (at the protein concentration of 1 mg/mL) was also used to estimate the biotransformation of IMQ amide prodrugs. All tested prodrugs were stable in the presence of BBMVs (**Figure 5- 8**). Taking together the artificial CMs affinity, long-chain triglycerides solubility and the rate of IMQ release in the biorelevant media, prodrugs 5 and 8 were selected as the most promising candidates to proceed to *in vivo* studies.

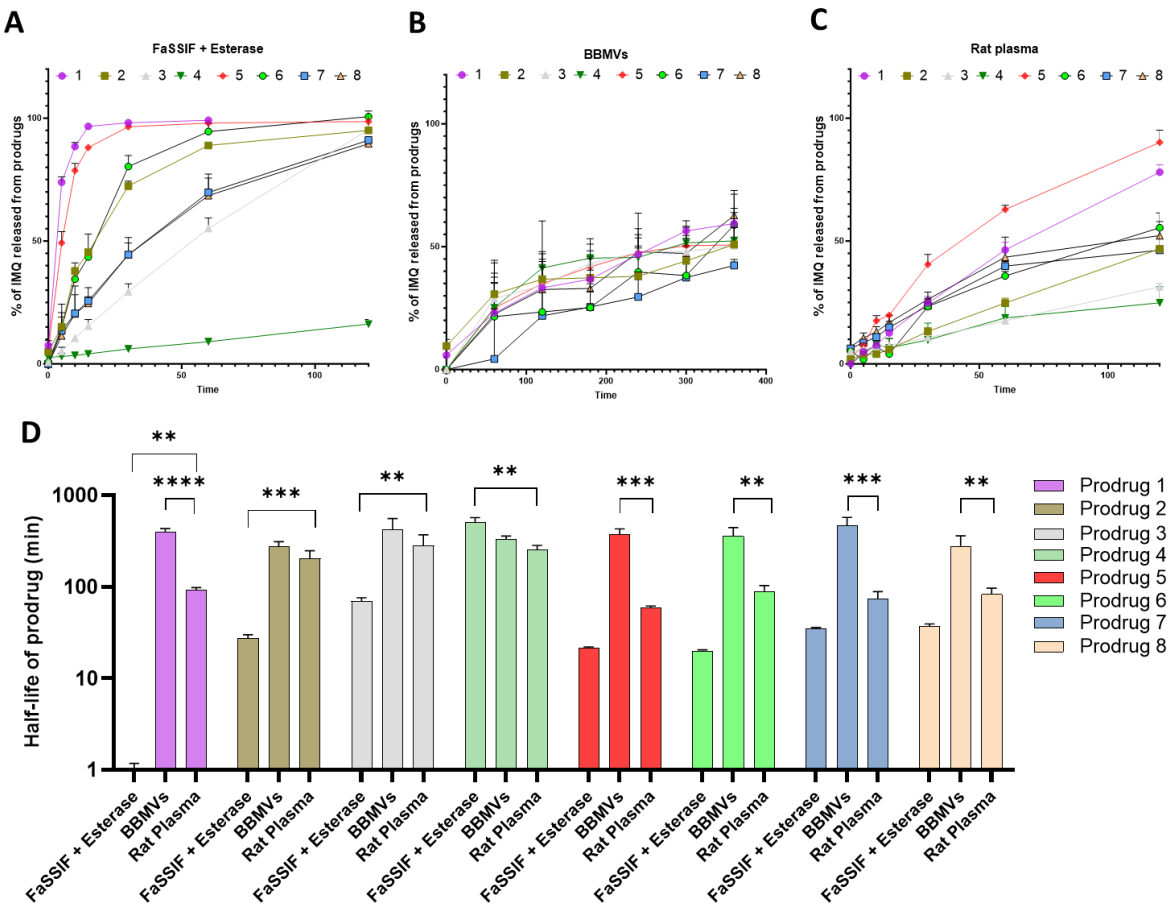

Figure 5-7 The biotransformation of prodrugs to IMQ (n = 3, mean ± SD). Panels (A), (B) and (C) show the kinetics of IMQ release from prodrugs in FaSSIF with porcine esterase (20 IU/mL), BBMVs (1 mg/mL of total protein level) and rat plasma, respectively. Panel D shows the half-lives (t1/2) of prodrugs in tested relevant media. One-way ANOVA, followed by Dunnett's comparison, was used for statistical analysis. Asterisks denote significance against the half-life of the prodrug in plasma. **,p < .01; ***,p < .001; ****,p < .0001.

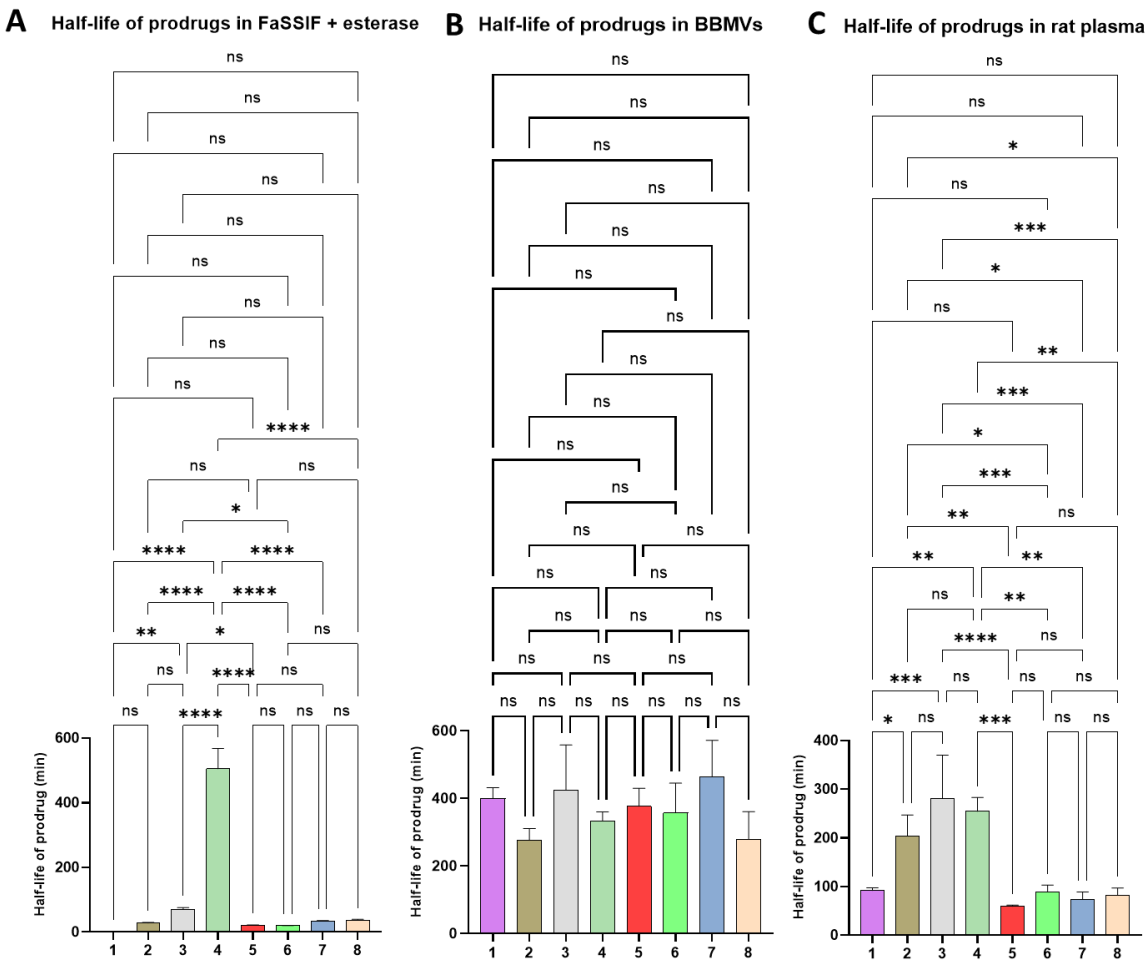

Figure 5- 8 Half-lives of prodrugs in (A) FaSSIF with porcine esterase (20 IU/mL), (B) BBMVs (1 mg/mL of total protein level) and (C) rat plasma. One-way ANOVA followed by Tukey's comparison was used for statistical analysis. ***,p < .01; ***,p < .001; ****,p < .0001.*

5.3.7 Pharmacokinetic studies of prodrug 5, prodrug 8 and IMQ that released from prodrugs

The pharmacokinetic profiles of prodrugs 5 and 8 were generated following the protocol described in **Section 2.7.3.2**, and pharmacokinetic parameters were calculated as described in **Section 2.7.3.3**.

The plasma concentration-time profiles of IMQ that were released from prodrugs and the profile of prodrugs 5 and 8 were generated following IV and PO administration of prodrugs (**Figure 5-9**).

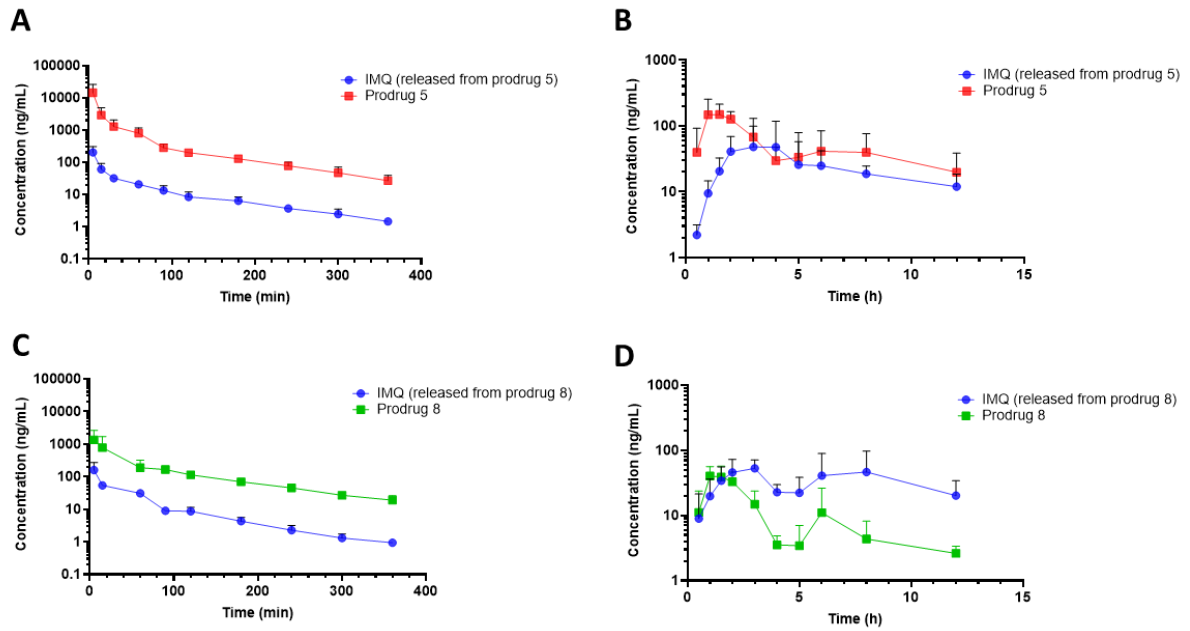

Figure 5-9 Plasma concentration-time profiles of IMQ, prodrug 5 and prodrug 8 (mean ± SD) following: panel (A) IV bolus of prodrug 5 (1.49 mg/Kg, n=4); panel (B) Oral administration of prodrug 5 in lipid-based formulation (14.9 mg/Kg, n=6); panel (C) IV bolus of prodrug 8 (1.69 mg/Kg, n=4); panel (D) Oral administration of prodrug 8 in lipid-based formulation (16.9 mg/Kg, n=5).

The PK parameters of IMQ (released from prodrugs), prodrugs 5 and 8 were calculated using a non-compartmental approach and summarised in

Table 5- 4 and **Table 5-5**.

A statistically significant difference was found between the terminal slope half-lives ($t_{1/2}$) of IMQ following IV administration of IMQ itself and IV administration of prodrugs 5 and 8, suggesting that the rate of IMQ release from prodrugs was slower than the rate of elimination of IMQ (**Table 4- 3** and

Table 5- 4).

Table 5- 4 Pharmacokinetic parameters of IMQ following administrations of different compounds to rats: 1) prodrug 5 (1.49 mg/kg for IV and 14.9 mg/kg for PO); and 2) prodrug 8 (1.69 mg/kg for IV and 16.9 mg/kg for PO) (mean ± SD).

Compound dose	Prodrug 5		Prodrug 8	
Administration route	i.v.	p.o.	i.v.	p.o.
AUC_{inf} (h·ng/mL)	105.6 ± 26.5	415.4 ± 225.1	97.3 ± 27.6	531.6 ± 398.3
AUC_{last} (h·ng/mL)	102.5 ± 26.1	313.8 ± 198.1	95.4 ± 27.4	404.3 ± 301.3
C_0 or C_{max} (ng/mL)	390.2 ± 243.8	78.0 ± 66.3	310.4 ±	72.8 ± 37.7
CL (mL/h/kg)	-	-	-	-
V_{ss} (mL/kg)	-	-	-	-
T_{max} (h)	-	2 - 6	-	2 - 6
$t_{1/2}$ (h)	1.47 ± 0.2 *a	2.2 ± 0.9	1.1 ± 0.2 *a	4.9 ± 2.7
F_{oral} (%)	-	15.6 ± 9.8 ns, b	-	20.1 ± 15.0 ns,b

AUC_{inf} area under the curve from time zero to infinity; AUC_{last} area under the curve from time zero to the last observed time point (0 – 360 min for IV administration of prodrugs; 0 – 12 h for PO administration of prodrugs); C_0, concentration extrapolated to time zero; CL, clearance; V_{ss}, volume of distribution at steady state; T_{max} maximum concentration; $t_{1/2}$, half-life; F_{oral}, absolute oral bioavailability. The absolute oral bioavailability was calculated using the AUC_{last} of IMQ following IV bolus (**Table 4-3**).

[a] One-way ANOVA followed by Dunnett's comparison was used to compare the $t_{1/2}$ of IMQ following IV administration of unmodified IMQ (**Table 4-3**), prodrug 5 and prodrug 8. Asterisks denote significance against IMQ. ^{ns}, p>.05 *, p < .05.

[a] One-way ANOVA followed by Dunnett's comparison was used to compare the F_{oral} of IMQ following administration of unmodified IMQ (using lipid-based formulation) (**Table 4-3**), prodrug 5 and prodrug 8. Asterisks denote significance against IMQ. ^{ns}, p>.05 *, p < .05.

Following oral administration of prodrugs 5 and 8, the T_{max} of prodrugs themselves was between 1-2 h, while the T_{max} of IMQ was 2-6 h (

Table 5- 4 and **Table 5-5**). The plasma concentration-time profile of IMQ following oral administration of prodrugs 5 and 8 is not erratic and prolonged, as opposed to the oral administration of IMQ itself (**Figure 4-2** and **Figure 5-9**). There is no difference in the F_{oral} of IMQ between administrations of equimolar doses of the parent drug and prodrugs (**Table 4- 3** and

Table 5- 4).

Table 5-5 Pharmacokinetic parameters prodrugs following administration of prodrug 5 (1.49 mg/kg for IV and 14.9 mg/kg for PO) and prodrug 8 to rats (1.69 mg/kg for IV and 16.9 mg/kg for PO) (mean ± SD).

Compound dose	Prodrug 5		Prodrug 8	
Administration	i.v.	p.o.	i.v.	p.o.
AUC_{inf}	5280.8 ± 1601.2	749.3 ± 520.9	1186.4 ± 602.1	143.1 ± 18.0
AUC_{last}	5223.0 ± 3516.0	609.9 ± 286.7	1062.1 ±614.3	129.6 ± 23.2
C_0 or C_{max}	33102.0 ± 27251.7	185.3 ± 87.0	2882.2 ± 2564.6	51.8 ± 10.3
CL (mL/h/kg)	434.8 ± 327.1	-	1814.5 ± 683.1	-
V_{ss} (mL/kg)	433.9 ± 202.7 *, [b]	-	2263.8 ± 1221.3 [ns, b]	-
T_{max} (h)	-	1 - 2	-	1 - 2
$t_{1/2}$ (h)	1.4 ± 0.3	4.4 ± 3.1	1.4 ± 0.2	3.3 ± 1.2
F_{oral} (%)	-	1.2 ± 0.8 [a]	-	1.3 ± 0.3 [a]

AUC_{inf} area under the curve from time zero to infinity; AUC_{last} area under the curve from time zero to the last observed time point (0 – 360 min for IV bolus administration of prodrugs; 0 – 12 h for PO administration of prodrugs); C_{max}, maximum observed concentration; C_0, concentration extrapolated to time zero; CL, clearance; V_{ss}, volume of distribution at steady state; T_{max} maximum concentration; $t_{1/2}$, half-life; F_{oral}, absolute oral bioavailability.

[a]The absolute oral bioavailability was calculated using the AUC_{last} of prodrugs following IV bolus.

[b] One-way ANOVA followed by Dunnett's comparison was used to compare the V_{ss} of IMQ (**Table 4-3**), V_{ss} of prodrug 5 and V_{ss} of prodrug 8. Asterisks denote significance against IMQ. [ns], p>.05 *, p < .05.

Additionally, the PK parameters of prodrugs 5 and 8 were also calculated using a two-compartmental model (

Table 5- 6). It should be noted that one data set of prodrug 5 was excluded due to the insufficient time point in the elimination phase.

It was found that the volume of distribution of the central compartment (V_1) of prodrug 5 was significantly lower than the V_1 of IMQ (

Table 5- 6 and

Table 4-4). However, no difference was found between the V_1 of prodrug 8 and V_1 of IMQ.

Table 5- 6 Two-compartment analysis of the volume of distribution of IMQ, prodrug5 and prodrug 8 (n = 3 to 4). (mean ± SD)

Compound dose	Prodrug 5	Prodrug 8
	(n = 3)	(n = 4)
Administration	IV	IV
AUC (h·ng/mL)	3975.4 ± 3090.7	1152.5 ± 234.7
CL (mL/h/kg)	544.1 ± 349.2	1719.7 ± 605.5
V_1 (mL/kg)	157.3 ± 144.0*	1213.1 ± 694.8^{ns}
V_2 (mL/kg)	457.5 ± 182.8^{ns}	1279.4 ± 1062.6^{ns}
V_{ss} (mL/kg)	614.8 ± 588.5^{ns}	2493.1 ± 941.7^{ns}
$t_{1/2}$ (h)	1.1 ± 0.2	1.5 ± 0.9

AUC, area under the curve; CL, clearance; V_1. volume of distribution in compartment 1; V_2, volume of distribution in compartment 2; V_{ss}, volume of distribution at steady state; T_{max} maximum concentration; $t_{1/2}$, ß elimination half-life .

[b] One-way ANOVA followed by Dunnett's comparison was used to compare the V_1, V_2 and V_{ss} of prodrugs 5 and 8 to those parameters of IMQ (**Table 4-4**). Asterisks denote significance against IMQ. ^{ns}, p>.05 *, p < .05

5.3.8 Biodistribution of prodrugs 5 and 8 and IMQ released by prodrugs

For assessment of intestinal lymphatic delivery of IMQ using prodrugs 5 and 8, biodistribution (BD) studies were conducted at 1.5 h and 6 h following an oral gavage of prodrugs. It should be noted that the concentration of IMQ in plasma, lymph fluid, and whole blood is expressed in ng/mL, whereas in tissue, it is reported in ng/g. As described in **Section 4.3.3**, the density of the analysed biofluids is approximately 1 g/mL, allowing for a direct comparison of IMQ concentrations in blood and tissue using one-way ANOVA. Additionally, the concentrations of tested compounds in the examined biofluids are presented as ng/g in the **Appendix** (**Figure Appx.-2 to Figure Appx.-4**).

The selection of the time points was based on our previous works suggesting that when the intestinal lymphatic transport occurs, the concentration of drugs in the intestinal lymphatics could be highest at or just before the T_{max} in plasma [190,191]. **Figure 5- 10 A** shows that substantial delivery of prodrug 5 to the mesenteric lymph was achieved with 50-fold higher average concentration of IMQ in the lymph fluid in comparison to plasma at 1.5 h. Similarly, the average concentrations of prodrug 8 in mesenteric lymph were 11-fold higher than in plasma at 1.5 h (**Figure 5- 10 C**).

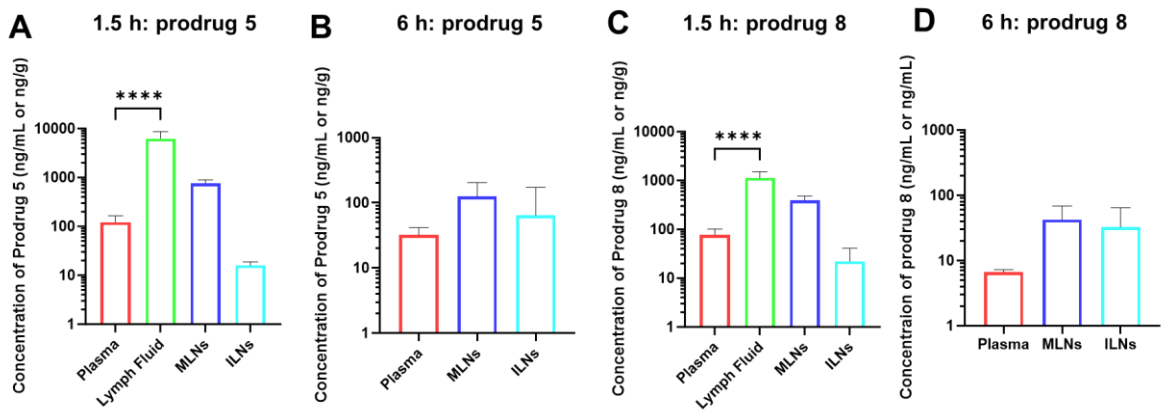

Figure 5- 10 The biodistribution of prodrugs 5 and 8 in plasma, mesenteric lymph, mesenteric lymph nodes (MLNs) and iliac lymph nodes (ILNs) (mean ± SD, n = 4 to 8). Panels (A) and (B) show the distribution of prodrug 5 (14.9 mg/kg) following oral administration at 1.5 and 6 h, respectively. Panels (C) and (D) show the distribution of prodrug 8 (16.7 mg/kg) following oral administration at 1.5 and 6 h, respectively. One-way ANOVA, followed by Dunnett's comparison, was used for statistical analysis. Asterisks denote statistical significance against plasma. ****,$p < .0001$.

At 1.5 h after administration, the concentration of active IMQ released from prodrug 5 in MLNs was significantly higher than the concentration of IMQ in plasma (**Figure 5-11**), indicating that prodrug 5 efficiently released IMQ in the intestinal lymphatic system. The tissue-to-plasma ratio of IMQ levels in the mesenteric lymph and MLNs was significantly increased from 0.5-fold to 1.9-fold and from 5-fold to 11-fold, respectively, following the oral administration of prodrug 5 (**Figure 5-12**). A similar result was also found with the administration of prodrug 8 (**Figure 5- 11** and **Figure 5-12**). However, as opposed to MLNs, the tissue-to-plasma ratio of IMQ in the ILNs was similar following the administration of the prodrugs and unmodified IMQ.

Additionally, the average concentration of IMQ in MLNs and ILNs following oral administration of unmodified IMQ and prodrugs was also separately compared (**Figure 5-13**). It was shown that the concentration of IMQ in the MLNs was significantly higher

following the oral administration of prodrugs in comparison to the oral administration of unmodified IMQ.

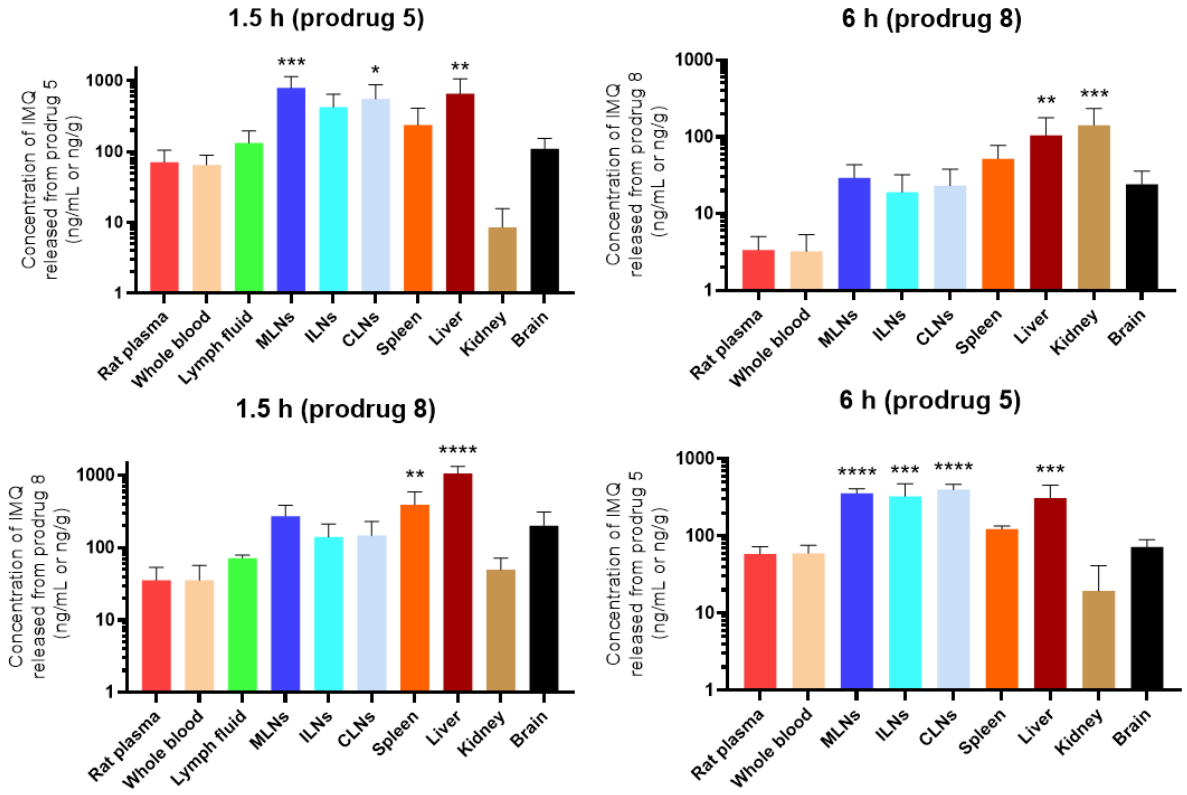

Figure 5- 11 The distribution of IMQ in plasma, mesenteric lymph fluid, lymph nodes and main organs following oral administrations of prodrug 5 (14.9 mg/kg) and 8 (16.7 mg/kg) using lipid-based formulation at 1.5 and 6 h (mean ± SD, n = 5 to 8). MLN, mesenteric lymph node; ILNs, iliac lymph nodes; CLNs, cervical lymph nodes. One-way ANOVA, followed by Dunnett's comparison, was used for statistical analysis. Asterisks denote statistical significance against plasma. * $p < .05$; ** ,$p < .01$, ***,$p < .001$, ****,$p < .0001$.

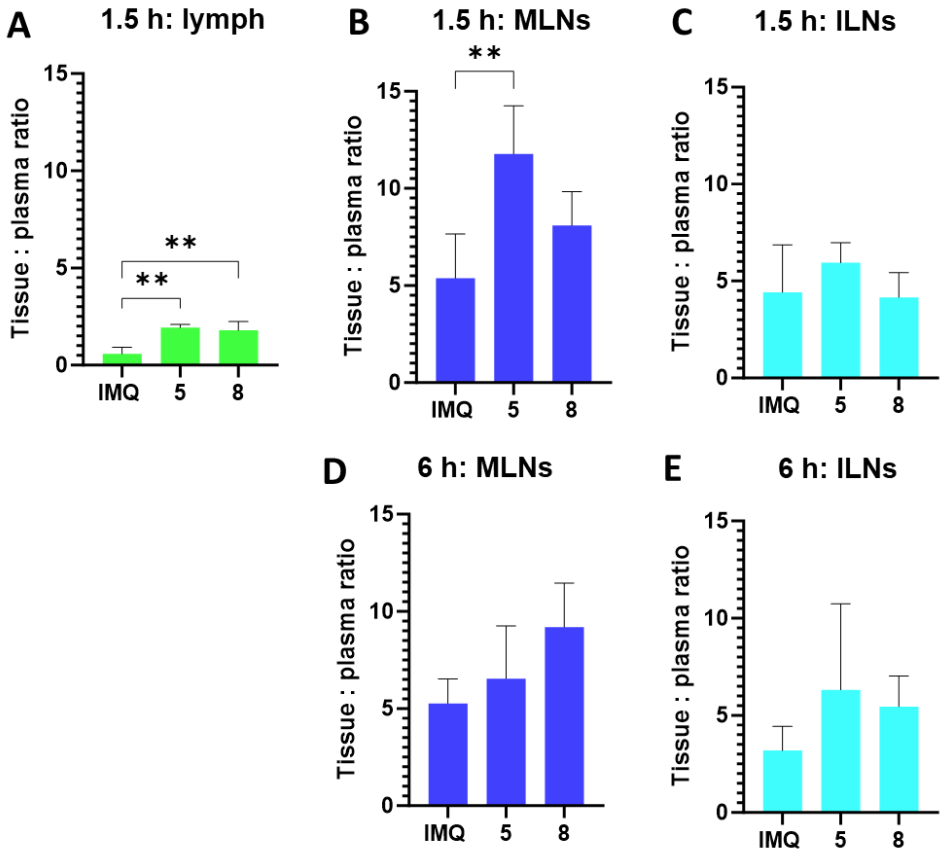

Figure 5-12 The ratios of distribution of IMQ into panel (A) mesenteric lymph, panel (B) mesenteric lymph nodes (MLNs) and panel (C) iliac lymph nodes (ILNs) following oral administration of unmodified IMQ (8 mg/kg) with lipid, prodrug 5 (14.9 mg/kg) and prodrug 8 (16.7 mg/kg). All results are presented as mean ± SD (n = 4 to 8). One-way ANOVA, followed by Dunnett's comparison, was used for statistical analysis. ***, p < .01*.

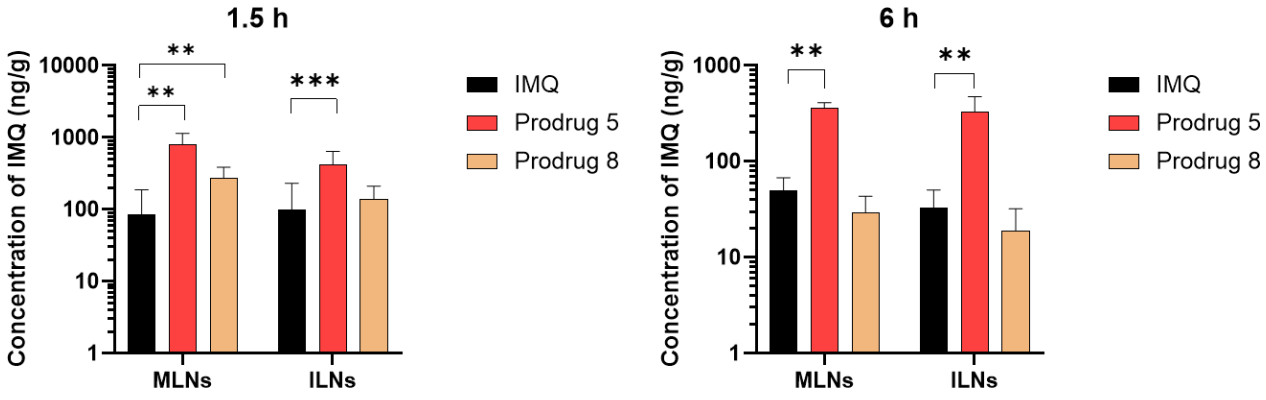

Figure 5-13 The distribution of IMQ mesenteric lymph nodes (ILNs) and iliac lymph nodes (ILNs) following oral administrations of prodrug 5 (14.9 mg/kg) and 8 (16.7 mg/kg) using lipid-based formulation at 1.5 and 6 h (mean ± SD, n = 4 to 8). One-way ANOVA, followed by Dunnett's comparison, was used for statistical analysis. Asterisks denote significance against IMQ. ** p < .05*; *** ,p < .01, ***,p < .001, ****,p < .0001.*

To understand if the distribution pattern of IMQ into tissues (**Figure 4-3**, **Chapter 4**) was altered when prodrugs were administered, we compared the tissue-to-plasma ratio of IMQ in main tissues following oral administration of IMQ and its prodrugs (**Figure 5- 14**). It was shown that with the oral administration of prodrug 5 in particular, the tissue-to-plasma ratio of IMQ was significantly decreased in comparison to the administration of unmodified IMQ and prodrug 8.

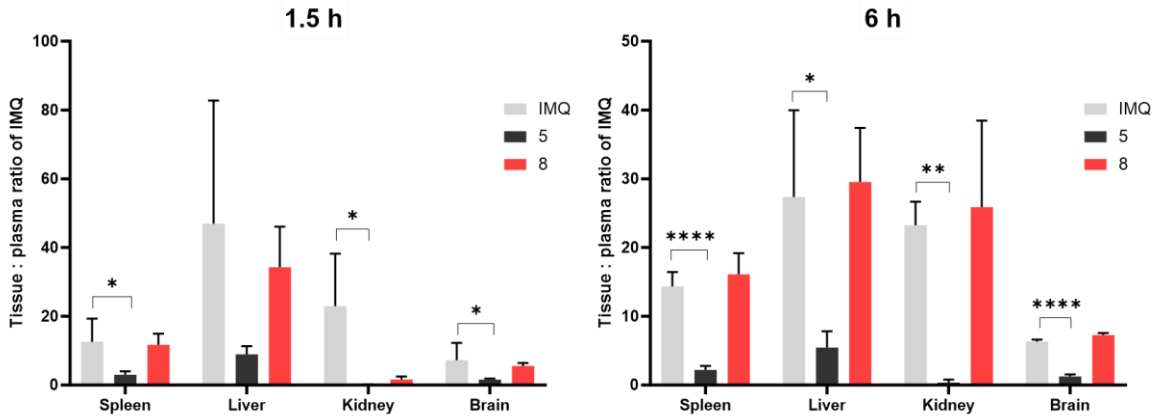

Figure 5- 14 The distribution of IMQ into the spleen, liver, kidney and brain following oral administration of IMQ (8 mg/kg) with lipids, prodrug 5 (14.9 mg/kg) and prodrug 8 (16.7 mg/kg) present as the ratio of IMQ concentration in the analysed sample to IMQ concentration in plasma at 1.5 h and 6 h. All results are presented as mean ± SD (n = 4 to 8). One-way ANOVA, followed by Dunnett's comparison, was used for statistical analysis. Asterisks denote statistical significance against IMQ **, p < .05*; ***,p < .01; ****,p < .0001.*

Additionally, the biodistribution of prodrugs 5 and 8 following oral administration showed that prodrugs were not as widely distributed to various tissues and organs in comparison to IMQ (**Figure 5- 15** and **Figure 4-3**, **Chapter 4**).

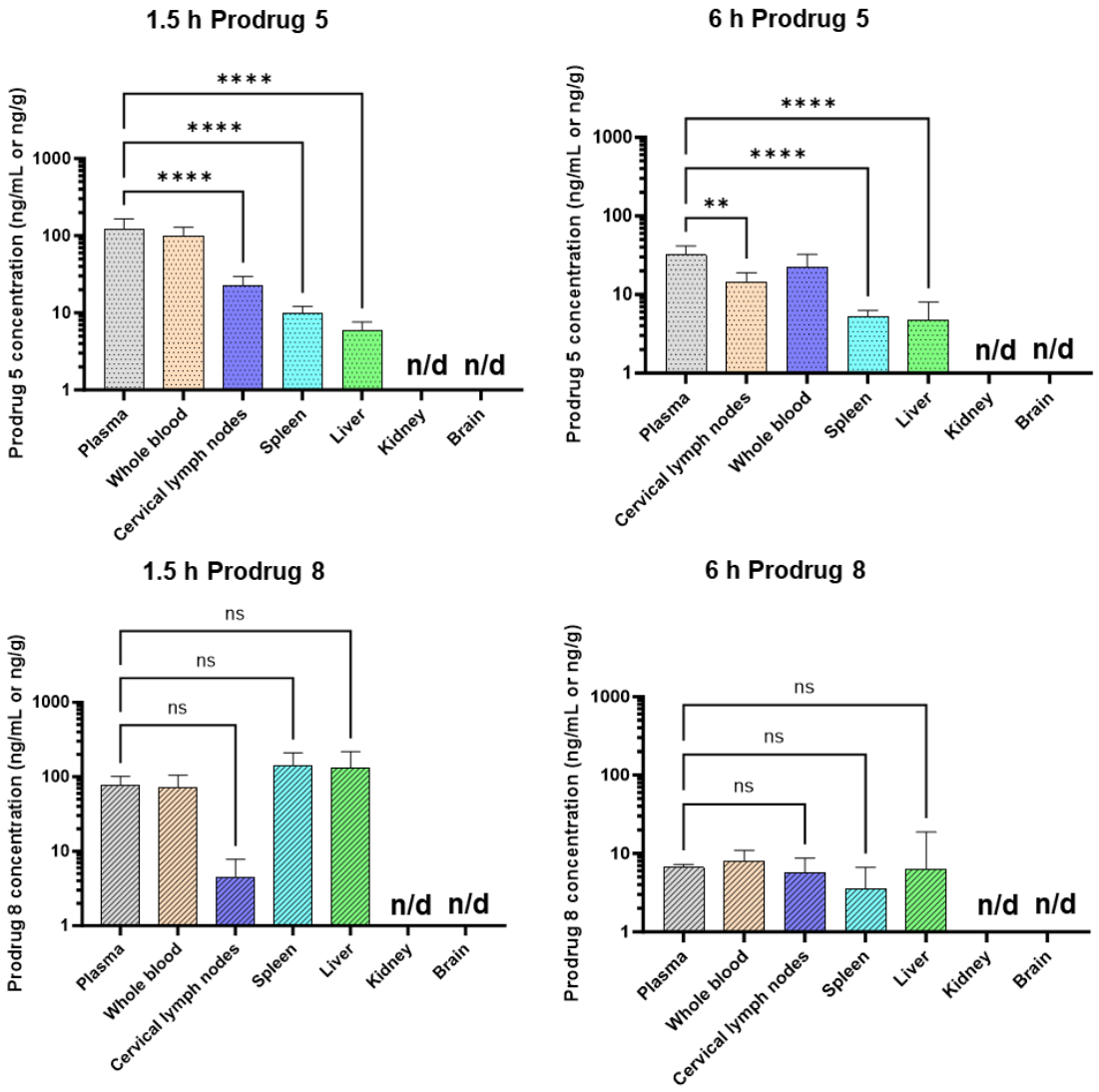

Figure 5- 15 The distribution of prodrug 5 and prodrug 8 following oral administrations of prodrug 5 (14.9 mg/kg) and 8 (16.7 mg/kg) using lipid-based formulation at 1.5 and 6 h (mean ± SD, n = 5 to 6). One-way ANOVA, followed by Dunnett's comparison, was used for statistical analysis. Asterisks denote significance against plasma. * $p < .05$; ** ,$p < .01$, ***,$p < .001$, ****,$p < .0001$. n/d: below the limit of quantification.

5.4 Discussion

In CRC patients, immature DCs can capture tumour-associated antigens (TAAs), inducing their maturation. Only mature DCs are able to present the TAAs through MHC II to naïve T cells in the tumour-draining lymph nodes (LNs), resulting in activation of the anti-cancer immune response [119,155]. The mesenteric lymph nodes (MLNs) and iliac lymph nodes (ILNs) are enriched in DCs and lymphocytes and drain the lymph from the colorectal regions [30,32,34,153]. Previously, it was suggested that the poor therapeutic outcomes of immunomodulators in CRC patients were associated with the suppression of DCs maturation in LNs, resulting in inhibition of activation of $CD8^+$ and CD4+ T cells and also a reduction in T cell infiltration into tumour regions [77,93,120,156,157]. IMQ is the only TRL7 agonist that is currently clinically approved for cancer treatment. It was shown that IMQ activates the DCs *via* the MyD88 signalling pathway, which results in the facilitation of the maturation of DCs and secretion of immunostimulatory signals [111,119]. Therefore, targeted delivery of IMQ to MLNs and ILNs has the potential to facilitate the maturation of DCs and stimulate the anti-tumour immune response, overcoming immune suppression and eventually improving the treatment outcomes for CRC patients. Therefore, in this work, the approach of highly lipophilic amide prodrugs of IMQ in combination with LCT formulation was utilised to deliver IMQ specifically into the intestinal lymphatics following oral administration.

5.4.1 Design of promising prodrug candidates for targeted delivery into intestinal lymph nodes following oral administration

It has been shown previously that one of the main predictors for intestinal lymphatic transport of a molecule is its affinity to CMs [181]. Gershkovich *et al*. suggested that

there were several physicochemical properties of a drug molecule, such as lipophilicity, ionization of molecule at physiological pH, and number of free rotatable bonds, that can be used to predict the affinity of the molecule to CMs [182]. The authors suggested that the most important property of molecules is Log $D_{7.4}$, which is positively related to the affinity of molecules to CMs. By contrast, the ionization of drugs (Log P– Log $D_{7.4}$) and polar surface area are two significant properties that negatively impact drugs' affinity to CMs.

In this work, we aimed to design a series of highly lipophilic prodrugs by conjugating a fatty acid to the amine group present in IMQ (prodrugs 1 – 8, **Figure 5-2**). As expected, the predicted affinities of prodrugs 1 – 8 were significantly increased in comparison to IMQ, which has neglectable association to CMs (< 2 %) (**Table 4-1** and **Table 5-1**).

In addition to high affinity to CMs, efficient biotransformation from prodrugs to IMQ should also be carefully considered in the development of lipophilic prodrugs of IMQ. It is well-known that an amide is generally more stable to hydrolysis than an ester. Therefore, we designed coumarin-based prodrugs 9 and 10 which were expected to facilitate the biotransformation of prodrugs to IMQ (**Figure 5-3 A**). An increase in lipophilicity was found with the conjugation of coumarin-derived structures (**Table 5-1**). Importantly, it was reported that a modification of the phenol group with ester could build up an esterase-sensitive prodrug, which might promote the release of the IMQ (**Figure 5-3 B**) [275].

In addition to the prodrugs of IMQ that were developed in this chapter work, there are several prodrugs of IMQ that have been previously reported. Hantho *et al.* reported an enzyme-directed imiquimod-β-galactopyranoside prodrug. This prodrug was expected

to selectively release IMQ in the tumour microenvironment, which is rich in β-galactosidase (the enzyme for galactopyranoside), potentially resulting in a local immune response in the tumour microenvironment [276]. Kang *et al.* previously designed an IMQ prodrug that was conjugated with a long-chain alkyl group through a disulfide-bound [201]. The authors proposed that since the concentration of reductive glutathione (the reactive agent required to break disulfide bond) is 1,000-fold higher in the tumour intracellular environment than it is in the extracellular environment, this prodrug could selectively release the parent drug within tumour cells. Additionally, it was reported that a TLR 7 agonist conjugated with phospholipids was approximately 1,000-fold more potent for inducing cytokines production than an unconjugated drug [277]. The explanation for this result was that the phospholipid-conjugated TLR 7 agonist might be efficiently transported into plasmacytoid dendritic cells.

In our initial screening of potential prodrug candidates of IMQ for lymphatic delivery following oral administration, none of the proposed prodrugs had sufficient predicted affinity to CMs. The low predicted CMs affinities of these prodrugs could be a result of increased ionization in the plasma, a higher number of H-bond acceptors, and insufficient increase in lipophilicity.

5.4.2 Synthesis of IMQ prodrugs using a simple and high-yielding reaction

The amine present in the chemical structure of IMQ is a primary amine. Theoretically, it should be relatively easy to react with carboxylic acids. However, it was found that the yield of prodrugs using the chemical reaction described in **Figure 2-1** (**Chapter 2**) was low (< 10 %). Hydrochloric acid (HCl) is a byproduct of this reaction. In the reaction solvent, HCl could protonate IMQ (a weak base). As a result, the progress of this reaction was limited. To neutralise HCl in the reaction, potassium carbonate or

trimethylamine was added. However, the yield of prodrugs in this reaction remained low. A cloudy mixture was found in this reaction, suggesting a poor solubilization of the starting materials in the reaction solvent (anhydrous dimethylformamide, DMF). Therefore, in the next step, we tried several alternative solvents, such as dichloromethane (DCM), methanol, DMSO and *N*-methyl-2-pyrrolidone (NMP), to improve the dissolution. It was found that NMP significantly improved the solubilization of the starting materials.

It is worth noting that the primary amine in IMQ is not actually nucleophilic due to resonance of the lone pair into the imidazoquinoline ring. Beutner *et al.* previously reported a reaction using the coupling reagents hexafluorophosphate (TCFH) and *N*-methylimidazole (NMI), for the challenging amide bond formation [194]. This reaction produced a highly reactive acyl imidazolium intermediate of the carboxylic acid. This highly electrophilic intermediate can react with the non-nucleophilic amine on IMQ, resulting in a high yield of amide product (> 70 %).

5.4.3 The potential for intestinal lymphatic transport of IMQ prodrugs

It has been shown previously that the main predictor for intestinal lymphatic transport of a molecule is its affinity to CMs [181]. The affinity of IMQ prodrugs to CMs was substantially higher than that of IMQ (which was undetectable) (**Figure 5-4**). Previously, Chu *et al.* suggested that the degree of unsaturation of the conjugated fatty acid could facilitate the affinity of prodrugs to CMs [192]. In this study, we observed a similar trend (prodrug 4 vs. prodrugs 7 and 8); however, no statistically significant difference was found (**Figure 5-4**).

In this work, the *in vitro* affinity of prodrugs to CMs was assessed by artificial CMs. However, in our previous studies, a significant difference in prodrugs' affinity between artificial CMs and *in vivo*-derived CMs was found in some cases [190–192]. This could suggests that there were certain limitations in the current assessment of intestinal lymphatic transport using only artificial CMs.

The artificial CMs used in our assay were prepared using a protein-free triglyceride emulsion (Intralipid®) *via* ultracentrifugation following a previously described method [182]. Different from protein-free artificial CMs, *in vivo*-derived CMs contain about 2.1 – 6.4 % of protein [278]. The presence of apolipoproteins on the surface of CMs could be one of the reasons for the difference in prodrugs' affinity between artificial CMs and plasma-derived CMs [279]. Additionally, previous measurements showed that the size of particles in 10 % intralipid® emulsion was mainly distributed around 200 ± 10 nm [280]. However, animal- or human-derived CMs contain both small and large sizes of CMs, covering the range from 75 to 1,500 nm [173,174,181]. The limited particle size of artificial CMs could also result in an inaccurate prediction of prodrugs' affinity to natural CMs. Moreover, it has been reported that the plasma clearance of larger size of artificial CMs was slower than the clearance of smaller size of artificial CMs [278]. It suggests that differences in the size of CMs could result in varying clearance and catabolism kinetics. Therefore, it may be worth including natural CMs in the assessment of the intestinal lymphatic absorption of prodrugs before *in vivo* studies. Moreover, Chu *et al.* previously suggested that the spatial binding sites of molecules to CMs (for example, within the core or on the surface of CMs) may also impact their affinities to CMs [195]. CMs are large lipoproteins that consist of amphiphilic lipids on the surface and tri/di/mono-glycerides and fatty acids in the core [281]. The

conjugation of alkyl chains to IMQ may facilitate the encapsulation of prodrugs within the lipophilic core of CMs.

In addition to the CMs affinity, the high solubility in long-chain triglycerides (LCT) (> 50 mg/mL) is another important predictor for intestinal lymphatic transport [182,273]. Combined LCT solubility and CM affinity results suggest that prodrugs 3-8 have a high potential to be transported into the intestinal lymphatics following oral administration (**Table 5-2** and **Figure 5-4**) [192].

5.4.4 The biotransformation and stability of IMQ prodrugs in biorelevant media

The rate of IMQ released from the prodrugs in tested media directly corresponded to the hydrolysis half-life of prodrugs (**Figure 5-7**), suggesting that the hydrolysis of the amide bond was the primary metabolic pathway of IMQ amide prodrugs in the tested conditions. For effective delivery of the active drug to the intestinal lymphatics, prodrug candidates should resist enzymatic hydrolysis in the gastrointestinal (GI) tract but quickly release IMQ once they enter the lymphatic system.

The FaSSIF + esterase medium was previously used to estimate the hydrolysis of the ester prodrugs in the GI lumen [190–192]. This *in vitro* model was originally developed to evaluate the enzymatic hydrolysis of ester prodrugs in human intestine by Stappaerts *et al.* [282]. The authors reported that the biotransformation kinetics of the ester prodrug in the FaSSIF + esterase medium were similar to the kinetics in the human intestinal fluid. Additionally, this *in vitro* model has been previously used by us to assess the intraluminal hydrolysis of ester prodrugs, which were designed for targeted delivery of small molecules to MLNs following oral administration [190–192].

Interestingly, it was found that the hydrolysis of prodrugs was relatively fast in the FaSSIF + esterase medium, especially for prodrug 1 ($t_{1/2}$ < 5 min) (**Figure 5- 8 A**). It should be kept in mind that all tested prodrugs in this work were designed by conjugating IMQ with fatty acids *via* an amide bond (**Figure 5-2**). As a result, the hydrolysis of amide prodrugs should not be rapid with the presence of esterase. Herein, we proposed two hypotheses to explain this phenomenon. Firstly, it is was worth mentioning that the esterase added to the FaSSIF + esterase medium was a crude porcine hepatic extract, with only the esterase activity being quantified. Therefore, additional hepatic enzymes with no quantified activity may exist, resulting in the rapid hydrolysis of prodrugs with the presence of multiple enzymes. Secondly, the amide prodrugs of IMQ might be a substrate for carboxylesterase. It was previously reported that drug molecules that contain amide-derived structures, such as irinotecan, were metabolized by mammalian carboxylesterase [283]. Moreover, Wang *et al.* suggested that carboxylesterase 1 hydrolase both ester and amide molecules containing a small alcohol group or a bulky acyl group [284]. The biochemical structure of primate carboxylesterase showed that there are two ligand-binding sites of carboxylesterase 1. One is rigid, and the other is flexible, resulting in its capacity for catalytic hydrolysis of a wide range of substrates [285]. The chemical structure of IMQ lipophilic prodrugs is similar to a bulky acyl molecule (**Figure 5-2**). As a result, the IMQ prodrug may be a substrate of porcine esterase.

A direct assessment of the prodrug stability in the superior mesenteric lymph was difficult to perform as the lymph is limited in volume and difficult to collect. Previously, plasma has been used as a surrogate for mesenteric lymph to assess the biotransformation of prodrugs in the intestinal lymphatics [190–192]. In general, the mesenteric lymph and plasma share a similar composition of electrolytes, lipids and

proteins, but with some differences [286]. A proteomics study showed that the major difference between lymph fluid and plasma is that the former is significantly enriched in intracellular enzymes that were released from cells during cell apoptosis [287]. Moreover, it was reported that the concentration of carboxylesterase 1 in the mice blood fraction was approximately 2-fold higher than it was in the lymph [288]. Additionally, since the composition of lymph is highly related to the regions in which it is drained, the mesenteric lymph that drains from the small intestine is enriched with lipids [274].

We are aware that plasma could not completely overlap with enzymes and other components of mesenteric lymph. However, to the best of our knowledge, blood fraction is one of the current best available surrogates for lymph fluid. Therefore, rat plasma was used as a surrogate for lymph to assess the biotransformation of prodrugs.

Results from the biotransformation assay using the FaSSIF + esterase medium and rat plasma indicated that, except prodrug 4, synthesised amide prodrugs efficiently released IMQ in the FaSSIF + esterase medium and rat plasma, suggesting an efficient hydrolysis of the amide bond (**Figure 5-7**). Previously, a lipidised IMQ prodrug was synthesized by conjugating IMQ with cholesterol *via* an amide bond. It was observed that this IMQ-cholesterol prodrug can efficiently release the active molecule in a PBS/DMSO mixture [230]. It was suggested that the hydrolysis of the amide bond in the IMQ prodrug could easily happen even without the presence of hydrolase. However, one of the well-known challenges for amide prodrugs is that the amide bond is substantially more stable than ester [188,275,289]. Therefore, we hypothesised that the rapid release of IMQ from prodrugs is related to its unique chemical structure and its properties as a leaving group. The amine in the IMQ is not an electrophile amine

but an aniline. The electronic resonance could facilitate the release of IMQ, resulting in rapid hydrolysis of IMQ prodrugs.

In addition, it was noted that with an increase in the length of the alkyl chain (prodrugs 1-4), the half-lives of prodrugs in FaSSIF with added esterase activity and rat plasma were also increased, most likely due to steric hindrance [290,291]. Therefore, IMQ amide prodrugs 5-8 were designed as conjugates with unsaturated fatty acids to minimise steric hindrance. As expected, the introduction of unsaturation to prodrugs resulted in a faster conversion to active moiety.

It was previously reported that a decrease in the concentration of carboxylesterase 1 (which was likely related to the enzymatic hydrolysis of IMQ prodrugs) was observed in the mice lymph during the intraduodenal infusion of Intralipid ® [288]. In *in vivo* studies, lipids were co-administered with IMQ prodrugs to facilitate the production of CMs (**Section 2.7.4**). Therefore, the actual biotransformation of prodrugs to IMQ in the intestinal lymph could be slower than the *ex vivo* prediction. However, for rats, the flow rate of intestinal lymph is approximately 470-fold slower than the flow rate of intestinal blood (0.9 mL/h vs. 426 mL/h) [170,171]. Similarly, the flow rate of intestinal lymph is approximately 754-fold slower than that of blood in humans (1.16 mL/min vs. 500-750 mL/min) [170,172]. Considering the slow flow rate of intestinal lymph, it may allow prodrugs sufficient time to release the active drug in the lymphatics.

To evaluate the biotransformation of IMQ amide prodrugs in the GI tract more accurately, in this work, the brush border enzyme vesicles (BBMVs) medium was also evaluated for assessment of the hydrolysis of amide prodrugs. The BBMVs medium represents the enzymatic conditions in the enterocytes. In the GI tract, BBMVs are

mainly located within the brush border microvilli of epithelia (enterocytes) and about 16-25 % of BBMVs are secreted into the intestinal lumen [292]. These vesicles are enriched in metabolic enzymes, including alkaline phosphodiesterase, aminopeptidase and carboxypeptidase [293]. Previously, BBMVs pellets have been used for assessing the stability of peptides, digestion of nutrients and transport of drug molecules during GI absorption [294–298]. The brush border membrane could be one of the primary hydrolysis sites for amide prodrugs *in vivo*. The biotransformation assessment using BBMVs showed that all prodrugs were quite stable (**Figure 5-7**), suggesting that designed prodrugs are likely to be resistant to hydrolysis, especially near and in the enterocytes, before entering the intestinal lymphatics.

Taken together, the results of CM affinity, LCT solubility, biotransformation and stability, prodrugs 5 and 8, were selected as the most promising candidates for delivering IMQ into mesenteric and retroperitoneal lymphatics *via* the CM pathway.

5.4.5 Pharmacokinetics of prodrugs 5 and 8 and IMQ

It was shown previously that the lipophilic prodrug approach combined with a lipid-based formulation could increase the F_{oral} of drugs [190,191]. However, in this work, there was no statistically significant difference in the F_{oral} of IMQ between the administration of unmodified IMQ and the administration of prodrugs 5 and 8 (**Table 4- 3** and

Table 5- 4). The plasma concentration-time profile of IMQ following oral administration of prodrugs 5 and 8 was not prolonged and erratic as was the case for unmodified IMQ (**Figure 5-9**). Therefore, we hypothesised that prodrugs 5 and 8 did not increase the extent of IMQ absorption but potentially changed the absorption pattern and pathway. To test this hypothesis, the biodistribution of prodrug 5, prodrug 8 and IMQ released from the prodrugs was assessed following oral administration of prodrugs 5 and 8. Prodrugs 5 and 8 have significantly higher affinity to CMs than unmodified IMQ (**Figure 5-4**). As a result, high concentrations of prodrugs 5 and 8 were found in mesenteric lymph, strongly suggesting that the affinities of prodrugs 5 and 8 to CMs (70.3 % and 76.5 %, respectively) were sufficient for the substantial lymphatic uptake to occur *in vivo* (**Figure 5- 10 A** and **C**). It should be mentioned that the amine group on the 4-position of IMQ is an essential functional group responsible for its pharmacological effect. Therefore, although the off-target distribution of prodrugs could not be completely excluded (**Figure 5- 15**), the amidation of the amine on the 4-position with alkyl chains is unlikely to increase the toxicity of IMQ [230].

It should be noted that previously reported lipophilic prodrugs designed by us and others for intestinal lymphatics targeting mainly used an ester bond to conjugate active moiety with lipophilic structures [187,188,190–192,299]. To the best of our knowledge, only one work by Han *et al.* has previously attempted to design lipophilic prodrugs for targeting intestinal lymphatics through an amide bond [188]. The authors reported that the amide lipophilic prodrug approach did not improve intestinal lymphatic targeting

due to insufficient release of the active drug within the mesenteric lymph [188]. Notably, this amide prodrug was developed for mycophenolic acid, an immunomodulator with a distinct chemical structure from IMQ. In the case of the mycophenolic acid prodrug, the amide bond is not directly attached to the benzophenone-like aromatic core but is instead linked *via* an ethyl chain. As a result, the electron-withdrawing effect of the aromatic system does not effectively facilitate amide bond hydrolysis, limiting the release of the active parent drug in the lymphatic system.However, in the current study, a significant increase in the lymph-to-plasma concentration ratio of IMQ was observed when prodrugs were administered, in comparison to the administration of the unmodified IMQ (**Figure 5-12 A**). Moreover, a substantial increase was found in the MLNs-to-plasma concentration ratio of IMQ from 5.3-fold to 11.8-fold with prodrug 5 ($p = 0.0029$) and to 8.0-fold with prodrug 8 ($p = 0.079$) in comparison to unmodified IMQ (**Figure 5-12 B)**. Most importantly, following oral administration of prodrug 5, IMQ concentrations in MLNs were significantly higher than in plasma, indicating that IMQ was targeted into intestinal LNs (**Figure 5- 11**)**.**

However, as opposed to prodrug 5, IMQ concentrations in MLNs were not significantly higher than in plasma following the administration of prodrug 8 and unmodified IMQ. Additionally, prodrug 5 achieved a higher concentration of IMQ in MLNs and a higher MLNs-to-plasma ratio in comparison to prodrug 8 (**Figure 5- 11 and Figure 5-12 B)**. This is probably because the lymphatic delivery of prodrug 8 was lower than that of prodrug 5 (**Figure 5- 10 A** and **C**) and the biotransformation of prodrug 8 to IMQ in intestinal lymphatics was slower than that of prodrug 5 (**Figure 5- 8**).

It is important to note that MLNs are important targets for immune activators, such as toll-like receptor 7 (TLR 7) agonists. These lymph nodes are rich in DCs that are derived from the primary lymphoid tissues and DCs that migrate from the intestinal tissue, as well as naïve T cells, providing an environment for immune cells cross-communication in CRC patients [300]. The concentration of IMQ in MLNs is 1.6-fold higher than its EC_{50} (around 2 μM) as a TLR7 agonist, suggesting that targeted delivery IMQ to MLNs using prodrug 5 can potentially improve the treatment for CRC [301].

Concerning ILNs targeting, results suggest that following oral administration of prodrug 5, IMQ concentrations in ILNs were significantly higher in comparison to oral administration of unmodified IMQ (**Figure 5-13**). However, the ILNs-to-plasma concentration ratio of IMQ was not significantly different between oral administration of unmodified IMQ and prodrugs (**Figure 5-12 C**). This could suggest that the increase in the IMQ concentrations in ILNs may not be a direct result of intestinal lymphatic transport.

Additionally, compared to the V_{ss} of IMQ (3376.3 ± 1842.0 mL/kg) (**Table 4- 3**), a lower V_{ss} of prodrug 5 (434.8 ± 327.1 mL/kg, $p < 0.05$) and the V_{ss} of prodrug 8 (2241.7 ± 1221.3 mL/kg, $p > 0.05$) was found (**Table 5-5**). Moreover, results from the two-compartmental analysis model suggested that the unusually high distribution volume of the central compartment (in comparison to the distribution volume of the peripheral compartment) of IMQ was not present for prodrugs 5 and 8 (**Table 4-4** and

Table 5- 6). As a result, when prodrug 5 was administered, this non-specific distribution of IMQ was reduced (**Figure 5- 14**), suggesting that the off-target toxicity of IMQ could be potentially reduced using the prodrug approach.

5.5 Conclusion

In this chapter, lipophilic amide prodrugs were designed and assessed for their potential for intestinal transport and targeting of active IMQ into mesenteric and retroperitoneal lymph nodes following oral administration *via* the CMs pathway. In the design and *in vitro* assessment for prodrugs, we found that: 1) conjugation with a linear alkyl chain resulted in a substantial affinity of prodrugs to artificial CM; 2) inclusion of unsaturated bonds in the alkyl chain facilitated the active moiety released from amide prodrugs. Prodrugs 5 and 8 were selected as the most promising candidates and, therefore, were orally administered to rats. They were efficiently delivered to mesenteric lymphatics and released active IMQ in mesenteric lymph and lymph nodes. This work suggests that the approach of targeting IMQ to the mesenteric lymphatic system using lipophilic amide prodrugs is efficient. This study demonstrates more generally that the lipophilic amide prodrug approach for amine molecules for intestinal lymphatic targeting is feasible.

Chapter 6 General discussion and future work

6.1 General discussion

The aim of this PhD project was to deliver imiquimod (IMQ) to mesenteric and retroperitoneal lymph nodes (LNs) in a targeted manner using the lipophilic prodrug approach following oral administration. We aimed to achieve the activation of the antigen-presenting cells, such as dendritic cells (DCs), in the LNs, which drain lymph from the colorectal regions. As a result, the inhibitory immune responses that are regulated by the tumour cells could potentially be minimised, and the anti-tumour immune responses could be facilitated by the activation of DCs. Therefore, this approach could potentially improve the therapeutic outcome of patients diagnosed with colorectal cancer (CRC).

In this work, the lipophilic prodrug approach for intestinal lymphatic targeting was applied to the toll-like receptor 7 agonist, IMQ. To the best of our knowledge, the prodrugs of IMQ developed in this project were the first amide prodrugs that have been designed for intestinal lymphatic transport and could efficiently release the active parent molecule into the intestinal lymphatic system.

This project achieved the following:

1) Sensitive bioanalytical methods using high-performance liquid chromatography with UV detection (HPLC-UV) or with tandem mass spectrometry (LC-MS/MS) for the determination of the concentrations of IMQ and its prodrugs in biological samples.

2) Obtaining pharmacokinetics (PK) parameters and the biodistribution profile of IMQ in various LNs and tissues.

3) Design and synthesis of lipophilic prodrugs of IMQ using a high-yielding amidation reaction.

4) Establishment and validation of BBMVs *ex vivo* model for understanding the biotransformation of prodrugs to IMQ in the gastrointestinal tract.

5) Obtaining the PK profile of prodrugs 5 and 8 which were the most promising prodrugs and the PK profile of IMQ that was released from prodrugs.

6) Obtaining biodistribution profile of IMQ, prodrug 5 and prodrug 8 following the oral administration of prodrugs.

6.1.1 Bioanalytical method for the determination of IMQ and its prodrugs in biological samples

In **chapter 3** of this thesis, a sensitive, accurate and robust bioanalytical method for the determination of the concentrations of IMQ was developed and partially validated following the FDA guidelines [206]. Most previously developed analytical methods for IMQ only allowed the quantification of IMQ in a simple solvent matrix [212–215]. The HPLC-UV bioanalytical method of IMQ developed in this chapter can be used for the determination of the concentrations of IMQ in biological matrix samples, such as rat plasma, with a lower limit of quantification (LLOQ) at 15 ng/mL. The LLOQ of this method was more sensitive than previously reported methods [216,219]. Although one previous study reported a bioanalytical method for IMQ using HPLC-UV with an LLOQ of 1 ng/mL, the high volume of blood required (2 mL of whole blood) limited the application of this method in animal studies with rodents [140].

Additionally, in a previously reported bioanalytical method, a costly solid-phase extraction was required for sample preparation [302]. In our developed method, a

simple and cost-effective liquid-liquid extraction was used to minimize the potential endogenous interference and provide an efficient recovery of IMQ after the sample preparation. The cost-effectiveness of sample preparation is important in PK and BD studies since there will be a substantial amount of samples to be analysed.

It was reported that the oral bioavailability (F_{oral}) of IMQ was close to zero due to the extensive first-pass metabolism of IMQ in rats [252]. This suggests that a more sensitive bioanalytical method was needed to complete the PK profile of IMQ following the oral administration. Therefore, a tandem mass spectrometry (MS/MS) detector methodology was used to improve the LLOQ of this current assay. The LC-MS/MS bioanalytical method developed by us had an LLOQ at 1.25 ng/mL and only required 100 µL of plasma as sample volume. Moreover, the range of detection could be extended from 1.25 – 200 ng/mL to 1.25 – 4,000 ng/mL after the dilution of samples with blank plasma. The small volume of sample and the wide range of detection concentrations guarantee the application of this LC-MS/MS in various conditions.

In the current method, IMQ was eluted at the initial isocratic stage of the mobile phase (30:70 ammonia formate, pH = 3, and methanol) within 10 min. The composition of the organic solvent can be increased for the elution of lipophilic prodrugs of IMQ. As a result, IMQ, propranolol (internal standard), and its prodrugs were eluted at different retention times, avoiding cross-interferences. Moreover, this method could be potentially used for the simultaneous determination of the concentrations of IMQ and other compounds with minor adjustments.

The targeted delivery of IMQ with other chemotherapeutic agents (such as doxorubicin and irinotecan) or immunotherapeutic agents (such as PD-1/PD-L1 inhibitor) to tumour-associated regions demonstrated a promising therapeutic outcome in CRC

models [210,303,304]. The simultaneous determination of the local concentration of IMQ and the co-administrated drugs using bioanalytical assay is crucial. Due to the different lipophilicity between IMQ and the co-administrated drugs, the separation of analytes can be potentially achieved with the gradient increase (or decrease) in the proportion of the organic solvent in the mobile phase after the elution of IMQ.

6.1.2 intravenous formulation of IMQ

The poor solubility of IMQ in commonly used intravenous (IV) formulations was an obvious challenge in completing the PK profile of IMQ following IV bolus administration. Previously reported IV formulations of IMQ were not commercially available (under the protection of a patent) [137] or had other concerns about animal safety [140,210]. Therefore, in this chapter, we first developed a safe IV formulation of IMQ at a concentration of 0.8 mg/mL using a propylene glycol (PG)-water mixture (80:20, *v/v*) at the pH range of 6 - 6.5. With this formulation, the PK profile and parameters of IMQ in rats following (IV) bolus administration and oral administration were reported in **Chapter 4**.

Alternatively, nanoemulsion could be a potential formulation for poor water-soluble drugs, such as IMQ. Nanoemulsion consists of an oil and aqueous phase, which is supplemented with surfactants. Previously, a nanoemulsion of IMQ was developed using oleic acid, rose oil and PG [238]. Results showed that this formulation could efficiently encapsulate IMQ in nanoparticles (> 90 %) found in the size range of 150 – 400 nm. However, this formulation only allowed the dissolving of 12.5 mg of IMQ in a volume of 25 mL (a.k.a 0.5 mg/mL), which limits its application as an IV formulation of IMQ in our preclinical studies. Moreover, the oil used in this formulation is another safety concern for IV administration.

6.1.3 Pharmacokinetics and biodistribution profile of unmodified IMQ

It was found that the elimination rate of IMQ in rat plasma was fast ($t_{1/2}$ = 0.73 ± 0.05 h), which was consistent with previous reports [140,252]. The BD studies of unmodified IMQ show that the distribution of IMQ in plasma, serum and blood is not significantly different, and the blood-to-plasma ratio or the blood-to-serum ratio of IMQ was close to 1, suggesting a low intracellular distribution of IMQ in red blood cells. The clearance of IMQ in plasma was 4.468 ± 1.569 L/h/kg,[294] indicating a high hepatic extraction ratio of IMQ. The PK studies of IMQ showed that the oral bioavailability (F_{oral}) of the drug is limited (< 10 %), which may be a direct result of the rapid hepatic first-pass metabolism of IMQ. A clinical study of IMQ reported that the clearance of IMQ in humans was 0.963 ± 0.158 L/h/kg following an oral administration of the drug, which is slower than the clearance of IMQ in rats reported in our studies [140]. An *in vitro* metabolism study using human cytochrome P450 and mouse liver showed that IMQ was predominantly mediated by cytochrome P450 1A1 and 1A2 [305]. It was reported that the human's hepatic CYP 1A1 is less responsive and less sensitive to its substrate in comparison to rats' CYP 1A1 [254]. Therefore, we suggested that the difference in the clearance of IMQ between humans and rats could be a result of various activities of hepatic enzymes that are responsible for the metabolism of IMQ.

A similar fast clearance and low F_{oral} of another TLR 7 agonist, isatoribine, was reported, which limits the clinical application of isatoribine [306]. ANA975 is a prodrug of isatoribine (**Figure 6- 1**). The phase I clinical trial showed that the bioavailability of isatoribine was over 85 % following the oral administration of ANA975 [307].

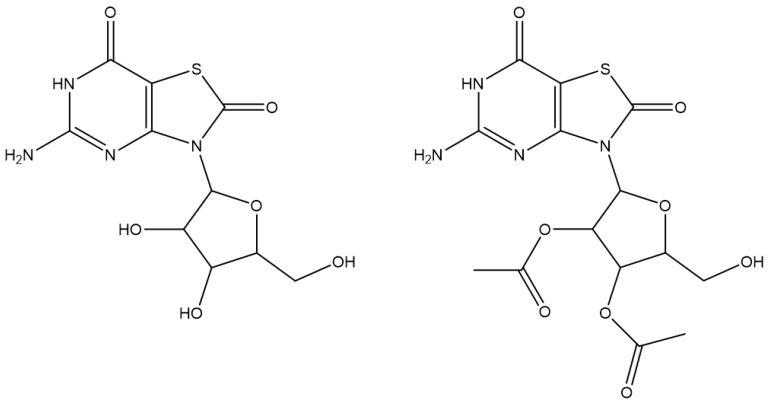

Figure 6- 1 The chemical structure of isatoribine and its prodrug ANA975 [307].

A high volume of distribution (V_{ss}) of IMQ (3.376 L/Kg) was observed in our work, which is consistent with previous studies [140,241]. Considering the moderate lipophilicity of IMQ (Log P = 3.46), the V_{ss} of IMQ is unusually high. Moreover, a low distribution of IMQ into the blood cells was found in our study, which could not explain the high V_{ss} of IMQ. Therefore, we also included a two-compartmental model to explain the relatively high V_{ss}. The compartmental modelling suggested that IMQ was mainly distributed into the central compartment (V_1) which represents the blood circulation and highly blood-perfused organs (such as the liver, kidney and spleen) rather than the peripheral compartment (V_2). A similarly high volume of distribution of a non-lipophilic drug molecule has been observed in animals following the IV administration of metformin. Metformin is a hydrophilic drug (Log P = -1.43), which was found to have a V_{ss} of 1311 mL/kg in rats. It was suggested that the high V_{ss} of metformin could be a result of the drug's accumulation in the GI wall and liver [256]. Our studies showed the average concentration of IMQ in the liver is the highest, and the concentration of IMQ in the liver is significantly higher than it in the plasma (**Figure 4-3**, **Chapter 4**). The high distribution of IMQ in the liver could potentially explain the large V_{ss} of IMQ.

Previously, the lipid-based formulation was used to improve the F_{oral} of lipophilic compounds because it could potentially enhance intraluminal solubility and facilitate the intestinal lymphatic absorption of the drugs, resulting in partial avoidance of the first-pass metabolism [179,183,203]. Since IMQ does not show lipophilic physicochemical properties, it was expected that the intestinal lymphatic transport of IMQ following oral administration was limited [182]. As we expected, the F_{oral} of IMQ in the lipid-based formulation group did improve in comparison to the lipid-free formulation group, suggesting that there was a low chance for IMQ itself without chemical modifications to be absorbed into the intestinal lymphatics following oral administration. Moreover, the low solubility of IMQ in long-chain triglycerides and the low affinity of IMQ to artificial chylomicrons confirmed the limited potential of lymphatic absorption of unmodified IMQ [181–184].

Although there was no statistically significant difference between the concentration of IMQ in LNs and in plasma, the average concentrations of IMQ in the examined LNs (MLNs, iliac LNs, cervical LNs and inguinal LNs) were 3- to 5-fold higher than it in the plasma. It should be noted that the BD of IMQ in the LNs, which are the main areas of therapeutic targeting of TLR 7 agonists, were reported in our work for the first time.

In our previous studies, it was found that when drug molecules were absorbed into intestinal lymphatics *via* the CMs pathway, the concentration of the drug in the mesenteric lymph was much higher than its concentration in the plasma [180,190–192,195,196,203]. However, in the case of IMQ, similar average concentrations of the drug in the mesenteric lymph and in plasma suggested that the accumulation of IMQ in the LNs was not a direct result of intestinal lymphatic transport. It should be kept in mind that the V_{ss} of IMQ was quite high, which suggests that the high concentration of

IMQ in the LNs could be a result of the wide distribution of the drug into tissues. The high distribution of IMQ was also found in highly blood-perfused organs, as well as the relatively medium to low blood-perfused regions, such as skeleton muscle and the brain. The unspecific systemic distribution of IMQ may be responsible for the various adverse effects of the drug and the poor therapeutic outcomes in the clinical trials [131,141]. Therefore, in **chapter 5**, a series of highly lipophilic prodrugs of IMQ were designed and synthesised, which were expected to deliver the drug to the intestinal LNs on a targeted manner, and also minimise the wide systemic distribution.

6.1.4 Design and selection of promising prodrug candidates for targeted delivery of IMQ to intestinal lymphatic

Chapter 5 of this thesis started with the design of lipophilic prodrugs of IMQ based on a previously reported *in silico* model [182]. The first generation of prodrugs (prodrugs 1-4) was designed by conjugating IMQ with medium-chain (C10) to long-chain (C18) saturated fatty acid structures. The second generation of prodrugs 5-8 was designed by conjugating IMQ with unsaturated alkyl chains (a.k.a. unsaturated fatty acid). The unsaturated long-chain structure was expected to improve the affinity of CMs and facilitate the release of the parent molecules. Additionally, it was previously reported that the conjugation of IMQ with unsaturated fatty acid could also improve the molecular penetration into cells [193].

In the next step, we aimed to synthesize the designed prodrugs 1-8 with a high-yield amidation reaction. In this work, we found that the primary amine on the C4 position of the imidazoquinoline structure was not nucleophilic due to the attached imidazoquinoline structure but more electrophilic. As a result, the amidation of IMQ with acyl halide had a limited yield. An amidation reaction for producing IMQ-oleate

prodrugs using coupling reagents *N*-Hydroxysuccinimide (NHS) and *N, N'*-Dicyclohexylcarbodiimide (DCC) was previously reported [193]. However, we found that no product of the IMQ's prodrugs when the same reaction was applied. Moreover, during the reaction, a cloudy mixture of the starting materials was noticed. This observation suggested that the limited production of the IMQ prodrugs could be a result of IMQ itself not being dissolved in the reaction solvents. In this work, we found that *N*-methyl-2-pyrrolidone (NMP) could be used to improve the dissolution of IMQ. Moreover, a previously reported reaction for challenged amidation involving coupling reagents hexafluorophosphate (TCFH) and *N*-methylimidazole (NMI) was used in the synthesis of prodrugs 1-8 of IMQ [194], which offered a relatively high yield (> 70 %).

It has been shown that the high affinity of drugs to the CMs is important for the intestinal lymphatic transport of drugs following oral administration [181,182,190–192,195]. Previously, Porter's group suggested that the prodrugs designed with alkyl derivatives structures had limited lymphatic transport following oral administration in comparison to triglyceride (TG)-mimetic structures [186,188,281]. However, *in silico* and *in vitro* results in our work show that the simple alkyl prodrugs of IMQ have a significantly higher affinity to CMs (> 60 %) in comparison to IMQ itself, which has a negligible affinity to CMs (< 2 %). The results from *in vivo* studies show that the concentrations of prodrugs 5 and 8 in mesenteric lymph were 50- and 11-fold, respectively, higher than their concentrations in the plasma, confirming a high lymphatic absorption of these two prodrugs. This suggests that the TG-mimetic structures were not necessary in the case of IMQ. Additionally, cannabidiol, testosterone and halofantrine do not contain a biomimetic structure (such as triglycerides) but are still largely absorbed into intestinal lymphatics following oral administration [180,308,309]. It suggests that other physicochemical properties, such

as lipophilicity and ionisation, may predominately decide the lymphatic absorption of the drug molecules [182].

It should be noted that the amine group on the C4 position of IMQ is the key functional group for the pharmacological effects of the drug [230]. Therefore, the substantial amounts of prodrugs 5 and 8 in the intestinal lymphatic systems were not likely to introduce any adverse effect.

Optimal prodrug candidates should resist enzymatic hydrolysis before they are absorbed into the lymphatics and efficiently release the active drug in the lymphatic system, ensuring effective delivery of IMQ to the intestinal LNs following oral administration. Previously, the biotransformation of the prodrugs in the GI tract was assessed by *in vitro* models, such as FaSSIF supplemented with esterase [190–192,282] and lipid-digestion buffer [186], as well as *ex vivo* models, such as bile and pancreatic fluid [289]. These models are only able to estimate the enzymatic hydrolysis of the prodrugs in the intestinal fluid. However, the association between prodrugs and CMs actually happens in the intracellular space of enterocytes [185]. Previous work from our group and others did not include the assessment of the stability of prodrugs in the enterocytes. In this project, the brush border membrane vesicles (BBMVs) were first used to assess the biotransformation of prodrugs when the compounds pass through the brush border microvilli of epithelia. It was found that all synthesised prodrugs had a long half-life in the presence of BBMVs, suggesting reasonable stability of the prodrugs in the enterocytes.

The biotransformation of the prodrugs to IMQ in the lymphatics was evaluated using rat plasma as a surrogate for lymph following a previously reported protocol [190–192]. Previous studies in ours and Prof Christopher Porter's group have shown that the

simple alkyl prodrug structure could not efficiently release the active moiety in the lymphatic system, limiting the local concentration of active drugs in the targeted sites within intestinal lymphatics [188,190,191]. It was found that synthesised prodrugs (except prodrug 4) had a relatively short half-life in the rat plasma, suggesting that they could be efficiently converted to the parent drug in the lymph. Moreover, it was found that the increase in the alkyl chain length could significantly prolong the half-lives of prodrugs in the plasma. By contrast, the addition of unsaturated bonds to the alkyl chain could facilitate the release of IMQ from prodrugs in the plasma (prodrugs 2 vs 5, 3 vs 6, and 4 vs 7 or 8). These results suggested that unsaturated moieties could potentially overcome the steric hindrances introduced by the elongation of alkyl chains, resulting in the efficient release of active drugs [291].

6.1.5 Targeted delivery of IMQ to intestinal lymphatics using the lipophilic prodrug approach

The MLNs drain lymph from the colorectal regions and are enriched in DCs which can be activated by IMQ *via* binding to the TLR 7 [30,32,34,153]. In the patients affected by CRC, the activation of DCs is inhibited by the suppressive signals that are regulated by the tumour cells. Therefore, targeted delivery of IMQ using the lipophilic prodrug approach into the MLNs can potentially facilitate the anti-tumour immune response that is regulated by the activated DCs. In previous studies from our group and others, chemical structures of prodrugs were mainly designed through an ester linker. Only the ester-type prodrugs have been reported as successful for targeted delivery of the active parent drugs into the MLNs [185–192,310]. In contrast, the amide bond is generally considered unsuitable for lymphatic targeting of drugs due to their high stability, which makes them difficult to hydrolysed within the lymphatic system

[275,311]. Moreover, Han *et al.* reported that although an amide prodrug itself can be transported into the mesenteric lymph following oral administration, it could not enhance the local concentration of the parent molecule (mycophenolic acid) in the intestinal lymphatics because the prodrug failed to convert into the active parent compound in lymphatic system.

Amide structure was thought not suitable for chemical structures of prodrugs due to the high stability of this chemical bond [289]. However, in the case of IMQ, it only contains an amine group which is prodrug-able. Our results showed that following the oral administration of prodrugs 5 or 8, the average concentration of IMQ (released from the prodrugs) in MLNs was 11- or 8-fold higher, respectively, than its concentration in plasma. The lymph-to-plasma ratio of IMQ concentration significantly increased from 0.5-fold to 1.9-fold in the mesenteric lymph following the oral administration of prodrug 5. The tissue-to-plasma ratio of drug concentration is an important indicator for targeted delivery and has been used to evaluate the specific distribution of drugs [312–314]. Therefore, our results indicate that the amide prodrug could efficiently release IMQ in the intestinal lymphatics and targeted delivered the parent molecules in the LNs.

Similar to IMQ, some other chemotherapeutic agents and immunomodulators contain only the amine group as the prodrug-able structure (**Figure 6-2**). This current work shows the feasibility of using amide prodrugs in targeted delivery to the MLNs for the first time.

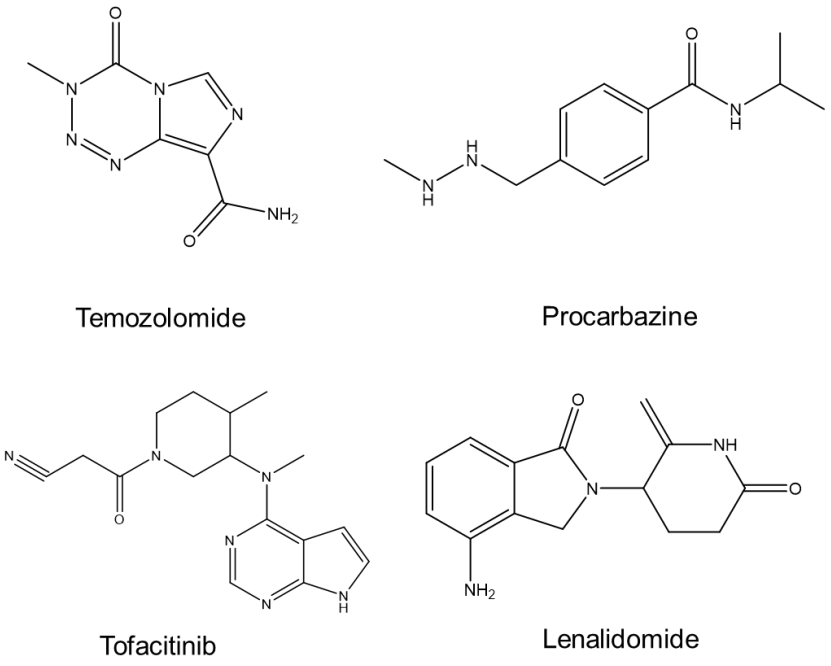

Figure 6-2 Examples of chemotherapeutic agents (temozolomide and procarbazine) and immunomodulators (tofacitinib and lenalidomide) that contain only amide group as a prodrug-able structure.

The lymphatics from the lower part of colorectal regions and the upper part of the anus also drain into the iliac LNs [176,177,315], suggesting that iliac LNs are also an important targeting area of IMQ. It was reported that lipophilic molecules could be absorbed in the colorectal areas [316,317] and be drained into iliac LNs following the pattern of lymphatic drainage [176,177,315]. Our results showed that a significantly higher average concentration of IMQ in iliac LNs, compared to the plasma concentration of IMQ, was only observed following the oral administration of prodrug 5. Following the oral administration of prodrug 5 or prodrug 8, the tissue-to-plasma ratio of the concentration of IMQ in the iliac LNs was not different in comparison to the oral administration of IMQ itself. These results suggest that the lipophilic prodrug approach may not effectively deliver drug molecules to the iliac LNs following oral administration.

Previously, small drug molecules were delivered to iliac LNs using nanoparticles *via* intramuscular injection (on the leg) or microneedles *via* subcutaneous injection (on the back skin) [318,319]. This delivery approach is based on the lymphatic drainage pattern from the popliteal and inguinal LNs to the iliac LNs [178]. Additionally, Galandiuk *et al.* reported that the concentration of 5-fluorouracil in the iliac LNs was higher following rectal administration in comparison to other administration routes [320], suggesting that the suppository formulation may be useful in the targeted delivery of drugs to the iliac LNs.

In addition to delivering IMQ to LNs, in this work, the wide and unspecific distribution of IMQ was minimized. Our results show that the tissue-to-plasma ratio of IMQ in the highly blood-perfused organs and the low blood-perfused organs was significantly decreased following the oral administration of prodrugs in comparison to the administration of unmodified IMQ. This suggests that the off-target toxicity of IMQ could be minimized due to the decrease in the systemic distribution of IMQ using the lipophilic prodrug approach.

It should be noted that the primary purpose of this project is to deliver IMQ into intestinal lymphatics. On the other hand, prodrugs 5 and 8 were expected to improve the F_{oral} of IMQ because they can transport IMQ into the systemic circulation, avoiding hepatic first-pass metabolism [190,191,321]. However, in this work, the F_{oral} of IMQ was not significantly improved after the oral administration of prodrugs 5 and 8 (15.6 ± 9.8 % and 20.1 ± 15.0 %, respectively) in comparison to the oral administration of unmodified IMQ (6.7 ± 4.2 %). It was found that the F_{oral} of the prodrugs 5 and 8 were only 1.5 ± 1.5 % and 1.29 ± 0.3 %, respectively. The limited F_{oral} of the prodrugs may be one of the reasons for the lack of improvement in the F_{oral} of IMQ using prodrug approach.

6.2 Future work

6.2.1 *In vivo* efficacy and toxicological study of prodrugs of IMQ

The local concentration of IMQ in the intestinal lymphatics was significantly improved using the lipophilic prodrug approach. Following the assessment of the biodistribution of IMQ in the lymphatics in rats, the therapeutic efficacy of prodrug candidates can be evaluated using animal models.

The primary pharmacological effect of IMQ is activating the unmatured DCs [119,124,125,130,142]. The activation of DCs in the targeted area, such as MLNs, following administration of the prodrugs of IMQ can be examined using health rat models. In the LNs of non-infected animal models, the population of MHC II^+ and MHC II^- is not significantly different [322]. Once the DCs are activated in the presence of antigens or immune activators, the population of DCs and the percentage of activated DCs will increase. The change in the DCs' population and phenotypes can be monitored using flow cytometry analysis and immunostaining microscopy [323,324].

Additionally, it is important to understand the potential toxicological effects of the prodrugs of IMQ. Although the prodrugs themselves are less likely have any pharmacological effects as an immunoactivitor, increased local concentration of IMQ in the MLNs after the administration of the prodrugs may introduce an inflammatory storm (a.k.a cytokine storm) in the lymphatic system [325]. The local inflammatory signals may be magnified during the signal pathway and eventually damage the secondary organs after a few days [326]. To address this concern, a toxicology study should be conducted on the amide prodrugs of IMQ. For example, the EC50 values of prodrugs 5 and 8 could be determined using human or animal-derived immature dendritic cells (DCs). In preclinical studies, the prodrugs should be orally administered

to in vivo models at three different dose levels to establish the no observed adverse effect level (NOAEL) dose and maximum tolerated dose (MTD). Additionally, relevant toxicity endpoints, including both local and systemic inflammatory responses, should be assessed by measuring proinflammatory cytokines such as TNF-α using ELISA.

6.2.2 Applying the simple alkyl prodrugs structure to other imidazoquinoline derivatives

The simple alkyl amide prodrug structure of IMQ could potentially also be applied to other TLR agonists, such as resiquimod (a TLR 7/8 agonist) [327] and gardiquimod (TLR 7/8 agonist) [328], as well as TLR antagonists [329], which contain an amine group attached to the imidazoquinoline ring (**Figure 6-3**).

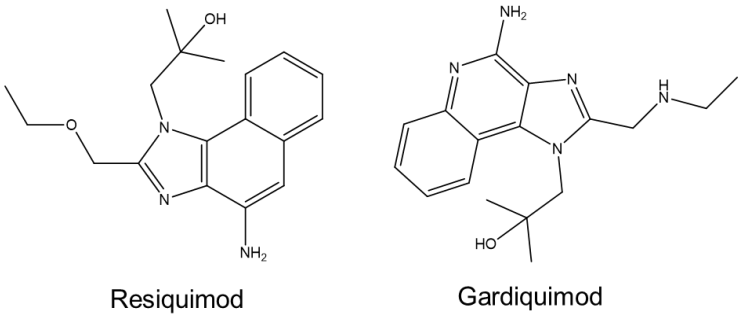

Figure 6-3 Chemical structure of resiquimod and gardiquimod.

Resiquimod is a second-generation derivative of IMQ that can activate the immune response *via* TLR7/8 [207]. It has two prodrug-able chemical functional groups. One is the primary amine on the imidazoquinoline ring, and the other is the tertiary hydroxyl group on the substituent side chain. A previous study has shown that a prodrug of resiquimod, designed *via* the tertiary hydroxyl group, demonstrated certain cytotoxicity [330]. Moreover, another prodrug of resiquimod, targeting local LNs through liposomal

delivery, did not enhance the immune response, indicating limited biotransformation of the prodrug into resiquimod [331]. In this work, we demonstrated several advantages of using simple alkyl prodrugs of imidazoquinoline derivatives: 1) the potential toxicity of the prodrug is minimized due to chemical blocking of the key functional amine group, and 2) the release of the parent molecule is relatively efficient, facilitated by electronic resonance between the amine group and the imidazoquinoline ring. Therefore, the application of the lipophilic prodrug approach to TLR ligands with primary amine attached to the imidazoquinoline structure may enhance immunotherapy treatments.

6.2.3 Co-delivery of IMQ and other drug molecules using prodrug approach

TLR 7 agonist has been previously co-administered with an immune checkpoint inhibitor in mouse model bearing with neck and head cancer. Results showed that the combination of TLR 7 and checkpoint inhibitors can: 1) suppress the progression of both primary tumour and metastatic tumour; 2) upregulate the anti-tumour related genes; 3) adjust the ratio of M1 proinflammatory macrophages in the tumour microenvironment and 4) stimulate the activation of CD8+ T cells and improve the T cell infiltration in the tumour sites [332]. Additionally, many studies have demonstrated the therapeutic benefit of using TLR agonists as an adjuvant in combination with checkpoint inhibitors using tumour cell lines or preclinical models [333–335]. Therefore, targeted co-delivery of both IMQ and checkpoint inhibitors using the lipophilic prodrug approach could potentially improve the therapeutic outcome in patients with CRC.

BMS-1 is a small-molecule PD-1 inhibitor from Bristol-Myers Squibb [336] (**Figure 6-4 A**). BMS-1 contains a carboxylic acid, which can be conjugated with a lipophilic

structure *via* an ester bond. The *in silico* predicted affinity of BMS-1 to CMs is less than 1 %. However, the affinity prodrug structure, which contains both BMS-1 and IMQ (**Figure 6-4 B**), increases to 82.2 %. Moreover, the affinity of the prodrug structure can be further improved by increasing the length of the alkyl chain (**Figure 6-4 C**).

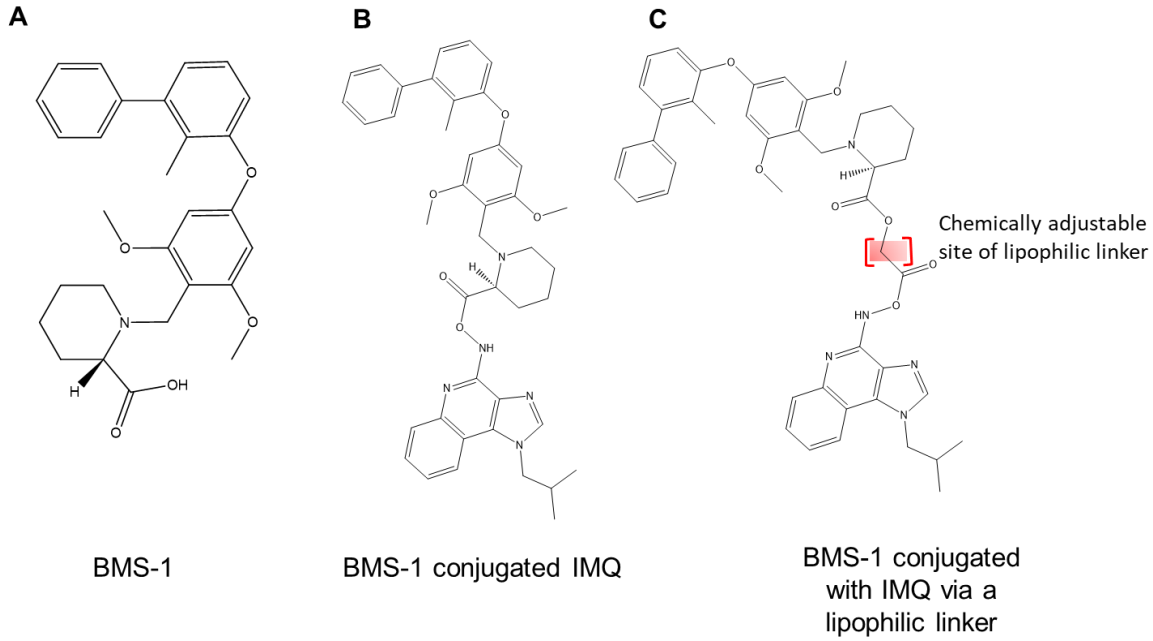

Figure 6-4 The chemical structure of BMS-1 and its prodrugs.

Appendix

Characterization of purified prodrugs

Prodrug 1 (IMQ decanoic acid), *N*-(1-isobutyl-1H-imidazo[4,5-c]quinolin-4-yl) decanamide; Prodrug 1 was synthesized with IMQ and decanoic acid as starting materials. The melting point of prodrug1 is in the range of 70 – 87 °C. The purity of the final product (> 95%) was confirmed by HPLC-UV. ^{1}H NMR (400 MHz, $CDCl_3$): δ 8.22 (s, 1H), 7.54 (d, J = 8.4 Hz, 1H), 7.42 (dd, J = 8.3, 1.4 Hz, 1H), 7.06 (ddd, J = 8.4, 7.1, 1.4 Hz, 1H), 6.94 (s, 1H), 3.75 (d, J = 7.4 Hz, 2H), 2.52 (s, 2H), 1.86 – 1.71 (m, J = 6.7 Hz, 1H), 1.28 (p, J = 7.6 Hz, 2H), 0.97 – 0.86 (m, 2H), 0.85 – 0.66 (m, 12H), 0.47 (d, J = 6.6 Hz, 6H), 0.32 (t, J = 6.8 Hz, 2H). ^{13}C NMR (101 MHz, $CDCl_3$) δ 144.37, 143.96, 142.97, 133.31, 129.87, 129.45, 127.59, 124.99, 119.92, 116.71, 55.23, 37.95, 31.99, 29.62, 29.59, 29.41, 28.95, 25.27, 22.78, 19.89, 14.22. HR-MS (ESI$^+$): m/z $[M+H]^+$ calculated for $C_{24}H_{34}N_4O$ m/z 395.2805, found m/z 395.2819.

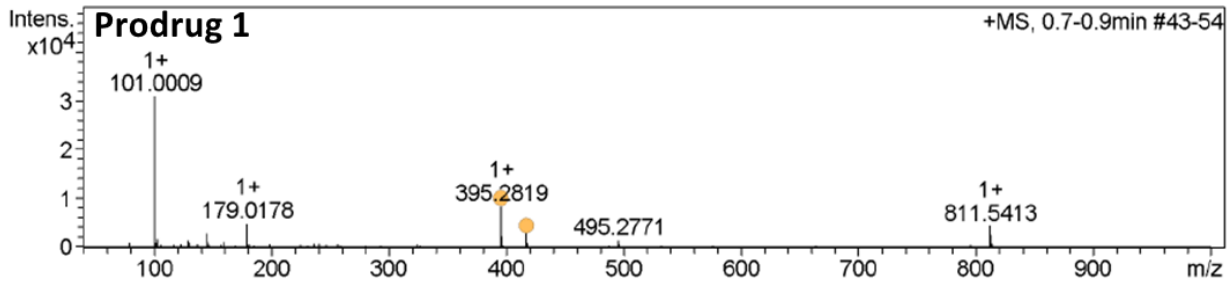

Prodrug 2 (IMQ tetradecanoid acid), *N*-(1-isobutyl-1H-imidazo[4,5-c]quinolin-4-yl) tetradecanamide. Prodrug 2 was synthesized with IMQ and tetradecanoic acid. The melting point of prodrug 2 is in the range of 45-68 °C. The purity of the final product (> 95%) was confirmed by HPLC-UV.^{1}H NMR (400 MHz, $CDCl_3$) δ 8.13 (s, 1H), 7.56 (d, J = 8.4 Hz, 1H), 7.44 (dd, J = 8.2, 1.4 Hz, 1H), 7.07 (ddd, J = 8.4, 7.1, 1.4 Hz, 1H),

6.96 (ddd, J = 8.3, 7.0, 1.3 Hz, 1H), 3.77 (d, J = 7.4 Hz, 2H), 2.52 (s, 2H), 1.81 (hept, J = 6.8 Hz, 1H), 1.28 (p, J = 7.6 Hz, 2H), 0.92 (p, J = 6.8 Hz, 2H), 0.85 – 0.77 (m, 1H), 0.70 (s, 18H), 0.49 (d, J = 6.7 Hz, 6H), 0.32 (t, J = 6.7 Hz, 3H). ^{13}C NMR (101 MHz, $CDCl_3$) δ 143.03, 133.44, 127.73, 125.11, 120.01, 116.80, 55.37, 38.07, 32.13, 29.90, 29.88, 29.86, 29.77, 29.69, 29.56, 29.06, 25.37, 22.89, 20.00, 14.32. HR-MS (ESI+): m/z $[M+H]^+$ calculated for $C_{28}H_{42}N_4O$ m/z 451.3431, found m/z 451.3442.

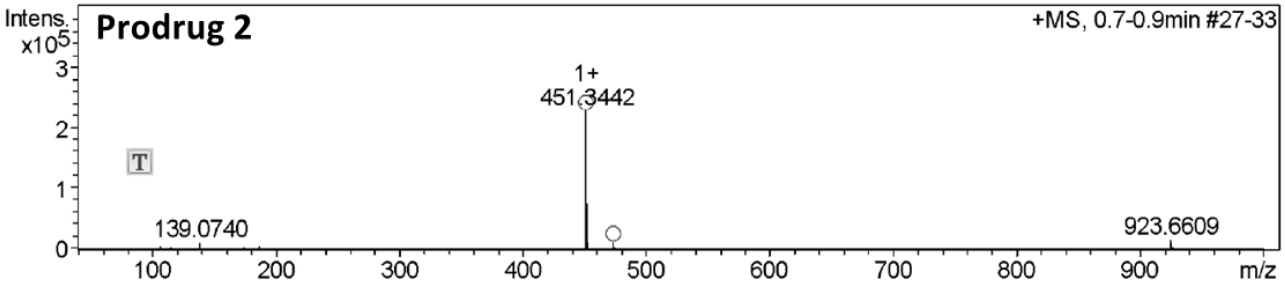

Prodrug 3 (IMQ palmitic acid), *N*-(1-isobutyl-1H-imidazo[4,5-c]quinolin-4-yl) palmitamide. Prodrug 3 was synthesized with IMQ and palmitic acid. The melting point of prodrug 3 is in the range of 45-58 °C. The purity of the final product (> 95%) was confirmed by HPLC-UV. ^{1}H NMR (400 MHz, $CDCl_3$) δ 8.71 (s, 1H), 8.14 (d, J = 8.4 Hz, 1H), 8.02 (d, J = 8.2 Hz, 1H), 7.84 (s, 1H), 7.69 – 7.61 (m, 1H), 7.58 – 7.49 (m, 1H), 4.35 (d, J = 7.4 Hz, 2H), 3.10 (s, 2H), 2.39 (hept, J = 6.8 Hz, 1H), 1.86 (p, J = 7.6 Hz, 2H), 1.55 – 1.44 (m, 2H), 1.38 (dq, J = 16.2, 6.3 Hz, 2H), 1.31 (s, 5H), 1.30 (s, 1H), 1.28 (s, 13H), 1.06 (d, J = 6.6 Hz, 6H), 0.90 (t, J = 6.7 Hz, 3H). ^{13}C NMR (101 MHz, $CDCl_3$) δ 144.22 (d, J = 39.3 Hz), 142.95, 133.38, 130.04 (d, J = 7.3 Hz), 129.93, 129.52, 127.68, 125.05, 119.95, 116.76, 77.36, 55.32, 37.99, 31.92, 29.89 (d, J = 1.7 Hz), 29.57 (d, J = 6.5 Hz), 29.36, 29.13, 29.01, 27.36, 25.28, 22.80, 19.95, 14.25. HR-MS (ESI+): m/z $[M+H]^+$ calculated for $C_{30}H_{46}N_4O$ m/z 479.3744 , found m/z 479.3766.

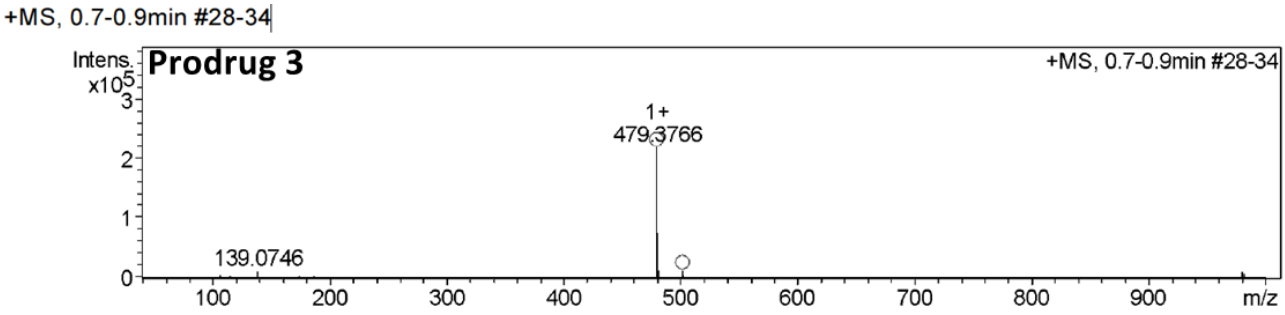

Prodrug 4 (IMQ stearic acid), N-(1-isobutyl-1H-imidazo[4,5-c]quinolin-4-yl) stearamide. Prodrug 4 was synthesized with IMQ and stearic acid. The melting point of prodrug 4 is in the range of 40-54 °C. The purity of the final product (> 95%) was confirmed by HPLC-UV. ^{1}H NMR (400 MHz, $CDCl_3$) δ 14.76 (s, 1H), 14.11 (d, J = 8.4 Hz, 1H), 14.00 (dd, J = 8.2, 1.4 Hz, 1H), 13.83 (s, 1H), 13.63 (ddd, J = 8.4, 7.0, 1.4 Hz, 1H), 13.52 (ddd, J = 8.4, 7.0, 1.3 Hz, 1H), 10.33 (d, J = 7.4 Hz, 2H), 9.07 (s, 2H), 8.37 (dp, J = 13.7, 7.0 Hz, 1H), 7.84 (p, J = 7.6 Hz, 2H), 7.48 (dq, J = 9.2, 6.6 Hz, 2H), 7.35 (ddd, J = 18.5, 8.5, 4.1 Hz, 3H), 7.26 (s, 23H), 7.05 (d, J = 6.6 Hz, 6H), 6.88 (t, J = 6.8 Hz, 3H). ^{13}C NMR (101 MHz, CDCl3) δ 142.95, 133.38, 129.97, 129.90, 129.53, 127.67, 125.05, 119.95, 116.76, 77.36, 55.32, 38.01, 32.07, 29.85, 29.83, 29.81, 29.71, 29.63, 29.51, 29.01, 25.30, 22.84, 19.95, 14.27.HR-MS (ESI$^+$): m/z $[M+H]^+$ calculated for $C_{32}H_{50}N_4O$ m/z 507.4057, found m/z 507.4073.

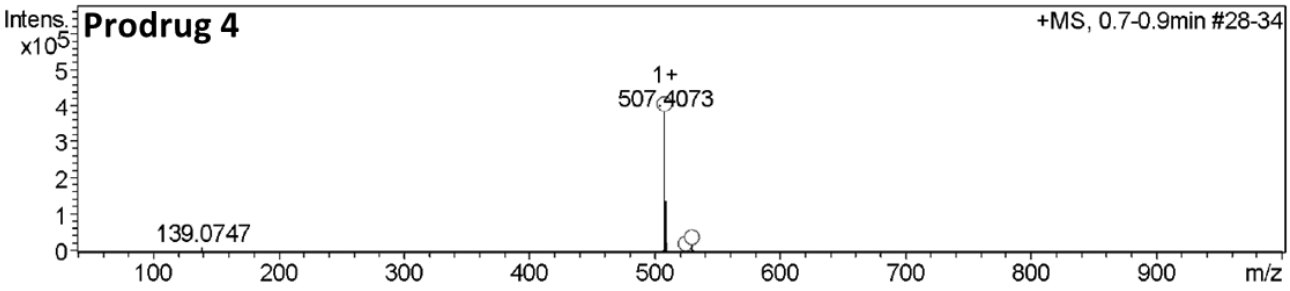

Prodrug 5 (IMQ myristoleic acid), (E)-N-(1-isobutyl-1H-imidazo[4,5-c]quinolin-4-yl) tetradec-9-enamide. Prodrug 5 was synthesized with IMQ and myristoleic acid. Prodrug 5 is melted at room temperature. The purity of the final product (> 95%) was confirmed by HPLC-UV. ^{1}H NMR (400 MHz, $CDCl_3$) δ 8.15 (s, 1H), 7.59 – 7.50 (m, 1H), 7.43 (dd, J = 8.2, 1.4 Hz, 1H), 7.06 (ddd, J = 8.4, 7.1, 1.4 Hz, 1H), 6.95 (ddd, J = 8.3, 7.1, 1.3 Hz, 1H), 4.85 – 4.71 (m, 2H), 3.76 (d, J = 7.4 Hz, 2H), 2.51 (s, 2H), 1.87 – 1.70 (m, 1H), 1.46 (q, J = 7.3 Hz, 4H), 1.28 (p, J = 7.6 Hz, 2H), 0.90 (dt, J = 18.2, 9.5 Hz, 2H), 0.87 – 0.60 (m, 11H), 0.48 (d, J = 6.6 Hz, 6H), 0.37 – 0.24 (m, 3H). ^{13}C NMR (101 MHz, CDCl3) δ 142.98, 130.00, 129.52, 127.66, 125.04, 119.96, 116.75, 55.30, 38.00, 32.10, 29.89, 29.69 – 29.20 (m), 29.00, 27.33, 27.05, 25.27, 22.47, 19.94, 14.14. HR-MS (ESI^+): m/z $[M+H]^+$ calculated for $C_{28}H_{40}N_4O$ m/z 449.3275, found m/z 449.3286.

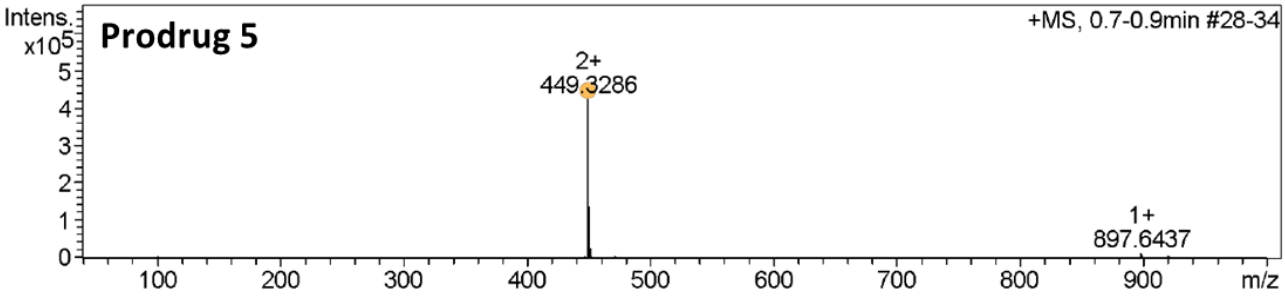

Prodrug 6 (IMQ palmitoleic acid), (E)-N-(1-isobutyl-1H-imidazo[4,5-c]quinolin-4-yl) hexadec-9-enamide. Prodrug 6 was synthesized with IMQ and palmitoleic acid. Prodrug 6 is melted at room temperature. The purity of the final product (> 95%) was confirmed by HPLC-UV. ^{1}H NMR (400 MHz, $CDCl_3$) δ 8.71 (s, 1H), 8.10 (d, J = 8.3 Hz,

1H), 8.05 – 7.94 (m, 1H), 7.82 (s, 1H), 7.62 (ddd, J = 8.4, 7.0, 1.4 Hz, 1H), 7.51 (td, J = 7.5, 1.4 Hz, 1H), 5.39 – 5.28 (m, 2H), 4.32 (d, J = 7.4 Hz, 2H), 3.08 (s, 2H), 2.36 (dp, J = 13.6, 6.8 Hz, 1H), 2.01 (dq, J = 12.0, 5.7 Hz, 4H), 1.84 (p, J = 7.6 Hz, 2H), 1.47 (q, J = 7.4 Hz, 2H), 1.43 – 1.22 (m, 14H), 1.04 (d, J = 6.6 Hz, 6H), 0.93 – 0.79 (m, 3H). ^{13}C NMR (101 MHz, $CDCl_3$) δ 174.04, 144.39, 144.01, 142.95, 133.33, 129.93, 129.47, 127.62, 125.01, 119.93, 116.75, 77.36, 55.28, 37.97, 32.05, 29.83, 29.81, 29.78, 29.69, 29.62, 29.49, 28.98, 25.28, 22.82, 19.92, 14.25.HR-MS (ESI^+): m/z $[M+H]^+$ calculated for $C_{30}H_{44}N_4O$ m/z 477.3588, found m/z 477.3598.

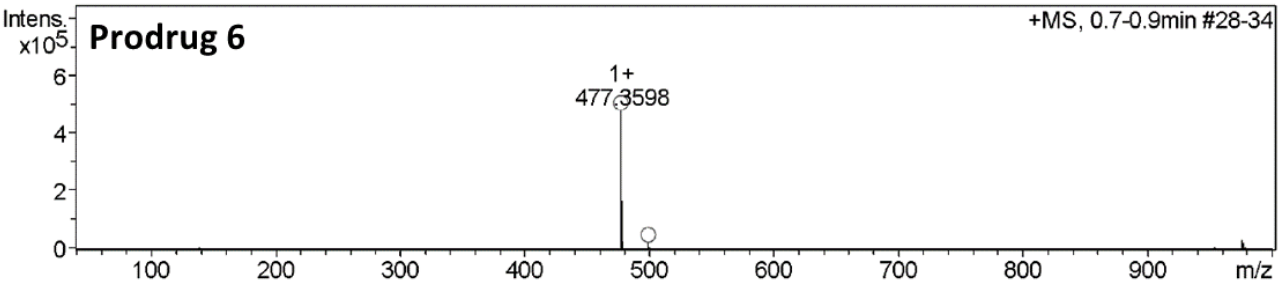

Prodrug 7 (IMQ oleic acid), N-(1-isobutyl-1H-imidazo[4,5-c]quinolin-4-yl) oleamide. Prodrug 7 was synthesized with IMQ and oleic acid. Prodrug 7 is melted at room temperature. The purity of the final product (> 95%) was confirmed by HPLC-UV. ^1H NMR (400 MHz, $CDCl_3$) δ 8.09 (d, J = 8.4 Hz, 1H), 7.98 (dd, J = 8.3, 1.4 Hz, 1H), 7.81 (s, 1H), 7.61 (ddd, J = 8.4, 7.0, 1.4 Hz, 1H), 7.50 (ddd, J = 8.3, 7.1, 1.3 Hz, 1H), 5.39 – 5.28 (m, 2H), 4.31 (d, J = 7.4 Hz, 2H), 3.07 (s, 2H), 2.71 (s, 1H), 2.35 (dp, J = 13.7, 7.1 Hz, 1H), 2.00 (hept, J = 4.7 Hz, 4H), 1.83 (p, J = 7.6 Hz, 2H), 1.53 – 1.43 (m, 2H), 1.40 – 1.20 (m, 18H), 1.03 (d, J = 6.6 Hz, 6H), 0.86 (t, J = 6.7 Hz, 3H). ^{13}C NMR (101 MHz, $CDCl_3$) δ 207.05, 144.47, 143.90, 142.96, 133.34, 130.05, 129.96, 129.80, 129.50, 127.64, 125.02, 119.94, 116.72, 77.36, 55.27, 37.98, 32.01, 31.04, 29.89, 29.88, 29.82, 29.78, 29.64, 29.61, 29.58, 29.51, 29.43, 29.34, 28.97, 28.33, 27.33,

25.25, 22.79, 19.91, 14.23. HR-MS (ESI+): m/z $[M+H]^+$ calculated for $C_{32}H_{48}N_4O$ m/z 505.3901, found m/z 505.3912.

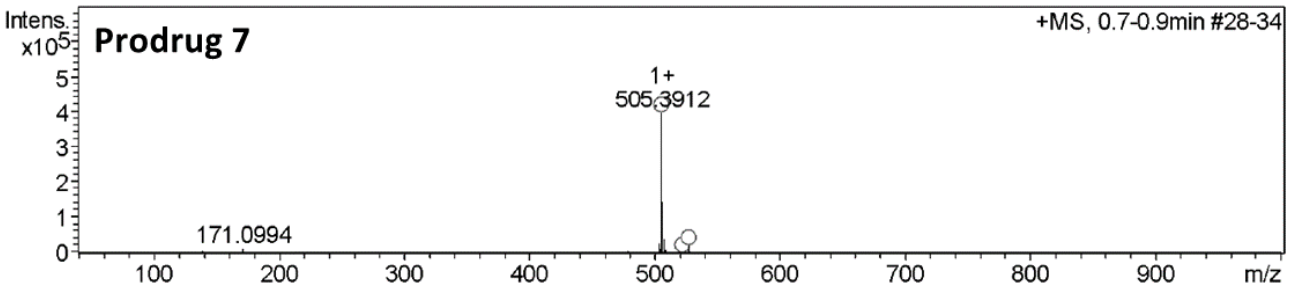

Prodrug 8 (IMQ linoleic acid), (9Z,12Z)-N-(1-isobutyl-1H-imidazo[4,5-c]quinolin-4-yl) octadeca-9,12-dienamide. Prodrug 8 was synthesized with IMQ and linoleic acid. Prodrug 8 is melted at room temperature. The purity of the final product (> 95%) was confirmed by HPLC-UV. ^{1}H NMR (400 MHz, $CDCl_3$) δ 8.74 (s, 1H), 8.09 (d, J = 8.4 Hz, 1H), 7.97 (d, J = 8.2 Hz, 1H), 7.81 (s, 1H), 7.61 (ddd, J = 8.4, 7.0, 1.4 Hz, 1H), 7.49 (ddd, J = 8.2, 7.0, 1.3 Hz, 1H), 5.41 – 5.25 (m, 4H), 4.30 (d, J = 7.4 Hz, 2H), 3.07 (s, 2H), 2.76 (t, J = 6.5 Hz, 2H), 2.33 (dq, J = 13.8, 6.9 Hz, 1H), 2.03 (dq, J = 10.1, 4.9 Hz, 4H), 1.83 (p, J = 7.6 Hz, 2H), 1.47 (h, J = 6.6 Hz, 2H), 1.42 – 1.22 (m, 12H), 1.02 (d, J = 6.6 Hz, 6H), 0.87 (t, J = 6.7 Hz, 3H). ^{13}C NMR (101 MHz, $CDCl_3$) δ 144.35, 143.96, 142.96, 130.28, 130.24, 129.87, 129.44, 128.07, 128.04, 127.60, 124.99, 119.92, 116.72, 55.24, 37.91, 31.61, 29.76, 29.55, 29.50, 29.44, 29.33, 28.95, 27.34, 27.29, 25.73, 25.23, 22.66, 19.89, 14.17. HR-MS (ESI^+): m/z $[M+H]^+$ calculated for $C_{32}H_{46}N_4O$ m/z 503.3744, found m/z 503.3754.

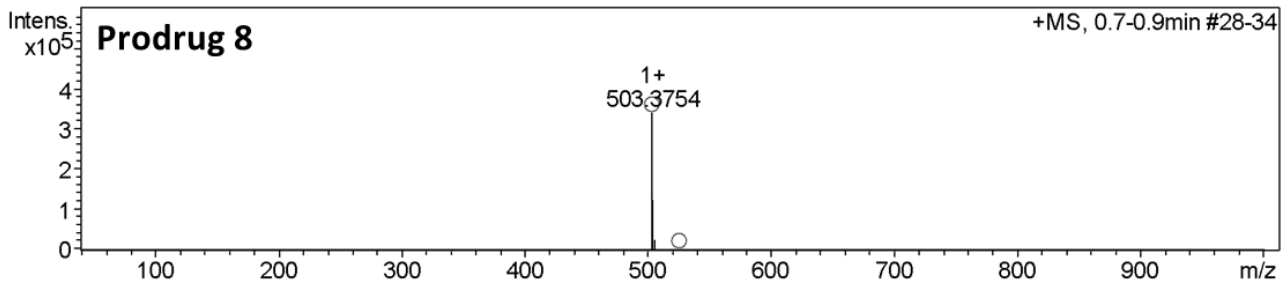
Intens.
x10^5
Prodrug 8
+MS, 0.7-0.9min #28-34
1+
503.3754
4
3
2
1
0
100
200
300
400
500
600
700
800
900
m/z

Biodistribution of IMQ and its prodrugs

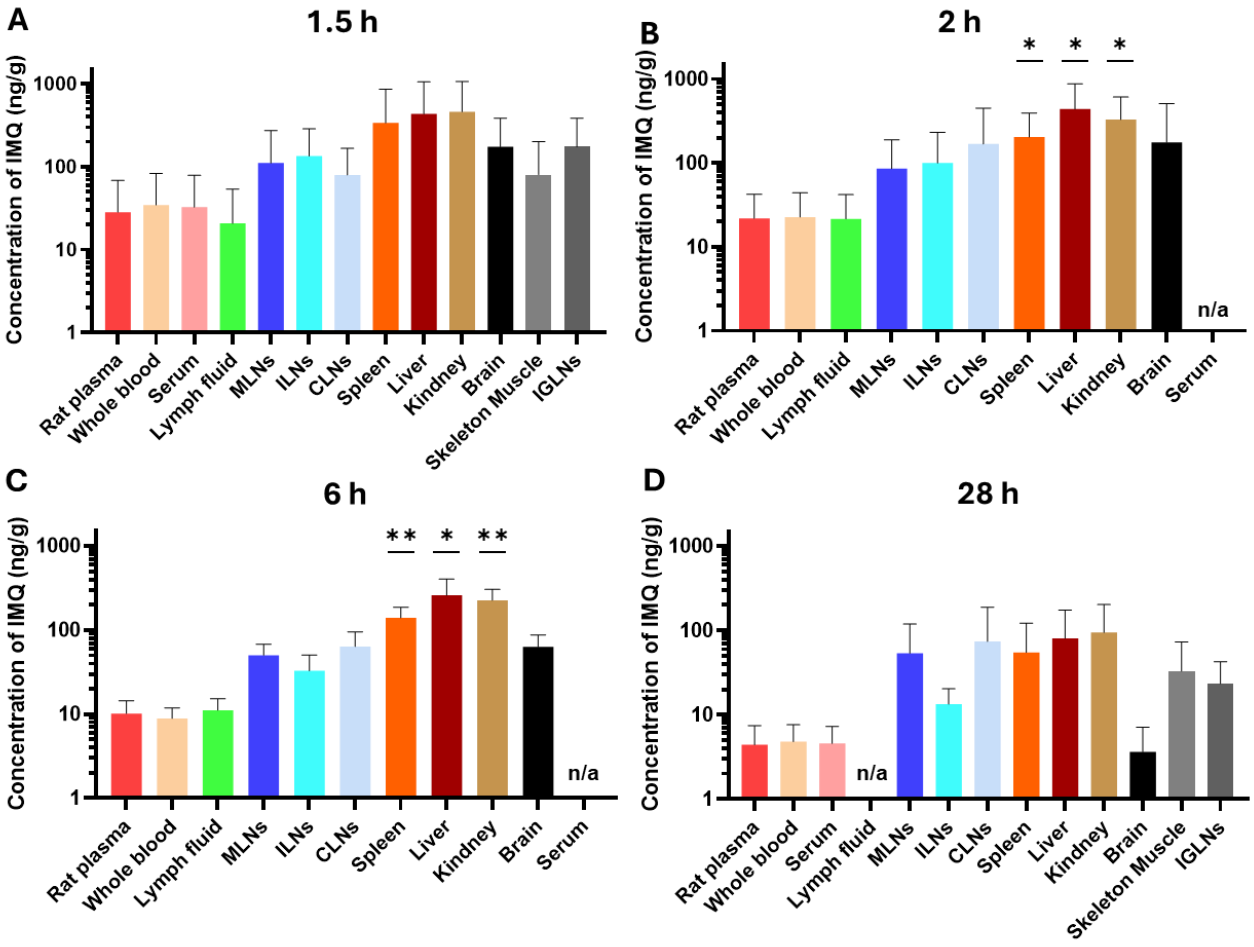

Figure Appx.-1 The biodistribution of IMQ following oral administration of IMQ (8 mg/kg) with lipids at local Tmax 1.5 h, 2 h, 6 h and 28 h (mean ± SD, n = 4 to 6). The concentrations of IMQ in plasma, whole blood, serum, and lymph fluid were converted from ng/mL to ng/g based on biofluid density (plasma, serum, and lymph fluid: 1.006 g/mL; whole blood: 1.056 g/mL) [235–237]. MLN, mesenteric lymph node; ILNs, iliac lymph nodes; CLNs, cervical lymph nodes; IGLNs, inguinal lymph nodes. An unpaired t-test was used for the comparison of IMQ concentration in plasma and other samples. One-way ANOVA followed by Turkey's comparison was used to compare the concentration of IMQ in the plasma, serum and whole blood at 2 h and 28 h. *, $p < .05$; **,$p < .01$. n/a: Samples were not collected.

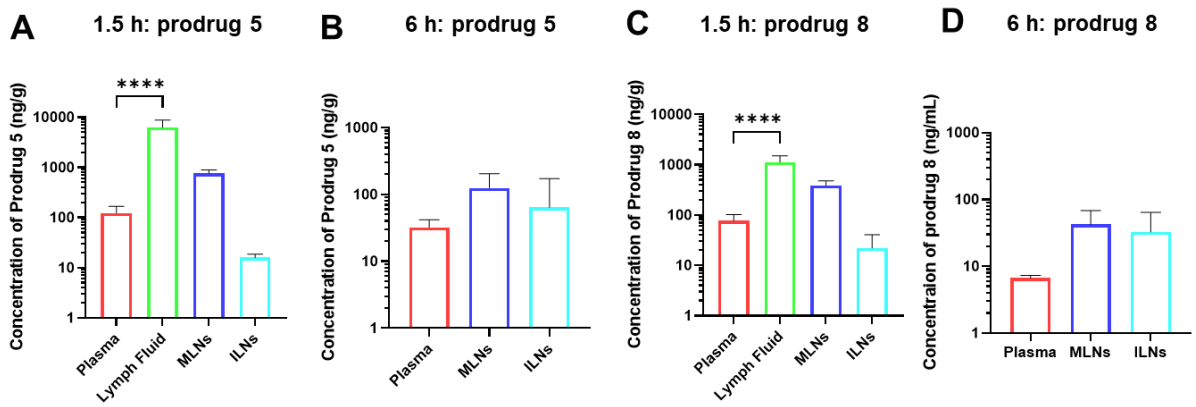

Figure Appx.- 2 The biodistribution of prodrugs 5 and 8 in plasma, mesenteric lymph, mesenteric lymph nodes (MLNs) and iliac lymph nodes (ILNs) (mean ± SD, n = 4 to 8). The concentrations of prodrugs in plasma, whole blood, serum, and lymph fluid were converted from ng/mL to ng/g based on biofluid density (plasma, serum, and lymph fluid: 1.006 g/mL; whole blood: 1.056 g/mL) [235–237]. Panels (A) and (B) show the distribution of prodrug 5 (14.9 mg/kg) following oral administration at 1.5 and 6 h, respectively. Panels (C) and (D) show the distribution of prodrug 8 (16.7 mg/kg) following oral administration at 1.5 and 6 h, respectively. One-way ANOVA, followed by Dunnett's comparison, was used for statistical analysis. Asterisks denote statistical significance against plasma. ****,$p < .0001$.

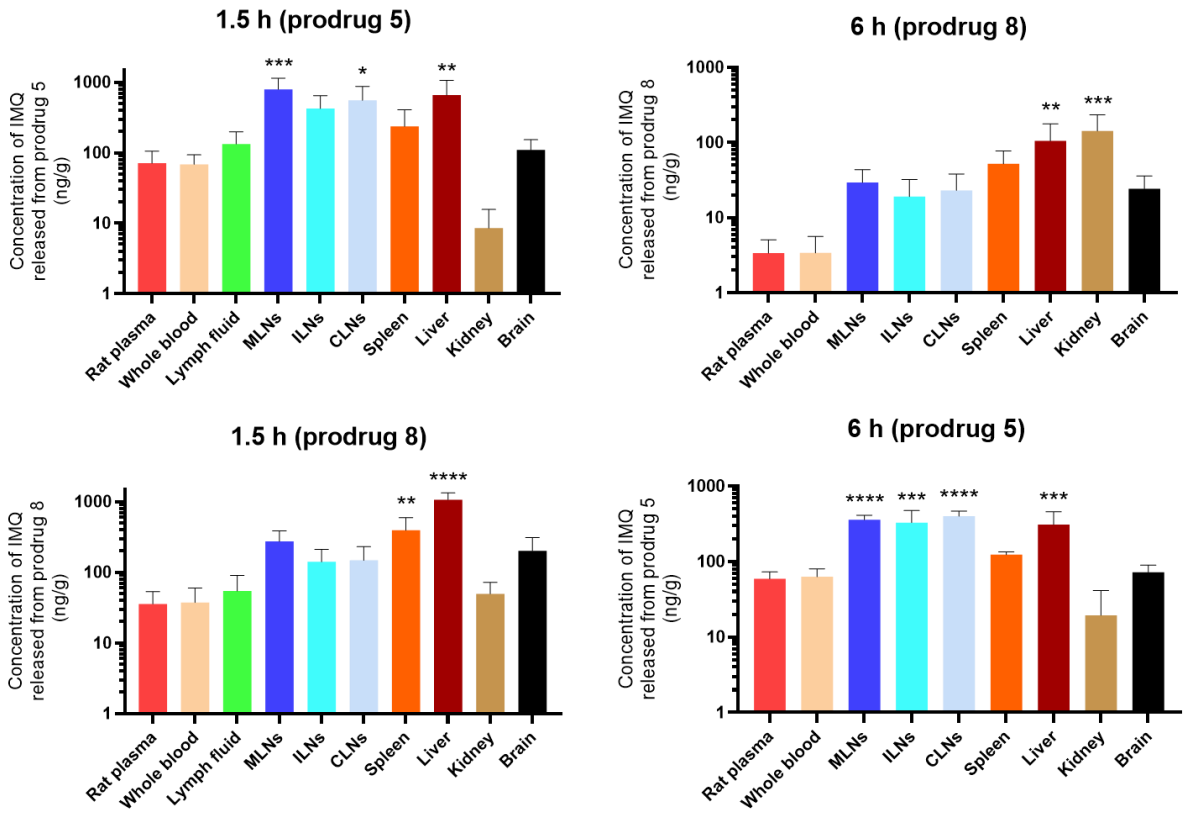

Figure Appx.- 3 The distribution of IMQ in plasma, mesenteric lymph fluid, lymph nodes and main organs following oral administrations of prodrug 5 (14.9 mg/kg) and 8 (16.7 mg/kg) using lipid-based formulation at 1.5 and 6 h (mean ± SD, n = 5 to 8). The concentrations of IMQ in plasma, whole blood, serum, and lymph fluid were converted from ng/mL to ng/g based on biofluid density (plasma, serum, and lymph fluid: 1.006 g/mL; whole blood: 1.056 g/mL) [235–237]. MLN, mesenteric lymph node; ILNs, iliac lymph nodes; CLNs, cervical lymph nodes. One-way ANOVA, followed by Dunnett's comparison, was used for statistical analysis. Asterisks denote statistical significance against plasma. * p < .05; ** ,p < .01, ***,p < .001, ****,p < .0001.

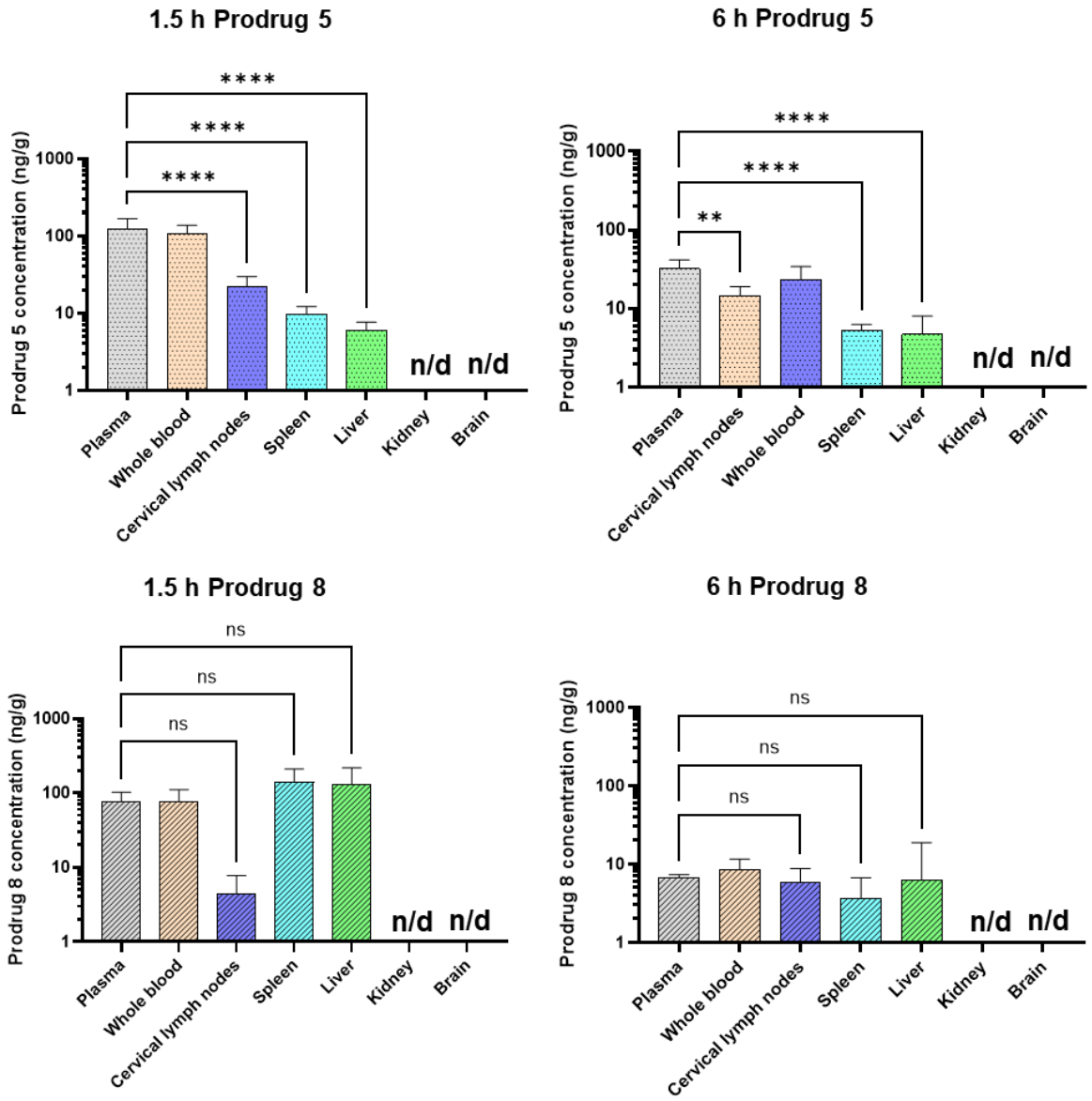

Figure Appx.- 4 The distribution of prodrug 5 and prodrug 8 following oral administrations of prodrug 5 (14.9 mg/kg) and 8 (16.7 mg/kg) using lipid-based formulation at 1.5 and 6 h (mean ± SD, n = 5 to 6). The concentrations of prodrugs in plasma, whole blood, serum, and lymph fluid were converted from ng/mL to ng/g based on biofluid density (plasma, serum, and lymph fluid: 1.006 g/mL; whole blood: 1.056 g/mL) [235–237]. One-way ANOVA, followed by Dunnett's comparison, was used for statistical analysis. Asterisks denote significance against plasma. * p < .05; ** ,p < .01, ***,p < .001, ****,p < .0001. n/d: below the limit of quantification.

Reference

[1] Ferlay J, Colombet M, Soerjomataram I, Mathers C, Parkin DM, Piñeros M, et al. Estimating the global cancer incidence and mortality in 2018: GLOBOCAN sources and methods. Int J Cancer 2019;144:1941–53. https://doi.org/10.1002/ijc.31937.

[2] Sung H, Ferlay J, Siegel RL, Laversanne M, Soerjomataram I, Jemal A, et al. Global Cancer Statistics 2020: GLOBOCAN Estimates of Incidence and Mortality Worldwide for 36 Cancers in 185 Countries. CA Cancer J Clin 2021;71:209–49. https://doi.org/10.3322/caac.21660.

[3] Smittenaar CR, Petersen KA, Stewart K, Moitt N. Cancer incidence and mortality projections in the UK until 2035. Br J Cancer 2016;115:1147–55. https://doi.org/10.1038/bjc.2016.304.

[4] Aran V, Victorino AP, Thuler LC, Ferreira CG. Colorectal Cancer: Epidemiology, Disease Mechanisms and Interventions to Reduce Onset and Mortality. Clin Colorectal Cancer 2016;15:195–203. https://doi.org/10.1016/j.clcc.2016.02.008.

[5] Morgan E, Arnold M, Gini A, Lorenzoni V, Cabasag CJ, Laversanne M, et al. Global burden of colorectal cancer in 2020 and 2040: Incidence and mortality estimates from GLOBOCAN. Gut 2023;72:338–44. https://doi.org/10.1136/gutjnl-2022-327736.

[6] Klimeck L, Heisser T, Hoffmeister M, Brenner H. Colorectal cancer: A health and economic problem. Best Pract Res Clin Gastroenterol 2023;66. https://doi.org/10.1016/j.bpg.2023.101839.

[7] Siegel RL, Miller KD, Jemal A. Cancer statistics, 2019. CA Cancer J Clin 2019;69:7–34. https://doi.org/10.3322/caac.21551.

[8] Sinicrope FA. Increasing Incidence of Early-Onset Colorectal Cancer. New England Journal of Medicine 2022;386:1547–58. https://doi.org/10.1056/nejmra2200869.

[9] Willauer AN, Liu Y, Pereira AAL, Lam M, Morris JS, Raghav KPS, et al. Clinical and molecular characterization of early-onset colorectal cancer. Cancer 2019;125:2002–10. https://doi.org/10.1002/cncr.31994.

[10] Araghi M, Soerjomataram I, Jenkins M, Brierley J, Morris E, Bray F, et al. Global trends in colorectal cancer mortality: projections to the year 2035. Int J Cancer 2019;144:2992–3000. https://doi.org/10.1002/ijc.32055.

[11] Quirke P, Risio M, Lambert R, Von Karsa L, Vieth M. Quality assurance in pathology in colorectal cancer screening and diagnosis-European recommendations. Virchows Archiv 2011;458:1–19. https://doi.org/10.1007/s00428-010-0977-6.

[12] Siegel RL, Wagle NS, Cercek A, Smith RA, Jemal A. Colorectal cancer statistics, 2023. CA Cancer J Clin 2023;73:233–54. https://doi.org/10.3322/caac.21772.

[13] Hamilton SR, Aaltonen LA. Pathology and Genetics of Tumours of the Digestive System. 2000.

[14] Muzny DM, Bainbridge MN, Chang K, Dinh HH, Drummond JA, Fowler G, et al. Comprehensive molecular characterization of human colon and rectal cancer. Nature 2012;487:330–7. https://doi.org/10.1038/nature11252.

[15] Zhang L, Shay JW. Multiple Roles of APC and its Therapeutic Implications in Colorectal Cancer. J Natl Cancer Inst 2017;109. https://doi.org/10.1093/jnci/djw332.

[16] Guinney J, Dienstmann R, Wang X, De Reyniès A, Schlicker A, Soneson C, et al. The consensus molecular subtypes of colorectal cancer. Nat Med 2015;21:1350–6. https://doi.org/10.1038/nm.3967.

[17] Noack P, Langer R. Molecular pathology of colorectal cancer. Memo - Magazine of European Medical Oncology 2023;16:116–21. https://doi.org/10.1007/s12254-023-00893-2.

[18] Müller MF, Ibrahim AEK, Arends MJ. Molecular pathological classification of colorectal cancer. Virchows Archiv 2016;469:125–34. https://doi.org/10.1007/s00428-016-1956-3.

[19] Berg KCG, Sveen A, Høland M, Alagaratnam S, Berg M, Danielsen SA, et al. Gene expression profiles of CMS2-epithelial/canonical colorectal cancers are largely driven by DNA copy number gains. Oncogene 2019;38:6109–22. https://doi.org/10.1038/s41388-019-0868-5.

[20] László L, Kurilla A, Takács T, Kudlik G, Koprivanacz K, Buday L, et al. Recent updates on the significance of kras mutations in colorectal cancer biology. Cells 2021;10:1–19. https://doi.org/10.3390/cells10030667.

[21] Liu YH, Hu CM, Hsu YS, Lee WH. Interplays of glucose metabolism and KRAS mutation in pancreatic ductal adenocarcinoma. Cell Death Dis 2022;13. https://doi.org/10.1038/s41419-022-05259-w.

[22] Hoorn S Ten, De Back TR, Sommeijer DW, Vermeulen L. Clinical Value of Consensus Molecular Subtypes in Colorectal Cancer: A Systematic Review and Meta-Analysis. J Natl Cancer Inst 2022;114:503–16. https://doi.org/10.1093/jnci/djab106.

[23] Jung G, Hernández-Illán E, Moreira L, Balaguer F, Goel A. Epigenetics of colorectal cancer: biomarker and therapeutic potential. Nat Rev Gastroenterol Hepatol 2020;17:111–30. https://doi.org/10.1038/s41575-019-0230-y.

[24] Sawayama H, Miyamoto Y, Ogawa K, Yoshida N, Baba H. Investigation of colorectal cancer in accordance with consensus molecular subtype classification. Ann Gastroenterol Surg 2020;4:528–39. https://doi.org/10.1002/ags3.12362.

[25] Hanahan D, Weinberg RA. Hallmarks of cancer: The next generation. Cell 2011;144:646–74. https://doi.org/10.1016/j.cell.2011.02.013.

[26] van der Geest LGM, Lam-Boer J, Koopman M, Verhoef C, Elferink MAG, de Wilt JHW. Nationwide trends in incidence, treatment and survival of colorectal cancer patients with synchronous metastases. Clin Exp Metastasis 2015;32:457–65. https://doi.org/10.1007/s10585-015-9719-0.

[27] Riihimaki M, Hemminki A, Sundquist J, Hemminki K. Patterns of metastasis in colon and rectal cancer. Sci Rep 2016;6. https://doi.org/10.1038/srep29765.

[28] Ji H, Hu C, Yang X, Liu Y, Ji G, Ge S, et al. Lymph node metastasis in cancer progression: molecular mechanisms, clinical significance and therapeutic interventions. Signal Transduct Target Ther 2023;8. https://doi.org/10.1038/s41392-023-01576-4.

[29] Stacker SA, Williams SP, Karnezis T, Shayan R, Fox SB, Achen MG. Lymphangiogenesis and lymphatic vessel remodelling in cancer. Nat Rev Cancer 2014;14:159–72. https://doi.org/10.1038/nrc3677.

[30] Kim JC, Lee KH, Yu CS, Kim HC, Chang HM, Kim JH, et al. The clinicopathological significance of inferior mesentric lymph node metastasis in colorectal cancer. European Journal of Surgical Oncology 2004;30:271–9. https://doi.org/10.1016/j.ejso.2003.12.002.

[31] Ong MLH, Schofield JB. Assessment of lymph node involvement in colorectal cancer. World J Gastrointest Surg 2016;8:179. https://doi.org/10.4240/wjgs.v8.i3.179.

[32] Sasaki T, Shigeta K, Matsui S, Seishima R, Okabayashi K, Kitagawa Y. Mesenteric location of lymph node metastasis for colorectal cancer. ANZ J Surg 2023;93:1257–61. https://doi.org/10.1111/ans.18221.

[33] Naxerova K, Reiter JG, Brachtel E, Lennerz JK, van de Wetering M, Rowan A, et al. Origins of lymphatic and distant metastases in human colorectal cancer. Science (1979) 2017;357:55–60. https://doi.org/10.5061/dryad.vv53d.

[34] Yeo SG, Kim DY, Kim TH, Jung KH, Hong YS, Kim SY, et al. Curative chemoradiotherapy for isolated retroperitoneal lymph node recurrence of colorectal cancer. Radiotherapy and Oncology 2010;97:307–11. https://doi.org/10.1016/j.radonc.2010.05.021.

[35] NICE guidline. Colorectal cancer NICE guideline. 2020.

[36] Ciombor KK, Wu C, Goldberg RM. Recent therapeutic advances in the treatment of colorectal cancer. Annu Rev Med 2015;66:83–95. https://doi.org/10.1146/annurev-med-051513-102539.

[37] Morris VK, Kennedy EB, Baxter NN, Al ;, Benson Iii B, Cercek A, et al. Treatment of Metastatic Colorectal Cancer: ASCO Guideline. J Clin Oncol 2022;41:678–700. https://doi.org/10.1200/JCO.22.

[38] Longley DB, Harkin DP, Johnston PG. 5-Fluorouracil: Mechanisms of action and clinical strategies. Nat Rev Cancer 2003;3:330–8. https://doi.org/10.1038/nrc1074.

[39] Miwa M, Ura M, Nishida M, Sawada N, Ishikawa T, Mori K, et al. Original Paper Design of a Novel Oral Fluoropyrimidine Carbamate, Capecitabine, which Generates 5-Fluorouracil Selectively in Tumours by Enzymes Concentrated in Human Liver and Cancer Tissue. vol. 34. 1998.

[40] André T, Boni C, Mounedji-Boudiaf L, Navarro M, Tabernero J, Hickish T, et al. Oxaliplatin, Fluorouracil, and Leucovorin as Adjuvant Treatment for Colon Cancer for the Multicenter International Study of Oxaliplatin/5-Fluorouracil/Leucovorin in the Adjuvant Treatment of Colon Cancer (MOSAIC) Investigators. vol. 23. 2004.

[41] Kelland L. The resurgence of platinum-based cancer chemotherapy. Nat Rev Cancer 2007;7:573–84. https://doi.org/10.1038/nrc2167.

[42] Dasari S, Bernard Tchounwou P. Cisplatin in cancer therapy: Molecular mechanisms of action. Eur J Pharmacol 2014;740:364–78. https://doi.org/10.1016/j.ejphar.2014.07.025.

[43] Pommier Y. Topoisomerase I inhibitors: Camptothecins and beyond. Nat Rev Cancer, vol. 6, 2006, p. 789–802. https://doi.org/10.1038/nrc1977.

[44] Mathijssen RHJ, Van Alphen RJ, Verweij J, Loos WJ, Nooter K, Stoter G, et al. Clinical Pharmacokinetics and Metabolism of Irinotecan (CPT-11). n.d.

[45] de Man FM, Goey AKL, van Schaik RHN, Mathijssen RHJ, Bins S. Individualization of Irinotecan Treatment: A Review of Pharmacokinetics, Pharmacodynamics, and Pharmacogenetics. Clin Pharmacokinet 2018;57:1229–54. https://doi.org/10.1007/s40262-018-0644-7.

[46] Luchini C, Bibeau F, Ligtenberg MJL, Singh N, Nottegar A, Bosse T, et al. ESMO recommendations on microsatellite instability testing for immunotherapy in cancer, and its relationship with PD-1/PD-L1 expression and tumour mutational burden: A systematic review-based approach. Annals of Oncology 2019;30:1232–43. https://doi.org/10.1093/annonc/mdz116.

[47] Arora SP, Mahalingam D. Immunotherapy in colorectal cancer: For the select few or all? J Gastrointest Oncol 2018;9:170–9. https://doi.org/10.21037/jgo.2017.06.10.

[48] Ahmadzadeh M, Johnson LA, Heemskerk B, Wunderlich JR, Dudley ME, White DE, et al. Tumor antigen-specific CD8 T cells infiltrating the tumor express high levels of PD-1 and are functionally impaired n.d. https://doi.org/10.1182/blood-2008.

[49] Sharpe AH, Wherry EJ, Ahmed R, Freeman GJ. The function of programmed cell death 1 and its ligands in regulating autoimmunity and infection. Nat Immunol 2007;8:239–45. https://doi.org/10.1038/ni1443.

[50] Han Y, Liu D, Li L. PD-1/PD-L1 pathway: current researches in cancer. vol. 10. 2020.

[51] Tang Q, Chen Y, Li X, Long S, Shi Y, Yu Y, et al. The role of PD-1/PD-L1 and application of immune-checkpoint inhibitors in human cancers. Front Immunol 2022;13. https://doi.org/10.3389/fimmu.2022.964442.

[52] Vaddepally RK, Kharel P, Pandey R, Garje R, Chandra AB. Review of indications of FDA-approved immune checkpoint inhibitors per NCCN guidelines with the level of evidence. Cancers (Basel) 2020;12. https://doi.org/10.3390/cancers12030738.

[53] Overman MJ, McDermott R, Leach JL, Lonardi S, Lenz HJ, Morse MA, et al. Nivolumab in patients with metastatic DNA mismatch repair-deficient or microsatellite instability-high colorectal cancer (CheckMate 142): an open-label, multicentre, phase 2 study. Lancet Oncol 2017;18:1182–91. https://doi.org/10.1016/S1470-2045(17)30422-9.

[54] André T, Shiu K-K, Kim TW, Jensen BV, Jensen LH, Punt C, et al. Pembrolizumab in Microsatellite-Instability–High Advanced Colorectal Cancer. New England Journal of Medicine 2020;383:2207–18. https://doi.org/10.1056/nejmoa2017699.

[55] Ribas A, Wolchok JD. Cancer immunotherapy using checkpoint blockade. n.d.

[56] Buchbinder EI, Desai A. CTLA-4 and PD-1 pathways similarities, differences, and implications of their inhibition. American Journal of Clinical Oncology: Cancer Clinical Trials 2016;39:98–106. https://doi.org/10.1097/COC.0000000000000239.

[57] Hoos A. Development of immuno-oncology drugs-from CTLA4 to PD1 to the next generations. Nat Rev Drug Discov 2016;15:235–47. https://doi.org/10.1038/nrd.2015.35.

[58] Piccirillo CA, Shevach EM. Naturally-occurring CD4+CD25+ immunoregulatory T cells: Central players in the arena of peripheral tolerance. Semin Immunol 2004;16:81–8. https://doi.org/10.1016/j.smim.2003.12.003.

[59] Sobhani N, Tardiel-Cyril DR, Davtyan A, Generali D, Roudi R, Li Y. CTLA-4 in regulatory T cells for cancer immunotherapy. Cancers (Basel) 2021;13:1–18. https://doi.org/10.3390/cancers13061440.

[60] Lenz H-J, Eric ;, Cutsem V, Limon ML, Yeung K, Wong M, et al. First-Line Nivolumab Plus Low-Dose Ipilimumab for Microsatellite Instability-High/ Mismatch Repair-Deficient Metastatic Colorectal Cancer: The Phase II CheckMate 142 Study. J Clin Oncol 2021;40:161–70. https://doi.org/10.1200/JCO.21.

[61] Berraondo P, Sanmamed MF, Ochoa MC, Etxeberria I, Aznar MA, Pérez-gracia JL. Cytokines in clinical cancer immunotherapy. Br J Cancer 2019. https://doi.org/10.1038/s41416-018-0328-y.

[62] Jiang T, Zhou C, Ren S. Role of IL-2 in cancer immunotherapy. Oncoimmunology 2016;5. https://doi.org/10.1080/2162402X.2016.1163462.

[63] Srivastava N, McDermott D. Update on benefit of immunotherapy and targeted therapy in melanoma: The changing landscape. Cancer Manag Res 2014;6:279–89. https://doi.org/10.2147/CMAR.S64979.

[64] J Y Douillard DCADRMNRDJPKPJTIJCMAGgLAPR. Irinotecan combined with fluorouracil compared with fluorouracil alone as first-line treatment for metastatic colorectal cancer: a multicentre randomised trial. THE LANCET 2000;355.

[65] A. de Gramont AFMSMHAHJCCBHC-FACGFDPNLBCLDHF de BCWFM and AB. Leucovorin and Fluorouracil With or Without Oxaliplatin as First-Line Treatment in Advanced Colorectal Cancer. Journal of Clinical Oncology 2000;18.

[66] Brezden-Masley C, Polenz C. Current practices and challenges of adjuvant chemotherapy in patients with colorectal cancer. Surg Oncol Clin N Am 2014;23:49–58. https://doi.org/10.1016/j.soc.2013.09.009.

[67] Amarjothi JMV, Ramasamy V, Senthil Kumaran GR, Naganath Babu OL. Challenges associated with colorectal cancer in pregnancy. Case Rep Gastroenterol 2019;13:253–7. https://doi.org/10.1159/000500078.

[68] Saif MW, Lichtman SM. Chemotherapy options and outcomes in older adult patients with colorectal cancer. Crit Rev Oncol Hematol 2009;72:155–69. https://doi.org/10.1016/j.critrevonc.2009.02.006.

[69] Kamat N, Khidhir MA, Hussain S, Alashari MM, Rannug U. Chemotherapy induced microsatellite instability and loss of heterozygosity in chromosomes 2, 5, 10, and 17 in solid tumor patients. 2014.

[70] Martinez-Balibrea E, Martínez-Cardus A, Gines A, Ruiz De Porras V, Moutinho C, Layos L, et al. Tumor-related molecular mechanisms of oxaliplatin resistance. Mol Cancer Ther 2015;14:1767–76. https://doi.org/10.1158/1535-7163.MCT-14-0636.

[71] Cao X, Hou J, An Q, Assaraf YG, Wang X. Towards the overcoming of anticancer drug resistance mediated by p53 mutations. Drug Resistance Updates 2020;49. https://doi.org/10.1016/j.drup.2019.100671.

[72] Gmeiner WH. Entrapment of DNA topoisomerase-DNA complexes by nucleotide/nucleoside analogs. Cancer Drug Resistance 2019;2:994–1001. https://doi.org/10.20517/cdr.2019.95.

[73] Arango D, Wilson AJ, Shi Q, Corner GA, Arañes MJ, Nicholas C, et al. Molecular mechanisms of action and prediction of response to oxaliplatin in colorectal cancer cells. Br J Cancer 2004;91:1931–46. https://doi.org/10.1038/sj.bjc.6602215.

[74] Blondy S, David V, Verdier M, Mathonnet M, Perraud A, Christou N. 5-Fluorouracil resistance mechanisms in colorectal cancer: From classical pathways to promising processes. Cancer Sci 2020;111:3142–54. https://doi.org/10.1111/cas.14532.

[75] Bouwman P, Jonkers J. The effects of deregulated DNA damage signalling on cancer chemotherapy response and resistance. Nat Rev Cancer 2012;12:587–98. https://doi.org/10.1038/nrc3342.

[76] Sui X, Chen R, Wang Z, Huang Z, Kong N, Zhang M, et al. Autophagy and chemotherapy resistance: A promising therapeutic target for cancer treatment. Cell Death Dis 2013;4. https://doi.org/10.1038/cddis.2013.350.

[77] Ciardiello D, Vitiello PP, Cardone C, Martini G, Troiani T, Martinelli E, et al. Immunotherapy of colorectal cancer: Challenges for therapeutic efficacy. Cancer Treat Rev 2019;76:22–32. https://doi.org/10.1016/j.ctrv.2019.04.003.

[78] Jia-Liang Liu, Ming Yang, Jun-Ge Bai, Zheng Liu, Xi-Shan Wang. Cold" colorectal cancer faces a bottleneck in immunotherapy. 2023.

[79] Dobosz P, Stępień M, Golke A, Dzieciątkowski T. Challenges of the Immunotherapy: Perspectives and Limitations of the Immune Checkpoint Inhibitor Treatment. Int J Mol Sci 2022;23. https://doi.org/10.3390/ijms23052847.

[80] Johnson FL. IMMUNOLOGICAL ASPECTS OF MALIGNANT DISEASE. Medical Journal of Australia 1971;2:317–25. https://doi.org/10.5694/j.1326-5377.1971.tb50568.x.

[81] Teng MWL, Kershaw MH, Smyth MJ. Cancer Immunoediting: From Surveillance to Escape. Cancer Immunotherapy: Immune Suppression and Tumor Growth: Second Edition 2013;3:85–99. https://doi.org/10.1016/B978-0-12-394296-8.00007-5.

[82] Nelson BH. The impact of T-cell immunity on ovarian cancer outcomes. Immunol Rev 2008;222:101–16. https://doi.org/10.1111/j.1600-065X.2008.00614.x.

[83] Shankaran V, Ikeda H, Bruce AT, White JM, Swanson PE, Old LJ, et al. IFNgamma and lympohcytes prevent primary tomour development and shape tomour immunogenicity. Nature 2001;410:1107–11.

[84] Finn OJ. Immuno-oncology: Understanding the function and dysfunction of the immune system in cancer. Annals of Oncology 2012;23:viii6–9. https://doi.org/10.1093/annonc/mds256.

[85] Wagner S, Mullins CS, Linnebacher M. Colorectal cancer vaccines: Tumor-associated antigens neoantigens. World J Gastroenterol 2018;24:5418–32. https://doi.org/10.3748/wjg.v24.i48.5418.

[86] Lewis JD, Reilly BD, Bright RK. Tumor-associated antigens: From discovery to immunity. Int Rev Immunol 2003;22:81–112. https://doi.org/10.1080/08830180305221.

[87] Joshi S, Kumar S, Choudhury A, Ponnusamy MP, Batra SK. Altered Mucins (MUC) Trafficking in Benign and Malignant Conditions. vol. 5. 2014.

[88] Kasprzak A, Siodła E, Andrzejewska M, Szmeja J, Seraszek-Jaros A, Cofta S, et al. Differential expression of mucin 1 and mucin 2 in colorectal cancer. World J Gastroenterol 2018;24:4164–77. https://doi.org/10.3748/wjg.v24.i36.4164.

[89] Knutson KL, Disis ML. Tumor antigen-specific T helper cells in cancer immunity and immunotherapy. Cancer Immunology, Immunotherapy 2005;54:721–8. https://doi.org/10.1007/s00262-004-0653-2.

[90] Liu CC, Yang H, Zhang R, Zhao JJ, Hao DJ. Tumour-associated antigens and their anti-cancer applications. Eur J Cancer Care (Engl) 2017;26. https://doi.org/10.1111/ecc.12446.

[91] Wurz GT, Kao CJ, Wolf M, DeGregorio MW. Tecemotide: An antigen-specific cancer immunotherapy. Hum Vaccin Immunother 2014;10:3383–93. https://doi.org/10.4161/hv.29836.

[92] Inamura K. Colorectal cancers: An update on their molecular pathology. Cancers (Basel) 2018;10. https://doi.org/10.3390/cancers10010026.

[93] Gulubova M V., Ananiev JR, Vlaykova TI, Yovchev Y, Tsoneva V, Manolova IM. Role of dendritic cells in progression and clinical outcome of colon cancer. Int J Colorectal Dis 2012;27:159–69. https://doi.org/10.1007/s00384-011-1334-1.

[94] Guilliams M, Ginhoux F, Jakubzick C, Naik SH, Onai N, Schraml BU, et al. Dendritic cells, monocytes and macrophages: A unified nomenclature based on ontogeny. Nat Rev Immunol 2014;14:571–8. https://doi.org/10.1038/nri3712.

[95] Ziegler-Heitbrock L, Ancuta P, Crowe S, Dalod M, Grau V, Hart DN, et al. Nomenclature of monocytes and dendritic cells in blood. Blood 2010;116. https://doi.org/10.1182/blood-2010-02-258558.

[96] Sato K, Fujita S. Dendritic Cells-Nature and Classification. vol. 56. 2007.

[97] Nfon CK, Dawson H, Toka FN, Golde WT. Langerhans cells in porcine skin. Vet Immunol Immunopathol 2008;126:236–47. https://doi.org/10.1016/j.vetimm.2008.07.012.

[98] Lommatzsch M, Bratke K, Stoll P, Mülleneisen N, Prall F, Bier A, et al. Bronchoalveolar lavage for the diagnosis of Pulmonary Langerhans cell histiocytosis. Respir Med 2016;119:168–74. https://doi.org/10.1016/j.rmed.2016.09.004.

[99] T.C.R. PARIKETT JLM. Characterization of Interstitial Dendritic cells in Human Liver. Transplantation 1988;46:754–61.

[100] Merad M, Sathe P, Helft J, Miller J, Mortha A. The dendritic cell lineage: Ontogeny and function of dendritic cells and their subsets in the steady state and the inflamed setting. Annu Rev Immunol 2013;31:563–604. https://doi.org/10.1146/annurev-immunol-020711-074950.

[101] Caetano Reis e Sousa. Dendritic cells in a mature age. Perspectives (Montclair) 2006;6. https://doi.org/https://doi.org/10.1038/nri1845.

[102] Clark G], Angel N, Kato M, Lopez] Alejandro, Macdonald K, Vuckovic S, et al. The role of dendritic cells in the innate immune system. vol. 2. 2000.

[103] de Winde CM, Munday C, Acton SE. Molecular mechanisms of dendritic cell migration in immunity and cancer. Med Microbiol Immunol 2020;209:515–29. https://doi.org/10.1007/s00430-020-00680-4.

[104] Wong JL, Muthuswamy R, Bartlett DL, Kalinski P. Il-18-based combinatorial adjuvants promote the intranodal production of ccl19 by nk cells and dendritic cells of cancer patients. Oncoimmunology 2013;2. https://doi.org/10.4161/onci.26245.

[105] Hansson M, Lundgren A, Elgbratt K, Quiding-Järbrink M, Svennerholm AM, Johansson EL. Dendritic cells express CCR7 and migrate in response to CCL19 (MIP-3β) after exposure to Helicobacter pylori. Microbes Infect 2006;8:841–50. https://doi.org/10.1016/j.micinf.2005.10.007.

[106] Sabado RL, Balan S, Bhardwaj N. Dendritic cell-based immunotherapy. Cell Res 2017;27:74–95. https://doi.org/10.1038/cr.2016.157.

[107] Bryant CE, Sutherland S, Kong B, Papadimitrious MS, Fromm PD, Hart DNJ. Dendritic cells as cancer therapeutics. Semin Cell Dev Biol 2019;86:77–88. https://doi.org/10.1016/j.semcdb.2018.02.015.

[108] Berger A. Science commentary : Th1 and Th2 responses : what are they ? 2000;321:5500. https://doi.org/https://doi.org/10.1136/bmj.321.7258.424.

[109] Raskov H. Cytotoxic CD8 + T cells in cancer and cancer immunotherapy. Br J Cancer 2021. https://doi.org/10.1038/s41416-020-01048-4.

[110] Schreibelt G, Bol KF, Aarntzen EHJG, Gerritsen WR, Punt CJA, Figdor CG, et al. Importance of helper T-cell activation in dendritic cell-based anticancer immunotherapy. Oncoimmunology 2013;2. https://doi.org/10.4161/onci.24440.

[111] Patente TA, Pinho MP, Oliveira AA, Evangelista GCM, Bergami-Santos PC, Barbuto JAM. Human dendritic cells: Their heterogeneity and clinical application potential in cancer immunotherapy. Front Immunol 2019;10:1–18. https://doi.org/10.3389/fimmu.2018.03176.

[112] Gee K, Guzzo C, Mat NFC, Ma W, Kumar A. The IL-12 family of cytokines in infection, inflammation and autoimmune disorders. Inflamm Allergy Drug Targets 2009;8:40–52. https://doi.org/10.2174/187152809787582507.

[113] Michielsen AJ, Ryan EJ, O'Sullivan JN. Dendritic cell inhibition correlates with survival of colorectal cancer patients on bevacizumab treatment. Oncoimmunology 2012;1:1445–7. https://doi.org/10.4161/onci.21318.

[114] Janssen E, Subtil B, Ortiz F de la J, Verheul HMW, Tauriello DVF. Combinatorial immunotherapies for metastatic colorectal cancer. Cancers (Basel) 2020;12:1–29. https://doi.org/10.3390/cancers12071875.

[115] Hinshaw DC, Shevde LA. The tumor microenvironment innately modulates cancer progression. Cancer Res 2019;79:4557–67. https://doi.org/10.1158/0008-5472.CAN-18-3962.

[116] Kubiczkova L, Sedlarikova L, Hajek R, Sevcikova S. TGF-β-an excellent servant but a bad master. 2012.

[117] Zong J, Keskinov AA, Shurin G V., Shurin MR. Tumor-derived factors modulating dendritic cell function. Cancer Immunology, Immunotherapy 2016;65:821–33. https://doi.org/10.1007/s00262-016-1820-y.

[118] Tang M, Diao J, Gu H, Khatri I, Zhao J, Cattral MS. Toll-like Receptor 2 Activation Promotes Tumor Dendritic Cell Dysfunction by Regulating IL-6 and IL-10 Receptor Signaling. Cell Rep 2015;13:2851–64. https://doi.org/10.1016/j.celrep.2015.11.053.

[119] Wculek SK, Cueto FJ, Mujal AM, Melero I, Krummel MF, Sancho D. Dendritic cells in cancer immunology and immunotherapy. Nat Rev Immunol 2020;20:7–24. https://doi.org/10.1038/s41577-019-0210-z.

[120] Kusume A, Sasahira T, Luo Y, Isobe M, Nakagawa N, Tatsumoto N, et al. Suppression of dendritic cells by HMGB1 is associated with lymph node metastasis of human colon cancer. Pathobiology 2009;76:155–62. https://doi.org/10.1159/000218331.

[121] Seidel JA, Otsuka A, Kabashima K. Anti-PD-1 and Anti-CTLA-4 Therapies in Cancer: Mechanisms of Action, Efficacy, and Limitations. Front Oncol 2018;8:1–14. https://doi.org/10.3389/fonc.2018.00086.

[122] Bai L, Li W, Zheng W, Xu D, Chen N, Cui J. Promising targets based on pattern recognition receptors for cancer immunotherapy. Pharmacol Res 2020;159:105017. https://doi.org/10.1016/j.phrs.2020.105017.

[123] Rezaei N. Therapeutic targeting of pattern-recognition receptors. Int Immunopharmacol 2006;6:863–9. https://doi.org/10.1016/j.intimp.2006.02.005.

[124] Tartey S, Takeuchi O. Pathogen recognition and Toll-like receptor targeted therapeutics in innate immune cells. Int Rev Immunol 2017;36:57–73. https://doi.org/10.1080/08830185.2016.1261318.

[125] O'Neill LAJ, Hennessy EJ, Parker AE. Targeting Toll-like receptors: Emerging therapeutics? Nat Rev Drug Discov 2010;9:293–307. https://doi.org/10.1038/nrd3203.

[126] Chi H, Li C, Zhao FS, Zhang L, Ng TB, Jin G, et al. Anti-tumor activity of toll-like receptor 7 agonists. Front Pharmacol 2017;8:1–10. https://doi.org/10.3389/fphar.2017.00304.

[127] Maeda K, Akira S. TLR7 Structure: Cut in Z-Loop. Immunity 2016;45:705–7. https://doi.org/10.1016/j.immuni.2016.10.003.

[128] Rolfo C, Giovannetti E, Martinez P, McCue S, Naing A. Applications and clinical trial landscape using Toll-like receptor agonists to reduce the toll of cancer. NPJ Precis Oncol 2023;7. https://doi.org/10.1038/s41698-023-00364-1.

[129] Garris CS, Arlauckas SP, Kohler RH, Trefny MP, Garren S, Piot C, et al. Successful Anti-PD-1 Cancer Immunotherapy Requires T Cell-Dendritic Cell Crosstalk Involving the Cytokines IFN-γ and IL-12. Immunity 2018;49:1148-1161.e7. https://doi.org/10.1016/j.immuni.2018.09.024.

[130] Javaid N, Choi S. Toll-like receptors from the perspective of cancer treatment. Cancers (Basel) 2020;12:1–33. https://doi.org/10.3390/cancers12020297.

[131] Vacchelli E, Galluzzi L, Eggermont A, Fridman WH, Galon J, Sautès-Fridman C, et al. Trial watch: FDA-approved Toll-like receptor agonists for cancer therapy. Oncoimmunology 2012;1:894–907. https://doi.org/10.4161/onci.20931.

[132] Bauer S, Pigisch S, Hangel D, Kaufmann A, Hamm S. Recognition of nucleic acid and nucleic acid analogs by Toll-like receptors 7, 8 and 9. Immunobiology 2008;213:315–28. https://doi.org/10.1016/j.imbio.2007.10.010.

[133] Witt PL, Ritch PS, Reding D, McAuliffe TL, Westrick L, Grossberg SE, et al. Phase I Trial of an Oral Immunomodulator and Interferon Inducer in Cancer Patients. Cancer Res 1993;53:5176–80.

[134] Reiter MJ, Testerman TL, Miller RL, Weeks CE, Tomai MA. Cytokine induction in mice by the immunomodulator imiquimod. J Leukoc Biol 1994;55:234–40. https://doi.org/10.1002/jlb.55.2.234.

[135] Sidky YA, Borden EC, Weeks CE, Reiter MJ, Hatcher JF, Bryan GT. Inhibition of Murine Tumor Growth by an Interferon-inducing Imidazoquinolinamine. Cancer Res 1992;52:3528–33.

[136] Arentsen HC, Hulsbergen-Van de Kaa CA, Jansen CFJ, Maj R, Leoni LM, Oosterwijk E, et al. Pharmacokinetics and toxicity of intravesical TMX-101: a preclinical study in pigs. BJU Int 2011;108:1210–4. https://doi.org/10.1111/j.1464-410X.2010.10055.x.

[137] Falke J, Hulsbergen-van de Kaa CA, Maj R, Oosterwijk E, Witjes JA. Pharmacokinetics and pharmacodynamics of intravesical and intravenous TMX-101 and TMX-202 in a F344 rat model. Urologic Oncology: Seminars and Original Investigations 2018;36:242.e1-242.e7. https://doi.org/10.1016/j.urolonc.2018.01.016.

[138] Goldstein D, Hertzog P, Tomkinson E, Couldwell D, McCarville S, Parrish S, et al. Administration of imiquimod, an interferon inducer, in asymptomatic human immunodeficiency virus-infected persons to determine safety and biologic response modification. Journal of Infectious Diseases 1998;178:858–61. https://doi.org/10.1086/515343.

[139] Savage P, Horton V, Moore J, Owens M, Witt P, Gore ME. A phase I clinical trial of imiquimod, an oral interferon inducer, administered daily. Br J Cancer 1996;74:1482–6. https://doi.org/10.1038/bjc.1996.569.

[140] Soria I, Myhre P, Horton V, Ellefson P, McCarville S, Schmitt K, et al. Effect of food on the pharmacokinetics and bioavailability of oral imiquimod relative to a subcutaneous dose. Int Journal of Clinical Pharmacology and Therapeutics 2000;38:476–81. https://doi.org/10.5414/CPP38476.

[141] Smith M, García-Martínez E, Pitter MR, Fucikova J, Spisek R, Zitvogel L, et al. Trial Watch: Toll-like receptor agonists in cancer immunotherapy. Oncoimmunology 2018;7:1–15. https://doi.org/10.1080/2162402X.2018.1526250.

[142] Tomai MA, Miller RL, Lipson KE, Kieper WC, Zarraga IE, Vasilakos JP. Resiquimod and other immune response modifiers as vaccine adjuvants. Expert Rev Vaccines 2007;6:835–47. https://doi.org/10.1586/14760584.6.5.835.

[143] Vasilakos JP, Tomai MA. The use of Toll-like receptor 7/8 agonists as vaccine adjuvants. Expert Rev Vaccines 2013;12:809–19. https://doi.org/10.1586/14760584.2013.811208.

[144] Dindo D, Nocito A, Schettle M, Clavien PA, Hahnloser D. What should we do about anal condyloma and anal intraepithelial neoplasia? Results of a survey. Colorectal Disease 2011;13:796–801. https://doi.org/10.1111/j.1463-1318.2010.02258.x.

[145] Gkegkes ID, Iavazzo C, Stamatiadis AP. Intra-anal use of imiquimod: what is the clinical evidence? Int J STD AIDS 2019;30:1018–24. https://doi.org/10.1177/0956462419855828.

[146] Yi JY, Jung YJ, Choi SS, Hwang J, Chung E. Autophagy-mediated anti-tumoral activity of imiquimod in Caco-2 cells. Biochem Biophys Res Commun 2009;386:455–8. https://doi.org/10.1016/j.bbrc.2009.06.046.

[147] Lin X, Zhang J, Wang X, Lin G, Chen T. Pre-activation with TLR7 in combination with thioridazine and loratadine promotes tumoricidal T-cell activity in colorectal cancer. Anticancer Drugs 2020;31:989–96. https://doi.org/10.1097/CAD.0000000000000972.

[148] Rostamizadeh L, Ramezani M, Monirinasab H, Rostamizadeh K, Sabzichi M, Bahavarnia SR, et al. Modulating the tumor microenvironment in a mouse model of colon cancer using a combination of HIF-1α inhibitors and Toll-Like Receptor 7 agonists. Naunyn Schmiedebergs Arch Pharmacol 2024. https://doi.org/10.1007/s00210-024-03658-8.

[149] Yang X, Huang C, Wang H, Yang K, Huang M, Zhang W, et al. Multifunctional Nanoparticle-Loaded Injectable Alginate Hydrogels with Deep Tumor Penetration for Enhanced Chemo-Immunotherapy of Cancer. ACS Nano 2024;18:18604–21. https://doi.org/10.1021/acsnano.4c04766.

[150] Swartz MA. The physiology of the lymphatic system. Adv Drug Deliv Rev 2001;50:3–20. https://doi.org/10.1016/S0169-409X(01)00150-8.

[151] Farnsworth RH, Achen MG, Stacker SA. The evolving role of lymphatics in cancer metastasis. Curr Opin Immunol 2018;53:64–73. https://doi.org/10.1016/j.coi.2018.04.008.

[152] Kesler CT, Liao S, Munn LL, Padera TP. Lymphatic vessels in health and disease. Wiley Interdiscip Rev Syst Biol Med 2013;5:111–24. https://doi.org/10.1002/wsbm.1201.

[153] Shu P, Ouyang G, Wang F, Zhou J, Shen Y, Li Z, et al. The role of radiotherapy in the treatment of retroperitoneal lymph node metastases from colorectal cancer. Cancer Manag Res 2020;12:8913–21. https://doi.org/10.2147/CMAR.S249248.

[154] Willard-Mack CL. Normal Structure, Function, and Histology of Lymph Nodes. Toxicol Pathol 2006;34:409–24. https://doi.org/10.1080/01926230600867727.

[155] Miller MJ, Hejazi AS, Wei SH, Cahalan MD, Parker I. T cell repertoire scanning is promoted by dynamic dendritic cell behavior and random T cell motility in the lymph node 2004.

[156] Dhodapkar M V., Dhodapkar KM, Palucka AK. Interactions of tumor cells with dendritic cells: Balancing immunity and tolerance. Cell Death Differ 2008;15:39–50. https://doi.org/10.1038/sj.cdd.4402247.

[157] McDonnell AM, Robinson BWS, Currie AJ. Tumor antigen cross-presentation and the dendritic cell: Where it all begins? Clin Dev Immunol 2010;2010. https://doi.org/10.1155/2010/539519.

[158] Feeney OM, Gracia G, Brundel DHS, Trevaskis NL, Cao E, Kaminskas LM, et al. Lymph-directed immunotherapy – Harnessing endogenous lymphatic distribution pathways for enhanced therapeutic outcomes in cancer. Adv Drug Deliv Rev 2020;160:115–35. https://doi.org/10.1016/j.addr.2020.10.002.

[159] Trevaskis NL, Kaminskas LM, Porter CJH. From sewer to saviour-targeting the lymphatic system to promote drug exposure and activity. Nat Rev Drug Discov 2015;14:781–803. https://doi.org/10.1038/nrd4608.

[160] Francis DM, Manspeaker MP, Schudel A, Sestito LF, O'Melia MJ, Kissick HT, et al. Blockade of immune checkpoints in lymph nodes through locoregional delivery augments cancer immunotherapy. Sci Transl Med 2020;12:1–12. https://doi.org/10.1126/scitranslmed.aay3575.

[161] Mu H, Høy CE. The digestion of dietary triacylglycerols. Prog Lipid Res 2004;43:105–33. https://doi.org/10.1016/S0163-7827(03)00050-X.

[162] Carey MC, Bliss CM. LIPID DIGESTION AND ABSORPTION. vol. 45. 1983.

[163] Jackson AD, McLaughlin J. Digestion and absorption. Surgery 2009;27:231–6. https://doi.org/10.1016/j.mpsur.2009.03.003.

[164] Xiao C, Stahel P, Lewis GF. Regulation of Chylomicron Secretion: Focus on Post-Assembly Mechanisms. Cmgh 2019;7:487–501. https://doi.org/10.1016/j.jcmgh.2018.10.015.

[165] Johnston JM, Borgstrom B. THE INTESTINAL ABSORPTION AND METABOLISM OF MICELLAR SOLUTIONS OF LIPIDS. 1963. https://doi.org/https://doi.org/10.1016/0926-6542(64)90005-8.

[166] Buttet M, Traynard V, Tran TTT, Besnard P, Poirier H, Niot I. From fatty-acid sensing to chylomicron synthesis: Role of intestinal lipid-binding proteins. Biochimie 2014;96:37–47. https://doi.org/10.1016/j.biochi.2013.08.011.

[167] Shi Y, Cheng D. Beyond triglyceride synthesis: The dynamic functional roles of MGAT and DGAT enzymes in energy metabolism. Am J Physiol Endocrinol Metab 2009;297. https://doi.org/10.1152/ajpendo.90949.2008.

[168] Xiao C, Stahel P, Lewis GF. Regulation of Chylomicron Secretion: Focus on Post-Assembly Mechanisms. CMGH 2019;7:487–501. https://doi.org/10.1016/j.jcmgh.2018.10.015.

[169] Biochi ~mi C~a BB, Hussain MM, Kancha RK, Zhou Z, Luchoomun J, Zu H, et al. Chylomicron assembly and catabolism: role of apolipoproteins and receptors. vol. 1300. 1996.

[170] Trevaskis NL, Lee G, Escott A, Phang KL, Hong J, Cao E, et al. Intestinal Lymph Flow, and Lipid and Drug Transport Scale Allometrically From Pre-clinical Species to Humans. Front Physiol 2020;11. https://doi.org/10.3389/fphys.2020.00458.

[171] Park H, Yeom E, Lee SJ. X-ray PIV measurement of blood flow in deep vessels of a rat: An in vivo feasibility study. Sci Rep 2016;6. https://doi.org/10.1038/srep19194.

[172] Granger DN, Kvietys PR. Circulation, Overview. 2004.

[173] Porsgaard T, Kánsky´, JK, Mason S, Mu H. Size and Number of Lymph Particles Measured by a Particle Sizer During Absorption of Structured Oils in Rats. vol. 40. 2005.

[174] Horst Ruf · Barry J. Gould. Size distributions of chylomicrons from human lymph from dynamic light scattering measurements. Eur Biophys J 1998;28:1–11.

[175] Zhang F, Zarkada G, Yi S, Eichmann A. Lymphatic Endothelial Cell Junctions: Molecular Regulation in Physiology and Diseases. Front Physiol 2020;11. https://doi.org/10.3389/fphys.2020.00509.

[176] Bartholdson L, Hultborn A, Hulten L, Roos B, Rosencrantz M, Ahrén C. Lymph drainage from the upper and middle third of the rectum as demonstrated by 198Au. Acta Radiologica - Series Therapy, Physics and Biology 1977;16:352–60. https://doi.org/10.3109/02841867709133955.

[177] Cho HS, Ahn JH. Nomenclature and Lymphatic Drainage Patterns of Abdominal Lymph Nodes. Journal of the Korean Society of Radiology 2022;83:1240–58. https://doi.org/10.3348/jksr.2021.0189.

[178] Tilney NL. Patterns of lymphatic drainage in the adult laboratory rat. J Anat 1971;109:369–83.

[179] Zgair A, Wong JCM, Lee JB, Mistry J, Sivak O, Wasan KM, et al. Dietary fats and pharmaceutical lipid excipients increase systemic exposure to orally administered cannabis and cannabis-based medicines. Am J Transl Res 2016;8:3448–59.

[180] Zgair A, Lee JB, Wong JCM, Taha DA, Aram J, Di Virgilio D, et al. Oral administration of cannabis with lipids leads to high levels of cannabinoids in the intestinal lymphatic system and prominent immunomodulation. Sci Rep 2017;7. https://doi.org/10.1038/s41598-017-15026-z.

[181] Gershkovich P, Hoffman A. Uptake of lipophilic drugs by plasma derived isolated chylomicrons: Linear correlation with intestinal lymphatic bioavailability. European Journal of Pharmaceutical Sciences 2005;26:394–404. https://doi.org/10.1016/j.ejps.2005.07.011.

[182] Gershkovich P, Fanous J, Qadri B, Yacovan A, Amselem S, Hoffman A. The role of molecular physicochemical properties and apolipoproteins in association of drugs with triglyceride-rich lipoproteins: in-silico prediction of uptake by chylomicrons. Journal of Pharmacy and Pharmacology 2008;61:31–9. https://doi.org/10.1211/jpp/61.01.0005.

[183] Trevaskis NL, Charman WN, Porter CJH. Lipid-based delivery systems and intestinal lymphatic drug transport: A mechanistic update. Adv Drug Deliv Rev 2008;60:702–16. https://doi.org/10.1016/j.addr.2007.09.007.

[184] Porter CJH, Trevaskis NL, Charman WN. Lipids and lipid-based formulations: Optimizing the oral delivery of lipophilic drugs. Nat Rev Drug Discov 2007;6:231–48. https://doi.org/10.1038/nrd2197.

[185] Han S, Hu L, Quach T, Simpson JS, Trevaskis NL, Porter CJH. Profiling the Role of Deacylation-Reacylation in the Lymphatic Transport of a Triglyceride-Mimetic Prodrug. Pharm Res 2015;32:1830–44. https://doi.org/10.1007/s11095-014-1579-9.

[186] Quach T, Hu L, Han S, Lim SF, Senyschyn D, Yadav P, et al. Triglyceride-Mimetic Prodrugs of Buprenorphine Enhance Oral Bioavailability via Promotion of Lymphatic Transport. Front Pharmacol 2022;13. https://doi.org/10.3389/fphar.2022.879660.

[187] Hu L, Quach T, Han S, Lim SF, Yadav P, Senyschyn D, et al. Glyceride-Mimetic Prodrugs Incorporating Self-Immolative Spacers Promote Lymphatic Transport, Avoid First-Pass Metabolism, and Enhance Oral Bioavailability. Angewandte Chemie 2016;128:13904–9. https://doi.org/10.1002/ange.201604207.

[188] Han S, Quach T, Hu L, Wahab A, Charman WN, Stella VJ, et al. Targeted delivery of a model immunomodulator to the lymphatic system: Comparison of alkyl ester versus triglyceride mimetic lipid prodrug strategies. Journal of Controlled Release 2014;177:1–10. https://doi.org/10.1016/j.jconrel.2013.12.031.

[189] Kochappan R, Cao E, Han S, Hu L, Quach T, Senyschyn D, et al. Targeted delivery of mycophenolic acid to the mesenteric lymph node using a triglyceride mimetic prodrug approach enhances gut-specific immunomodulation in mice. Journal of Controlled Release 2021;332:636–51. https://doi.org/10.1016/j.jconrel.2021.02.008.

[190] Lee JB, Zgair A, Malec J, Kim TH, Kim MG, Ali J, et al. Lipophilic activated ester prodrug approach for drug delivery to the intestinal lymphatic system. Journal of Controlled Release 2018;286:10–9. https://doi.org/10.1016/j.jconrel.2018.07.022.

[191] Qin C, Chu YJ, Feng W, Fromont C, He S, Ali J, et al. Targeted delivery of lopinavir to HIV reservoirs in the mesenteric lymphatic system by lipophilic ester prodrug approach. Journal of Controlled Release 2020. https://doi.org/10.1016/j.jconrel.2020.10.036.

[192] Chu Y, Wong A, Chen H, Ji L, Qin C, Feng W, et al. Development of lipophilic ester prodrugs of dolutegravir for intestinal lymphatic transport. European Journal of Pharmaceutics and Biopharmaceutics 2023;191:90–102. https://doi.org/10.1016/j.ejpb.2023.08.015.

[193] Sharma A, Sharma D, Baldi A, Jyoti K, Chandra R, Madan J. Imiquimod-oleic acid prodrug-loaded cream reduced drug crystallinity and induced indistinguishable cytotoxicity and apoptosis in mice melanoma tumour. J Microencapsul 2019;36:759–74. https://doi.org/10.1080/02652048.2019.1677796.

[194] Beutner GL, Young IS, Davies ML, Hickey MR, Park H, Stevens JM, et al. TCFH-NMI: Direct Access to N-Acyl Imidazoliums for Challenging Amide Bond Formations. Org Lett 2018;20:4218–22. https://doi.org/10.1021/acs.orglett.8b01591.

[195] Chu Y, Qin C, Feng W, Sheriston C, Jane Khor Y, Medrano-Padial C, et al. Oral administration of tipranavir with long-chain triglyceride results in moderate intestinal lymph targeting but no efficient delivery to HIV-1 reservoir in mesenteric lymph nodes. Int J Pharm 2021;602. https://doi.org/10.1016/j.ijpharm.2021.120621.

[196] Wong A, Chu Y, Chen H, Feng W, Ji L, Qin C, et al. Distribution of lamivudine into lymph node HIV reservoir. Int J Pharm 2023;648:123574. https://doi.org/10.1016/j.ijpharm.2023.123574.

[197] Kessler M, Acuto O, Storelli C, Murer H, Müller M, Semenza G. A MODIFIED PROCEDURE FOR THE RAPID PREPARATION OF EFFICIENTLY TRANSPORTING VESICLES FROM SMALL INTESTINAL BRUSH BORDER MEMBRANES THEIR. Biochim Biophys Acta 1978;506:136–54.

[198] Farooq N, Yusufi ANK, Mahmood R. Effect of fasting on enzymes of carbohydrate metabolism and brush border membrane in rat intestine. Nutrition Research 2004;24:407–16. https://doi.org/10.1016/j.nutres.2004.01.004.

[199] Walsky RL, Obach RS. VALIDATED ASSAYS FOR HUMAN CYTOCHROME P450 ACTIVITIES. 2004.

[200] Marques M. Dissolution media simulating fasted and fed states. Dissolut Technol 2004;11:16. https://doi.org/10.14227/DT110204P16.

[201] Kang T, Li Y, Wang Y, Zhu J, Yang L, Huang Y, et al. Modular Engineering of Targeted Dual-Drug Nanoassemblies for Cancer Chemoimmunotherapy. ACS Appl Mater Interfaces 2019;11:36371–82. https://doi.org/10.1021/acsami.9b11881.

[202] Zgair A, Lee JB, Wong JCM, Taha DA, Aram J, Di Virgilio D, et al. Oral administration of cannabis with lipids leads to high levels of cannabinoids in the intestinal lymphatic system and prominent immunomodulation. Sci Rep 2017;7:1–12. https://doi.org/10.1038/s41598-017-15026-z.

[203] Feng W, Qin C, Chu YJ, Berton M, Lee JB, Zgair A, et al. Natural sesame oil is superior to pre-digested lipid formulations and purified triglycerides in promoting the intestinal lymphatic transport and systemic bioavailability of cannabidiol. European Journal of Pharmaceutics and Biopharmaceutics 2021;162:43–9. https://doi.org/10.1016/j.ejpb.2021.02.013.

[204] Qin C, Feng W, Chu YJ, Lee JB, Berton M, Bettonte S, et al. Development and validation of a cost-effective and sensitive bioanalytical HPLC-UV method for determination of lopinavir in rat and human plasma. Biomedical Chromatography 2020;34:1–10. https://doi.org/10.1002/bmc.4934.

[205] Webb K, Fogarty A, Barrett DA, Nash EF, Whitehouse JL, Smyth AR, et al. Clinical significance of Pseudomonas aeruginosa 2-alkyl-4-quinolone quorum-sensing signal molecules for long-term outcomes in adults with cystic fibrosis. J Med Microbiol 2019;68:1823–8. https://doi.org/10.1099/jmm.0.001099.

[206] U.S. Department of Health and Human Services Food and Drug Administration Center for Drug Evaluation and Research (CDER) Center for Veterinary Medicine (CVM). Bioanalytical Method Validation Guidance for Industry Biopharmaceutics Bioanalytical Method Validation Guidance for Industry Biopharmaceutics Contains Nonbinding Recommendations. 2018.

[207] Frega G, Wu Q, Le Naour J, Vacchelli E, Galluzzi L, Kroemer G, et al. Trial Watch: experimental TLR7/TLR8 agonists for oncological indications. Oncoimmunology 2020;9. https://doi.org/10.1080/2162402X.2020.1796002.

[208] Gao Y, Zhang Y, Xia H, Ren Y, Zhang H, Huang S, et al. Biomimetic virus-like mesoporous silica nanoparticles improved cellular internalization for co-delivery of antigen and agonist to enhance Tumor immunotherapy. Drug Deliv 2023;30. https://doi.org/10.1080/10717544.2023.2183814.

[209] Wang L, He Y, He T, Liu G, Lin C, Li K, et al. Lymph node-targeted immune-activation mediated by imiquimod-loaded mesoporous polydopamine based-nanocarriers. Biomaterials 2020;255. https://doi.org/10.1016/j.biomaterials.2020.120208.

[210] Yan W, Li Y, Zou Y, Zhu R, Wu T, Yuan W, et al. Co-delivering irinotecan and imiquimod by pH-responsive micelle amplifies anti-tumor immunity against colorectal cancer. Int J Pharm 2023;648:123583. https://doi.org/10.1016/j.ijpharm.2023.123583.

[211] Singh B, Maharjan S, Pan DC, Zhao Z, Gao Y, Zhang YS, et al. Imiquimod-gemcitabine nanoparticles harness immune cells to suppress breast cancer. Biomaterials 2022;280. https://doi.org/10.1016/j.biomaterials.2021.121302.

[212] Jain S, Diwan A, Sardana S. Development and validation of UV spectroscopy and RP-HPLC methods for estimation of Imiquimod. Int J Pharm Sci Rev Res 2015;35:16–21.

[213] Bachute MT, Turwale SL. A rapid and validated reverse phase liquid chromatographic method for determination of imiquimod from topical cream formulations. J Pharm Res 2013;6:73–7. https://doi.org/10.1016/j.jopr.2012.11.016.

[214] Hussain S, Shaikh T, Farooqui M. Development and Validation of Liquid Chromatography Method for the Determination and Quantification of Impurities in Imiquimod. Br J Pharm Res 2016;13:1–9. https://doi.org/10.9734/bjpr/2016/28020.

[215] Sharma M, Sharma G, Singh B, Katare OP. Stability Kinetics of Imiquimod: Development and Validation of an Analytical Method. J Chromatogr Sci 2019;57:583–91. https://doi.org/10.1093/chromsci/bmz030.

[216] De Paula D, Original Research al, De Paula D, Azenha Martins C, Vitória Lopes Badra Bentley M. Development and validation of HPLC method for imiquimod determination in skin penetration studies. BIOMEDICAL CHROMATOGRAPHY Biomed Chromatogr 2008;22:1416–23. https://doi.org/10.1002/bmc.

[217] Ramineni SK, Dziubla TD, Cunningham LL, Puleo DA. Local delivery of imiquimod in hamsters using mucoadhesive films and their residence time in human patients. Oral Surg Oral Med Oral Pathol Oral Radiol 2014;118:665–73. https://doi.org/10.1016/j.oooo.2014.08.015.

[218] Al-Mayahy MH, Sabri AH, Rutland CS, Holmes A, McKenna J, Marlow M, et al. Insight into imiquimod skin permeation and increased delivery using microneedle pre-treatment. European Journal of Pharmaceutics and Biopharmaceutics 2019;139:33–43. https://doi.org/10.1016/j.ejpb.2019.02.006.

[219] Kim S, Youssef SH, Song Y, Garg S. Development and application of a chromatographic method for simultaneous quantification of 5-fluorouracil and imiquimod in drug-in-adhesive topical patches. Sustain Chem Pharm 2022;27. https://doi.org/10.1016/j.scp.2022.100711.

[220] Chan D, Tarbin J, Sharman M, Carson M, Smith M, Smith S. Screening method for the analysis of antiviral drugs in poultry tissues using zwitterionic hydrophilic interaction liquid chromatography/tandem mass spectrometry. Anal Chim Acta 2011;700:194–200. https://doi.org/10.1016/j.aca.2010.11.015.

[221] Liu ZC, Yang F, Yao M, Lin YH, Su ZJ. Simultaneous determination of antiviral drugs in chicken tissues by ultra high performance liquid chromatography with tandem mass spectrometry. J Sep Sci 2015;38:1784–93. https://doi.org/10.1002/jssc.201401461.

[222] Balireddi V, Tirukkovalluri SR, Murthy Tatikonda K, Surikutchi BT, Mitra P. Development and Validation of Stability Indicating UPLC-PDA/MS for the Determination of Imiquimod and its

Eight Related Substances: Application to Topical Cream. J Chromatogr Sci 2019;57:249–57. https://doi.org/10.1093/chromsci/bmy108.

[223] D. K. MYERS & A. KEMP JUN. Inhibition of Esterases by the Fluorides of Organic Acids. Nature 1954;173:33–4.

[224] S Loevenhart BA. THE INHiBITING EFFECT OF SODIUM FLUORIDE ON THE ACTION OF LIPASE. (Second Paper.). 1906.

[225] Alapafuja SO, Nikas SP, Bharathan IT, Shukla VG, Nasr ML, Bowman AL, et al. Sulfonyl fluoride inhibitors of fatty acid amide hydrolase. J Med Chem 2012;55:10074–89. https://doi.org/10.1021/jm301205j.

[226] Bowen RAR, Remaley AT. Interferences from blood collection tube components on clinical chemistry assays. Biochem Med (Zagreb) 2014;24:31–44. https://doi.org/10.11613/BM.2014.006.

[227] Adams JL, Smothers J, Srinivasan R, Hoos A. Big opportunities for small molecules in immuno-oncology. Nat Rev Drug Discov 2015;14:603–21. https://doi.org/10.1038/nrd4596.

[228] De Vries IJM, Krooshoop DJEB, Scharenborg NM, Lesterhuis WJ, Diepstra JHS, Van Muijen GNP, et al. Effective migration of antigen-pulsed dendritic cells to lymph nodes in melanoma patients is determined by their maturation state. Cancer Res 2003;63:12–7.

[229] Lei H, Kim JH, Son S, Chen L, Pei Z, Yang Y, et al. Immunosonodynamic Therapy Designed with Activatable Sonosensitizer and Immune Stimulant Imiquimod. ACS Nano 2022;16:10979–93. https://doi.org/10.1021/acsnano.2c03395.

[230] Yin W, Deng B, Xu Z, Wang H, Ma F, Zhou M, et al. Formulation and Evaluation of Lipidized Imiquimod as an Effective Adjuvant. ACS Infect Dis 2023;9:378–87. https://doi.org/10.1021/acsinfecdis.2c00583.

[231] Yin W, Xuan D, Wang H, Zhou M, Deng B, Ma F, et al. Biodegradable Imiquimod-Loaded Mesoporous Organosilica as a Nanocarrier and Adjuvant for Enhanced and Prolonged Immunity against Foot-and-Mouth Disease Virus in Mice. ACS Appl Bio Mater 2022;5:3095–106. https://doi.org/10.1021/acsabm.2c00382.

[232] Liu T, Zhu M, Chang X, Tang X, Yuan P, Tian R, et al. Tumor-Specific Photothermal-Therapy-Assisted Immunomodulation via Multiresponsive Adjuvant Nanoparticles. Advanced Materials 2023;35. https://doi.org/10.1002/adma.202300086.

[233] Sorgi D, Sartori A, Germani S, Gentile RN, Bianchera A, Bettini R. Imiquimod Solubility in Different Solvents: An Interpretative Approach. Pharmaceutics 2024;16:282. https://doi.org/10.3390/pharmaceutics16020282.

[234] Macpherson AJ, Smith K. Mesenteric lymph nodes at the center of immune anatomy. Journal of Experimental Medicine 2006;203:497–500. https://doi.org/10.1084/jem.20060227.

[235] Oschry Y, Eisenberg S. Rat plasma lipoproteins: re-evaluation of a lipoprotein system in an animal devoid of cholesteryl ester transfer activity. J Lipid Res 1982;23:1099–106. https://doi.org/10.1016/s0022-2275(20)38046-9.

[236] Tso P, Ragland JB, Sabesin SM. Isolation and characterization of lipoprotein of density less than 1.006 g/ml from rat hepatic lymph. J Lipid Res 1983;24:810–20. https://doi.org/10.1016/s0022-2275(20)37926-8.

[237] Lasser NL, Roheim PS, Edelstein D, Eder HA. Serum lipoproteins of normal and cholesterol fed rats. J Lipid Res 1973;14:1–8. https://doi.org/10.1016/s0022-2275(20)39322-6.

[238] Jadhav ST, Salunkhe VR, Bhinge SD. Nanoemulsion drug delivery system loaded with imiquimod: a QbD-based strategy for augmenting anti-cancer effects. Futur J Pharm Sci 2023;9:120. https://doi.org/10.1186/s43094-023-00568-z.

[239] Alqahtani MS, Kazi M, Alsenaidy MA, Ahmad MZ. Advances in Oral Drug Delivery. Front Pharmacol 2021;12. https://doi.org/10.3389/fphar.2021.618411.

[240] Augustijns P, Wuyts B, Hens B, Annaert P, Butler J, Brouwers J. A review of drug solubility in human intestinal fluids: Implications for the prediction of oral absorption. European Journal of Pharmaceutical Sciences 2014;57:322–32. https://doi.org/10.1016/j.ejps.2013.08.027.

[241] Lamb K, Kang YM, Gebhart GF, Bielefeldt K. Gastric Inflammation Triggers Hypersensitivity to Acid in Awake Rats. Gastroenterology 2003;125:1410–8. https://doi.org/10.1016/j.gastro.2003.07.010.

[242] Robert A, Nezamis JE, Lancaster C. Mild irritants prevent gastric necrosis through “adaptive cytoprotection” mediated by prostaglandins. Am J Physiol Gastrointest Liver Physiol 1983;8. https://doi.org/10.1152/ajpgi.1983.245.1.g113.

[243] Solanki SS, Soni LK, Maheshwari RK. Study on Mixed Solvency Concept in Formulation Development of Aqueous Injection of Poorly Water Soluble Drug. J Pharm (Cairo) 2013;2013:1–8. https://doi.org/10.1155/2013/678132.

[244] Padiyar A, Agrawal OP, Rajpoot K, Tekade RK. Hydrotropy, mixed hydrotropy, and mixed solvency as trending concept for solubilization of lipophilic drugs. The Future of Pharmaceutical Product Development and Research, Elsevier; 2020, p. 145–78. https://doi.org/10.1016/b978-0-12-814455-8.00005-0.

[245] Simamora P, Alvarez JM, Yalkowsky SH. Solubilization of rapamycin. vol. 213. 2001.

[246] El Hamd MA, Obaydo RH, Nashed D, El-Maghrabey M, Lotfy HM. Hydrotropy and co-solvency: Sustainable strategies for enhancing solubility of poorly soluble pharmaceutical active ingredients. Talanta Open 2025;11. https://doi.org/10.1016/j.talo.2024.100391.

[247] Ward FW, Coates ME. Gastrointestinal pH measurement in rats: influence of the microbial flora, diet and fasting. vol. 21. 1987.

[248] McNeil NI, Ling KLE, Wager J. Mucosal surface pH of the large intestine of the rat and of normal and inflamed large intestine in man. Gut 1987;28:707–13. https://doi.org/10.1136/gut.28.6.707.

[249] McConnell EL, Basit AW, Murdan S. Measurements of rat and mouse gastrointestinal pH, fluid and lymphoid tissue, and implications for in-vivo experiments. Journal of Pharmacy and Pharmacology 2010;60:63–70. https://doi.org/10.1211/jpp.60.1.0008.

[250] Neena Washington CW and CW. Chapter Seven: Drug Delivery to the Large Intestine and Rectum. Physiological Pharmaceutics. 2nd ed., London: 2000, p. 114–79.

[251] Hurst S, Loi C-M, Brodfuehrer J, El-Kattan A. Impact of physiological, physicochemical and biopharmaceutical factors in absorption and metabolism mechanisms on the drug oral bioavailability of rats and humans. Expert Opin Drug Metab Toxicol 2007;3:469–89. https://doi.org/10.1517/17425225.3.4.469.

[252] Jianyong Wang. PHARMACOLOGY/TOXICOLOGY NDA REVIEW AND EVALUATION APPLICATION NUMBER: 201153Orig1s000. Department of Health and Human Services Public Health Service FOOD AND DRUG ADMINISTRATION CERTER FOR DRUG EVALUATION AND RESEARCH 2010.

[253] Mescher M, Tigges J, Rolfes KM, Shen AL, Yee JS, Vogeley C, et al. The Toll-like receptor agonist imiquimod is metabolized by aryl hydrocarbon receptor-regulated cytochrome P450 enzymes in human keratinocytes and mouse liver. Arch Toxicol 2019;93:1917–26. https://doi.org/10.1007/s00204-019-02488-5.

[254] Budinsky RA, LeCluyse EL, Ferguson SS, Rowlands JC, Simon T. Human and rat primary hepatocyte CYP1A1 and 1A2 induction with 2,3,7,8-tetrachlorodibenzo-p-dioxin, 2,3,7,8-tetrachlorodibenzofuran, and 2,3,4,7,8-pentachlorodibenzofuran. Toxicological Sciences 2010;118:224–35. https://doi.org/10.1093/toxsci/kfq238.

[255] Feng W, Qin C, Chu YJ, Berton M, Lee JB, Zgair A, et al. Natural sesame oil is superior to pre-digested lipid formulations and purified triglycerides in promoting the intestinal lymphatic transport and systemic bioavailability of cannabidiol. European Journal of Pharmaceutics and Biopharmaceutics 2021;162:43–9. https://doi.org/10.1016/j.ejpb.2021.02.013.

[256] Stepensky D, Friedman M, Raz I, Hoffman A. PHARMACOKINETIC-PHARMACODYNAMIC ANALYSIS OF THE GLUCOSE-LOWERING EFFECT OF METFORMIN IN DIABETIC RATS REVEALS FIRST-PASS PHARMACODYNAMIC EFFECT. 2002.

[257] Lee G, Han S, Lu Z, Hong J, Phillips ARJ, Windsor JA, et al. Intestinal delivery in a long-chain fatty acid formulation enables lymphatic transport and systemic exposure of orlistat. Int J Pharm 2021:120247. https://doi.org/10.1016/j.ijpharm.2021.120247.

[258] Suami H, Scaglioni MF. Lymphatic territories (lymphosomes) in the rat: An anatomical study for future lymphatic research. Plast Reconstr Surg 2017;140:945–51. https://doi.org/10.1097/PRS.0000000000003776.

[259] Sainathan SK, Bishnupuri KS, Aden K, Luo Q, Houchen CW, Anant S, et al. Toll-like receptor-7 ligand imiquimod induces type I interferon and antimicrobial peptides to ameliorate dextran sodium sulfate-induced acute colitis. Inflamm Bowel Dis 2012;18:955–67. https://doi.org/10.1002/ibd.21867.

[260] Abdallah M, Müllertz OO, Styles IK, Mörsdorf A, Quinn JF, Whittaker MR, et al. Lymphatic targeting by albumin-hitchhiking: Applications and optimisation. Journal of Controlled Release 2020;327:117–28. https://doi.org/10.1016/j.jconrel.2020.07.046.

[261] CAPT E. Dennis Bashaw. Imiquimod Cream 3.75% (ZYCLARA/Marketed 5% name-ALDARA) In: Clinical Pharmacology [database on the Internet]， NDA 201153, n.d.

[262] Khier S, Gattacceca F, El Messaoudi S, Lafaille F, Deleuze-Masquéfa C, Bompart J, et al. Metabolism and pharmacokinetics of EAPB0203 and EAPB0503, two imidazoquinoxaline compounds previously shown to have antitumoral activity on melanoma and T-lymphomas.

Drug Metabolism and Disposition 2010;38:1836–47. https://doi.org/10.1124/dmd.110.034579.

[263] Zahr NM, Zhao Q, Goodcase R, Pfefferbaum A. Systemic Administration of the TLR7/8 Agonist Resiquimod (R848) to Mice Is Associated with Transient, In Vivo-Detectable Brain Swelling. Biology (Basel) 2022;11. https://doi.org/10.3390/biology11020274.

[264] Buchbinder EI, Desai A. CTLA-4 and PD-1 pathways similarities, differences, and implications of their inhibition. American Journal of Clinical Oncology: Cancer Clinical Trials 2016;39:98–106. https://doi.org/10.1097/COC.0000000000000239.

[265] Ganesan A, Ahmed M, Okoye I, Arutyunova E, Babu D, Turnbull WL, et al. Comprehensive in vitro characterization of PD-L1 small molecule inhibitors. Sci Rep 2019;9:12392. https://doi.org/10.1038/s41598-019-48826-6.

[266] Jia L, Liu K, Fei T, Liu Q, Zhao X, Hou L, et al. Programmed cell death-1/programmed cell death-ligand 1 inhibitors exert antiapoptosis and antiinflammatory activity in lipopolysaccharide stimulated murine alveolar macrophages. Exp Ther Med 2021;21:400. https://doi.org/10.3892/etm.2021.9831.

[267] Bai H, Wang Z, Li M, Sun P, Wei S, Wang W, et al. Inhibition of programmed death-1 decreases neointimal hyperplasia after patch angioplasty. J Biomed Mater Res B Appl Biomater 2021;109:269–78. https://doi.org/10.1002/jbm.b.34698.

[268] Lichtenstern CR, Ngu RK, Shalapour S, Karin M. Immunotherapy, Inflammation and Colorectal Cancer. Cells 2020;9. https://doi.org/10.3390/cells9030618.

[269] Zhu S, Zhang T, Zheng L, Liu H, Song W, Liu D, et al. Combination strategies to maximize the benefits of cancer immunotherapy. J Hematol Oncol 2021;14. https://doi.org/10.1186/s13045-021-01164-5.

[270] Dudek AZ, Yunis C, Harrison LI, Kumar S, Hawkinson R, Cooley S, et al. First in human phase I trial of 852A, a novel systemic toll-like receptor 7 agonist, to activate innate immune responses in patients with advanced cancer. Clinical Cancer Research 2007;13:7119–25. https://doi.org/10.1158/1078-0432.CCR-07-1443.

[271] Y-H Wu T, Singh M, Miller AT, De Gregorio E, Doro F, G Skibinski DA, et al. Rational design of small molecules as vaccine adjuvants. ADJUVANTS 2014;6. https://doi.org/10.1126/scitranslmed.3009980.

[272] Yáñez JA, Wang SWJ, Knemeyer IW, Wirth MA, Alton KB. Intestinal lymphatic transport for drug delivery. Adv Drug Deliv Rev 2011;63:923–42. https://doi.org/10.1016/j.addr.2011.05.019.

[273] Charman WNA, Stella VJ. Estimating the maximal potential for intestinal lymphatic transport of lipophilic drug molecules. vol. 34. 1986.

[274] Fanous MYZ, Phillips AJ, Windsor JA. Mesenteric lymph: The bridge to future management of critical illness. Journal of the Pancreas 2007;8:374–99.

[275] Simplício AL, Clancy JM, Gilmer JF. Prodrugs for amines. Molecules 2008;13:519–47. https://doi.org/10.3390/molecules13030519.

[276] Hantho JD, Strayer TA, Nielsen AE, Mancini RJ. An Enzyme-Directed Imidazoquinoline for Cancer Immunotherapy. ChemMedChem 2016;11:2496–500. https://doi.org/10.1002/cmdc.201600443.

[277] Chan M, Hayashi T, Kuy CS, Gray CS, Wu CCN, Corr M, et al. Synthesis and immunological characterization of toll-like receptor 7 agonistic conjugates. Bioconjug Chem 2009;20:1194–200. https://doi.org/10.1021/bc900054q.

[278] Martins IJ, Mortimer B, Miller J, Redgrave TG. Effects of particle size and number on the plasma clearance of chylomicrons and remnants. vol. 37. 1996.

[279] Trevaskis NL, Shanker RM, Charman WN, Porter CJH. The mechanism of lymphatic access of two cholesteryl ester transfer protein inhibitors (CP524,515 and CP532,623) and evaluation of their impact on lymph lipoprotein profiles. Pharm Res 2010;27:1949–64. https://doi.org/10.1007/s11095-010-0199-2.

[280] Férézou J, Gulik A, Domingo N, Milliat F, Dedieu J-C, Dunel-Erb S, et al. Intralipid 10%: Physicochemical Characterization. n.d.

[281] Elz AS, Trevaskis NL, Porter CJH, Bowen JM, Prestidge CA. Smart design approaches for orally administered lipophilic prodrugs to promote lymphatic transport. Journal of Controlled Release 2022;341:676–701. https://doi.org/10.1016/j.jconrel.2021.12.003.

[282] Stappaerts J, Geboers S, Snoeys J, Brouwers J, Tack J, Annaert P, et al. Rapid conversion of the ester prodrug abiraterone acetate results in intestinal supersaturation and enhanced absorption of abiraterone: In vitro, rat in situ and human in vivo studies. European Journal of Pharmaceutics and Biopharmaceutics 2015;90:1–7. https://doi.org/10.1016/j.ejpb.2015.01.001.

[283] Di L. The Impact of Carboxylesterases in Drug Metabolism and Pharmacokinetics. Curr Drug Metab 2018;20:91–102. https://doi.org/10.2174/1389200219666180821094502.

[284] Wang D, Zou L, Jin Q, Hou J, Ge G, Yang L. Human carboxylesterases: a comprehensive review. Acta Pharm Sin B 2018;8:699–712. https://doi.org/10.1016/j.apsb.2018.05.005.

[285] Holmes RS, Glenn JP, Vandeberg JL, Cox LA. Baboon carboxylesterases 1 and 2: Sequences, structures and phylogenetic relationships with human and other primate carboxylesterases. J Med Primatol 2009;38:27–38. https://doi.org/10.1111/j.1600-0684.2008.00315.x.

[286] Clement CC, Cannizzo ES, Nastke MD, Sahu R, Olszewski W, Miller NE, et al. An expanded self-antigen peptidome is carried by the human lymph as compared to the plasma. PLoS One 2010;5. https://doi.org/10.1371/journal.pone.0009863.

[287] Santambrogio L. The Lymphatic Fluid. Int Rev Cell Mol Biol, vol. 337, Elsevier Inc.; 2018, p. 111–33. https://doi.org/10.1016/bs.ircmb.2017.12.002.

[288] Wassmer B, Augenstein U, Ronai A, De Looze S, Deimling O Von. LYMPH ESTERASES OF THE HOUSE MOUSE (MUS MUSCULUS)-II. THE ROLE OF ESTERASE-2 IN FAT RESORPTION. vol. 9. 1988.

[289] Han S, Quach T, Hu L, Lim SF, Gracia G, Trevaskis NL, et al. The Impact of Conjugation Position and Linker Chemistry on the Lymphatic Transport of a Series of Glyceride and Phospholipid

Mimetic Prodrugs. J Pharm Sci 2021;110:489–99. https://doi.org/10.1016/j.xphs.2020.10.021.

[290] Burke M, Redden PR, Douglas J-A, Dick A, Horrobin DF. In vitro hydrolysis of novel gamma-linolenoyloxyalkyl derivatives of theophylline. vol. 157. 1997.

[291] Redden PR, Melanson RL, Douglas J-AE, Dick AJ. Acyloxymethyl acidic drug derivatives: in vitro hydrolytic reactivity. vol. 180. 1999.

[292] McConnell RE, Higginbotham JN, Shifrin DA, Tabb DL, Coffey RJ, Tyska MJ. The enterocyte microvillus is a vesicle-generating organelle. Journal of Cell Biology 2009;185:1285–98. https://doi.org/10.1083/jcb.200902147.

[293] Hooton D, Lentle R, Monro J, Wickham M, Simpson R. The secretion and action of brush border enzymes in the mammalian small intestine. Rev Physiol Biochem Pharmacol 2015;168:59–118. https://doi.org/10.1007/112_2015_24.

[294] Hess S, Ovadia O, Shalev DE, Senderovich H, Qadri B, Yehezkel T, et al. Effect of structural and conformation modifications, including backbone cyclization, of hydrophilic hexapeptides on their intestinal permeability and enzymatic stability. J Med Chem 2007;50:6201–11. https://doi.org/10.1021/jm070836d.

[295] Schumacher-Klinger A, Fanous J, Merzbach S, Weinmüller M, Reichart F, Räder AFB, et al. Enhancing Oral Bioavailability of Cyclic RGD Hexa-peptides by the Lipophilic Prodrug Charge Masking Approach: Redirection of Peptide Intestinal Permeability from a Paracellular to Transcellular Pathway. Mol Pharm 2018;15:3468–77. https://doi.org/10.1021/acs.molpharmaceut.8b00466.

[296] Di Stasio L, d'Acierno A, Picariello G, Ferranti P, Nitride C, Mamone G. In vitro gastroduodenal and jejunal brush border membrane digestion of raw and roasted tree nuts. Food Research International 2020;136:109597. https://doi.org/10.1016/j.foodres.2020.109597.

[297] Salam S, Iqbal Z, Khan AA, Mahmood R. Oral administration of thiram inhibits brush border membrane enzymes, oxidizes proteins and thiols, impairs redox system and causes histological changes in rat intestine: A dose dependent study. Pestic Biochem Physiol 2021;178:104915. https://doi.org/10.1016/j.pestbp.2021.104915.

[298] Oulianova N, Cheng D, Huebert N, Chen Y. Human oral drugs absorption is correlated to their in vitro uptake by brush border membrane vesicles. Int J Pharm 2007;336:115–21. https://doi.org/10.1016/j.ijpharm.2006.11.045.

[299] Amory JK, Scriba GKE, Amory DW, Bremner WJ. Oral Testosterone-Triglyceride Conjugate in Rabbits: Single-Dose Pharmacokinetics and Comparison with Oral Testosterone Undecanoate. J Androl 2003;24:716–20. https://doi.org/10.1002/j.1939-4640.2003.tb02732.x.

[300] Houston SA, Cerovic V, Thomson C, Brewer J, Mowat AM, Milling S. The lymph nodes draining the small intestine and colon are anatomically separate and immunologically distinct. Mucosal Immunol 2016;9:468–78. https://doi.org/10.1038/mi.2015.77.

[301] Shukla NM, Malladi SS, Mutz CA, Balakrishna R, David SA. Structure-activity relationships in human toll-like receptor 7-active imidazoquinoline analogues. J Med Chem 2010;53:4450–65. https://doi.org/10.1021/jm100358c.

[302] Sabri AH, Cater Z, Gurnani P, Ogilvie J, Segal J, Scurr DJ, et al. Intradermal delivery of imiquimod using polymeric microneedles for basal cell carcinoma. Int J Pharm 2020;589. https://doi.org/10.1016/j.ijpharm.2020.119808.

[303] Liu Y, Han J, Bo Y, Bhatta R, Wang H. Targeted delivery of liposomal chemoimmunotherapy for cancer treatment. Front Immunol 2022;13. https://doi.org/10.3389/fimmu.2022.1010021.

[304] Rodell CB, Arlauckas SP, Cuccarese MF, Garris CS, Li R, Ahmed MS, et al. TLR7/8-agonist-loaded nanoparticles promote the polarization of tumour-associated macrophages to enhance cancer immunotherapy. Nat Biomed Eng 2018;2:578–88. https://doi.org/10.1038/s41551-018-0236-8.

[305] Mescher M, Tigges J, Rolfes KM, Shen AL, Yee JS, Vogeley C, et al. The Toll-like receptor agonist imiquimod is metabolized by aryl hydrocarbon receptor-regulated cytochrome P450 enzymes in human keratinocytes and mouse liver. Arch Toxicol 2019;93:1917–26. https://doi.org/10.1007/s00204-019-02488-5.

[306] Horsmans Y, Berg T, Desager JP, Mueller T, Schott E, Fletcher SP, et al. Isatoribine, an agonist of TLR7, reduces plasma virus concentration in chronic hepatitis C infection. Hepatology 2005;42:724–31. https://doi.org/10.1002/hep.20839.

[307] Xiang AX, Webber SE, Kerr BM, Rueden EJ, Lennox JR, Haley GJ, et al. Discovery of ANA975: An oral prodrug of the TLR-7 agonist isatoribine. Nucleosides Nucleotides Nucleic Acids, vol. 26, 2007, p. 635–40. https://doi.org/10.1080/15257770701490472.

[308] Klossner R, Groessl M, Schumacher N, Fux M, Escher G, Verouti S, et al. Steroid hormone bioavailability is controlled by the lymphatic system. Sci Rep 2021;11. https://doi.org/10.1038/s41598-021-88508-w.

[309] Caliph SM, Charman WN, Porter CJH. Effect of Short-, Medium-, and Long-Chain Fatty Acid-Based Vehicles on the Absolute Oral Bioavailability and Intestinal Lymphatic Transport of Halofantrine and Assessment of Mass Balance in Lymph-Cannulated and Non-Cannulated Rats. vol. 89. 2000.

[310] Han S, Quach T, Hu L, Lim SF, Zheng D, Leong NJ, et al. Increasing Linker Chain Length and Intestinal Stability Enhances Lymphatic Transport and Lymph Node Exposure of Triglyceride Mimetic Prodrugs of a Model Immunomodulator Mycophenolic Acid. Mol Pharm 2023. https://doi.org/10.1021/acs.molpharmaceut.3c00099.

[311] Mahesh S, Tang KC, Raj M. Amide bond activation of biological molecules. Molecules 2018;23. https://doi.org/10.3390/molecules23102615.

[312] Labarthe L, Gelé T, Gouget H, Benzemrane MS, Le Calvez P, Legrand N, et al. Pharmacokinetics and tissue distribution of tenofovir, emtricitabine and dolutegravir in mice. Journal of Antimicrobial Chemotherapy 2022;77:1094–101. https://doi.org/10.1093/jac/dkab501.

[313] Binkhathlan Z, Ali R, Qamar W, Al-Lawati H, Lavasanifar A. Pharmacokinetic and Tissue Distribution of Orally Administered Cyclosporine A-Loaded poly(ethylene oxide)-block-Poly(ε-caprolactone) Micelles versus Sandimmune® in Rats. Pharm Res 2021;38:51–65. https://doi.org/10.1007/s11095-021-02990-5.

[314] Zhang D, Hop CECA, Patilea-Vrana G, Gampa G, Seneviratne HK, Unadkat JD, et al. Drug concentration asymmetry in tissues and plasma for small molecule-related therapeutic modalities. Drug Metabolism and Disposition 2019;47:1122–35. https://doi.org/10.1124/dmd.119.086744.

[315] Looney WW. Lymphatic distribution of the colon and rectum. The American Journal of Surgery 1939;46:143–8. https://doi.org/10.1016/S0002-9610(39)90246-1.

[316] Jørgensen J, Holtug K, Jeppesen PB, Mortensen PB. Human rectal absorption of short- and medium-chain C2-C10 fatty acids. Scand J Gastroenterol 1998;33:590–4. https://doi.org/10.1080/00365529850171846.

[317] Jorgensen JR, Fitch MD, Mortensen PB, Fleming SE. In vivo absorption of medium-chain fatty acids by the rat colon exceeds that of short-chain fatty acids. Gastroenterology 2001;120:1152–61. https://doi.org/10.1053/gast.2001.23259.

[318] Abdallah M, Lin L, Styles IK, Mörsdorf A, Grace JL, Gracia G, et al. Impact of conjugation to different lipids on the lymphatic uptake and biodistribution of brush PEG polymers. Journal of Controlled Release 2024;369:146–62. https://doi.org/10.1016/j.jconrel.2024.03.032.

[319] Mc Crudden MTC, Larrañeta E, Clark A, Jarrahian C, Rein-Weston A, Lachau-Durand S, et al. Design, formulation and evaluation of novel dissolving microarray patches containing a long-acting rilpivirine nanosuspension. Journal of Controlled Release 2018;292:119–29. https://doi.org/10.1016/j.jconrel.2018.11.002.

[320] Galandiuk S, Wrightson W, Marr L, Myers S, LaRocca R V. Suppository Delivery of 5-Fluorouracil in Rectal Cancer. vol. 3. 1996.

[321] Al Nebaihi HM, Davies NM, Brocks DR. Pharmacokinetics of cycloheximide in rats and evaluation of its effect as a blocker of intestinal lymph formation. European Journal of Pharmaceutics and Biopharmaceutics 2023;193:89–95. https://doi.org/10.1016/j.ejpb.2023.10.016.

[322] Bode U, Lörchner M, Ahrendt M, Blessenohl M, Kalies K, Claus A, et al. Dendritic cell subsets in lymph nodes are characterized by the specific draining area and influence the phenotype and fate of primed T cells. Immunology 2008;123:480–90. https://doi.org/10.1111/j.1365-2567.2007.02713.x.

[323] Wang N, Zhang G, Zhang P, Zhao K, Tian Y, Cui J. Vaccination of TLR7/8 Agonist-Conjugated Antigen Nanoparticles for Cancer Immunotherapy. Adv Healthc Mater 2023;12. https://doi.org/10.1002/adhm.202300249.

[324] Cao Y, Long J, Sun H, Miao Y, Sang Y, Lu H, et al. Dendritic Cell-Mimicking Nanoparticles Promote mRNA Delivery to Lymphoid Organs. Advanced Science 2023;10. https://doi.org/10.1002/advs.202302423.

[325] Joffre O, Nolte MA, Spörri R, Sousa CRE. Inflammatory signals in dendritic cell activation and the induction of adaptive immunity. Immunol Rev 2009;227:234–47. https://doi.org/10.1111/j.1600-065X.2008.00718.x.

[326] Jarczak D, Nierhaus A. Cytokine Storm—Definition, Causes, and Implications. Int J Mol Sci 2022;23. https://doi.org/10.3390/ijms231911740.

[327] Zhang H, Tang W, Kheirolomoom A, Fite BZ, Wu B, Lau K, et al. Development of thermosensitive resiquimod-loaded liposomes for enhanced cancer immunotherapy. Journal of Controlled Release 2020. https://doi.org/10.1016/j.jconrel.2020.11.013.

[328] Ma F, Zhang J, Zhang J, Zhang C. The TLR7 agonists imiquimod and gardiquimod improve DC-based immunotherapy for melanoma in mice. Cell Mol Immunol 2010;7:381–8. https://doi.org/10.1038/cmi.2010.30.

[329] Patinote C, Karroum NB, Moarbess G, Cirnat N, Kassab I, Bonnet P-A, et al. Agonist and antagonist ligands of toll-like receptors 7 and 8: Ingenious tools for therapeutic purposes. Eur J Med Chem 2020;193:112238. https://doi.org/10.1016/j.ejmech.2020.112238.

[330] Qu H, Li L, Chen H, Tang M, Cheng W, Lin T yin, et al. Drug-drug conjugates self-assembled nanomedicines triggered photo−/immuno- therapy for synergistic cancer treatments. Journal of Controlled Release 2023;363:361–75. https://doi.org/10.1016/j.jconrel.2023.09.042.

[331] Wilkinson A, Lattmann E, Roces CB, Pedersen GK, Christensen D, Perrie Y. Lipid conjugation of TLR7 agonist Resiquimod ensures co-delivery with the liposomal Cationic Adjuvant Formulation 01 (CAF01) but does not enhance immunopotentiation compared to non-conjugated Resiquimod+CAF01. Journal of Controlled Release 2018;291:1–10. https://doi.org/10.1016/j.jconrel.2018.10.002.

[332] Sato-Kaneko F, Yao S, Ahmadi A, Zhang SS, Hosoya T, Kaneda MM, et al. Combination immunotherapy with TLR agonists and checkpoint inhibitors suppresses head and neck cancer. JCI Insight 2017;2. https://doi.org/10.1172/jci.insight.93397.

[333] Cho JH, Lee H-J, Ko H-J, Yoon B-I, Choe J, Kim K-C, et al. The TLR7 agonist imiquimod induces anti-cancer effects via autophagic cell death and enhances anti-tumoral and systemic immunity during radiotherapy for melanoma. vol. 8. 2017.

[334] Oya K, Nakamura Y, Zhenjie Z, Tanaka R, Okiyama N, Ichimura Y, et al. Combination treatment of topical imiquimod plus anti-pd-1 antibody exerts significantly potent antitumor effect. Cancers (Basel) 2021;13. https://doi.org/10.3390/cancers13163948.

[335] Tambunlertchai S, Geary SM, Salem AK. Topically Applied Resiquimod versus Imiquimod as a Potential Adjuvant in Melanoma Treatment. Pharmaceutics 2022;14. https://doi.org/10.3390/pharmaceutics14102076.

[336] Tsuruta A, Shiiba Y, Matsunaga N, Fujimoto M, Yoshida Y, Koyanagi S, et al. Diurnal Expression of PD-1 on Tumor-Associated Macrophages Underlies the Dosing Time-Dependent Antitumor Effects of the PD-1/PD-L1 Inhibitor BMS-1 in B16/BL6 Melanoma-Bearing Mice. Molecular Cancer Research 2022;20:972–82. https://doi.org/10.1158/1541-7786.MCR-21-0786.